Updated Cosmology

with Python

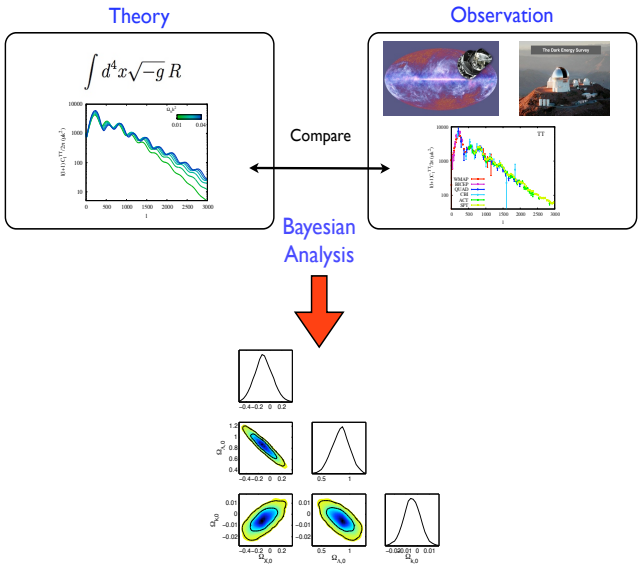

José-Alberto Vázquez

ICF-UNAM / Kavli-Cambridge

In progress

August 12, 2017

Contents

List of Figures vii

List of Tables xi

Acronyms xiii

1 Notation and conventions 7

1.1 Fundamental constants . . . 8

1.2 Distances . . . 9

1.3 Masses . . . 13

2 Homogeneous and Isotropic Universe 15

2.1 The cosmological principle . . . 16

2.2 The Geometry . . . 20

2.2.1 The spatial metric g_{ab} . . . 20

2.2.2 Lengths, areas and volumes . . . 24

2.3 The Einstein Tensor . . . 29

2.3.1 Christoffel symbols . . . 29

2.3.2 The curvature tensor . . . 30

2.3.3 Ricci tensor . . . 31

2.3.4 Einstein tensor . . . 33

2.4 The spacetime metric $g_{\mu\nu}$ . . . 40

2.5 The Friedmann-Robertson-Walker metric . . . 41

2.5.1 Geometric properties of the FRW metric . . . 46

2.6 Kinematics . . . 50

2.6.1 Geodesics in the FRW metric . . . 56
2.6.2 Redshift . . . 57
2.6.3 Hubble and Deceleration parameter . . . 59
2.6.4 Integrales . . . 62
2.7 The Friedmann-Lemaître equations . . . 67
2.8 The Energy-momentum tensor . . . 70
2.8.1 Cosmic Inventory . . . 72
2.8.2 The cosmological field equations . . . 77
2.9 Scalar Fields . . . 79
2.10 World Models . . . 81
2.11 Distances and Horizons . . . 85
2.11.1 Look-back time . . . 89
2.11.1.1 Alternatives to the ΛCDM model . . . 90

3 Inflation **93**
3.0.1 Shortcomings of the Hot Big Bang . . . 93
3.0.2 Cosmological Inflation . . . 96
3.0.3 Single-field Inflation . . . 99
3.0.4 Slow-Roll Inflation . . . 101
3.0.5 Slow-Roll approximation . . . 102

4 Thermal history of the Universe **107**
4.1 History . . . 111
4.1.1 The Hot Big Bang . . . 113
4.1.2 Local Thermal equilibrium . . . 115
4.1.3 Equilibrium Thermodynamics . . . 115
4.1.4 Densities and Pressure . . . 117
4.1.5 Effective number of Relativistic Species . . . 119
4.1.6 Conservation of Entropy . . . 121
4.1.7 Effective number of degrees of freedom in entropy . . . 122
4.1.8 Neutrino decoupling . . . 123
4.1.9 Electron-Positron Annihilation . . . 123
4.1.10 Cosmic Neutrino Background . . . 124

5 Beyond the Equilibrium **127**

5.1 Recombination . . . 127

5.1.1 Saha Equilibrium . . . 127

5.1.2 Hydrogen Recombination . . . 129

5.2 Photon Decoupling . . . 129

5.3 Last Scattering . . . 131

6 Big-Bang Nucleosynthesis **133**

6.1 BBN as a Probe of BSM physics . . . 137

6.2 Light Element Synthesis . . . 137

7 The Perturbed Universe **139**

7.1 Newtonian Perturbation Theory . . . 141

7.1.1 Perturbation analysis . . . 143

7.2 The Jean's length . . . 146

8 Applications to cold-Dark matter **149**

8.1 Solutions in a Einstein -de Sitter phase ($\bar{P} \approx 0,\ k = \Lambda = 0$) . . . 149

8.2 The Meszaros effect . . . 150

8.3 Late-time suppression of structure formation by Λ . . . 151

8.4 Evolution of baryon fluctuations after decoupling . . . 151

9 Relativistic Perturbation Theory **153**

9.1 Perturbed Spacetime . . . 153

9.2 Scalar, vector and tensor decomposition . . . 154

9.3 Orthogornal frame vectors . . . 155

9.4 Matter perturbations . . . 156

9.5 The gauge problem . . . 159

9.6 Gauge transformations . . . 160

9.7 Gauge invariant perturbations . . . 161

9.7.1 Gauge fixing . . . 162

9.8 Perturbations of the Stress-Energy tensor . . . 163

9.9 Gauge invariant perturbations . . . 164

9.10 Gauge fixing . . . 164

9.10.1 Uniform density gauge . . . 164

9.10.2 comoving gauge . . . 164
9.11 Adiabatic fluctuations . . . 164
9.12 Isocurvature fluctuations . . . 165

10 Linerised Evolution Equations **167**
10.1 Conformal Newtonian Gauge . . . 167
10.2 Perturbed Stress-Energy Conservation . . . 168
10.3 Euler equation . . . 169
10.4 Perturbed Einstein equations . . . 170
10.5 Einstein equations . . . 172
10.5.1 Conserved curvature perturbation . . . 175
10.5.2 A conservation law . . . 176
10.6 Summary . . . 178

11 Initial conditions **179**
11.0.1 Super horizon limit . . . 179
11.1 Evolution fo fluctuations . . . 181
11.2 Matter era . . . 182
11.3 Radiation . . . 183
11.3.1 Evolution of perturbations . . . 183

12 Initial conditions from inflation **189**
12.1 Canonical quantization . . . 191
12.2 Power spectrum . . . 192
12.3 Primordial perturbations from inflation . . . 194
12.4 The matter power spectrum . . . 196

13 CMB **201**
13.1 Isotropic CMB . . . 202

14 The Boltzmann equation **205**
14.1 Collisionless Part . . . 207
14.1.1 Perturbed temperature . . . 208
14.2 The Collision Term from Compton Scattering . . . 209
14.3 The Line of Sight Strategy . . . 212

15 Statistics of Random Fields **215**

15.0.1 CMB power spectrum . . . 215

15.1 Codes . . . 218

15.2 Description of fluctuations . . . 220

16 Bayesian Statistics **223**

16.1 Introduction . . . 223

16.2 Bayesian vs Frequentist statistics . . . 225

16.2.1 Frequentist statistics . . . 226

16.2.2 Bayesian statistics . . . 227

16.2.3 Comparing both descriptions . . . 227

16.3 A first look at Bayesian statistics . . . 229

16.3.1 Bayes theorem, priors, posteriors and all that stuff . . . 229

16.3.2 Updating the probability distribution . . . 232

16.3.3 About the Likelihood . . . 234

16.3.4 Letting aside the priors . . . 235

16.3.5 Chi-square and goodness of fit . . . 236

16.3.6 Contour plots and confidence regions . . . 238

16.3.7 Marginalization . . . 239

16.3.8 Fisher Matrix . . . 239

16.3.8.1 Constructing Fisher Matrices: A simple description . . . 240

16.3.9 Importance Sampling . . . 241

16.3.10 Combining datasets: Hyperparameter method . . . 242

16.4 Numerical tools . . . 244

16.4.1 MCMC techniques for parameter inference . . . 244

16.4.1.1 Metropolis-Hastings algorithm . . . 245

16.4.1.2 A first example of parameter inference . . . 246

16.4.1.3 Convergence test . . . 247

16.4.1.4 Some useful details . . . 248

16.5 Fitting a straight-line . . . 253

16.5.1 Case 1 . . . 254

16.5.2 Case 2 . . . 256

17 Statistics in Cosmology **261**

17.1 The Cosmological Parameters 261

17.1.1 Base parameters 261

17.1.2 Nuisance parameters 265

17.1.3 Derived parameters 266

17.1.4 Beyond the concordance ΛCDM 266

17.2 Observations 266

17.2.1 Current observations 267

17.2.2 Future surveys 272

17.3 Bayesian Analysis 274

17.3.1 Parameter estimation 274

17.3.2 Model selection 275

17.3.3 Dataset consistency 278

17.4 The concordance ΛCDM model 279

Bibliography **285**

List of Figures

1.1 Notation . . . 9
1.2 Parsec, and motion of earth and sun around the milky way. . . . 10
1.3 Size of the Universe . . . 11
1.4 Parsec, and motion of earth and sun around the milky way. . . . 12
1.5 Size of the Universe . . . 13
1.6 Rotation curves . . . 14

2.1 The Universe . . . 16
2.2 CMB Planck . . . 17
2.3 Homogeneity and Isotropy . . . 17
2.4 CMB anisotropies . . . 18
2.5 Points in space . . . 20
2.6 Line . . . 24
2.7 orthogonal coordinates . . . 25
2.8 Sphere . . . 25
2.9 worldlines . . . 40
2.10 coordinates . . . 41
2.11 Curvatures . . . 45
2.12 Hubble parameter . . . 47
2.13 Free particle . . . 50
2.14 Hubble parameter . . . 59
2.15 Hubble parameter . . . 60
2.16 Hubble parameter . . . 69

2.17 The evolution of the density parameters $\Omega_i(a)$ for different components of the universe . . . 78
2.18 Deceleration parameter $q(z)$ corresponding to a multi-fluid universe . . . 79
2.19 Hubble parameter . . . 82
2.20 Hubble parameter . . . 83
2.21 Hubble parameter . . . 86
2.22 Hubble parameter . . . 88
2.23 Hubble parameter . . . 88
2.24 Hubble parameter . . . 89
2.25 Comoving distance $d_{\rm c}$, luminosity distance d_L, and angular distance $d_{\rm A}$ . . . 90

3.1 Hubble parameter . . . 94
3.2 Temperature fluctuations observed in the CMB measured by the WMAP-7 experiment . . . 95
3.3 Schematic behaviour of the comoving Hubble radius during the Inflationary period. 96
3.4 Evolution of the density parameter Ω_T, during the inflationary period. . . . 98
3.5 Physical evolution of the observable universe during the inflationary period. . . . 99
3.6 Schematic Inflationary process followed by a reheating epoch . . . 103

5.3 Geometries of the spacetime . . . 131

7.1 Outline of the theoretical concepts reviewed throughout this chapter. . . . 142

11.1 CMB Planck . . . 181
11.2 CMB Planck . . . 185
11.3 CMB Planck . . . 187

12.1 CMB Planck . . . 198
12.2 CMB Planck . . . 199
12.3 CMB Planck . . . 200

15.1 Adiabatic CMB spectra for all the contributions: Temperature, E-mode, B-mode and T-E cross-correlation . . . 218
15.3 Total CMB temperature-spectrum and its different contributions: Sachs-Wolfe (SW); Doppler effect; and the integrated Sachs-Wolfe effect (ISW) . . . 220

16.1 The coin example: blue figure displays the prior distribution $P(p)$ which is updated, using the data, to get the posterior distribution $P(p|D)$, (red). The vertical black line corresponds to the real value, $p = 0.5$. 232

16.2 Posterior distributions $P(p|D)$, when the data is increased. Notice that while we continue increasing the experimental results, the posterior distribution starts to be more localized near by the real value $p = 0.5$. 233

16.3 Converging views in Bayesian inference (taken from [**?**]). A and B have different priors $P(\theta|I_i)$ for a value θ (panel (a)). Then, they observe one datum with an apparatus subject to a Gaussian noise and they obtained a likelihood $L(\theta; HI)$ (panel (b)), after which their posteriors $P(\theta|m_1)$ are obtained (panel (c)). Then, after observing 100 data, it can be seen how both posteriors are practically indistinguishable (panel (d)). 237

16.4 Left panel: 1D posterior distribution for our example. We plot the prior distribution (red), true posterior (dashed-black) and the posterior calculated by the MHA (blue). We plot 1,2 and 3σ confidence regions for the estimation of p. Right panel: associated Markov chain. We use $p_i = 0.1$ as our first "guess" for p. 247

16.5 Multiple MCMC. We use five Markov Chains to estimate the convergence. 249

16.6 Two Markov Chains considering different variance for our Gaussian proposal distribution. Left panel corresponds to $\hat{\sigma} = 0.002$, while right panel corresponds to $\hat{\sigma} = 0.8$. 250

16.7 Datasets D_1 and D_2 measured by our straight-line theory. Case 1 (left) and case 2 (right). . . 253

16.8 Left panel: 1D marginalized posterior distributions for our samples and the Markov chains for model H_0. Right panel: 2D marginalized posterior distributions along with 1-4 confidence regions for our parameters for model H_0. The red point corresponds to the true value. 254

16.9 Autocorrelation plots for model H_0. 256

16.10 Left panel: confidence regions for the parameters in model H_1. Right panel: the best-fit for the straight-lines inferred by the data. 257

16.11 Top left panel: confidence regions for the parameters in model H_0. Top right panel: confidence regions for the parameters in model H_1. Bottom panel: Best-fit values for the straight-lines for Case 2 inferred by our with data. 259

17.1 Variations of the CMB temperature power spectrum in terms of three fundamental quantities: Curvature, Baryons and Dark energy 262

17.2 Theoretical values of the distance modulus μ for three different models 263

17.4 Variations of the C^{TT} scalar spectrum and C^{BB} tensor spectrum for different values of n_s and r 265
17.5 Current status of temperature (TT), polarisation (EE) and cross-correlation (T-E) measurements of the CMB power spectra, by various observational probes. . . 269
17.6 WMAP, BICEP and QUaD constraints for the B-mode power spectrum. 270
17.7 Current status of measurements of the Hubble diagram of type Ia supernovae. . . 270
17.8 Current status of the perturbation power spectrum as measured by different experiments. 271
17.9 Polarisation noise power spectra for forthcoming experiments 273
17.10 Marginalised posterior distributions on the standard ΛCDM parameters using current cosmological observations 281
17.11 Summary of the work performed throughout this dissertation. 283

List of Tables

2.1 A Summary of possible geometries 46

2.2 Summary of the constituents of the universe along with their cosmological behaviour 77

16.1 Main differences between the Bayesian and Frequentist interpretations. 227

16.2 Jeffreys guideline scale for evaluating the strength of evidence when two models are compared. 230

16.3 $\Delta\chi^2$ for the conventional 68.3%, 95.4% and 99.73% as a function of the number of parameters (M) for the joint confidence level. 238

17.1 Candidate parameters used to describe models beyond the concordance ΛCDM. . 267

17.2 Jeffreys guideline scale for evaluating the strength of evidence when two models are compared. 277

17.3 Parameter description along with the flat-uniform priors assumed on the standard ΛCDM. 279

17.4 The constraints on the cosmological parameters using our dataset I 282

Acronyms

LMC - Large Magellanic Cloud

WMAP - Wilkinson Microwave Anisotropy Probe

ACT - Atacama Cosmology Telescope

SPT - South Pole Telescope

SNLS - SuperNovae Legacy Survey

LRG - Luminous Red Galaxies

HST - Hubble Space Telescope

CMB - Cosmic Microwave Background

FRW - Friedmann Robertson Walker

BBN - Big Bang Nucleosyntesis

GR - General Relativity

MG - Modified Gravity

LSS - Large Scale Structure

ly - light year

pc - parsec

1.- Compute the following integral

$$t = \frac{1}{H_0}\int_0^a \left[\frac{x}{\sqrt{\Omega_{r,0} + (1-\Omega_{r,0})x^2}}\right] dx, \tag{1}$$

for $\Omega_{r,0} < 1$ ($k = -1$) & $\Omega_{r,0} > 1$ ($k = 1$), to get

$$a(t) = (2H_0\Omega_{r,0}^{1/2}t)^{1/2}\left(1 + \frac{1-\Omega_{r,0}}{2\Omega_{r,0}^{1/2}}H_0 t\right)^{1/2}. \tag{2}$$

2.- Compute

$$t = \frac{1}{H_0}\int_0^a \left[\frac{x}{\sqrt{\Omega_{m,0}x + \Omega_{r,0}}}\right] dx, \tag{3}$$

to get

$$H_0 t = \frac{2}{3\Omega_{m,0}^2}\left[(\Omega_{m,0}a + \Omega_{r,0})^{1/2}(\Omega_{m,0}a - 2\Omega_{r,0}) + 2\Omega_{r,0}^{3/2}\right]. \tag{4}$$

3.- Compute

$$t = \frac{1}{H_0}\int_0^a \sqrt{\frac{x}{(1-\Omega_{\Lambda,0}) + \Omega_{\Lambda,0}x^3}}dx, \tag{5}$$

to get

$$H_0 t = \frac{2}{3\sqrt{|\Omega_{\Lambda,0}|}}f(x) = \begin{cases} \sinh^{-1}[\sqrt{a^3|\Omega_{\Lambda,0}|(1-\Omega_{\Lambda,0})}], & \Omega_{\Lambda,0} > 0. \\ . \\ \sin^{-1}[\sqrt{a^3|\Omega_{\Lambda,0}|(1-\Omega_{\Lambda,0})}], & \Omega_{\Lambda,0} < 0. \end{cases} \tag{6}$$

4.- We start by assuming the components of the Universe behave as perfect fluids and hence described by a barotropic equation of state $p_i = (\gamma_i - 1)\rho_i c^2$, where γ_i describes each fluid: radiation ($\gamma_r = 4/3$), baryonic and dark matter ($\gamma_m = 1$), and dark energy in the form of cosmological constant ($\gamma_\Lambda = 0$). Once we introduce the dimensionless *density parameters*, defined as

$$\Omega_i = \frac{\kappa_0}{3H^2}\rho_i, \tag{7}$$

a) Show that the continuity eqns. can be written as a dynamical system with the following form:

$$\Omega_i' = 3(\Pi - \gamma_i)\Omega_i, \tag{8}$$

with $\Pi = \sum_i \gamma_i \Omega_i$, and prime notation means derivative with respect to the e-fold parameter $N = \ln(a)$.

b) Also, show that the Friedmann equation becomes a constraint for the density parameters at all time $\sum_i \Omega_i = 1$.

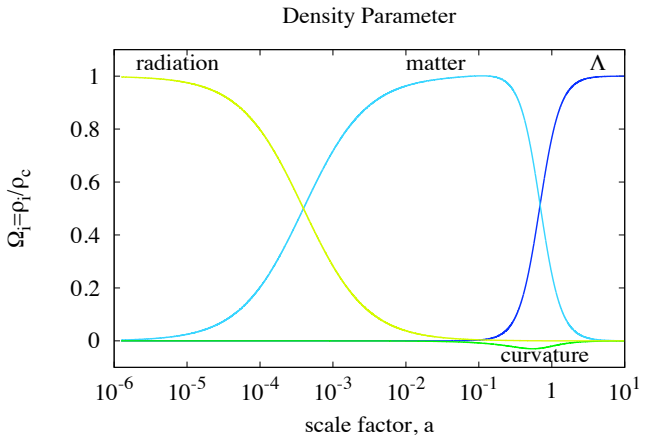

Figure 1: The evolution of the density parameters $\Omega_i(a)$.

c) Considering the initial conditions ($a = 1$) $\Omega_{r,0} = 10^{-4}$, $\Omega_{m,0} = 0.3$, $\Omega_{k,0} = -0.01$, $H_0 = 68\text{kms}^{-1}\text{Mpc}$, with cosmological constant, solve the dynamical system (**??**), along with the Friedmann constraint to get the following plot.

d) The deceleration parameter is computed in terms of the contents of the universe, as $q = \frac{1}{2}\sum_i \Omega_i(1 + 3w_i)$. Use the solutions from above to plot $q(z)$, where $1 + z = 1/a$.

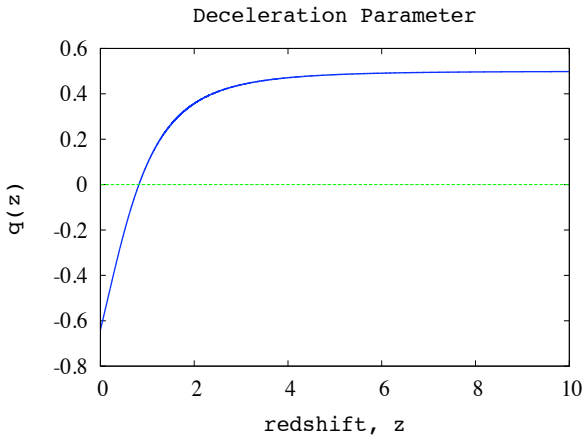

Figure 2: Deceleration parameter $q(z)$ as a function of redshift z for a multi-fluid universe. Notice that the universe is currently accelerating ($q(z = 0) < 0$).

5.- Consider the Universe from the previous exercise.

The *comoving distance* $d_{\rm c}$ is defined as

$$\chi_e = c\int_t^{t_0} \frac{dt}{R(t)} = \frac{c}{R_0}\int_0^z \frac{dz}{H(z)}. \tag{9}$$

The *luminosity distance* d_L is given by

$$d_L \equiv (1+z)R_0 S_k(\chi). \tag{10}$$

The angular distance is given by

$$d_{\rm A} \equiv \frac{R_0 S_k(\chi)}{(1+z)}. \tag{11}$$

where

$$R_0 = h_0^{-1}\sqrt{-k/\Omega_{k,0}} = \frac{H_0^{-1}}{\sqrt{|\Omega_{k,0}|}}. \tag{12}$$

.

Plot these three distances

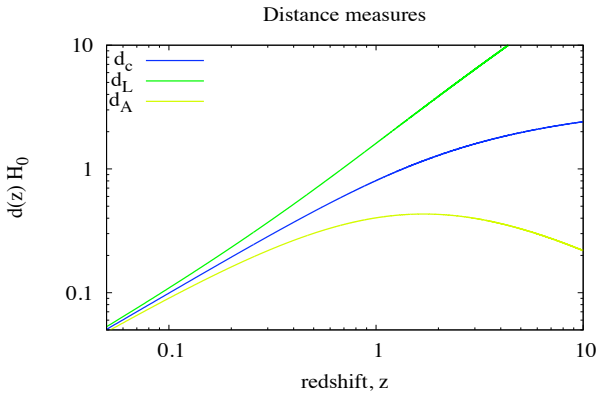

Figure 3: Comoving distance $d_{\rm c}$, luminosity distance d_L, and angular distance $d_{\rm A}$ for a universe filled with the same constituents as in Figure 2.17.

1) The most general spherically symmetric metric can be written as

$$ds^2 = -e^{2F(r,t)}dt^2 + e^{2H(r,t)}dr^2 + r^2(d\theta^2 + \sin^2\theta dphi^2). \tag{13}$$

This metric is very important as it underlies the theory of both homogeneous cosmological models and of spherically symmetric fluid models for massive stars and black holes. The functions $F(r,t)$ and $H(r,t)$ are determined by the material content of the space-time as described by the energy–momentum tensor and by the boundary conditions defining the problem.
Compute the components of the Einstein tensor.

$$\begin{aligned}
G_{00} &= e^{-2H}\left(\frac{2}{r}H' - \frac{1}{r^2}\right) + \frac{1}{r^2},\\
G_{11} &= e^{-2H}\left(\frac{2}{r}F' + \frac{1}{r^2}\right) - \frac{1}{r^2},\\
G_{22} = G_{33} &= e^{-2H}\left(F'' + F'^2 - H'F' + \frac{1}{r}(F' - H')\right)\\
&\quad - e^{-2F}\left(\ddot{H} + \dot{H}^2 - \dot{H}\dot{F}\right),\\
G_{01} = G_{10} &= \frac{2}{r}\dot{H}\, e^{-(F+H)}.
\end{aligned}$$

2) The Bianchi models are a large family of homogeneous but anisotropic cosmological models. We consider the homogenous and anisotropic space-time described by Bianchi type-III metric in the form

$$ds^2 = dt^2 - A(t)^2dx^2 - B(t)^2e^{-2\alpha x}dy^2 - C(t)^2dz^2, \tag{14}$$

where $A(t), B(t) and C(t)$ are the scale factors (metric tensors) and functions of the cosmic time t, and $\alpha = 0$ is a constant. (Bianchi type-I metric can be recovered by choosing $\alpha = 0$). Here, we assume an anisotropic fluid whose energy-momentum tensor is in diagonal form:

$$T_\nu{}^\mu = \mathrm{diag}[1, -w_x, -w_y, -w_z] = \mathrm{diag}[1, -w, -(w+\gamma), -(w+\delta)]\rho, \tag{15}$$

where ρ is the energy density of the fluid, w_x, w_y and w_z are the directional EoS parameters on the x, y and z axes respectively; w is the deviation-free EoS parameter of the fluid. δ and γ are not necessarily constants and can be functions of the cosmic time t.
a) Compute the components of the Einstein's field equations

$$\frac{\dot{A}}{A}\frac{\dot{B}}{B} + \frac{\dot{A}}{A}\frac{\dot{C}}{C} + \frac{\dot{B}}{B}\frac{\dot{C}}{C} - \frac{\alpha^2}{A^2} = \rho, \tag{5}$$

$$\frac{\ddot{B}}{B} + \frac{\ddot{C}}{C} + \frac{\dot{B}}{B}\frac{\dot{C}}{C} = -w\rho, \tag{6}$$

$$\frac{\ddot{A}}{A} + \frac{\ddot{C}}{C} + \frac{\dot{A}}{A}\frac{\dot{C}}{C} = -(w+\delta)\rho, \tag{7}$$

$$\frac{\ddot{A}}{A} + \frac{\ddot{B}}{B} + \frac{\dot{A}}{A}\frac{\dot{B}}{B} - \frac{\alpha^2}{A^2} = -(w+\gamma)\rho, \tag{8}$$

$$\alpha\left(\frac{\dot{A}}{A} - \frac{\dot{B}}{B}\right) = 0 \tag{9}$$

where the over dot denotes derivation with respect to the cosmic time t.
b) Show the solution of Eqn. (4) gives $B = c_1 A$, where c_1 is the positive constant of integration.
c) Substitute this solution into (7), and subtract the result from (6), to show that the the skewness parameter on the y axis is null, i.e. $\delta = 0$, which means that the directional EoS parameters, hence the pressures, on the x and y axes are equal.

The directional Hubble parameters in the directions of x, y and z for the Bianchi type-III metric may be defined as follows,

$$H_x \equiv \frac{\dot{A}}{A}, \quad H_y \equiv \frac{\dot{B}}{b}, \quad H_z \equiv \frac{\dot{C}}{C}. \tag{16}$$

and the mean Hubble parameter is given as

$$H = \frac{1}{3}\frac{\dot{V}}{V} = \frac{1}{3}\left(\frac{\dot{A}}{A} + \frac{\dot{B}}{B} + \frac{\dot{C}}{C}\right) \tag{17}$$

By solving the set of field equations, the difference between the expansion rates on x and z axes could be found $H_x - H_z$, [see Gen Relativ Gravit (2010) 42:763–775].

3) A step further to the standard model is to consider the dark energy being dynamic, where the evolution of its EoS is usually parameterised. A commonly used form of $w(z)$ is to take into account the next contribution of a Taylor expansion in terms of the scale factor $w(a) = w_0 + (1-a)w_a$ or in terms of redshift $w(z) = w_0 + \frac{z}{1+z}w_a$; we refer to this model as CPL. The parameters w_0 and w_a are real numbers such that at the present epoch $w|_{z=0} = w_0$ and $dw/dz|_{z=0} = -w_a$; we recover ΛCDM when $w_0 = -1$ and $w_a = 0$.

a) Show the Friedmann equation for the CPL parameterisation turns out to be:

$$\frac{H(z)^2}{H_0^2} = \Omega_{m,0}(1+z)^3 + \Omega_{k,0}(1+z)^2 + (1-\Omega_{m,0}-\Omega_{k,0})(1+z)^{3(1+w_0+w_a)}e^{-\frac{3w_a z}{1+z}}.$$

By using the initial conditions from the previous homework, plot the Comoving distance $d_{\rm c}$, luminosity distance d_L, and angular distance $d_{\rm A}$ for $[w_0 = 0.9, w_a = 0.5]$ and $[w_0 = -1.1, w_a = -0.5]$.

b) Repeat the same process in a), but now use the equation of state $w(z) = w_0 + w_a ln(1+z)$

4) As part of some models that allow deviations from ΛCDM we also use the polynomial-CDM model, that can be thought as a parameterisation of the Hubble function. This model has the following Friedmann equation:

$$\frac{H(z)^2}{H_0^2} = \Omega_{m,0}(1+z)^3 + (\Omega_{1,0}+\Omega_{k,0})(1+z)^2 + \Omega_{2,0}(1+z)^1 + (1-\Omega_{m,0}-\Omega_{1,0}-\Omega_{2,0}-\Omega_{k,0}),$$

where $\Omega_{1,0}$ and $\Omega_{2,0}$ are two additional parameters, which within the ΛCDM both of them remain absent ($\Omega_{1,0} = 0$ and $\Omega_{2,0} = 0$). Nevertheless, $\Omega_{2,0}$ could be interpreted as a 'missing matter' component introduced to allow a symmetry that relates the big bang to the future conformal singularity [see JCAP09(2012)020].

By using the initial conditions from the previous homework, plot the Comoving distance $d_{\rm c}$, luminosity distance d_L, and angular distance $d_{\rm A}$ for $[\Omega_{1,0} = 0.2, \Omega_{2,0} = -0.2]$ and $[\Omega_{1,0} = -0.2, \Omega_{2,0} = 0.2]$.

5) The action of a massive scalar field, with potential $V(\phi)$, is given by

$$S = \int d^4x\,\sqrt{-g}\,\left[\frac{1}{2}\partial_\mu\phi\partial^\mu\phi - V(\phi)\right]. \tag{18}$$

a) Show that the corresponding field equation for ϕ, obtained from the Euler-Lagrange equations, reads as

$$\Box^2\phi + \frac{dV}{d\phi} = 0. \tag{19}$$

where the *d'Alembertian* is : $\Box^2 = \partial_a\partial^a$.

0.1 Examen 1

1.- (0.5) Enunciar y explicar el Principio Cosmológico.

(0.5) Explicar homogeneidad e Isotropía, diferencia y dar ejemplos.

(1.0) Esbozar la materia oscura, i.e. historia, observaciones, candidatos, problemas.

(1.0) Esbozar la energía oscura, i.e. historia, observaciones, candidatos, problemas.

2.- Para el elemento de linea $d\sigma^2 = B(r)dr^2 + r^2 d\Omega^2$.

(1.0) Calcular ${\Gamma^r}_{rr}, {\Gamma^r}_{\theta\theta}, {\Gamma^r}_{\phi\phi}$.

Los componentes no nulos del Tensor de Ricci son:

$$R_{rr} = \frac{1}{rB}\frac{dB}{dr}, \qquad R_{\theta\theta} = 1 - \frac{1}{B} + \frac{r}{2B^2}\frac{dB}{dr}, \qquad R_{\phi\phi} = R_{\theta\theta}\sin^2\theta.$$

(0.5) Calcular el escalar de Ricci.

(1.0) Considerando que es un espacio maximalmente simetrico, encontrar la funcion $B(r)$.

Another scalar that can be constructed from the Riemann tensor is the *Kretschmann scalar*:

$$K = R_{abcd}R^{abcd}. \tag{20}$$

(0.5) Compute the Kretschmann scalar for a FRW spacetime.

3.- La metric FRW se encuentra que es

$$ds^2 = c^2dt^2 - R^2(t)\left[\frac{d\tilde{r}^2}{1-\tilde{k}\tilde{r}^2} + \tilde{r}^2 d\Omega^2\right]. \tag{21}$$

(0.5) show that this metric has a rescaling symmetry, that leaves the metric invariant

$$R \to \lambda R, \qquad \tilde{r} \to r/\lambda, \qquad \tilde{k} \to \lambda^2 k. \tag{22}$$

(0.5) By redefining the **radial coordinate** $d\chi \equiv dr/\sqrt{1-kr^2}$ in the metric (**??**), show that:

$$ds^2 = c^2dt^2 - R^2(t)\left[d\chi^2 + S_k^2(\chi)d\Omega^2\right], \tag{23}$$

where the function $S_k(\chi)$ is specified by the curvature term:

$$S_k(\chi) = \begin{cases} \sin\chi, & \text{for} \quad k=1 \\ \chi, & \text{for} \quad k=0 \\ \sinh\chi, & \text{for} \quad k=-1 \end{cases} \tag{24}$$

(1.0) Esbozar las tres posibles curvaturas, i.e. geometria, circunferencia, angulos del triangulo, tipo de universo.

Acronyms

component	Ω_i	w_i	$\rho(R)$	$R(t)$	$H(t)$	$a(\eta)$
radiation	$\Omega_{\rm r}$	?	$\propto R^{-4}$	$\propto t^{1/2}$	1/2t	η
matter	$\Omega_{\rm m}$	0	?	$\propto t^{2/3}$	?	η^2
curvature	Ω_k	?	$\propto R^{-2}$	?	1/t	?
cosmological constant	Ω_Λ	-1	$\propto R^0$	?	?	?

Table 1: conformal time $d\eta = dt/R(t)$

4.- Expand the scale factor as a power series about the present epoch t_0

$$R(t) = R[t_0 - (t_0 - t)], \tag{25}$$

and assuming $|t_0 - t| \ll t_0$ (very close to today), then

(0.5) show that

$$z = (t_0 - t)H_0 + (t_0 - t)^2 \left(1 + \frac{1}{2}q_0\right) H_0^2 + \cdots . \tag{26}$$

Since z is an absolute quantity (observable), then the look-back time $t_0 - t$ can be written in terms of z. For $z \ll 1$, from the above equation,

(1.0) show that

$$t_0 - t = H_0^{-1} z - H_0^{-1} \left(1 + \frac{1}{2}q_0\right) z^2 + \cdots . \tag{27}$$

(0.5) Finally, show that

$$H(z) = H_0[1 + (1 + q_0)z - \cdots] \tag{28}$$

5.- From the conservation of the energy-momentum tensor, $\nabla_\mu T^\mu_\nu = \partial_\mu T^\mu_\nu + \Gamma^\mu_{\mu\lambda} T^\lambda_\nu - \Gamma^\lambda_{\mu\nu} T^\mu_\lambda = 0$,

(1.0) for a perfect fluid, obtain the *continuity equation*.

(1.0) Complete table 1.

(0.5) Calcular la densidad de energía para la ecuacion de estado $w(a) = w_0 + w_a(1 - a)$.

(0.5) Calcular la densidad de energía para la ecuacion de estado $w(z) = w_0 + w_a z$.

0.1.1 Definiciones

$$\Gamma^a{}_{bc} = \frac{1}{2}g^{ad}(\partial_c g_{db} + \partial_b g_{dc} - \partial_d g_{bc}) \tag{29}$$

$$R^a{}_{bcd} \equiv \Gamma^a{}_{bd,c} - \Gamma^a{}_{bc,d} + \Gamma^e{}_{bd}\Gamma^a{}_{ec} - \Gamma^e{}_{bc}\Gamma^a{}_{ed}. \tag{30}$$

The expansion rate of the universe is characterised by the **Hubble parameter** defined as

$$H(t) \equiv \frac{\dot{R}(t)}{R(t)}, \tag{31}$$

The **deceleration parameter** $q(t)$, is defined by

$$q(t) \equiv -\frac{\ddot{R}(t)R(t)}{\dot{R}^2(t)}. \tag{32}$$

The Christoffel symbols for FRW are

$$\Gamma^0_{ij} = R\dot{R}\gamma_{ij}, \qquad \Gamma^i_{0j} = \frac{\dot{R}}{R}\delta^i_j, \qquad \Gamma^i_{jk} = \frac{1}{2}\gamma^{il}(\partial_j\gamma_{kl} + \partial_k\gamma_{jl} - \partial_l\gamma_{jk}).$$

otherwise zero

A **maximally symmetric space** is defined as both homogeneous and isotropic. Such space possesses the largest possible number of Killing vectors which in an n-dimensional manifold equals $n(n+1)/2$. The following holds for such spaces:

1.- The scalar curvature R is a constant, i.e.

$$R = n(n-1)K.$$

2.- The Ricci tensor is proportional to the metric tensor, i.e.

$$R_{\mu\nu} = \frac{1}{n}Rg_{\mu\nu}.$$

3.- The Riemman curvature tensor is given by

$$R_{\mu\nu\lambda\rho} = \frac{R}{n(n-1)}(g_{\mu\lambda}g_{\nu\rho} - g_{\nu\lambda}g_{\mu\rho}).$$

0.2 Examen 2

1.- (0.5) Explicar el Universo estático de Einstein.

(0.5) Dado un modelo Einstein-de Sitter, probar los siguientes resultados

$$a(t) = \left(\frac{t}{t_0}\right)^{2/3}, \quad H(t) = \frac{2}{3t} = H_0(1+z)^{3/2}, \quad q_0 = \frac{1}{2}, \quad \rho_m(t) = \frac{1}{6\pi G t^2}. \tag{33}$$

(0.5) Dado un modelo de Friedamann, con solo radiación y espacialmente plano, mostrar:

$$a(t) = \left(\frac{t}{t_0}\right)^{1/2}, \quad H(t) = \frac{1}{2t} = H_0(1+z)^2, \quad q_0 = 1, \quad \rho_r(t) = \frac{3}{32\pi G t^2}. \tag{34}$$

(0.5) Para un modelo de Friedmann (con $k = 0$) que contiene materia y radiación, mostrar:

$$H_0 t = \frac{2}{3\Omega_{m,0}^2}\left[(\Omega_{m,0}a + \Omega_{r,0})^{1/2}(\Omega_{m,0}a - 2\Omega_{r,0}) + 2\Omega_{r,0}^{3/2}\right]. \tag{35}$$

2.- (0.5) Mostrar que el parámetro de Hubble H se puede escribir como (Cosmic Chronometers)

$$H = -\frac{1}{1+z}\frac{dz}{dt}. \tag{36}$$

Esta relación, junto con las Large Red Galaxies, es usada para estimar el factor de Hubble.

(0.5) Considerando un Universo que contiene polvo, constante cosmológica y curvatura, mostrar que la ecuación de Friedmann se puede reescribir como

$$\left(\frac{H}{H_0}\right)^2 = (1+z)^2(1+z\Omega_{m,0}) - z(2+z)\Omega_{\Lambda,0}. \tag{37}$$

Usando ambas relaciones e integrando numéricamente, es posible calcular $t(z)$. A esta cantidad se le conoce como lookback-time.

3.- (1.0) Para un modelo de Friedmann con solo polvo, mostrar que la relación distancia-luminosidad varia con z como (formula de Mattig)

$$d_L(z) = \frac{2c}{H_0\Omega_{m,0}^2}\left[\Omega_{m,0}z + (\Omega_{m,0} - 2)\left(\sqrt{\Omega_{m,0}z + 1} - 1\right)\right]. \tag{38}$$

(0.5) Calcular la distancia angular y el horizonte comovil para un modelo Einstein-de Sitter.

(0.5) Mostrar que esta tiene un máximo en $z = 5/4$.

(1.0) Evaluar ambas expresiones en el limite $z \to \infty$, para calcular el diámetro angular subtendido por el horizonte en la superficie de ultima dispersion, i.e. $z = 1100$ y mostrar que

$$\theta_H = \frac{d_H(z_{rec})}{d_A(z_{rec})} \simeq z_{rec}^{-1/2} \simeq 1.73^o. \tag{39}$$

Esto muestra que el CMB esta cubierto por pequeños parches, con este tamaño angular, que evolucionan independientemente del Big Bang.

4.- (1.0) Explicar el problema de la planitud y del Horizonte.

(0.5) Definir inflación cosmológica, y como esta propone resolver los problemas.

(0.5) Mostrar tres equivalencias

$$\text{INFLATION} \iff \frac{d}{dt}\left(\frac{1}{RH}\right) < 0, \tag{40}$$

$$\iff \ddot{R} > 0, \tag{41}$$

$$\iff \rho + 3p < 0, \tag{42}$$

$$\iff -\frac{\dot{H}}{H^2} < 1. \tag{43}$$

5.- El tensor de energía momento correspondiente a un campo escalar es:

$$T_{\mu\nu} = \partial_\mu\phi\partial_\nu\phi - g_{\mu\nu}\left[\frac{1}{2}\partial_\sigma\phi\partial^\sigma\phi - V(\phi)\right]. \tag{44}$$

comparándolo con el de un fluido perfecto, en un sistema coordenado en el cual el fluido esta en reposo,

(0.5) mostrar que la densidad de energía y presión efectivas son:

$$T_{00} = \rho_\phi = \frac{1}{2}\dot{\phi}^2 + V(\phi) + \frac{1}{2}(\nabla\phi)^2, \tag{45}$$

$$T_{ii} = p_\phi = \frac{1}{2}\dot{\phi}^2 - V(\phi) + \frac{1}{6}(\nabla\phi)^2, \tag{46}$$

(0.5) si el campo ϕ es espacialmente constante, mostrar que inflación ocurre cuando $\dot{\phi}^2 < V(\phi)$.

(0.5) Mostrar que la ecuación de movimiento de un campo escalar con potencial $V(\phi)$ es

$$\ddot{\phi} + 3H\dot{\phi} + V_{,\phi} = 0. \tag{47}$$

(0.5) considerando que H es aproximadamente constante, encontrar la solución general de un campo escalar libre ϕ, para el cual $V(\phi) = \frac{1}{2}m^2\phi^2$.

6.- Considerando el mismo potencial $V(\phi) = \frac{1}{2}m^2\phi^2$.

(1.0) Explicar la aproximación de slow-roll y con esta encontrar las soluciones para el campo ϕ y el factor de escala.

(0.5) Calcular los parámetros de slow-roll $\epsilon_{\rm v}, \eta_{\rm v}$ y encontrar la condición del campo para que ocurra inflación.

(0.5) Calcular el numero de e-folds, y encontrar el valor del campo para explicar la isotropia del CMB, i.e. $N \sim 60$.

0.2.1 Definiciones

The FRW Universes dominated by matter and vacuum energy are named as **Lemaitre models**. Cosmological models with zero cosmological constant, and strictly non-zero matter or radiation density, are known as the **Friedmann models**. Comoving horizon

$$d_H = \frac{c}{R_0}\int_z^\infty \frac{dz}{H(z)}. \tag{48}$$

The *luminosity distance* d_L in terms of measurable quantities is

$$d_L(z) \equiv (1+z)R_0 S_k(\chi). \tag{49}$$

The angular distance is given by

$$d_{\rm A} \equiv \frac{R_0 S_k(\chi)}{(1+z)}, \tag{50}$$

$$\chi = \frac{c}{R_0}\int_0^z \frac{dz}{H(z)}. \tag{51}$$

$$\epsilon_{\rm v}(\phi) \equiv \frac{1}{16\pi G}\left(\frac{V_{,\phi}}{V}\right)^2, \qquad |\eta_{\rm v}(\phi)| \equiv \frac{1}{8\pi G}\frac{|V_{,\phi\phi}|}{V}. \tag{52}$$

0.3 Examen 3

1.- (1.0) El modelo estandar de partículas elementales se conforma por Quarks, Leptones, Bosones de norma y Escalar. Enunciar las partículas que corresponden a cada categoría.
(0.5) Cual es la principal diferencia entre partículas fermionicas y bosonicas?
(0.5) De que estan hechos los bariones. Enunciar dos de ellos.

2.- (0.5) Definir equilibrio térmico.
(1.0) En el limite relativista, calcular la densidad de energia de partículas

$$\rho = \frac{\pi^2}{30} g T^4 \begin{cases} 1 & \text{bosons} \\ \frac{7}{8} & \text{fermions.} \end{cases} \tag{53}$$

Por tanto, con la temperatura del CMB, se puede calcular el parametro de densidad de fotones

$$\rho_{\gamma,0} = \frac{\pi^2}{15} T_0^4 \approx 4.6 \times 10^{-34} \text{g cm}^{-4} \quad \rightarrow \quad \Omega_{\gamma,0} h^2 \approx 2.5 \times 10^{-5}.$$

(0.5) Mostrar que para este fluido, podemos recuperar la relación presión-densidad para un gas relativista (radiación): $P = \frac{1}{3}\rho$.
3.- (1.0) En el limite no-relativista mostrar que la densidad de numero de particulas es igual para bosones que para fermiones y esta dada por [1]

$$n = g \left(\frac{mT}{2\pi} \right)^{3/2} e^{-m/T}.$$

(1.0) En el orden mas bajo del limite no-relativista, la densidad de energia es simplemente igual a la densidad de masa $\rho \approx mn$. En este limite, mostrar que el gas de partículas se comporta como polvo sin presión (materia), – la ley de gas ideal – :

$$P = nT \ll \rho = mn.$$

4.- Una de las consequencias de la conservacion de la entropia implica que $g_* T^3 a^3 =$const.
(0.5) Utilizando la ecn de Friedmann para particulas relativistas, mostrar que la temperatura se comporta como: $T \propto g_{*s}^{-1/4} t^{-1/2}$.
Si agregamos constantes, podemos obtener que la temperatura del Universo 1 segundo despues del Big Bang era de alrededor de 1MeV.

$$\frac{T}{1MeV} \simeq 1.5 g_{*s}^{-1/4} \left(\frac{1sec}{t} \right)^{1/2}. \tag{54}$$

[1] Particulas masivas son exponencialmente raras a bajas temperaturas.

(1.0) Cuando la densidad de energia y entropia de los electrones y positrones es transferida a los fotones ($e^+ + e^- \rightleftharpoons \gamma + \gamma$), se dice que los fotones "se calientan". Mostrar que la temperatura de los neutrinos despues de la aniquilacion $e^+ + e^-$ es ligeramente menor y esta dada por:

$$T_\nu = \left(\frac{4}{11}\right)^{1/3} T_\gamma. \tag{55}$$

(0.5) Considerando que los neutrinos no tienen masa, y que el numero efectivo de familias de neutrinos es N_{eff}, mostrar que

$$\rho_\nu = \frac{7}{8} N_{\text{eff}} \left(\frac{4}{11}\right)^{4/3} \rho_\gamma. \tag{56}$$

5.- (1.0) Bosquejar el proceso de Recombinacion, Desacomplamiento de fotones, esto es, explica la sig figura:

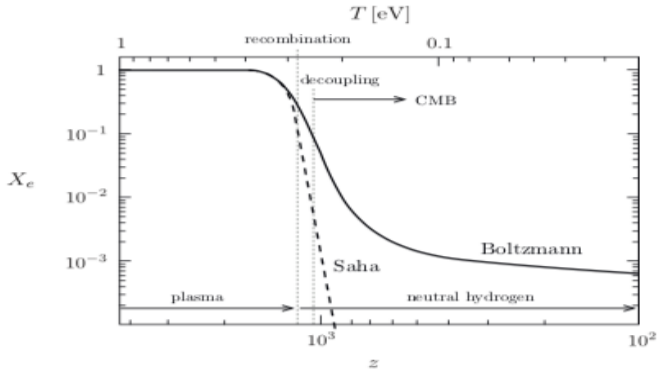

6.- (1.0) Calcular la abundancia relativa del neutron y proton

$$\left(\frac{n_n}{n_p}\right)_{eq} \tag{57}$$

y mostrar para que temperaturas hay el mismo numero de neutrones como de protones.
(0.5) Equilibrio termico ocurre hasta $T_{dec} \sim 0.8MeV$ (cuando los neutrinos se desacoplan). Muestra que la fracción de neutrones $X_n \equiv \frac{n_n}{n_n+n_p}$ es aproximadamente 1/6.
(0.5) A temperaturas $T > 0.2MeV$ ($t \sim 130$ sec) la vida media del neutro se vuelve importante, disminuyendo por un factor exponencial

$$X_n(T) = \frac{1}{6} e^{-t/\tau_n}.$$

Debido a que el nucleo de helio contiene 2 neutrones, todos los neutrones terminan formando helio (el nucleo ligero mas estable), y por tanto la densidad del numero de helio-4 es $N_{He-4} =$

$N_n/2$. Estimar la fraccion total de masa en helio-4

$$Y_4 \equiv \frac{2N_n}{N_n + N_p}.$$

Este tratamiento tan simple nos indica la fraccion de materia en el universo, la cual es principalmente He-4.

7.- (1.0) Explicar como la fracción de masa de Helio depende de diversos parametros iniciales (justifica tus enunciados).

(1.0) Explicar las sigs figuras.

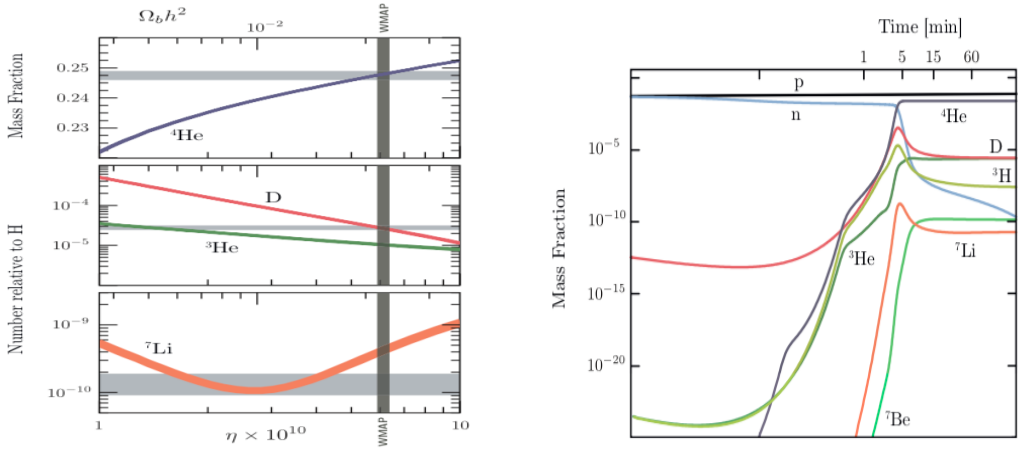

Figure 4: Helium production in the Universe

0.3.1 Definiciones

The number density (n), energy density (ρ) and pressure (P) of a gas of particles are given by

$$n = \frac{g}{(2\pi)^3}\int d^3p f(p), \qquad \rho = \frac{g}{(2\pi)^3}\int d^3p f(p)E(p), \qquad P = \frac{g}{(2\pi)^3}\int d^3p f(p)\frac{p^2}{3E}. \tag{58}$$

where g are the internal degrees of freedom, the particles energy $E(p) = \sqrt{m^2 + p^2}$ and its description is based on the *distribution function* $f(\vec{x}, \vec{p}, t)$.

Some useful integrals:

$$\int_0^\infty d\xi \frac{\xi^n}{e^\xi - 1} = \zeta(n+1)\Gamma(n+1), \qquad \int_0^\infty d\xi \xi^n e^{-\xi^2} = \frac{1}{2}\Gamma\left(\frac{1}{2}(n+1)\right), \tag{59}$$

with $\zeta(z)$ is the Riemann zeta-function, and $\Gamma(1/2) = \sqrt{\pi}$, $\Gamma(n+1) = n\Gamma(n)$.

La energia de enlace del Hidrogeno esta dada por $B_H = 1.3$MeV.

Vida media del neutron $\tau_n = 886$ sec.

0.4 Examen 4

1.- (1.0) Explicar teoría de perturbaciones Lagrangianas.

2.- (0.5) Encontrar las siguientes cantidades en coordenadas comoviles, donde la distancia física esta dada por $\vec{r} = a(t)\vec{x}$:

$$\left(\frac{\partial}{\partial t}\right)_{\vec{r}}, \qquad \vec{u} \equiv \frac{d\vec{r}}{dt}. \tag{60}$$

(1.5) Realizando el procedimiento de teoría de perturbaciones lineales, encontrar las ecuaciones que satisfacen $\delta, \vec{v}, \Phi$, o equivalentemente, encuentra:

$$\partial_t \delta, \quad \partial_t \vec{v}, \quad \nabla^2 \Phi. \tag{61}$$

3.- (0.5) A partir de las ecuaciones anteriores, obtener la ecuación de Jeans

$$\partial_t^2 \delta + 2H\partial_t \delta - 4\pi G\bar{\rho}\delta - \frac{1}{a^2\bar{\rho}}\nabla^2 \delta P = 0. \tag{62}$$

(1.0) Para un universo con presión cero, encontrar la manera alternativa de escribir esta ecuación, dada por:

$$\frac{d^2\delta}{da^2} + \frac{1}{a}\left[3 + \frac{d\ln H}{d\ln a}\right]\frac{d\delta}{da} - \frac{3}{2a^2}\Omega_m \delta = 0.$$

4.- (1.0) Muestra que los modos vectoriales en (**??**) pueden ser despreciados. Bajo que condiciones?

5.- El campo $\delta(\boldsymbol{x})$ puede ser escrito como la transformada de Fourier de $\delta(\boldsymbol{k})$ (o viceversa)

$$\delta(\boldsymbol{x}) = \int \delta(\boldsymbol{k}) e^{i\boldsymbol{k}\cdot\boldsymbol{x}} d^3\boldsymbol{k} \tag{63}$$

(0.5) Muestra que el gradiente de $\delta(\boldsymbol{x})$ es equivalente a multiplicar su transformada de Fourier por $i\boldsymbol{k}$.

(1.0) En una dimension, calcula la transformada de Fourier de la función $\delta(k) = e^{i\alpha k}$ y de $\delta(k) = e^{-\alpha x^2}$, con α =constante.

6.- Para un fluido barotropico $P = P(\rho)$, escribe la ecuacion de Jeans de la forma

$$\partial_t^2 \delta + 2H\partial_t \delta + w^2 \delta = 0. \tag{64}$$

(1.0) Para un Universo plano tipo Einstein-de Sitter, muestra que la solución a la ecuación esta dada por

$$\delta(t) = At^{2/3} + Bt^{-1}.$$

(0.5) Muestra que, para el modo creciente, el potencial gravitacional es constante.

7.- (1.0) Para un Universo con Ω_m, Ω_Λ y sin radiación $\Omega_r = 0$. Muestra que una solución a las perturbaciones de materia esta dada por el parámetro de Hubble $H(t)$ (solución decreciente).

8.- (1.0) La segunda solución linealmente independiente $D(t)$ se encuentra construyendo el Wronskiano $(\dot{D}H - D\dot{H})$. Encuentra que esta solución tiene la siguiente forma [hint: calcula $\frac{d}{dt}\left(\frac{D}{H}\right)$]

$$D(t) \propto H(t) \int_0^t \frac{dt'}{a^2(t')H^2(t')}.$$

Este se le conoce como el factor lineal de crecimiento de las perturbaciones. [1]

(0.5) Calcula $D(z)$ para el caso $\Omega_m = 1, \Omega_\Lambda = 0$.

9.- Para un universo dominado por la constante cosmológica:

(0.5) Encuentra las soluciones de las perturbaciones, esto es, muestra que las perturbaciones de materia no crecen.

(0.5) Muestra que el potential gravitacional decae con el factor de escala.

0.4.1 Definiciones

$$Continuity \quad : \quad \partial_t \rho + \nabla_{\vec{r}} \cdot (\rho \vec{u}) = 0, \qquad \text{(energy density conservation)}, \tag{65}$$

$$Euler \quad : \quad \partial_t \vec{u} + \vec{u} \cdot \nabla_{\vec{r}} \vec{u} = -\frac{1}{\rho} \nabla_{\vec{r}} \rho - \nabla_r \Phi, \qquad \text{(momentum conservation)}, \tag{66}$$

$$Poisson \quad : \quad \nabla^2_{\vec{r}} \Phi = 4\pi G \rho, \tag{67}$$

Teorema 2 (Abel-Liouville). *Sea*

$$x'' + a_1(t)x' + a_2(t)x = 0 \tag{8}$$

una ecuación diferencial lineal homogénea de segundo orden, donde $a_1(t)$ y $a_2(t)$ son funciones reales continuas en un intervalo I. Sean $x_1(t), x_2(t)$ dos soluciones de (8) y sea

$$W(t) = W[x_1(t), x_2(t)]$$

su wronskiano. Entonces,

$$\forall t \in I, \qquad W(t) = C\mathrm{e}^{-\int a_1(t)\,\mathrm{d}t}.$$

[1] La rapidez de crecimiento se define como $g(a) = \frac{dlnD}{dlna}$. Una aproximación util es parametrizandola como $g(z) = [\Omega_m(z)]^\gamma$, con $\gamma = 0.6$.

Numbers

1 Astronomical unit (AU)= 1.496×10^{13} cm

1 Parsec = 3.086×10^{18}cm

1 Solar Mass ($M_\odot$) = 2×10^{33}g

The Hubble constant: $H_0 = 67.5$ km s^{-1}Mpc^{-1}

Reduced Planck constant: $\hbar = h/2\pi =$

Concepts

- A **red dwarf** is the smallest and coolest kind of star on the main sequence.
- The **Cepheid variables** are (stars) considered as standard candles, as they have a relationship between their absolute luminosity and the pulsation period.
- A **satellite galaxy** is a smaller companion galaxy bound to its host galaxy (known as the primary galaxy).
- A **manifold** is a topological space that locally resembles Euclidean space near each point.

Copernican principle, Homogeneity → Isotropy?

Diferencia entre coordinate time and proper time.

Perfect Fluids

Bayesian vs Frequentists

Why MCMC (they scale approx linear with the dimension of the problem, rather than exponentially)

Convergence test (Gelma-Rubin)

Concepts

Scalar, Vectors, Tensor modes are completely decoupled? conditions

ξ is conserved for more than 1 field?

Temperature at decoupling time, z,t, T

Plots - CMB (scales, θ), first peak, odds and even peaks. color on the elipse.

when ocurred inflation? How long lasted? (a,t)

Explain equations, relevant terms.

horizon scale 1.7 degrees, $l \approx 100$, thickness $l \sim 10^3$, decoupling 1 degree, $l \sim 200$

Curvature parameter k, dimensions, magnitude.

Einstein equations and symmetries (10 eqs, 6 independent)

Gauges

Adiabatic & Isocurvature

Implications of a non-scale invariant spectrum $n \neq 1$

why $d_L > d_c > d_A$

understand step $\Delta \to \Delta'$

Implications of non-scale invariant $n \neq 1$

PCA

LD $\eta = \pi/2$, why?

Explain the shape of the LD model, why is it better than n_s

Bayesian vs Frequentist

PPF, perturbations

PDL (w=-1)

When the universe started accelerating (z)

Dependence on priors (why flat)

In the LD model, what if we choose another form of dark energy instead of the cosmological constant

Gelman Rubin and other convergence tests

Computational time for flat $\sim 10sec$, non flat 50 secs $10^4 - 10^4$ likelihood evaluations for. then 10 times more for model selection.

What are the MCMC methods in general, properties.

Jeffreys guideline is based on what, what are those numbers

Understand perturbation theory, parameters involved, gauge invariant quantities, sources (they are solutions of what)

line of sight integration.

Agregar modelos – Horota with (clase de cosmo cinves) inhomogeous (fernando, cosmo - icf)

Astronomical units, parsec

FLRW, GR, CMB, EL

mass of particles in ev, of the sun

value of H0

define conformal time, radial coordinate, rho crititcal, q, j,

epoch: aequiv,

(jav: Explain Einstein's derivation, the weak field limit, and R in terms of T)

(jav: add torsion discussion and models).

(jav: Palatini models too)

Show that In a *flat* space-time, $\Gamma^{a}{}_{bc}$ and its derivatives are zero

Explain the Weyl tensor and the Kretschmann scalar.

1

Notation and conventions

Some of the notation adopted throughout this book is as follows:

- Whenever indicated we use the **natural unit system**, where measurements are based on universal physical constants. That is, the speed of light c, the reduced Planck's constant $\hbar = h/2\pi$ and the Boltzmann's constant $k_{\rm B}$, are set equal to one (length and time have the same units):

$$c = \hbar = k_{\rm B} = 1. \tag{1.1}$$

- An **overdot** in any quantity denotes time (t) derivative, prime represents conformal-time (η) derivatives and a comma-subscript derivatives with respect to space coordinates or fields (ϕ):

$$\dot{f} \equiv \frac{\partial f}{\partial t}, \quad f' \equiv \frac{\partial f}{\partial \eta}, \quad \text{and} \quad f_{,\phi} \equiv \frac{\partial f}{\partial \phi}. \tag{1.2}$$

- Quantities evaluated at present time ($t = t_0$) are also expressed by a subscript '0', whereas vectors are represented by any of these forms: $\mathbf{x}, x^i, \vec{x}$.

- Greek indices run over time coordinate (labelled by '0') and three spatial-Latin coordinates:

$$\alpha, \beta, \cdots \in \{0, 1, 2, 3\}, \qquad \text{and} \qquad i, j, \cdots \in \{1, 2, 3\}. \tag{1.3}$$

- We adopt the sign convention commonly used in relativity and cosmology:

$$[\eta_{\mu\nu}] = \begin{pmatrix} +1 & 0 & 0 & 0 \\ 0 & -1 & 0 & 0 \\ 0 & 0 & -1 & 0 \\ 0 & 0 & 0 & -1 \end{pmatrix},$$

where $\eta_{\mu\nu}$ are the components of the tensor metric, and in a shorthand notation $[\eta_{\mu\nu}] = \text{diag}(+1, -1, -1, -1)$, such that the square line element is $ds^2 = \eta_{\mu\nu} dx^\mu dx^\nu = c^2 dt^2 - d\mathbf{x}^2$ for the Minkowski spacetime. This is the same signature used in Particle physics but often opposite in General Relativity.

- We adopt the Einstein's *summation convention*: whenever occur repeated indices (one as a covariant-subscript and one as a contravariant-superscript) in an expression they are summed over their range.

Example 1.0.1: Tensor metrico

In three dimensions:

$$a^i a_i \equiv \sum_{i=1}^{3} a_i a_i = (a_1)^2 + (a_2)^2 + (a_3)^2,$$

and

$$a^i{}_j a_{ik} = \sum_{i=1}^{3} a_{ij} a_{ik} = a_{1j} a_{1k} + a_{2j} a_{2k} + a_{3j} a_{3k}.$$

Here, the repeated index i is summed over all the components, and it is called a *dummy index*, as it can be replaced by any other index. Whereas the indices j and k, appearing on both sides of this equation, are said to be *free indices* as they can take any value from one to the dimension of the vector.

1.1 Fundamental constants

As we mentioned above, throughout this book we will mostly use natural units, however to make direct comparisons to physical quantities it is necessary to introduce the units back. Scipy has a library to perform this task.

HW 1.1.a: Covert the following quantities:

- $T_0 = 2.725K \to 0.2348$ meV, CMB temperature today.
- $\rho_{\gamma,0} = 4\sigma T_0^4/c \to 0.260$ eV cm^{-3} (411γ's cm^{-3}), CMB energy density.
- $c/H_0 \to$ Mpc, with $H_0 = 70$km sec^{-1}Mpc^{-1}, Hubble constant.

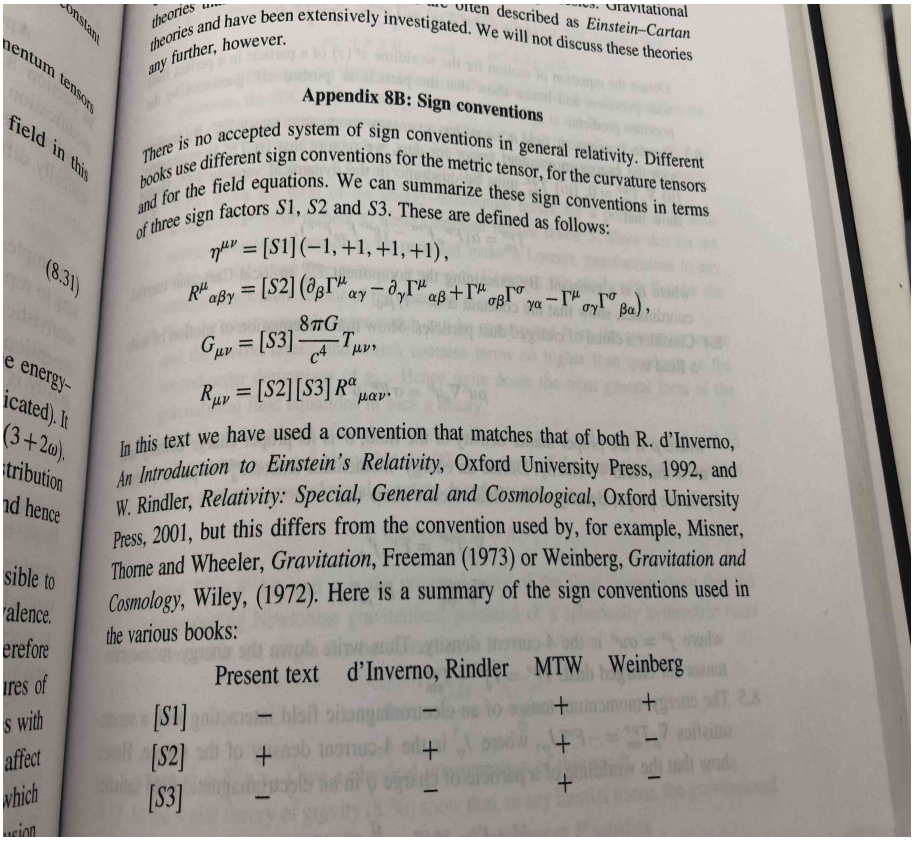

theories and have been extensively investigated. We will not discuss these theories any further, however.

Appendix 8B: Sign conventions

There is no accepted system of sign conventions in general relativity. Different books use different sign conventions for the metric tensor, for the curvature tensors and for the field equations. We can summarize these sign conventions in terms of three sign factors $S1$, $S2$ and $S3$. These are defined as follows:

$$\eta^{\mu\nu} = [S1](-1,+1,+1,+1),$$

$$R^{\mu}{}_{\alpha\beta\gamma} = [S2]\left(\partial_\beta \Gamma^{\mu}{}_{\alpha\gamma} - \partial_\gamma \Gamma^{\mu}{}_{\alpha\beta} + \Gamma^{\mu}{}_{\sigma\beta}\Gamma^{\sigma}{}_{\gamma\alpha} - \Gamma^{\mu}{}_{\sigma\gamma}\Gamma^{\sigma}{}_{\beta\alpha}\right),$$

$$G_{\mu\nu} = [S3]\frac{8\pi G}{c^4}T_{\mu\nu},$$

$$R_{\mu\nu} = [S2][S3]R^{\alpha}{}_{\mu\alpha\nu}.$$

In this text we have used a convention that matches that of both R. d'Inverno, *An Introduction to Einstein's Relativity*, Oxford University Press, 1992, and W. Rindler, *Relativity: Special, General and Cosmological*, Oxford University Press, 2001, but this differs from the convention used by, for example, Misner, Thorne and Wheeler, *Gravitation*, Freeman (1973) or Weinberg, *Gravitation and Cosmology*, Wiley, (1972). Here is a summary of the sign conventions used in the various books:

	Present text	d'Inverno, Rindler	MTW	Weinberg
$[S1]$	−	−	+	+
$[S2]$	+	+	+	−
$[S3]$	−	−	+	−

Figure 1.1: Comparison with several books/notes, i.e. Doran, Lasenby and Challinor, Baumman.

HW 1.1.b: Show the equivalence:

- $4.48146636 \times 10^{-7} = 8 * pi^5 * (boltzmannconstant)^4/(15 * (h * c)^3)) * (1 Kelvin) * *4/(3 * (100 km/s/Mpc)^2/(8 * Pi * G) * (speedoflight)^2)$.
- $0.2776566337 = 45 * \zeta(3)/(2 * \pi^4)$.
- $\rho_{c,0} = 1.87840\, h^2 \times 10^{-26}$ kg m^{-3} $= 2.775\, h^{-1} \times 10^{11} M_\odot/(h^{-1}\mathrm{Mpc})^3$.

1.2 Distances

Measuring distances is not an easy task, specially when such humongous lengths are considered in cosmology. Let us mention some of the most useful ones.

- The radius of the Earth's orbit around the Sun, that is, the mean distance from the centre

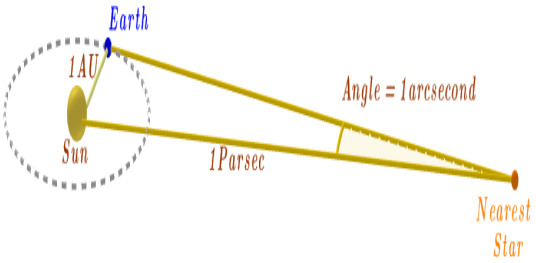

Figure 1.2: One Parsec (pc) is defined as the distance at which one astronomical unit subtends an angle of one second of arc.

of the earth to the centre of the sun is defined as 1 Astronomical Unit (AU) or equivalently 1 AU$= 1.496 \times 10^{13}$ cm. Note: astronomers mostly used units in cm, gr, etc.

- 1 Parsec (pc) is defined as the distance at which one astronomical unit subtends an angle of one second of arc (1 pc = 1 AU/tan(1")), as shown in Figure 1.2.

$$1 \text{ parsec} \equiv 1.496 \times 10^{13}\text{cm} \times \frac{360}{2\pi} \times 60 \times 60 = 3.086 \times 10^{18}\text{cm} \simeq 3.261 \text{ light years (ly)},$$

where a light year is the distance that light travels over the lapse of one year.

- Parsec, Kiloparsec (kpc) and Megaparsec (Mpc) are the most commonly used distance units in astronomy.

For instance:

- Proxima Centauri, meaning the *nearest [star] of Centaurus*, is 1.301 pc (4.244 lys) away to the Sun. Proxima Centauri, being the third member of the Alpha Centauri system, is a red dwarf star with a mass of about an eighth the mass of the Sun $M_\odot$. The other two members, Alpha Centauri A (Rigil Kentaurus) and Alpha Centauri B (Toliman), together form the binary star -Alpha Centauri AB- with an average distance of 4.3 lys from the sun.

- 8.5 kpc is the distance from the Sun to the Galactic Centre of the Milky Way[1], a barred spiral galaxy with the following features

  – Radius of the disk = 12.5 kpc.

[1]Was formed after the trickster god Hermes suckled the infant Heracles at the breast of Hera, the queen of the gods, while she was asleep. When Hera awoke, she tore Heracles away from her breast and splattered her breast milk across the heavens, see Figure 1.3.

- Thickness of the disk = 0.3 kpc.
- At our location, the galaxy rotates with a period of 200 million years.

Figure 1.3: The Origin of the Milky Way (source: Tintoretto).

- The *Canis Major Dwarf Galaxy* (a disputed dwarf irregular galaxy) is the closest neighbour galaxy, being located at about 7.7 kpc away from the Solar System and 13 kpc from the Galactic Centre. The previous contender for the closest galaxy corresponds to the *Sagittarius Dwarf Elliptical Galaxy* with a distance of ∼16kpc.
- Another satellite galaxy of the Milky Way is the Large Magellanic Cloud (LMC) [2], located at about 50 kpc. The Milky Way and the LMC are expected to collide in approximately 2.4 billion years [23].
- Andromeda, also known as Messier 31 or just M31, is the closest galaxy with similar size to our own with a distance of 780 kpc. This spiral galaxy, with a diameter of ∼67 kpc, is the largest within the Local Group. Andromeda is approaching the Milky Way at about 110 kilometres per second, and hence they are expected to collide in about 4.5 billion years [31].
- The *Local group* of galaxies, the one we live in, has a total diameter of roughly 3.1 Mpc. The Local Group comprises more than 54 galaxies, most of them are dwarf galaxies, and the two largest members include the Andromeda galaxy and the Milky Way (Triangulum

[2] An intermediate between dwarf spiral galaxies and irregular galaxies.

Galaxy being the third largest member). On the other hand, the Virgo cluster, comprises approximately 1300 (and possibly up to 2000) member galaxies and along with the Local Group they lay within the Virgo Supercluster.

- 33 Mpc is the diameter of Virgo Supercluster which contains at least 100 galaxy groups and clusters. The Virgo SC is only one of about 10 million superclusters in the observable universe.

- From the range of 10-100 Mpc are the sizes of Voids – spaces between filaments (Figure 1.4) – which contain very few or no galaxies. The *Local void*, lying adjacent to the Local Group, has a diameter of about 60 Mpc.

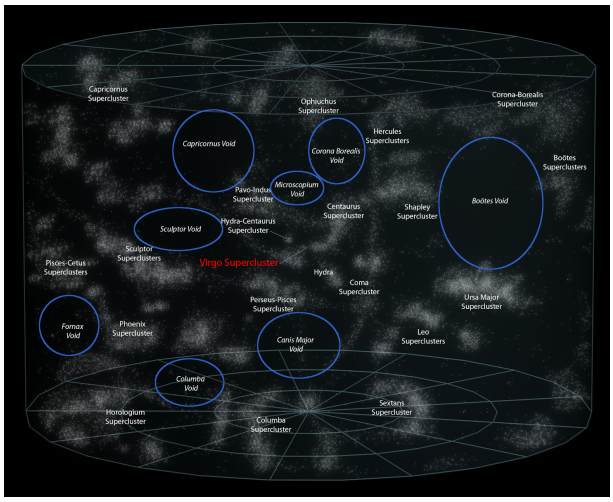

Figure 1.4: List of voids.

- The Laniakea Supercluster ("immense heaven" in Hawaiian), stretched out over 160 Mpc, encompasses approximately 100,000 galaxies. It has the approximate mass of 10^{17} solar masses and the closets supercluster consists of: Hydra-Centaurus (the closest neighbour), Perseus-Pisces and Pavo-Indus.

- The Hubble radius (radius of the observable universe) corresponds to c/H_0 =4450 Mpc (or 14.4 billion light years), as we shall see in the following sections.

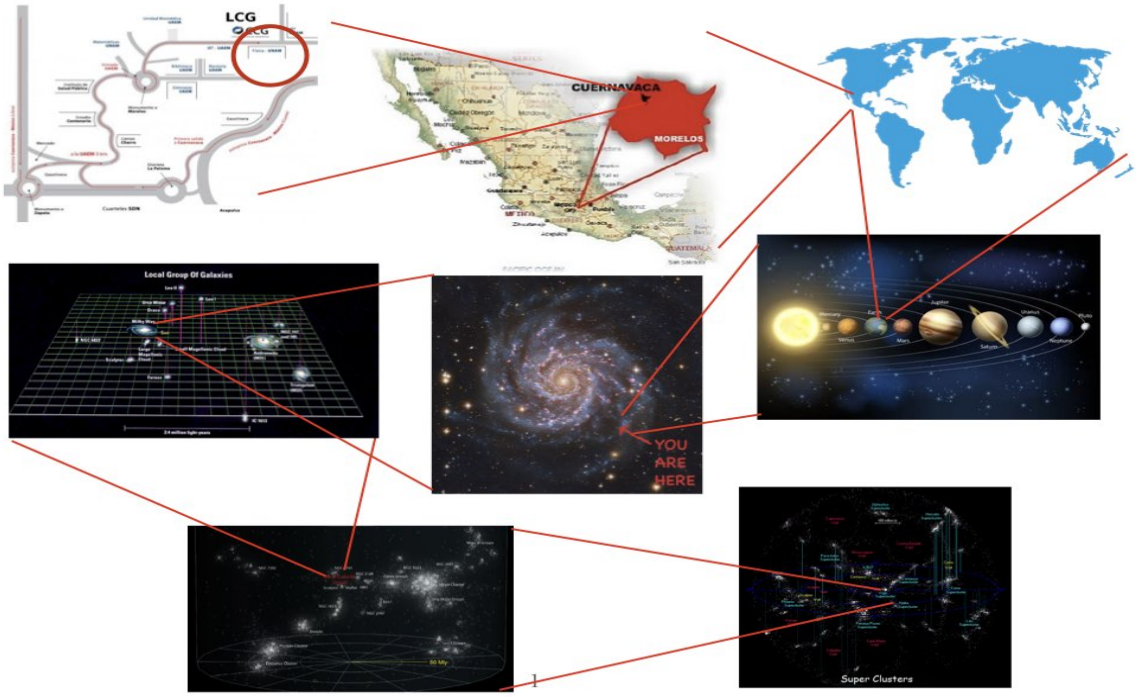

Figure 1.5: Size of the Universe.

1.3 Masses

- Stellar mass of the Milky Way $\simeq 1 \times 10^{11} M_{\odot}$.
- Dynamical mass of the Milky Way $\simeq 1 \times 10^{12} M_{\odot}$, measured from the motion of its satellites. Its difference compared to the stellar mass gives rise to the *Dark Matter* idea.
- Mass of giant elliptical galaxy $\simeq 1 \times 10^{13} M_{\odot}$.
- Mass of the Virgo cluster $\approx 10^{15} M_{\odot}$ (~ 1300 galaxies).
- Laniakea $\approx 10^{17} M_{\odot}$ ($\sim 1 \times 10^{5}$ galaxies).

HW 1.3: Compute the orbital speed of Neptune (5.43 km/s) given the mass of the sun and its distance, and compare with the real measurements (see Figure 1.6). Do the same with the Milky Way and the Sun.

The scale of the Universe: https://scaleofuniverse.com/

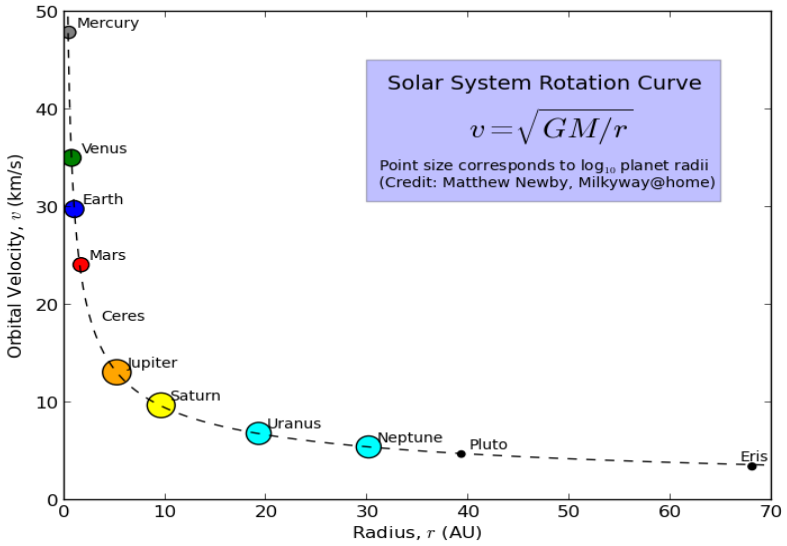

Figure 1.6: Rotation curves.

(jav: Use scipy constants)

2

Homogeneous and Isotropic Universe

In this Chapter, we start by introducing the theoretical framework that underlies the standard model of modern cosmology: the concordance ΛCDM model. We briefly review the equations determining the evolution of an homogeneous and isotropic universe. For the sake of completeness, in the following chapters, we have included the inflationary model as a solution to some of the shortcomings of the Hot Big Bang model. Finally, the computation of the distance modulus, cosmic microwave background spectrum and matter power spectrum allows us to establish a connection between cosmological models and current (future) observations through statistical tools, described in the next chapter. Some reference books have been used throughout this short review, they include: Dodelson [33], Hobson et al. [56], Liddle and Lyth [81], Mukhanov [98]; as well as some lecture notes: Peiris [105], Pettini [108], Challinor [24].

The standard description of the dynamical properties of the universe is provided by the Einstein's theory of General Relativity (GR), which builds a connection between the geometry of the space-time and its matter-content, through fundamental quantities: the *metric* $g_{\mu\nu}$ and the *energy-momentum* tensor $T_{\mu\nu}$

$$\underbrace{G_{\mu\nu}[g_{\mu\nu}]}_{\text{Geometry}} = \frac{8\pi G}{c^4} \underbrace{T_{\mu\nu}}_{\text{Matter}}. \tag{2.1}$$

Einstein equations are very elegant, however they are indeed very difficult to solve in the general case. Throughout this book we focus on the basic description of our Universe, an expanding

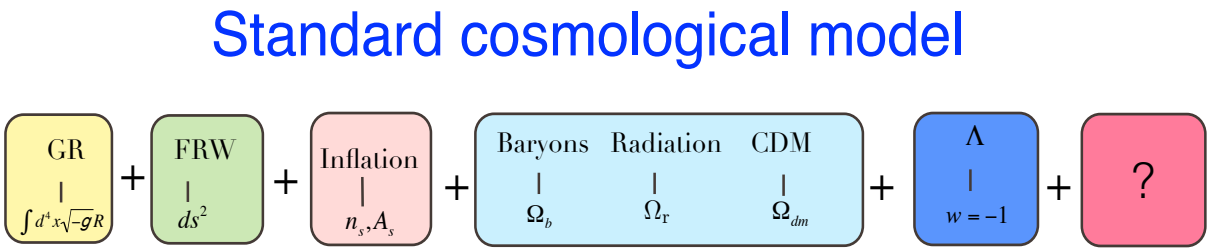

Figure 2.1: Main components of the Standard Cosmological Model.

homogeneous and isotropic described by the FLRW metric, and then move forward to the linear perturbation theory, as we shall see below.

2.1 The cosmological principle

In order to specify the global geometry of the universe, an essential assumption to do is the *Cosmological Principle*: when averaged over sufficiently large-scales at any particular time, the universe seems to be *Homogeneous* and *Isotropic* with a high accuracy. For instance, at scales larger than 150 Mpc, the distribution of galaxies over the celestial sphere does seem to justify the assumption of isotropy -i.e. independent of direction [28]. Moreover, the current uniformity in the temperature distribution of the *Cosmic Microwave Background* (CMB) radiation, to a few parts in 10^5, is the best observational evidence we have in support of an isotropic universe (see Figure 12.3; [67]). If isotropy is thus taken for granted and considering that our position in the universe is by no means preferred to any other, known as the *Copernican Principle*, then homogeneity -i.e. independent of position, follows from isotropy at every point.

Isotropy + Copernican Principle $\longrightarrow$ **Homogeneity.**

Isotropy states that the Universe looks the same in every direction.
Homogeneity states that the Universe looks the same at any point.

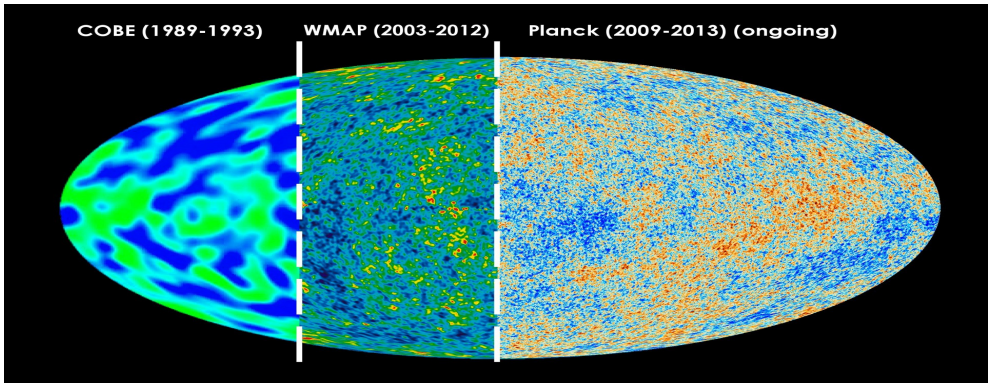

Figure 2.2: Anisotropies of the Universe seen by Planck satellite. Colours describe differences in temperatures, blue is cold and red hot, and they're about 10^{-6} (jav: use healpy to plot isotropy) www link (jav: show the great wall figure).

It is worth noting that isotropy about every point automatically implies homogeneity. However, homogeneity does not necessarily imply isotropy. For example, a universe with a large-scale electric field that points out in one direction everywhere and has the same magnitude at every point would be homogeneous but not isotropic (see Figure 2.3).

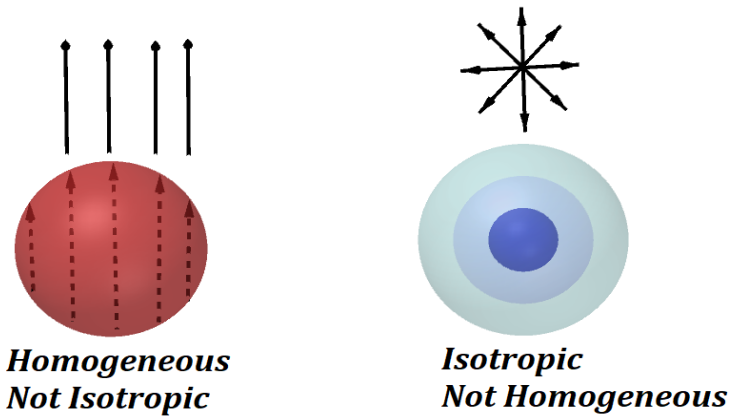

Figure 2.3: Illustration of how homogeneity and isotropy are not equivalent.

For those picky astrophysicist, who want to provide an explanation up to the most minimal detail, for instance the fingers of god (left of Figure 13.1) or the Stephen-Hawking letters (right of Figure 13.1) observed in the CMB, there exist models considering anisotropies in the Universe

(not to explain these silly things though). Some examples of anisotropic models are the Bianchi types [cite]. The type I models contain the Kasner metric, whereas the Bianchi IX includes the Taub metric; the isotropy of the FLRW metric is a particular case of the types I, V, VII and IX. Some inhomogeneous models are the Lemaitre-Tolman-Bondi [40] and Zsekeres [129]. For a review of the inhomogeneous framework, see [15]. In the following sections we will present a brief introduction to these alternative descriptions of the Universe.

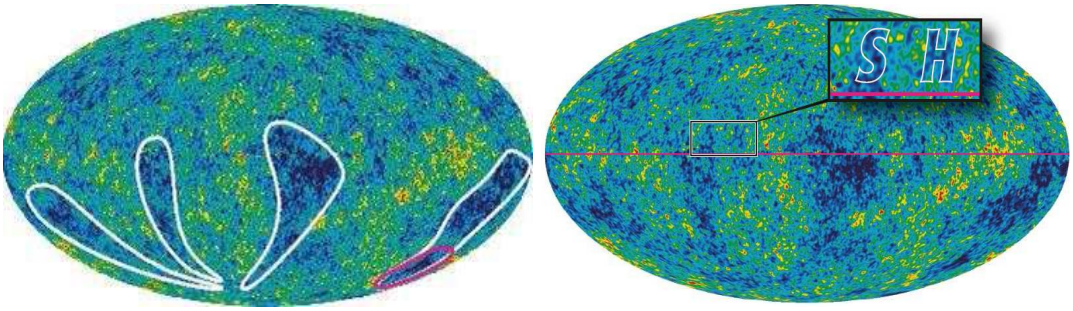

Figure 2.4: Anisotropies of the Universe seen by WMAP satellite.

HW 2.1.a: Describe some examples of non-homogeneous and non-isotropic universes

HW 2.1.b: The Anthropic Principle: Why the Universe is how it is?

Assumption 2.1.1:

Homogeneity and Isotropy.

Anthropic Principle

Why the Universe is how it is? This doubt has triggered a big debate among the scientific community during the last decades. However, even though the above question looks innocent, some people are still skeptical about the answers.

Despite the idea had been used previously by R. H. Dicke, the phrase **anthropic principle** was first attributed to the theoretical physicist Brandon Carter in 1974, who established the statement: "Although our situation is not necessarily central, it is inevitably privileged to some extent"[22]. In general, one can think about the anthropic principle as the idea that the behaviour and evolution of the Universe must be compatible with the conscious life we are observing and measuring. In other words, **the Universe has specific physical constants because they are the necessary ones to permit life** (jav: constant books cite[?]). However, these ideas have gone further, generating two variations of this concept [11]:

- Weak anthropic principle: "The observed values of all physical and cosmological quantities are not equally probable but they take on values restricted by the requirement that there exist sites where carbon-based life can evolve and by the requirements that the universe be old enough for it to have already done so".
- Strong anthropic principle: "The Universe must have those properties which allow life to develop within it at some stage in its history".

However, from the weak anthropic principle one can notice that this is very restrictive since it does not allow different kind of life apart of carbon-based, such as the possibility of silicon-based life which has been considered since a few years ago [6]. Meanwhile, the strong version can be criticised based upon the fact that it cannot be tested.
The philosophical conception that tries to explain why the universe is determined to be in the way we know it, could be summarised in a shallow way as follows: **The world is necessarily as it is because there are beings who wonder why it is so**. Even though this idea has received enough criticism and skepticism, it is the best explanation to some fundamental problems in physics, for instance, why the cosmological constant or the electroweak scale have that precise value. Therefore, until a more fundamental explanation to this kind of problems is proposed, the anthropic principle will be the most accepted answer.

2.2 The Geometry

The left hand side of Einstein's equations (2.1) contain, what is called the metric tensor $g_{\mu\nu}$ which describes the geometry of the space time. Let us start by defining this quantity.

2.2.1 The spatial metric g_{ab}

Consider two infinitesimally separated points P and Q in the manifold[1] (see Figure 2.5), with coordinates x^a and $x^a + dx^a$ respectively ($a = 1, 2, ..., N$), with N being the dimension of the space.

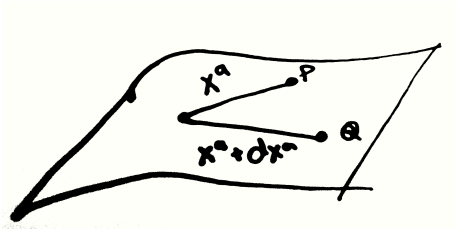

Figure 2.5: Points in space.

The local geometry of the manifold at the point P is determined by defining the squared *invariant distance* or *interval* (ds) between P and Q. In general, the interval is a function represented by

$$ds^2 = f(x^a, dx^a). \tag{2.2}$$

For developing general relativity we are interested in an expression of the form[1]

$$ds^2 = g_{ab}(x)dx^a dx^b, \tag{2.3}$$

where $g_{ab}(x)$ are the components of the *metric tensor* field, in our chosen coordinate system. Manifolds with a geometry express in the form of Eqn. (2.3) are called *Riemannian manifolds*. However, strictly speaking, the manifold is only Riemannian if $ds^2 > 0$, and because here ds^2 can be either positive, negative or zero, then the manifold should properly be called *pseudo-Riemannian* (we simply referred to it as Riemannian).

[1] In general terms, an n-dimensional manifold is an space that locally looks like $\mathbb{R}^n$.

[1] A consequence of the equivalence principle, is that it restricts the possible geometry of the curved space-time to a pseudo-Riemannian one.

The metric functions $g_{ab}(x)$ correspond to the elements of a position dependent squared matrix. These metric functions can be chosen such that the matrix is symmetric, that is $g_{ab}(x) = g_{ba}(x)$. Let us assume for a moment the matrix is a generic one, and hence it can be decomposed as the sum of a symmetric part and anti-symmetric component:

$$g_{ab}(x) = \underbrace{\frac{1}{2}[g_{ab}(x) + g_{ba}(x)]}_{\text{symmetric}} + \underbrace{\frac{1}{2}[g_{ab}(x) - g_{ba}(x)]}_{\text{anti-symmetric}}. \tag{2.4}$$

The contribution to the interval ds^2 from the antisymmetric part would be $\frac{1}{2}[g_{ab}(x) - g_{ba}(x)]dx^a dx^b$ which vanishes identically when the components a and b are interchanged. Therefore the antisymmetric part of g_{ab} can be safely neglected.

> Qz: How many independent variables have an N-dimensional symmetry matrix?

In a N-dimensional Riemannian manifold there are $\frac{1}{2}N(N+1)$ independent metric functions $g_{ab}(x)$. And since, in general, there are N arbitrary coordinate transformations, thus there are only $\frac{1}{2}N(N+1) - N = \frac{1}{2}N(N-1)$ independent degrees of freedom associated with $g_{ab}(x)$. For the particular case of a **diagonal metric**, i.e. $g_{ab}(x) = 0$ for $a \neq b$, the line element takes the form

$$ds^2 = g_{11}(dx^1)^2 + g_{22}(dx^2)^2 + \cdots + g_{NN}(dx^N)^2. \tag{2.5}$$

Such system of coordinates is called *orthogonal*, since any pair of coordinate curves cross at right angles.

Example 2.2.1: A trivial example

The **Euclidean metric** is the function $d : \mathbb{R}^n \times \mathbb{R}^n \to \mathbb{R}$ that assigns to any two vectors in Euclidean n-space $\vec{x} = (x^1, \ldots, x^n)$ and $\vec{y} = (y^1, \ldots, y^n)$ the number $d(\vec{x}, \vec{y}) = \sqrt{(x^1 - y^1)^2 + \cdots + (x^n - y^n)^2}$, that is, the *standard* distance between any two vectors in $\mathbb{R}^n$. The Euclidean metric (in a 3-dimensional space) is given by

$$g_{ij} = \begin{pmatrix} 1 & 0 & 0 \\ 0 & 1 & 0 \\ 0 & 0 & 1 \end{pmatrix},$$

giving the line element

$$ds^2 = g_{ij}dx^i dx^j = (dx)^2 + (dy)^2 + (dz)^2.$$

Examples of line elements:

- The 3-**Euclidean** spacetime

$$ds^2 = dx^2 + dy^2 + dz^2.$$

- The **Minkowski** spacetime, or the special relativistic line element

$$ds^2 = c^2dt^2 - dx^2 - dy^2 - dz^2.$$

- The **3-Sphere** $\mathbb{S}^3$ line element (with radius a)

$$ds^2 = \frac{a^2}{a^2 - r^2}dr^2 + r^2 d\theta^2 + r^2 \sin^2\theta d\phi^2.$$

- The **Friedmann-Lemaitre-Robertson-Walker** line element

$$ds^2 = c^2dt^2 - a^2(t)\left[\frac{dr^2}{1-\kappa r^2} + r^2(d\theta^2 + \sin^2\theta d\phi^2)\right].$$

- The locally rotationally symmetric (LRS) **Bianchi type-I** metric

$$ds^2 = c^2dt^2 - S^2(t)\left[e^{\frac{4}{\sqrt{6}}\varphi}\mathrm{d}x^2 + e^{-\frac{2}{\sqrt{6}}\varphi}(\mathrm{d}y^2 + \mathrm{d}z^2)\right].$$

- The **Kerr-Newman** line element that describes the geometry of spacetime for a rotating charged black hole with mass M, charge Q and angular momentum J, is

$$\begin{aligned} ds^2 &= \left(\frac{dr^2}{\Delta} + d\theta^2\right)\rho^2 - (c\ dt - a\sin^2\theta d\phi)^2\frac{\Delta}{\rho^2} \\ &\quad + ((r^2 + a^2)d\phi - ac\ dt)^2\frac{\sin^2\theta}{\rho^2}, \end{aligned}$$

with

$$a = \frac{J}{Mc}, \qquad \rho^2 = r^2 + a^2\cos^2\theta, \qquad \Delta = r^2 - r_s r + a^2 + r_Q^2.$$

Here r_s is the Schwarzschild radius of the massive body, related to its total mass-equivalent M by $r_s = 2GM/c^2$, and r_Q the length-scale corresponding to the electric charge Q of the mass $r_Q^2 = \frac{Q^2G}{4\pi\epsilon_0 c^4}$.

Here some particular examples for the Kerr-Newman metric

	$J = 0$	Rotating ($J \neq 0$)
$Q = 0$	Schwarzschild	Kerr
Charged ($Q \neq 0$)	Reissner-Nordström	Kerr-Newman

The 3-sphere example

Let us find the metric for a *3-sphere* $\mathbb{S}^3$ embedded in *four-dimensional* Euclidean space $\mathbb{R}^4$. First of all, the four-dimensional Euclidean space is described by the line element

$$ds^2 = dx^2 + dy^2 + dz^2 + dw^2, \tag{2.6}$$

however, we limit ourselves to move over the 3-dimensional-space restricted by the radius a

$$x^2 + y^2 + z^2 + w^2 = a^2. \tag{2.7}$$

Differentiating both sides of the equation, it yields to

$$2xdx + 2ydy + 2zdz + 2wdw = 0, \tag{2.8}$$

and substituting dw in (2.6) follows the line element:

$$ds^2 = dx^2 + dy^2 + dz^2 + \frac{(xdx + ydy + zdz)^2}{a^2 - (x^2 + y^2 + z^2)}. \tag{2.9}$$

Now, to get a better sense of the metric, transforming to spherical polar coordinates

$$x = r\sin\theta\cos\phi, \quad y = r\sin\theta\sin\phi, \quad z = r\cos\theta, \tag{2.10}$$

we obtain an alternative form for the line element (2.6)

$$\boxed{ds^2 = \frac{a^2}{a^2 - r^2}dr^2 + r^2 d\theta^2 + r^2\sin^2\theta d\phi^2.} \tag{2.11}$$

Notice that taking the limit for the radius of the sphere $a \to \infty$, the metric gets the form

$$ds^2 = dr^2 + r^2 d\theta^2 + r^2\sin^2\theta d\phi^2, \tag{2.12}$$

which is the ordinary Euclidean 3-dimensional space $ds^2 = dx^2 + dy^2 + dz^2$ but now written in spherical coordinates. The line element (2.11) therefore describes a non-Euclidean three-dimensional space.

Now that we have a description of the geometry of the space, we can compute physical quantities such as length, area and volume.

2.2.2 Lengths, areas and volumes

The lengths of curves follow immediately from the line element (ds^2). Suppose that the points A and B are joined by some path; then the length of this curve is given by

$$L_{AB} = \int_A^B ds = \int_A^B |g_{ab} dx^a dx^b|^{1/2}, \tag{2.13}$$

where the integral is evaluated along the curve. If the equation of the curve $x^a(u)$ is given in terms of some affine parameter u, as shown in Figure 2.6, then

$$L_{AB} = \int_{u_A}^{u_B} \left| g_{ab} \frac{dx^a}{du} \frac{dx^b}{du} \right|^{1/2} du, \tag{2.14}$$

where u_A and u_B are the values of the parameter u at the endpoints of the curve.

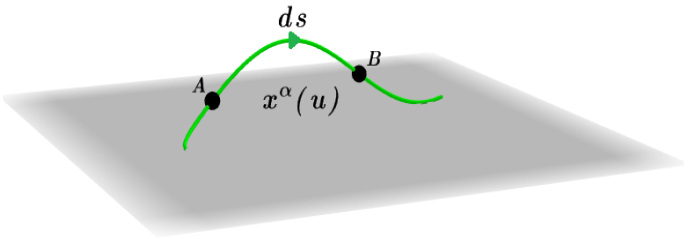

Figure 2.6: Two points describe a path defined by the line element $ds = |g_{ab} dx^a dx^b|^{1/2}$.

On the other hand, the proper lengths of two line segments will be $\sqrt{g_{11}} dx^1$ and $\sqrt{g_{22}} dx^2$ respectively. Thus the element of area is (see Figure 2.7)

$$dA = \sqrt{|g_{11} g_{22}|} dx^1 dx^2. \tag{2.15}$$

We can go even further and define a higher-dimensional *volume elements* in a similar way until we reach the N-dimensional volume element

$$d^N V = \sqrt{|g_{11} g_{22} \cdots g_{NN}|} dx^1 dx^2 \cdots dx^N. \tag{2.16}$$

In the general case, where the coordinates are not orthogonal, the volume elements may be rewritten as (with $g = det[g_{ij}]$),

$$d^N V = \sqrt{|g|} dx^1 dx^2 \cdots dx^N. \tag{2.17}$$

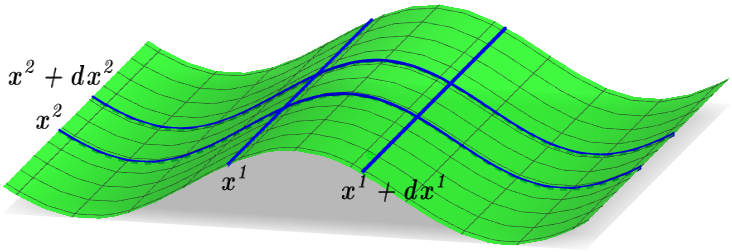

Figure 2.7: Element of Area. Orthogonal coordinates.

The Two-sphere

Let us consider the two-dimensional geometry of the surface of a sphere in terms of its radius ($\rho \in [0, a]$) and zenith angle ($\phi \in [0, 2\pi]$), assuming it is embedded in a three-dimensional Euclidean space (see Figure 2.8).

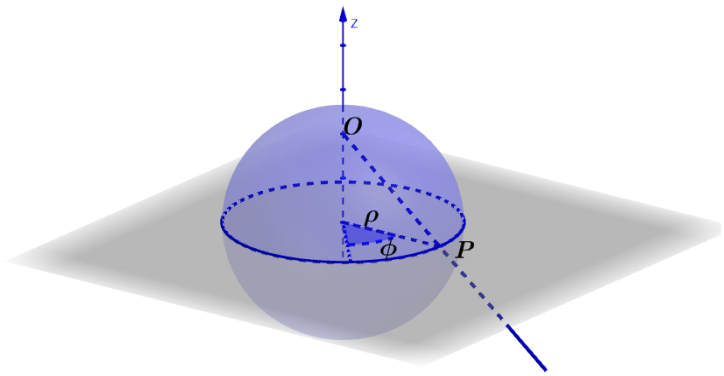

Figure 2.8: 2D - Sphere.

This can be seen as eliminating one dimension in (2.11) and making the substitutions

$$x = \rho \cos\phi, \qquad y = \rho \sin\phi, \tag{2.18}$$

with some algebra we obtain

$$ds^2 = \frac{a^2}{a^2 - \rho^2} d\rho^2 + \rho^2 d\phi^2. \tag{2.19}$$

Note that the line element contains a '*hidden symmetry*', namely our freedom to choose an arbitrary point on the sphere as the origin $\rho = 0$. There is also a *coordinate singularity*, which

has resulted simply from choosing coordinates with a restricted domain of validity. From Eqn. (2.19) we see that this coordinate system is orthogonal, with $g_{\rho\rho} = a^2/(a^2-\rho^2)$ and $g_{\phi\phi} = \rho^2$. From (2.13), the distance *in the surface* D from the centre to a particular radius $\rho = R$, at constant ϕ, is

$$D = \int_0^R \frac{a}{(a^2-\rho^2)^{1/2}} d\rho = a \sin^{-1}\left(\frac{R}{a}\right), \tag{2.20}$$

while the circumference of the circle is given by

$$C = \int_0^{2\pi} R d\phi = 2\pi R. \tag{2.21}$$

Similarly, from (2.15) we have the area within the circumference C

$$A = \int_0^{2\pi}\int_0^R \frac{a}{(a^2-\rho^2)^{1/2}} \rho d\rho d\phi = 2\pi a^2 \left[1 - \left(1 - \frac{R^2}{a^2}\right)^{1/2}\right]. \tag{2.22}$$

Writing the circumference C and the area A in terms of the distance D, we have

$$C = 2\pi a \sin\left(\frac{D}{a}\right) \qquad \text{and} \qquad A = 2\pi a^2 \left[1 - \cos\left(\frac{D}{a}\right)\right]. \tag{2.23}$$

As D increases, the circumference of the circle C do so until the point where $D = \pi a/2$ and then C becomes smaller as D increases. Then, the total area, by symmetry, is given by

$$A_{\text{tot}} = 2\int_0^{2\pi}\int_0^a \frac{a}{(a^2-r^2)^{1/2}} r dr d\phi = 4\pi a^2. \tag{2.24}$$

HW 2.2: hb.

1.- Compute the Volume of the 3D sphere [Eqn 2.11]. Hint:

$$V = \int_0^{2\pi} \int_0^{\pi} \int_0^{R} \frac{ar^2 \sin\theta}{(a^2 - r^2)^{1/2}} dr d\theta d\phi,$$

[the total volume $V_{\rm tot}$ is found when $R = a$].

2.- For this 3D-sphere, show that the line element can be written in the form

$$ds^2 = a^2[d\chi^2 + \sin^2\chi(d\theta^2 + \sin^2\theta d\phi^2)].$$

Then, calculate the area of the 2D sphere defined by $\chi = \chi_0$. Also find the total volume of the 3D space.

3.-By identifying a suitable coordinate transformation, show that the line element

$$ds^2 = (c^2 - a^2t^2)dt^2 - 2at\ dt\ dx - dx^2 - dy^2 - dz^2.$$

can be reduced to the Minkowski line element [a is a constant].

Python

In [1]:
```
from sympy import *
init_printing()
```

Distance in the surface

$$D = \int_0^R \frac{a}{(a^2-\rho^2)^{\frac{1}{2}}} d\rho$$

In [2]:
```
a, rho, R = symbols('a, \\rho, R', positive=True)
half = Rational(1, 2)
D = a / (a**2 - rho**2)**half

integrate(D, (rho, 0, R))
```

Out[2]:

$$a \operatorname{asin}\left(\frac{R}{a}\right)$$

Circumference

$$C = \int_0^{2\pi} R d\phi$$

In [3]:
```
phi = symbols ('\\phi')
C   = R

integrate(C,(phi,0,2*pi))
```

Out[3]:

$$2\pi R$$

Area

$$A = \int_0^{2\pi} \int_0^R \frac{a}{(a^2-\rho^2)^{\frac{1}{2}}} \rho d\rho d\phi$$

In [4]:
```
A = a / (a**2 - rho**2)**half*rho

simplify(integrate(A,(rho,0,R),(phi,0,2*pi)))
```

Out[4]:

$$2\pi a \left(a - \sqrt{-R^2 + a^2}\right)$$

2.3 The Einstein Tensor

2.3.1 Christoffel symbols

The coefficients $\Gamma^a{}_{bc}$ are known as the **affine connection**, or traditionally called as the *Christoffel symbol* (of the second kind). It can be easily shown that $\Gamma^a{}_{bc}$ do not transform as the components of a tensor, however

$$T^a{}_{bc} = \Gamma^a{}_{bc} - \Gamma^a{}_{cb}, \tag{2.25}$$

is indeed a third-rank tensor, namely the **torsion tensor**. For convenience we can assume torsion free $T^a{}_{bc} = 0$, that is, the *affine connection is symmetric in its covariant indices*, i.e.

$$\Gamma^a{}_{bc} = \Gamma^a{}_{cb}. \tag{2.26}$$

Assumption 2.3.1:

Torsion free: $T^a{}_{bc} = 0 \quad \Rightarrow \quad \Gamma^a{}_{bc} = \Gamma^a{}_{cb}$.

We will use the *ansatz* that the covariant derivative of the metric tensor vanishes

$$g_{ab;c} = 0. \tag{2.27}$$

The covariant derivative (expressed by ∇ or ;) of a tensor is

$$A_{ab;c} = A_{ab,c} - \Gamma^d{}_{ac}A_{db} - \Gamma^d{}_{bc}A_{ad}.$$

By cyclically permuting the three indices of Eqn. (2.27), summing them all over, and using the covariant derivative of a tensor, we get

$$\begin{aligned} \Gamma^a{}_{bc} &= \frac{1}{2}g^{ad}(\partial_c g_{db} + \partial_b g_{dc} - \partial_d g_{bc}) \\ &= \frac{1}{2}g^{ad}(g_{db,c} + g_{dc,b} - g_{bc,d}). \end{aligned} \tag{2.28}$$

Then, for the torsionless case, the quantity on the right hand side of Eqn. (2.28) is properly called the **metric connection** and often denoted by the symbol $\{{}^a_{bc}\}$. In a torsionless manifold the affine and metric connections are equivalent.

The quantity Γ_{abc}, traditionally known as the **Christoffel symbol of the first kind**, is given by

$$\begin{aligned} \Gamma_{abc} &\equiv g_{ad}\Gamma^d{}_{bc} \\ &= \frac{1}{2}(\partial_c g_{ab} + \partial_b g_{ac} - \partial_a g_{bc}). \end{aligned} \tag{2.29}$$

Adding Γ_{abc} to Γ_{bac} gives

$$g_{ab,c} = \Gamma_{abc} + \Gamma_{bac}, \tag{2.30}$$

which relates partial derivatives of the metric components to the connection coefficients. The contraction of the connection coefficients, leads to

$$\Gamma^a{}_{ab} = \partial_b \ln \sqrt{|g|} = \frac{1}{\sqrt{|g|}} \partial_b \sqrt{|g|}. \tag{2.31}$$

where the derivative of the determinant g of g_{ab} is

$$\begin{aligned} g_{,c} &= g g^{ab} g_{ab,c}, \\ &= 2g\Gamma^a{}_{ac}. \end{aligned} \tag{2.32}$$

HW 2.3.a: Show that the components of $\Gamma^a{}_{bc}$ do not transform as the components of a tensor, but $T^a{}_{bc}$ do.

HW 2.3.b: Prove (2.28), (2.30) and (2.32).

2.3.2 The curvature tensor

The **curvature tensor** (or the *Riemann-Christoffel tensor*) is defined in terms of the metric tensor g_{ab} and its first and second derivatives.

$$R^a{}_{bcd} \equiv \Gamma^a{}_{bd,c} - \Gamma^a{}_{bc,d} + \Gamma^e{}_{bd}\Gamma^a{}_{ec} - \Gamma^e{}_{bc}\Gamma^a{}_{ed}. \tag{2.33}$$

In a *flat* space-time, $\Gamma^a{}_{bc}$ and its derivatives are zero, and hence

$$R^a{}_{bcd} = 0. \tag{2.34}$$

The curvature tensor possesses a number of symmetries and satisfies certain identities, that are most easily derived in terms of its covariant components. An alternative way, and useful for this purpose, is the lowered version

$$R_{abcd} = g_{ae} R^e{}_{bcd}, \tag{2.35}$$

and after considerable algebra, we have

$$R_{abcd} = \frac{1}{2}\left(g_{bc,ad} - g_{ac,bd} + g_{ad,bc} - g_{bd,ac}\right) - g^{ef}\left(\Gamma_{eac}\Gamma_{fbd} - \Gamma_{ead}\Gamma_{fbc}\right), \tag{2.36}$$

and the symmetries can be expressed as follow

$$\begin{aligned} R_{abcd} &= -R_{bacd}, \\ &= -R_{abdc}, \\ &= R_{cdab}. \end{aligned} \tag{2.37}$$

From the first set of symmetries, we notice that for $a = b$ or $c = d$ all the components of the Riemann tensor are zero. Then, we may easily deduce the *cyclic identity* (or **1st Bianchi identity**)

$$R_{abcd} + R_{adbc} + R_{acdb} = 0, \tag{2.38}$$

which may be written as $R_{a[bcd]} = 0$. The conditions (2.37) and (2.38) reduce the number of independent components from N^4 to $N^2(N^2-1)/12$ (jav: do the math). In general, considering several dimensions, we have

No. of dimensions	2	3	4
No. of independent components of R_{abcd}	1	6	20

You can see from this table that in four dimensions the number of independent components is reduced from a possible 256 to 20.

Another useful relation we will need is the **2nd Bianchi identity**

$$R_{abcd;e} + R_{abde;c} + R_{abec;d} = 0, \tag{2.39}$$

and it can be written in the compact cyclic form $R_{ab[cd;e]}$.

HW 2.3.c: Show the validity of the expressions (2.37), (2.38) and (2.39).

2.3.3 Ricci tensor

From the symmetry properties, raising the index a and then contracting on the first two indices, gives

$$R^{a}{}_{acd} = 0. \tag{2.40}$$

Example 2.3.1: Show that $R^a{}_{acd}$=0.

Take the expression (2.35)

$$R_{abcd} = g_{ae} R^e{}_{bcd},$$

multiply $\times g^{ab}$ both sides

$$g^{ab} R_{abcd} = g^{ab} g_{ae} R^e{}_{bcd},$$

because the mood indices, we can interchanged $a \leftrightarrow b$ on the right hand side to get

$$g^{ba} \underbrace{g_{be} R^e{}_{acd}}_{\text{contraction}} = g^{ba} R_{bacd} = g^{ab} R_{bacd} = -g^{ab} R_{abcd},$$

where we have used the symmetry $g^{ba} = g^{ab}$ and the anti-symmetric relation in (2.37). Therefore $R^a{}_{acd} = 0$.

Contracting on the first and third indices, however, gives in general a non-zero result and this leads to a new tensor, the **Ricci tensor** (the trace of the Riemann tensor):

$$R_{ab} \equiv R^c{}_{acb} = g^{cd} R_{cadb}. \tag{2.41}$$

By raising the index a in the cyclic identity and contracting with d, one may easily show that the Ricci tensor is symmetric, $R^a{}_b = R_a{}^b$, and hence we can denote both by R^b_a. A further contraction gives the **Ricci scalar**, also known as the *curvature scalar*, which is the trace of the Ricci tensor:

$$R \equiv R^a{}_a = g^{ab} R_{ab} = g^{ab} g^{cd} R_{cadb}. \tag{2.42}$$

Example 2.3.2: Show R_{ab}=R_{ba}.

First, we write the cyclic expression (2.38) and multiply it by g^{cd} to get

$$g^{cd} R_{dacb} + g^{cd} R_{dcba} + g^{cd} R_{dbac} = 0,$$

notice the second term ($g^{cd} R_{dcba}$) vanishes by the first identity in (2.37). To then

$$\begin{aligned} g^{cd} R_{dacb} + g^{cd} R_{dbac} &= 0, \\ R^c{}_{acb} - g^{cd} R_{dbca} &= 0, \\ R^c{}_{acb} - R^c{}_{bca} &= 0, \\ R_{ab} &= R_{ba}. \end{aligned}$$

pb. The traceless part of the tensor R_{abcd} is defined by the equation

$$\begin{aligned} R_{abcd} &= \frac{1}{2}\left(g_{ac}R_{bd} - g_{ad}R_{bc} - g_{bc}R_{ad} + g_{bd}R_{ac}\right) \\ &\quad -\frac{1}{6}(g_{ac}g_{bd} - g_{ad}g_{bc})R \\ &\quad +C_{abcd}. \end{aligned} \tag{2.43}$$

The expressions in the first two lines have the symmetries of the curvature tensor, and C_{abcd} is called the *Weyl tensor*. The coefficients in the first two lines are chosen so the contraction of the Weyl tensor vanishes,

$$C^{a}{}_{bac} = 0.$$

The Weyl tensor will be helpful in simplifying the optical equation for the distortion in an inhomogeneous universe.

Another scalar that can be constructed from the Riemann tensor is the *Kretschmann scalar*:

$$K = R_{abcd}R^{abcd}. \tag{2.44}$$

For a Schwarzschild black hole of mass M, the Kretschmann scalar is

$$K = \frac{48G^2M^2}{c^4r^6},$$

which is not infinite at the event horizon $r = 2M$, hence we can tell immediately that the event horizon is a coordinate singularity not a real one. Likewise we can tell immediately that there is a real singularity at $r = 0$.

2.3.4 Einstein tensor

Taking the Bianchi identities (2.39), and raising a and contracting with c (i.e. $\times g^{ac}$) gives

$$\nabla_e R_{bd} + \nabla_c R^{c}{}_{bde} + \nabla_d R^{c}{}_{bec} = 0, \tag{2.45}$$

which, on using the antisymmetry property in the third term, gives the Ricci tensor

$$\nabla_e R_{bd} + \nabla_c R^{c}{}_{bde} - \nabla_d R_{be} = 0. \tag{2.46}$$

If we now raise b and contract with e ($\times g^{be}$), we find

$$\nabla_e R^{e}{}_{d} + \nabla_c R^{ce}{}_{de} - \nabla_d R = 0, \tag{2.47}$$

Using the antisymmetry properties of Ricci tensor we may write the second term as

$$\nabla_c R^{ce}{}_{de} = \nabla_c R^{ec}{}_{ed} = \nabla_c R^{c}{}_{d} = \nabla_e R^{e}{}_{d}, \tag{2.48}$$

so the first and secod terms in (2.47) are identical and we obtain

$$2\nabla_e R^{e}{}_{d} - \nabla_d R = \nabla_e (2R^{e}{}_{d} - \delta^{e}_{d} R) = 0. \tag{2.49}$$

Finally, raising the index d ($\times g^{db}$), we obtain the important result

$$\nabla_a (R^{ab} - \frac{1}{2} g^{ab} R) = 0. \tag{2.50}$$

The term in parentheses is called the **Einstein tensor**

$$G^{ab} \equiv R^{ab} - \frac{1}{2} g^{ab} R. \tag{2.51}$$

It is clearly symmetric $G^{ab} = G^{ba}$ and thus possesses only one independent divergence $\nabla_a G^{ab}$ which vanishes.

HW 2.3.d: Show that $\nabla_a G^{ab} = 0$.
Hint: by contracting the second Bianchi identities, show that $R^{a}{}_{b;a} = \frac{1}{2} R_{;b}$.

The trace

$$\begin{aligned} g^{ab} G_{ab} &= g^{ab} R_{ab} - \frac{1}{2} g^{ab} g_{ab} R, \\ G &= R - \frac{1}{2} n R, \\ G &= \frac{2-n}{2} R. \end{aligned} \tag{2.52}$$

The special case of $n = 4$ dimensions gives the trace of the Einstein tensor as the negative of the Ricci tensor's trace, i.e. $G = -R$. Thus another name for the Einstein tensor is the *trace-reversed Ricci tensor*.

Example 2.3.3: The 2D sphere.

Let us get back to the metric of the surface of a sphere, with radius a, in spherical polar coordinates.

$$ds^2 = a^2 d\theta^2 + a^2 \sin^2\theta d\phi^2.$$

Then, we have the metric and its inverse

$$g_{ab} = \begin{pmatrix} a^2 & 0 \\ 0 & a^2\sin^2\theta \end{pmatrix} \qquad g^{ab} = \begin{pmatrix} 1/a^2 & 0 \\ 0 & 1/a^2\sin^2\theta \end{pmatrix}$$

Therefore, $g_{\theta\theta} = a^2$, $g_{\phi\phi} = a^2\sin^2\theta$, $g^{\theta\theta} = 1/a^2$, $g^{\phi\phi} = 1/a^2\sin^2\theta$. In two dimensions there are only six (2^3 minus the symmetric part) independent connection coefficients,

$$\Gamma^{\theta}{}_{\theta\theta}, \quad \Gamma^{\theta}{}_{\theta\phi}, \quad \Gamma^{\theta}{}_{\phi\phi}, \quad \Gamma^{\phi}{}_{\theta\theta}, \quad \Gamma^{\phi}{}_{\theta\phi}, \quad \Gamma^{\phi}{}_{\phi\phi}.$$

and the only derivative different from zero is $g_{\phi\phi,\theta} = 2a^2\sin\theta\cos\theta$. Therefore the Christoffel symbols are given by

$$\begin{aligned} &\Gamma^{\theta}{}_{\theta\theta} = 0, \qquad \Gamma^{\theta}{}_{\theta\phi} = 0, \qquad \Gamma^{\theta}{}_{\phi\phi} = -\sin\theta\cos\theta, \\ &\Gamma^{\phi}{}_{\phi\phi} = 0 \qquad \Gamma^{\phi}{}_{\theta\theta} = 0, \qquad \Gamma^{\phi}{}_{\theta\phi} = \cot\theta. \end{aligned}$$

In two dimensions the Riemann tensor has only one independent non zero component, due to all the symmetries it satisfies: $R_{\theta\phi\theta\phi} = R_{\phi\theta\phi\theta} = -R_{\theta\phi\phi\theta} = -R_{\phi\theta\theta\phi}$. And according to previous calculations:

$$R^{\theta}{}_{\phi\theta\phi} = \partial_\theta\Gamma^{\theta}{}_{\phi\phi} - \partial_\phi\Gamma^{\theta}{}_{\phi\theta} + \Gamma^{i}{}_{\phi\phi}\Gamma^{\theta}{}_{i\theta} - \Gamma^{i}{}_{\phi\theta}\Gamma^{\theta}{}_{i\phi}.$$

Since there are no ϕ derivatives, the second term vanishes. Since $\Gamma^{\theta}{}_{i\theta} = 0$, the first double Γ term vanishes too. Therefore, we get

$$\begin{aligned} R^{\theta}{}_{\phi\theta\phi} &= \partial_\theta\Gamma^{\theta}{}_{\phi\phi} - \Gamma^{\phi}{}_{\phi\theta}\Gamma^{\theta}{}_{\phi\phi} - \Gamma^{\theta}{}_{\phi\theta}\Gamma^{\theta}{}_{\theta\phi} \\ &= \partial_\theta(-\sin\theta\cos\theta) - (\cot\theta)(-\sin\theta\cos\theta) \\ &= \sin^2\theta - \cos^2\theta + \cos^2\theta = \sin^2\theta. \end{aligned}$$

Therefore $R_{\theta\phi\theta\phi} = g_{\theta i}R^{i}{}_{\phi\theta\phi} = \sin^2\theta$ and

$$R^{\phi}{}_{\theta\phi\theta} = g^{\phi\phi}R_{\phi\theta\phi\theta} = \frac{1}{\sin^2\theta}\sin^2\theta = 1.$$

Example 2.3.4: The 2D sphere.

The Ricci tensor is then:

$$\begin{aligned} R_{\theta\theta} &= R^{i}{}_{\theta i\theta} = R^{\theta}{}_{\theta\theta\theta} + R^{\phi}{}_{\theta\phi\theta} = 1. \\ R_{\phi\phi} &= R^{i}{}_{\phi i\phi} = R^{\theta}{}_{\phi\theta\phi} + R^{\phi}{}_{\phi\phi\phi} = \sin^2\theta. \\ R_{\theta\phi} &= R_{\phi\theta} = R^{i}{}_{\theta i\phi} = R^{\theta}{}_{\theta\theta\phi} + R^{\phi}{}_{\theta\phi\phi} = 0. \end{aligned}$$

The Ricci scalar is:

$$R = g^{ab}R_{ab} = g^{\theta\theta}R_{\theta\theta} + g^{\phi\phi}R_{\phi\phi} = \frac{1}{a^2} + \left(\frac{1}{a^2\sin^2\theta}\right)(\sin^2\theta) = \frac{2}{a^2}.$$

The resulting Einstein tensor:

$$G_{ab} = R_{ab} - \frac{1}{2}Rg_{ab} = 0,$$

for all $a, b \in [\theta, \phi]$. Thus the Gaussian curvature K (defined later) of a spherical surface is given by

$$K = \frac{R_{1212}}{|g|} = \frac{a^2\sin^2\theta}{a^4\sin^2\theta} = \frac{1}{a^2}.$$

Alternatives to GR

"In general relativity (GR) it is assumed, without empirical support, that torsion vanishes identically. Of course, one may claim that the experimental success of GR justifies the vanishing-torsion hypothesis. However, as it is argued below, all GR tests are compatible with a non-vanishing torsion, and, as a basic assumption of the theory, it is paramount to experimentally test it."[**?**] Furthermore, another important hypothesis is the fact that c, G, and α are constant, nevertheless, some important cosmological implications emerge when these are not. In this paper some models where all this standard assumptions may change are discussed.

Einstein-Cartan theory

The theory was first proposed by Élie Cartan in 1922 [**?**] and expounded in the following few years. This model states that GR must be extended in order to include an affine torsion, which in contrast with GR, allows the possibility of having an asymmetric Ricci tensor. Nowadays, this theory that extend the Riemannian geometry in that direction is better known as Riemann-Einstein-Cartan geometry and is determined by the following features:

- A specific choice of the metric tensor.
- A specific affine torsion tensor.
- Parallel transport must preserve lengths and angles as in the usual Riemannian geometry.

The corresponding equations of motion derived from the action variation are given by:

$$R_{ak} - \frac{1}{2} g_{ak} R = \frac{8\pi G}{c^4} P_{ak},$$

$$S^k_{ab} = \frac{8\pi G}{c^4} \sigma^k_{ab},$$

where σ^k_{ab} is the spin tensor of the source. $S^k_{ab} = T^k_{ab} + g^k_a T^m_{bm} - g^k_b T^m_{am}$ is the modified torsion tensor. And, finally T^k_{ab} is the affine torsion tensor that characterised these models. In the first equation one can see that it has the same structure than the usual Einstein's equations. Meanwhile, the second equation expresses the angular momentum conservation considering the spin-orbit interaction. Therefore, GR can be understood as a limit of the more general Riemann-Einstein-Cartan theory of gravity. Moreover, it is expected that this theory will prove to be a better classical limit of a future quantum theory of gravitation than the theory without torsion [**?**].

Variable c and G

In contrast with what know from GR, the idea of a variable (non-constant) speed of light (VSL) has been considered over the years. Actually, Einstein itself thought seriously this idea in 1911 [**?**], where he assumed that clocks in a gravitational field run slower, whereby the corresponding frequencies are influenced by the gravitational potential. Later, in 1915 he concluded that light speed is constant when gravity does not have to be considered but that the speed of light cannot be constant in a gravitational field with variable strength [**?**].

Nowadays, this idea is still present but in cosmological models such as the alternative to inflation proposed by Jean-Pierre Petit, John Moffat, Andreas Albrecht and JoÃ£o Magueijo [**? ? ?**], where also the Newton's constant G is no longer a constant. In the minimally coupled theory one then simply replaces c by a field in a preferred frame. Hence, the action is given by

$$S = \int d^4x \left(\sqrt{-g} \left(\frac{\psi(R + 2\Lambda)}{16\pi G} + \mathcal{L}_{\text{mat}} \right) + \mathcal{L}_{\psi} \right),$$

where $\psi(x^{\mu}) = c^4$. One can solve the cosmological field equations that define it for general power-law variations of "c" and "G". This allows us to determine the rate and sense of the changes required in "c" if the flatness, horizon, and cosmological constant problems are to be solved. The period when "c" varies is expected to happen only during the very early universe, therefore its observational remnants should be observable through the CMB fluctuations.

Variable α

It has been suggested by some astronomical observation that perhaps α, the fine structure constant, should not be strictly a constant, and this idea led to a serious consideration of a variable α by Jacob Bekenstein in 1981 [**?**]. However, one big consequence is that Maxwell's equations must be modified, but in order to test the viability of this conception, purely electromagnetic experiments are not enough. On the other hand, since the cosmological perspective, the framework predicts an $\frac{\dot{\alpha}}{\alpha}$ which can be compatible with the astronomical constraints; hence, these are too insensitive to determine any possible variability. In VSL theories a varying α is interpreted as $c \propto h \propto \alpha^{-1/2}$ and e is constant, Lorentz invariance is broken, and so by construction there is a preferred frame for the formulation of the physical laws.

Thus, so far, this idea cannot be ruled out with the experimental evidence, and more future tests are needed in order to determine its viability.

Some model with torsion and c, G and α varying has been discussed. Although most of these theories are not in contradiction with observational evidence, sometimes the framework looks more complicated than the ordinary one. Nevertheless, they are a valid and consistent approach that could be helpful to solve for example some cosmological problems.

2.4 The spacetime metric $g_{\mu\nu}$

The most general expression for the metric $g_{\mu\nu}$ can be represented by a sequence of non-intersecting spacelike hypersurfaces labelled by some parameter t, see Figure 2.9.

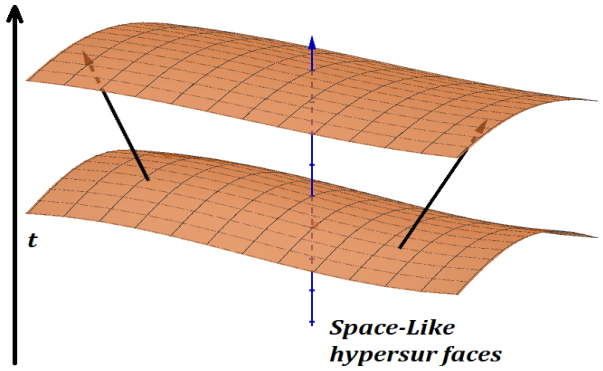

Figure 2.9: Worldlines.

This parameter may be taken to be the **proper time** along the worldline of any fundamental observer. The parameter t is then called the *synchronous time coordinate*. In addition, we may also introduce spatial coordinates (x^1, x^2, x^3) that are *constant* along any worldline. Thus, each fundamental observer has fixed (x^1, x^2, x^3) coordinates, and so the latter are called *comoving coordinates*, see for instance Figure 2.10.

Then the line element takes the form

$$ds^2 = g_{\mu\nu}dx^\mu dx^\nu = g_{00}c^2dt^2 + 2g_{0i}c\, dtdx^i + g_{ij}dx^i dx^j, \tag{2.53}$$

where the components of the spatial metric g_{ij} are functions of the coordinates (ct, x^1, x^2, x^3). Because the hypersurfaces $t =$ constant may be naturally constructed in such a way that the 4-velocity of any fundamental observer is orthogonal to the hypersurface, then the term g_{0i} must be zero. On the other hand, we may use the proper time of the coordinate system given by the fundamental observers to label the spacelike hypersurfaces (see Figure 2.9). This choice of coordinate time implies that $g_{00} = 1$, and therefore the space-time interval becomes

$$ds^2 = c^2dt^2 - g_{ij}dx^i dx^j. \tag{2.54}$$

2.5 The Friedmann-Robertson-Walker metric

Let us now incorporate the postulates of homogeneity and isotropy to the geometry of the Universe. The former demands that all points on a particular spacelike hypersurface are equivalent, whereas the latter demands that all directions on the hypersurface are equivalent for fundamental observers.

> Isotropy requires that the distribution of galaxies at two different times must be similar, and homogeneity requires that the magnification factor must be independent of the position for the distribution.

It thus follows that the time t can enter the g_{ij} only through a common factor, and hence the metric must take the following form

$$ds^2 = c^2dt^2 - S^2(t)d\sigma^2, \tag{2.55}$$

where $S(t)$ is a time-dependent scale factor (length-dimensions) and $d\sigma^2 = \gamma_{ij}dx^i dx^j$ contains functions of the coordinates (x^1, x^2, x^3) only. As we will see in the following section, the physical distance (r) is proportional to the comoving distance (x) times the scale factor $S(t)$ and hence it gets larger as time evolves. See Figure 2.10.

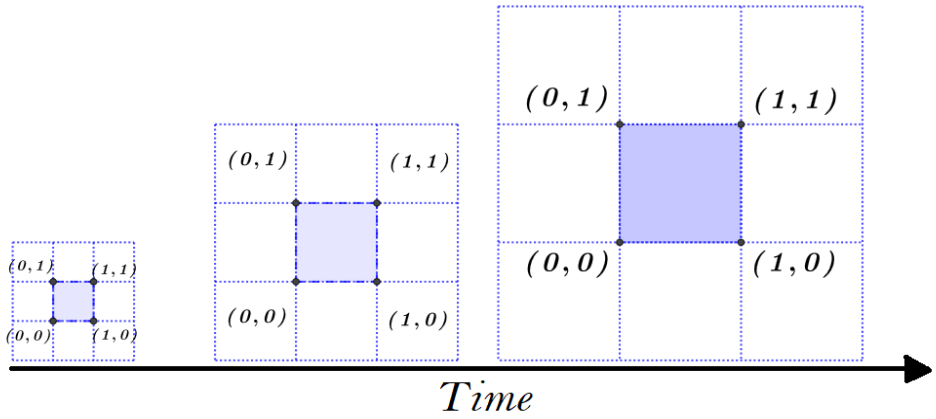

Figure 2.10: Comoving coordinates.

Over the years, cosmological observations have provided decisive evidence that the universe is currently expanding, therefore the scale factor satisfies $\dot{S}(t) > 0$ as we shall come back later,

see Hubble [59], Perlmutter et al. [106], Riess et al. [115].

On the other hand, a *maximally symmetric space* is specified by just one number – the *curvature* K, which is independent of the coordinates. Such *constant curvature* spaces must be homogeneous and isotropic, the key property we are looking for to describe the Universe at large scales.

Example 2.5.1: Maximally symmetric spaces

A **maximally symmetric space** is defined as both homogeneous and isotropic. Such space possesses the largest possible number of Killing vectors which in an n-dimensional manifold equals $n(n+1)/2$. The following holds for such spaces:

1.- The scalar curvature R is a constant, i.e.

$$R = n(n-1)K.$$

2.- The Ricci tensor is proportional to the metric tensor, i.e.

$$R_{\mu\nu} = \frac{1}{n} R g_{\mu\nu}.$$

3.- The Riemman curvature tensor is given by

$$R_{\mu\nu\lambda\rho} = \frac{R}{n(n-1)}(g_{\mu\lambda}g_{\nu\rho} - g_{\nu\lambda}g_{\mu\rho}).$$

Assuming general static isotropy, the line element of an isotropic 3-space in spherical coordinates (r, θ, ϕ) can be written as

$$d\sigma^2 = B(r)dr^2 + r^2(d\theta^2 + \sin^2\theta d\phi^2), \tag{2.56}$$

and its scalar curvature ${}^3R$ is computed to be

$${}^3R = \frac{2}{r^2}\frac{d}{dr}\left[r\left(1 - \frac{1}{B(r)}\right)\right]. \tag{2.57}$$

Homogeneity implies that all geometrical properties are independent of r and therefore ${}^3R$ must be constant. That is, equating Eq. (2.57) to a constant value $6K$ and integrating the result, this yields to the expression

$$r\left(1 - \frac{1}{B}\right) = Kr^3 + c, \tag{2.58}$$

with K and c constants. In order to avoid any singularity at $r = 0$ is compulsory to select $c = 0$ and therefore $B(r) = (1 - Kr^2)^{-1}$.

Example 2.5.2: An isotropic 3-space.

For the line element $d\sigma^2 = B(r)dr^2 + r^2 d\Omega^2$ the components of the metric tensor are, along with the inverse components:

$$g_{ab} = \begin{pmatrix} B(r) & 0 & 0 \\ 0 & r^2 & 0 \\ 0 & 0 & r^2\sin^2\theta \end{pmatrix}, \qquad g^{ab} = \begin{pmatrix} \frac{1}{B^2(r)} & 0 & 0 \\ 0 & \frac{1}{r^2} & 0 \\ 0 & 0 & \frac{1}{r^2\sin^2\theta} \end{pmatrix}.$$

By using the symmetric properties of the Christoffel symbols, the identity (2.32), that for three different indices (i.e. $\Gamma^r{}_{\theta\phi}$) the symbols are null, thus the non zero components are:

$$\begin{aligned} \Gamma^r{}_{rr} &= \frac{1}{2B(r)}\frac{dB(r)}{dr}, \qquad \Gamma^r{}_{\theta\theta} = -\frac{r}{B(r)}, \qquad \Gamma^r{}_{\phi\phi} = -\frac{r\sin^2\theta}{B(r)}. \\ \Gamma^\theta{}_{r\theta} &= \Gamma^\phi{}_{r\phi} = \frac{1}{r}, \qquad \Gamma^\theta{}_{\phi\phi} = -\sin\theta\cos\theta, \qquad \Gamma^\phi{}_{\phi\theta} = \cot\theta. \end{aligned}$$

The Riemann tensor components

$$\begin{aligned} R^r{}_{\theta r\theta} &= \Gamma^r{}_{\theta\theta,r} - \Gamma^r{}_{r\theta,\theta} + \Gamma^r{}_{r\lambda}\Gamma^\lambda{}_{\theta\theta} - \Gamma^r{}_{\theta\lambda}\Gamma^\lambda{}_{r\theta} = \frac{r}{2B^2(r)}\frac{dB(r)}{dr}. \\ R^r{}_{\phi r\phi} &= \Gamma^r{}_{\phi\phi,r} - \Gamma^r{}_{r\phi,\phi} + \Gamma^r{}_{r\lambda}\Gamma^\lambda{}_{\phi\phi} - \Gamma^r{}_{\phi\lambda}\Gamma^\lambda{}_{r\phi} = \frac{r\sin^2\theta}{2B^2(r)}\frac{dB(r)}{dr}. \\ R^\theta{}_{r\theta r} &= \Gamma^\theta{}_{rr,\theta} - \Gamma^\theta{}_{\theta r,r} + \Gamma^\theta{}_{\theta\lambda}\Gamma^\lambda{}_{rr} - \Gamma^\theta{}_{r\lambda}\Gamma^\lambda{}_{\theta r} = \frac{1}{2rB(r)}\frac{dB(r)}{dr}. \\ R^\theta{}_{\phi\theta\phi} &= \Gamma^\theta{}_{\phi\phi,\theta} - \Gamma^\theta{}_{\theta\phi,\phi} + \Gamma^\theta{}_{\theta\lambda}\Gamma^\lambda{}_{\phi\phi} - \Gamma^\theta{}_{\phi\lambda}\Gamma^\lambda{}_{\theta\phi} = \sin^2\theta\left(1 - \frac{1}{B(r)}\right). \\ R^\phi{}_{r\phi r} &= \Gamma^\phi{}_{rr,\phi} - \Gamma^\phi{}_{\phi r,r} + \Gamma^\phi{}_{\phi\lambda}\Gamma^\lambda{}_{rr} - \Gamma^\phi{}_{r\lambda}\Gamma^\lambda{}_{\phi r} = \frac{1}{2rB(r)}\frac{dB(r)}{dr}. \\ R^\phi{}_{\theta\phi\theta} &= \Gamma^\phi{}_{\theta\theta,\phi} - \Gamma^\phi{}_{\phi\theta,\theta} + \Gamma^\phi{}_{\phi\lambda}\Gamma^\lambda{}_{\theta\theta} - \Gamma^\phi{}_{\theta\lambda}\Gamma^\lambda{}_{\phi\theta} = 1 - \frac{1}{B(r)}. \end{aligned}$$

The non-null Ricci tensor components:

$$R_{rr} = \frac{1}{rB}\frac{dB}{dr}, \qquad R_{\theta\theta} = 1 - \frac{1}{B} + \frac{r}{2B^2}\frac{dB}{dr}, \qquad R_{\phi\phi} = R_{\theta\theta}\sin^2\theta.$$

Finally, the curvature scalar:

$$R = g^{rr}R_{rr} + g^{\theta\theta}R_{\theta\theta} + g^{\phi\phi}R_{\phi\phi} = \frac{2}{r^2}\frac{d}{dr}\left[r\left(1 - \frac{1}{B(r)}\right)\right].$$

Considering $R_{jk} = 2Kg_{jk}$

$$\frac{1}{rB}\frac{dB}{dr} = 2KB(r), \qquad \& \qquad 1 - \frac{1}{B} + \frac{r}{2B^2}\frac{dB}{dr} = 2Kr^2.$$

Integrating the first equation

$$B(r) = \frac{1}{A - Kr^2}.$$

Substituting into the second expression, then it gives $1 - A + Kr^2 = Kr^2$, from which we see that $A = 1$. Thus, we have constructed the line element for the maximally symmetric 3-space.

Finally, with the previous results we have that the spatial part of the metric is written as

$$d\sigma^2 = \gamma_{ij} dx^i dx^j = \frac{dr^2}{1 - Kr^2} + r^2 d\Omega^2, \tag{2.59}$$

where r is the radial coordinate and $d\Omega^2 = d\theta^2 + \sin^2\theta d\phi^2$ is the metric on the 2-sphere. Notice it has a similar form as the metric for a 3-sphere embedded in four-dimensional Euclidean space. The metric contains a 'hidden symmetry', since the origin of the radial coordinate is completely arbitrary. We can choose any point in this space as our origin since all points are equivalent. There is no centre in this space.

HW 2.5: Take metric (2.56) and compute Christoffel and Riemann to get (2.59). Make sure you do $R_{ij} = 2K g_{ij}$.

Plugging everything together into (2.55), we get the Friedmann-Robertson-Walker metric

$$ds^2 = c^2 dt^2 - S^2(t) \left[\frac{dr^2}{1 - Kr^2} + r^2 d\Omega^2 \right]. \tag{2.60}$$

Let us assume that $K \neq 0$, then we can define the variable $\tilde{k} = K/|K|$ such that $\tilde{k} = \pm 1$ depending on the sign of K. Moreover we introduce the rescale coordinate

$$\tilde{r} = |K|^{1/2} r, \tag{2.61}$$

so Eqn. (2.60) becomes

$$ds^2 = c^2 dt^2 - \frac{S^2(t)}{|K|} \left[\frac{d\tilde{r}^2}{1 - \tilde{k}\tilde{r}^2} + \tilde{r}^2 d\Omega^2 \right]. \tag{2.62}$$

and then, introducing the rescaled function $R(t)$ by (we keep $R(t)$ as the factor as it does contain the units, and the coordinates are still comoving [dimensionless])

$$R(t) = \begin{cases} \frac{S(t)}{|K|^{1/2}} & \text{if } K \neq 0, \\ \\ S(t) & \text{if } K = 0. \end{cases} \tag{2.63}$$

Eqn. (2.62) yields to

$$ds^2 = c^2 dt^2 - R^2(t) \left[\frac{d\tilde{r}^2}{1 - \tilde{k}\tilde{r}^2} + \tilde{r}^2 d\Omega^2 \right]. \tag{2.64}$$

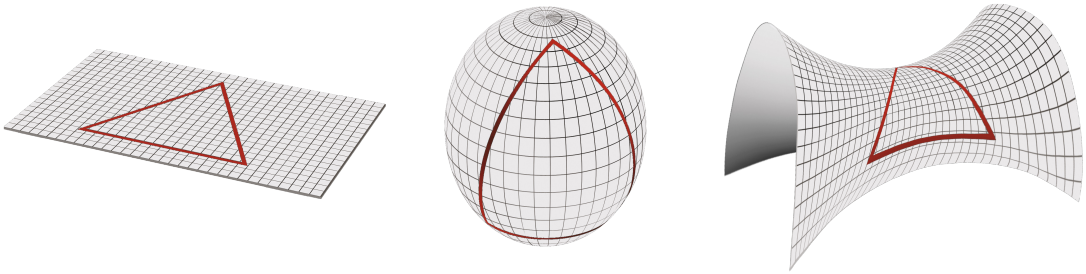

Figure 2.11: Three curvatures allowed for an Isotropic and Homogeneous space-time.

The constant k classifies the curvature of the spatial sections, with closed (S^3), flat (R^3) and open (H^3) universes corresponding to $\tilde{k} = +1, 0, -1$, respectively (see Figure 2.11).

Example 2.5.3: Curvature metrics.

For the flat case $\tilde{k} = 0$ the spatial metric is

$$\begin{aligned} d\sigma^2 &= dr^2 + r^2 d\Omega^2 \\ &= dx^2 + dy^2 + dz^2, \end{aligned}$$

which is simply a flat Euclidean space. For the closed case $\tilde{k} = +1$ we can define $r = \sin\chi$ to write the metric as

$$d\sigma^2 = d\chi^2 + \sin^2\chi d\Omega^2,$$

which is the metric of a three-sphere. In the open $\tilde{k} = -1$ case we can set $r = \sinh\chi$ to obtain

$$d\sigma^2 = d\psi^2 + \sinh^2\psi d\Omega^2.$$

This is the metric for a three-dimensional space of constant negative curvature.

Notice the line element (2.64) has a rescaling symmetry, that leaves the metric invariant

$$R \to \lambda R, \qquad \tilde{r} \to r/\lambda, \qquad \tilde{k} \to \lambda^2 k. \tag{2.65}$$

A convenient form to express the FRW metric is by choosing the rescaling factor as $\lambda = 1/R_0$. That is, using coordinates normalised to the present time, labelled with subscript '0', to defined *the normalised scale factor*

$$a(t) \equiv \frac{R(t)}{R_0}. \tag{2.66}$$

Curvature	Geometry	Angles of triangle	circumference of circle	Type of Universe
$k > 0$	Spherical	$> 180°$	$c < 2\pi r$	Closed
$k = 0$	Flat	$180°$	$c = 2\pi r$	Flat
$k > 0$	Hyperbolic	$< 180°$	$c > 2\pi r$	Open

Table 2.1: A Summary of possible geometries

Therefore the scale factor is set to unity today $a_0 \equiv a(t_0) \equiv 1$, $\tilde{r} \to R_0 r$ has units of [length] and the curvature parameter $\tilde{k} \to k/R_0^2$ has dimensions of [length]$^{-2}$. Note that in this case, k can take any value and not just be restricted to $\{+1, 0, -1\}$. The general properties of these three spaces can be summarised in Table 2.1. The *general FRW metric* written in terms of the normalised scale factor $a(t)$ is thus given by

$$ds^2 = c^2 dt^2 - a^2(t) \left[\frac{dr^2}{1 - kr^2} + r^2 d\Omega^2 \right]. \tag{2.67}$$

In general and throughout this book, we will use the metric (2.64) but dropping the tilde for convenience.

2.5.1 Geometric properties of the FRW metric

The physical meaning of the curvature term becomes more apparent by redefining the **radial coordinate** $d\chi \equiv dr/\sqrt{1 - kr^2}$ in the metric (2.64), that leads to

$$ds^2 = c^2 dt^2 - R^2(t) \left[d\chi^2 + S_k^2(\chi) d\Omega^2 \right], \tag{2.68}$$

where the function $S_k(\chi)$ is specified by the curvature term:

$$S_k(\chi) = \begin{cases} \sin\chi, & \text{for} \quad k = 1 \quad \text{(closed universe)} \\ \chi, & \text{for} \quad k = 0 \quad \text{(flat universe)} \\ \sinh\chi, & \text{for} \quad k = -1 \quad \text{(open universe)} \end{cases} \tag{2.69}$$

where the comoving coordinates remained. When using the symmetry shown above they get units by $\chi \to \chi/\lambda$ and $S_k^2 \to S_k^2/\lambda$.

The comoving radial χ-coordinate, on a null geodesic ($ds^2 = 0$), is computed from

$$\chi = \int \frac{c\ dt}{R(t)}. \tag{2.70}$$

The form of the metric (2.68) is particularly convenient to study the propagation of light. For this purpose, it is useful to introduce the **conformal time**:

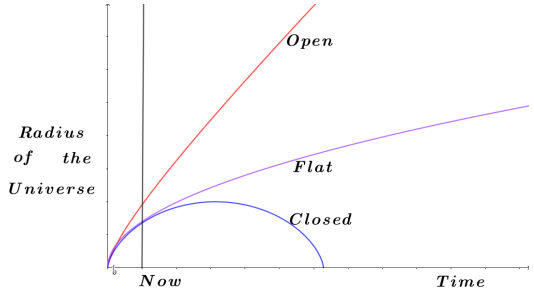

Figure 2.12: Figures for curve spaces. (jav: redo this figure)

$$d\eta = \frac{c\ dt}{R(t)}. \tag{2.71}$$

so that (2.68) becomes

$$ds^2 = \underbrace{R^2(\eta)}_{\text{Conformal}}\ \underbrace{\left[d\eta^2 - (d\chi^2 + S_k^2(\chi)d\Omega^2)\right]}_{\text{Minkowski}}. \tag{2.72}$$

We notice the presence of the static Minkowski space multiplied by a conformal factor $R^2(\eta)$. Because light moves along null geodesics, $ds^2 = 0$, the propagation of light in a FRW is the same as in Minkowski space firstly transformed to conformal time, and along the path we have

$$d\eta = d\chi. \tag{2.73}$$

Therefore the dynamics of the space-time, in a homogeneous and isotropic universe, reduces to determining the scale factor $R(t)$, which is computed from Einstein's equations once the matter content is specified, as we shall see below.

Introduction

In the Λ-CDM model a basic assumption is given by the cosmological principle, which establishes that the Universe where we live is **homogeneous** and **isotropic** at large scales. However, in this paper some models that do not meet those requirements are discussed.

Non-isotropic cosmological models

This type of models are characterised for being homogeneous but not necessarily isotropic in its spatial part, therefore they can be seen as generalisation of the FLRW Universe. Among the most famous are those known as Bianchi models, they are described by the metric (in natural units)[6]:

$$ds^2 = -dt^2 + a_x(t)dx^2 + a_y(t)dy^2 + a_z(t)dz^2.$$

Supposing a comoving test particle in this solution, it will follow the geodesic where (x, y, z) keep constant, however, since the scale factor is different in each direction, its volume and shape could be modified in general.

In order to test this models according to the experimental data, several calculation of nucleosynthesis and CMB anisotropies have been realised, nevertheless, the results have shown that these models are inconsistent with some cosmological parameters, ergo, they are usually only considered as toy models that are tractable exact solutions of Einstein's field equations.

Non-homogeneous cosmological models

These inhomogeneous models are those exact solutions of Einsteins equations that in analogy with the non-isotropic ones, can reproduce the FLRW solution as a limit. There are several proposals in these directions, where the best known are [15]:

(a) The Szekeres - Szafron family: These models are characterised by the metric:

$$ds^2 = dt^2 - e^{2\alpha(t,x,y,r)}dr^2 - e^{2\beta(t,x,y,r)}(dx^2 + dy^2),$$

and they meet the following properties

- They obey the Einstein equations with a perfect fluid source.
- The flow-lines of the perfect fluid are geodesic and nonrotating.

- The hypersurfaces orthogonal to the flow-lines are conformally flat.
- The Ricci tensor of those hypersurfaces has two of its eigenvalues equal. 5. The shear tensor has two of its eigenvalues equal.

(b) The Lemaitre model: This describes a spherically symmetric inhomogeneous fluid with anisotropic pressure. In comoving coordinates it has the following form.

$$ds^2 = e^{A(t,r)}dt^2 - e^{B(t,r)}dr^2 - R^2(t,r)(d\upsilon^2 + \sin^2\upsilon d\phi^2).$$

(c) In the special case of dust with the cosmological constant, the above model reproduces the Lemaitre-Tolman (LT) model which is described by the metric

$$ds^2 = dt^2 - \frac{R_{,r}^2}{1+2E}dr^2 - R^2(t,r)(d\upsilon^2 + \sin^2\upsilon d\phi^2).$$

Conclusion

Some non-standard cosmological models have been discussed. It is worth mentioning that these models can be seen as a generalisation of the FLRW solution which provides a good phenomenological landscape, and since the existence of gravitational lenses, we know that we do not live in a FLRW Universe, thus, considering more general and tractable exact solutions to Einstein's equations is very important.

2.6 Kinematics

In general, for a particle described with coordinates x^μ, we have the action $S[x^\mu(\lambda)]$ with an associated Lagrangian density, given by

$$S[x^\mu(\lambda)] \equiv L[x^\mu, \dot{x}^\mu]d\lambda, \tag{2.74}$$

where overdot means derivative respect to an affine parameter λ: $\dot{x}^\mu \equiv \frac{dx^\mu}{d\lambda}$.
The variation of the action yields to

Example 2.6.1: The Euler-Lagrange equations

$$\frac{d}{d\lambda}\left(\frac{\partial L}{\partial \dot{x}^\mu}\right) - \frac{\partial L}{\partial x^\mu} = 0.$$

Pee. Let us consider the motion of a massive particle between points A and B, displayed in Figure 2.13, the action is given by

$$S = m\int_A^B ds, \tag{2.75}$$

with boundary conditions defined as

$$\lambda(A) \equiv 0, \qquad \lambda(B) \equiv 1, \tag{2.76}$$

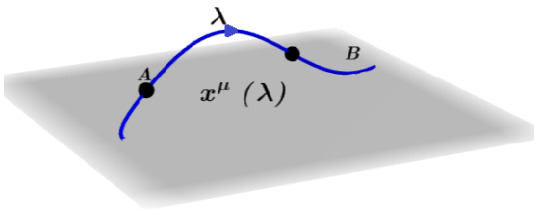

Figure 2.13: Free particle

where the interval ds in a generic space is $ds^2 = g_{\mu\nu}dx^\mu dx^\nu$, and hence

$$S[x^\mu(\lambda)] \quad = \quad m\int_0^1 [g_{\mu\nu}(x)\dot{x^\mu}\dot{x^\nu}]^{1/2}d\lambda. \tag{2.77}$$

The canonical momenta p_μ are the derivatives of the Lagrangian with respect to the coordinate velocities. Computing the derivatives of the density Lagrangian $L = m(g_{\mu\nu}\dot{x^\mu}\dot{x^\nu})^{1/2}$, and for

convenience making $m = 1$[1]:

$$p_\alpha \equiv \frac{\partial L}{\partial \dot{x}^\alpha} = \frac{1}{2}\left(g_{\mu\nu}\dot{x^\mu}\dot{x^\nu}\right)^{-1/2}\left[\frac{\partial \dot{x}^\mu}{\partial \dot{x}^\alpha}\dot{x}^\nu + \dot{x}^\mu\frac{\partial \dot{x}^\nu}{\partial \dot{x}^\alpha}\right]$$
$$= \frac{1}{2L}g_{\mu\nu}\left[\delta^\mu_\alpha\dot{x}^\nu + \dot{x}^\mu\delta^\nu_\alpha\right] = \frac{1}{2L}\left[g_{\alpha\nu}\dot{x}^\nu + g_{\mu\alpha}\dot{x}^\mu\right] = \frac{1}{L}g_{\mu\alpha}\dot{x}^\mu, \tag{2.78}$$

$$\frac{\partial L}{\partial x^\alpha} = \frac{1}{2L}\partial_\alpha g_{\mu\nu}\dot{x}^\mu\dot{x}^\nu. \tag{2.79}$$

By using the interval ds, we have

$$\left(\frac{ds}{d\lambda}\right)^2 = g_{\mu\nu}\frac{dx^\mu}{d\lambda}\frac{dx^\nu}{d\lambda} = L^2 \qquad \text{and} \qquad \frac{d}{d\lambda} \to L\frac{d}{ds}. \tag{2.80}$$

Writing the Einstein-Lagrange equations in terms of the interval ds, they yield to

$$\frac{d}{ds}\left(g_{\mu\alpha}\frac{dx^\mu}{ds}\right) - \frac{1}{2}\partial_\alpha g_{\mu\nu}\frac{dx^\mu}{ds}\frac{dx^\nu}{ds} = 0. \tag{2.81}$$

Expanding the first term in the previous expression

$$g_{\mu\alpha}\frac{d^2x^\mu}{ds^2} + \partial_\beta g_{\mu\alpha}\frac{dx^\beta}{ds}\frac{dx^\mu}{ds} - \frac{1}{2}\partial_\alpha g_{\mu\nu}\frac{dx^\mu}{ds}\frac{dx^\nu}{ds} = 0, \tag{2.82}$$

where the second term that contains $\partial_\beta g_{\mu\alpha}$ can be replaced by $\frac{1}{2}(\partial_\beta g_{\mu\alpha} + \partial_\mu g_{\beta\alpha})\frac{dx^\beta}{ds}\frac{dx^\mu}{ds}$. By contracting with the inverse metric, relabelling indices and using the Christoffel definition we find the

Geodesic equation

$$\frac{d^2x^\mu}{ds^2} + \Gamma^\mu{}_{\alpha\beta}\frac{dx^\alpha}{ds}\frac{dx^\beta}{ds} = 0.$$

Considering the particle has a four-velocity $u^\mu \equiv \frac{dx^\mu}{ds}$, from the geodesic equation we have

$$\frac{du^\mu}{ds} + \Gamma^\mu_{\alpha\beta}u^\alpha u^\beta = 0, \tag{2.83}$$

using the chain rule

$$\frac{d}{ds}u^\mu(x^\alpha(s)) = \frac{dx^\alpha}{ds}\frac{\partial u^\mu}{\partial x^\alpha} = u^\alpha\frac{\partial u^\mu}{\partial x^\alpha}, \tag{2.84}$$

so, we get

$$u^\alpha\left(\frac{\partial u^\mu}{\partial x^\alpha} + \Gamma^\mu_{\alpha\beta}u^\beta\right) = 0. \tag{2.85}$$

[1] where we have used $\frac{\partial \dot{x}^\nu}{\partial \dot{x}^\mu} = \delta^\nu_\mu$.

We notice the quantity within parenthesis defines the covariant derivative

$$\nabla_\alpha u^\mu \equiv \partial_\alpha u^\mu + \Gamma^\mu_{\alpha\beta} u^\beta, \tag{2.86}$$

and therefore, we have that $u^\alpha \nabla_\alpha u^\mu = 0$ (same result obtain in GR using parallel transport). Putting back the mass, and using the four-momentum of the particle $p^\mu = -mu^\mu$ [Pee], it yields to

$$p^\alpha \frac{\partial p^\mu}{\partial x^\alpha} = -\Gamma^\mu_{\alpha\beta} p^\alpha p^\beta. \tag{2.87}$$

Example 2.6.2: The Einstein-Hilbert action.

Let us consider the Einstein-Hilbert action, given by

$$S_{EH} = \int d^n x\sqrt{-g}R = \int d^n x\sqrt{-g}R_{\mu\nu}g^{\mu\nu},$$

where, as usual, the g is the determinant of the metric $g_{\mu\nu}$ and R is the Ricci scalar.

In General Relativity the metric $g_{\mu\nu}$ is the dynamical variable, whereas the Ricci scalar is the product of the metric and its derivatives, hence the integral contains all the dynamical variables that conform the Lagrangian (jav: Palatini formalism). Therefore, to minimise the action – by using the variational principle –, we perform the variation of the action equal to zero:

$$\delta S_{EH} = \delta \int d^n x\sqrt{-g}R = 0.$$

Then

$$\begin{aligned}\delta S_{EH} &= \int d^n x\sqrt{-g}g^{\mu\nu}\delta R_{\mu\nu} + \int d^n x\sqrt{-g}R_{\mu\nu}\delta g^{\mu\nu} + \int d^n x R_{\mu\nu}g^{\mu\nu}\delta\sqrt{-g} \\ &= \delta S_1 + \delta S_2 + \delta S_3.\end{aligned}$$

We compute separately the variation for each term S_i with $i = 1, 2, 3$.
For S_1, we first use the definition of the Christoffel symbols

$$R_{\mu\nu} = R^{\lambda}{}_{\mu\lambda\nu} = \partial_\lambda\Gamma^{\lambda}{}_{\mu\nu} - \partial_\nu\Gamma^{\lambda}{}_{\mu\lambda} + \Gamma^{\lambda}{}_{\lambda\epsilon}\Gamma^{\epsilon}{}_{\nu\mu} - \Gamma^{\lambda}{}_{\nu\epsilon}\Gamma^{\epsilon}{}_{\mu\lambda}.$$

Then, the corresponding variation is

$$\begin{aligned}\delta R_{\mu\nu} &= \partial_\lambda\delta\Gamma^{\lambda}_{\mu\nu} - \partial_\nu\delta\Gamma^{\lambda}_{\mu\lambda} + \delta\Gamma^{\lambda}_{\lambda\epsilon}\Gamma^{\epsilon}_{\nu\mu} + \Gamma^{\lambda}_{\lambda\epsilon}\delta\Gamma^{\epsilon}_{\nu\mu} - \delta\Gamma^{\lambda}_{\nu\epsilon}\Gamma^{\epsilon}_{\mu\lambda} - \Gamma^{\lambda}_{\nu\epsilon}\delta\Gamma^{\epsilon}_{\mu\lambda} \\ &= (\partial_\lambda\delta\Gamma^{\lambda}_{\mu\nu} + \Gamma^{\lambda}_{\lambda\epsilon}\delta\Gamma^{\epsilon}_{\nu\mu} - \Gamma^{\epsilon}_{\mu\lambda}\delta\Gamma^{\lambda}_{\nu\epsilon} - \Gamma^{\epsilon}_{\nu\lambda}\delta\Gamma^{\lambda}_{\mu\epsilon}) \\ &\quad -(\partial_\nu\delta\Gamma^{\lambda}_{\mu\lambda} + \Gamma^{\lambda}_{\nu\epsilon}\delta\Gamma^{\epsilon}_{\mu\lambda} - \Gamma^{\epsilon}_{\nu\mu}\delta\Gamma^{\lambda}_{\lambda\epsilon} - \Gamma^{\epsilon}_{\nu\lambda}\delta\Gamma^{\lambda}_{\mu\epsilon}).\end{aligned}$$

Using the covariant derivative

$$\nabla_c\delta\Gamma^{c}_{ab} = \partial_c\delta\Gamma^{c}_{ab} + \Gamma^{c}_{cd}\delta\Gamma^{d}_{ba} - \Gamma^{d}_{ac}\delta\Gamma^{c}_{bd} - \Gamma^{d}_{bc},\delta\Gamma^{c}_{ad},$$

in order to write the previous expression as

$$\delta R_{\mu\nu} = \nabla_\lambda\delta\Gamma^{\lambda}_{\mu\nu} - \nabla_\nu\delta\Gamma^{\lambda}_{\mu\lambda}.$$

Example 2.6.3:

The first part of the action, S_1, results in the following form:

$$\begin{aligned}\delta S_1 &= \int d^4x\sqrt{-g}g^{\mu\nu}(\nabla_\lambda\delta\Gamma^\lambda_{\mu\nu} - \nabla_\nu\delta\Gamma^\lambda_{\mu\lambda}) \\ &= \int d^4x\sqrt{-g}[\nabla_\lambda(g^{\mu\nu}\delta\Gamma^\lambda_{\mu\nu}) - \delta\Gamma^\lambda_{\mu\nu}\nabla_\lambda g^{\mu\nu} - \nabla_\nu(g^{\mu\nu}\delta\Gamma^\lambda_{\mu\lambda}) + \delta\Gamma^\lambda_{\mu\lambda}\nabla_\nu g^{\mu\nu}].\end{aligned}$$

Because the covariant derivative of the metric vanishes, thus the previous equation becomes:

$$\begin{aligned}\delta S_1 &= \int d^4x\sqrt{-g}[\nabla_\lambda(g^{\mu\nu}\delta\Gamma^\lambda_{\mu\nu}) - \nabla_\nu(g^{\mu\nu}\delta\Gamma^\lambda_{\mu\lambda})] \\ &= \int d^4x\sqrt{-g}\nabla_\lambda[g^{\mu\nu}\delta\Gamma^\lambda_{\mu\nu} - g^{\mu\lambda}\delta\Gamma^\nu_{\mu\nu}]. \qquad (2.88)\end{aligned}$$

Let be $J^\lambda = g^{\mu\nu}\delta\Gamma^\lambda_{\mu\nu} - g^{\mu\lambda}\delta\Gamma^\nu_{\mu\nu}$, a vectorial field defined over a region M with frontier Σ. Using the Stokes theorem:

$$\int_M d^4x\sqrt{|g|}\nabla_\lambda J^\lambda = \int_\Sigma d^3x\sqrt{|g|}n_\lambda J^\lambda,$$

with n_λ is a unitary normal vector to the hyper-surface Σ. In infinity J^λ becomes zero on the surfaces due to the variations in $g_{\mu\nu}$ tend to zero far away from the sources, and the variation of the Christoffel symbols are proporcional to the variations of the metric and its derivatives. Therefore, we have $S_1 = 0$, that is, the first term does not contribute to the variation of the Einstein-Hilbert action.

To compute the variations of S_2 y S_3, let us analyse the behaviour of the metric tensor under variations. First, consider that $g_{\lambda\mu}g^{\mu\nu} = \delta^\nu_\lambda$ Then, assuming the metric tensor has inverse, hence it exists a tensor $A^{\nu\mu}$ such that:

$$g^{\mu\nu} = \frac{1}{g}(A^{\mu\nu})^T = \frac{1}{g}A^{\nu\mu},$$

where g is the determinant of $g_{\mu\nu}$. From the two previous expressions, we have $g = g_{\mu\nu}A^{\mu\nu}$. From which we may infer that the partial derivative of the determinant is:

$$\frac{\partial g}{\partial g_{\mu\nu}} = A^{\mu\nu}.$$

Therefore

$$\delta g = \frac{\partial g}{\partial g_{\mu\nu}}\delta g_{\mu\nu} = A^{\mu\nu}\delta g_{\mu\nu} = gg^{\nu\mu}\delta g_{\mu\nu}.$$

and given that $g^{\mu\nu}$ is symetric, then:

$$\delta g = gg^{\mu\nu}\delta g_{\mu\nu}.$$

Example 2.6.4:

With the previous calculations in mind, we are able to compute the variation of the $\sqrt{-g}$ term:

$$\begin{aligned}\delta\sqrt{-g} &= -\frac{1}{2\sqrt{-g}}\delta g \\ &= \frac{1}{2}\frac{g}{\sqrt{-g}}g^{\mu\nu}\delta g_{\mu\nu}.\end{aligned} \tag{2.89}$$

We need $\delta g^{\mu\nu}$ instead of $\delta g_{\mu\nu}$; to do that, we consider the following:

$$\begin{aligned}\delta\delta_{\mu}{}^{\epsilon} = \delta(g_{\mu\lambda}g^{\lambda\epsilon}) &= 0 \\ g^{\lambda\epsilon}\delta g_{\mu\lambda}\delta g^{\lambda\epsilon} &= 0 \\ g^{\lambda\epsilon}\delta g_{\mu\lambda} &= -g_{\mu\lambda}\delta g^{\lambda\epsilon}.\end{aligned}$$

Multiplying both terms of the equation by $g_{\nu\epsilon}$, we have:

$$\begin{aligned}g_{\nu\epsilon}g^{\lambda\epsilon}\delta g_{\mu\lambda} &= -g_{\nu\epsilon}g_{\mu\lambda}\delta g^{\lambda\epsilon} \\ \delta^{\lambda}_{\nu}\delta g_{\mu\lambda} &= -g_{\nu\epsilon}g_{\mu\lambda}\delta g^{\lambda\epsilon} \\ \delta g_{\mu\nu} &= -g_{\mu\lambda}g_{\nu\epsilon}\delta g^{\epsilon\lambda}.\end{aligned} \tag{2.90}$$

Substituting the last results into equation 2.89:

$$\begin{aligned}\delta\sqrt{-g} &= -\frac{1}{2}\sqrt{-g}g^{\mu\nu}g_{\mu\lambda}g_{\nu\epsilon}\delta g^{\epsilon\lambda} \\ &= -\frac{1}{2}\sqrt{-g}\delta^{\nu}_{\lambda}g_{\nu\epsilon}\delta g^{\epsilon\lambda} \\ &= -\frac{1}{2}\sqrt{-g}g_{\lambda\epsilon}\delta g^{\epsilon\lambda}.\end{aligned} \tag{2.91}$$

Renaming the indices, then:

$$\delta\sqrt{-g} = -\frac{1}{2}\sqrt{-g}g_{\mu\nu}\delta g^{\mu\nu}.$$

Using that $S_1 = 0$ along with equations 2.90 and 2.91, finally we've got:

$$\begin{aligned}\delta S_{EH} &= \int d^4x\sqrt{-g}R_{\mu\nu}\delta g^{\mu\nu} - \frac{1}{2}\int d^4R\sqrt{-g}g_{\mu\nu}\delta g^{\mu\nu} \\ &= \int d^4x\sqrt{-g}[R_{\mu\nu} - \frac{1}{2}g_{\mu\nu}R]\delta g^{\mu\nu}.\end{aligned}$$

Notice the terms within brackets correspond to the definition of the Einstein tensor:

$$G_{\mu\nu} = R_{\mu\nu} - \frac{1}{2}g_{\mu\nu}R.$$

Modifications to the Einstein-Hilbert action.

The action of the $f(R)$ models is given by

$$S_{MG} = \int d^n x \sqrt{-g} f(R).$$

See [42], where the equations of motion are (2.15)-(2.16) and the dynamical system (4.63)-(4.66) to find the solutions.

Also, see [91] for a Brane-World Gravity review, where the action to take into account is

$$S_{\text{gravity}} = \frac{1}{2\kappa_{4+d}^2} \int d^4 d^d y \sqrt{-{}^{(4+d)}g} \left[{}^{(4+d)}R - 2\Lambda_{4+d} \right],$$

where d is the number of extra dimensions and κ_{4+d}^2 is the gravitation coupling constant.

2.6.1 Geodesics in the FRW metric

The FRW metric (2.64) is written in the following way

$$ds^2 = c^2 dt^2 - R^2(t) \gamma_{ij} dx^i dx^j. \tag{2.92}$$

HW 2.6: Compute the Christoffel symbols to get

$$\Gamma^0_{ij} = R\dot{R}\gamma_{ij}, \qquad \Gamma^i_{0j} = \frac{\dot{R}}{R}\delta^i_j, \qquad \Gamma^i_{jk} = \frac{1}{2}\gamma^{il}(\partial_j \gamma_{kl} + \partial_k \gamma_{jl} - \partial_l \gamma_{jk}).$$

otherwise zero (jav: plug back c).

The homogeneity of FRW implies that $\partial_i p^\mu = 0$ and hence only survives $\alpha = 0$. From the geodesic equation (2.87), we have

$$p^0 \frac{dp^\mu}{dt} = -\Gamma^\mu_{\rho\beta} p^\rho p^\beta \tag{2.93}$$

$$= -(2\Gamma^\mu_{0j} p^0 + \Gamma^\mu_{ij} p^i) p^j. \tag{2.94}$$

The implications of the expressions above are:

- A massive particle at rest - in the comoving frame - $p^j = 0$, will stay at rest

$$p^j = 0 \qquad \rightarrow \qquad \frac{dp^\mu}{dt} = 0. \tag{2.95}$$

- Considering the case $\mu = 0$, we have that the first Christoffel vanishes ($\Gamma^0_{0j} = 0$), and hence

$$E\frac{dE}{dt} = -\Gamma^0_{ij}p^i p^j = -\frac{\dot{R}}{R}p^2. \tag{2.96}$$

where we have written $p^0 = E$ and the physical three-momentum $p^2 = -g_{ij}p^i p^j = R^2\gamma_{ij}p^i p^j$, and the components of the four momentum satisfy the constraint $g_{\mu\nu}p^\mu p^\nu = m^2$ or $E^2 - p^2 = m^2$. Using the fact that $EdE = pdp$, then the equation can be written as

$$\frac{\dot{p}}{p} = -\frac{\dot{R}}{R} \qquad \rightarrow \qquad p \propto \frac{1}{R}, \tag{2.97}$$

the three momentum of any particle (either massive or massless) decays with the expansion of the universe.

  - For massless particle- The energy decays with the expansion of the scale factor

$$p = E \propto 1/R. \tag{2.98}$$

  - For massive

$$p = \frac{mv}{\sqrt{1-v^2}} \propto \frac{1}{R}, \tag{2.99}$$

where $v^i = dx^i/dt$ is the comoving peculiar velocity of the particles and $v^2 \equiv R^2\gamma_{ij}v^i v^j$. The freely-falling particles left on their own will converge onto the Hubble flow.

2.6.2 Redshift

The light emitted can be viewed either quantum mechanically as a free-propagating photons, or classically propagating electromagnetic waves

- Quantum.

  The wavelength $\lambda = h/p$ and since

$$p \propto \frac{1}{R(t)} \rightarrow \lambda \propto R(t). \tag{2.100}$$

  Light emitted at time t_1 with wavelength λ_1 will be observed at t_0 with

$$\lambda_0 = \frac{R(t_0)}{R(t_1)}\lambda_1. \tag{2.101}$$

  Since $R(t_0) > R(t_1)$ (with $t_0 > t_1$), then the wavelength of the light increases $\lambda_0 > \lambda_1$, that is, is red-shifted otherwise blue-shifted.

- Classical waves.

  (jav: Figure). Consider a galaxy at fixed comoving distance d. At a time η_1, the galaxy emits a signal of short conformal duration $\Delta\eta$. According to the geodesics $\Delta\eta = \Delta\chi$ (2.73) the light arrives at our telescope at time η_0. The conformal duration of the signal measured by the detector is the same as the source, but the physical time intervals are different at the points of emission and detection.

$$\Delta t_1 = R(\eta_1)\Delta\eta \qquad \& \qquad \Delta t_0 = R(\eta_0)\Delta\eta. \tag{2.102}$$

  If Δt is the period of the light wave, the light is emitted with wavelength $\lambda_1 = \Delta t_1$, but it is observed with wavelength $\lambda_0 = \Delta t_0$, so that

$$\frac{\lambda_0}{\lambda_1} = \frac{R(\eta_0)}{R(\eta_1)}. \tag{2.103}$$

For convenience, we express the fractional shift in wavelength of a photon emitted by a distant galaxy at time t_1 with wavelength λ_1 and the observer on Earth today (t_0), as:

$$z \equiv \frac{\lambda_0 - \lambda_1}{\lambda_1}, \tag{2.104}$$

and therefore the gravitational redshift in terms of the scale factor is

$$1 + z = \frac{R(t_0)}{R(t_1)}.$$

Example 2.6.5: Cosmological redshifts

In general it is shown (see [50]) that the redshift z can be computed given the conformal Killing vector field, giving

$$1 + z = \sqrt{\frac{g_{\alpha\beta}(y^\gamma)\xi^\alpha(y^\gamma)\xi^\beta(y^\gamma)}{g_{\alpha\beta}(x^\gamma)\xi^\alpha(x^\gamma)\xi^\beta(y^\gamma)}}.$$

The redshift is used to refer to the time at which the scale factor was a fraction $1/(1+z)$ of its present value. It is also used to refer to the distance that light has travelled since that time [81].

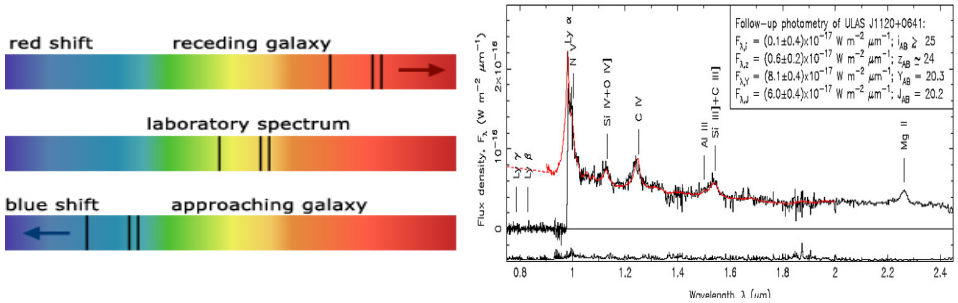

Figure 2.14: Redshift

Example 2.6.6: Times in the Universe

Some particular times in the history of the Universe

$$\begin{aligned} R &= 1, \quad z = 0, \quad t = 13.8Gys, \\ R &= 0, \quad z = \infty, \quad t = 0, \\ R &= 1/1101, \quad z = 1100, \quad t = 380,000ys. \end{aligned}$$

2.6.3 Hubble and Deceleration parameter

Let us expand the scale factor as a power series about the present epoch t_0

$$\begin{aligned} R(t) &= R[t_0 - (t_0 - t)] \\ &= R(t_0) - (t_0 - t)\dot{R}|_{t=t_0} + \frac{1}{2}(t_0 - t)^2\ddot{R}|_{t=t_0} - \cdots \\ &= R(t_0)\left[1 - (t_0 - t)H(t_0) - \frac{1}{2}(t_0 - t)^2 q(t_0)H^2(t_0) - \cdots\right]. \end{aligned} \tag{2.105}$$

HW: use simpy.

The expansion rate of the universe is characterised by the **Hubble parameter** defined as

$$H(t) \equiv \frac{\dot{R}(t)}{R(t)}, \tag{2.106}$$

where the present expansion rate, being $H(t = t_0)$, is called the Hubble constant H_0. Because the Hubble constant is still not known with great accuracy, it is conventional to denote it through the dimensionless parameter h, such that $H_0 = 100\,h\ \mathrm{km\,s^{-1}Mpc^{-1}} = h/3000\ \mathrm{Mpc}^{-1}$.

The **deceleration parameter** $q(t)$, is defined by

$$q(t) \equiv -\frac{\ddot{R}(t)R(t)}{\dot{R}^2(t)}. \tag{2.107}$$

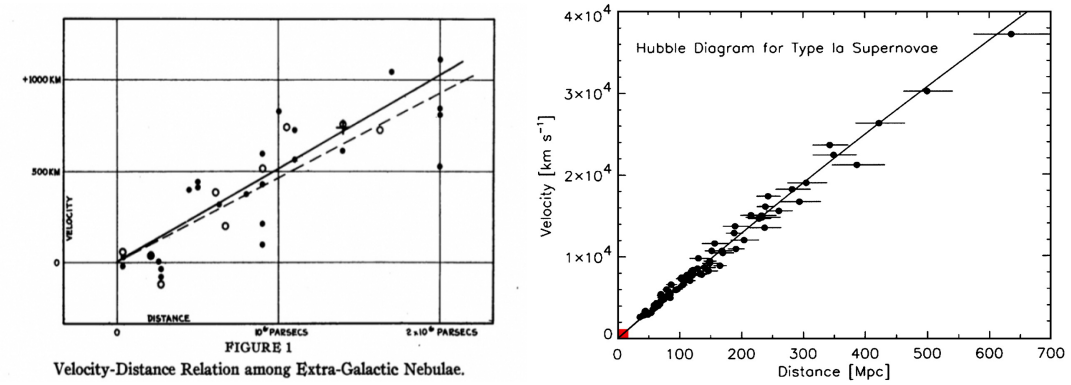

Figure 2.15: Hubble parameter

As the name suggests, it describes whether the expansion of the universe is slowing down ($q > 0$) or speeding up ($q < 0$). If the Taylor expansion keeps on going there come out several parameters, for instance the next two ones are the jerk $j \equiv \frac{R^2 \dddot{R}}{\dot{R}^3}$ and the snap $j \equiv \frac{R^3 \ddddot{R}}{\dot{R}^4}$ parameters. That is, the coefficients in the power series of the expansion of the scale factor are known as the *cosmography*. See for instance [8]

Now, let us write the redshift parameter in terms of the *look-back* time $t - t_0$

$$\frac{R(t_0)}{R(t)} = \left[1 - (t_0 - t)H_0 - \frac{1}{2}(t_0 - t)^2 q_0 H_0^2 - \cdots\right]^{-1} \approx [1 - \delta x]^{-1} \tag{2.108}$$

$$\approx 1 + (t_0 - t)H_0 + \frac{1}{2}(t_0 - t)^2 q_0 H_0^2 + (t_0 - t)^2 H_0^2. \tag{2.109}$$

assuming $|t_0 - t| \ll t_0$ (very close to today). Then, we have

$$z = \frac{R(t_0)}{R(t)} - 1 = (t_0 - t)H_0 + (t_0 - t)^2 \left(1 + \frac{1}{2}q_0\right) H_0^2 + \cdots . \tag{2.110}$$

Since z is an absolute quantity (observable), then the look-back time $t_0 - t$ can be written in terms of z. For $z \ll 1$, from the above equation, we have

$$(t_0 - t)H_0 = z - (t_0 - t)^2 \left(1 + \frac{1}{2}q_0\right) H_0^2 + \cdots . \tag{2.111}$$

and using the fact, at first order that $(t_0 - t)H_0 \approx z$, therefore

$$t_0 - t = H_0^{-1} z - H_0^{-1} \left(1 + \frac{1}{2}q_0\right) z^2 + \cdots . \tag{2.112}$$

The approximations depend only on the present-day values of H_0 and q_0, and no knowledge of the complete expansion history $R(t)$ of the universe.

The radial χ coordinate (Eq. 2.70) of the emitting galaxy

$$\chi = \int_t^{t_0} \frac{c\ dt}{R(t)} = c\ R_0^{-1} \int_t^{t_0} [1 - (t_0 - t)H_0 + \cdots]^{-1} dt, \tag{2.113}$$

assuming $t_0 - t \ll t_0$, expanding the terms and then integrating, we have

$$\chi = c\ R_0^{-1}[(t_0 - t) + \frac{1}{2}(t_0 - t)^2 H_0 + \cdots]. \tag{2.114}$$

using the expression (2.112), assuming $z \ll 1$,

$$\chi = \frac{c}{R_0 H_0}[z - \frac{1}{2}(1 + q_0)z^2 + \cdots], \tag{2.115}$$

it only depends on H_0 and q_0 and not on the full expansion $R(t)$.

The proper distance d_p of the emitting galaxy at cosmic time t_0 is $d \equiv R(t_0)\chi$, thus for nearby galaxies $d \approx cz/H_0$. Moreover, using that the cosmological redshift can be written as a Doppler shift due to recession velocity v of the emitting galaxy

$$v \equiv cz = H_0 d.$$

The galaxies appear to recede from us with a recesion speed proportional to their distance: *Hubble's law*. The Hubble constant has the dimensions of the inverse time and $1/H_0$ gives the age of the universe. It is important not to confuse the expansion redshift with a kinematic redshift. Also, take into account for relativistic velocities

$$1 + z = \sqrt{\frac{1 + v/c}{1 - v/c}}. \tag{2.116}$$

Combining Eqn. 2.105, we get an expression (for small redshift) (jav: do it)

$$H(z) = H_0[1 + (1 + q_0)z - \cdots] \tag{2.117}$$

Example 2.6.7: Hubble expansion

The Hubble expansion is a natural property of an homogeneous an isotropic universe. All observers see galaxies with the same Hubble law. For example, consider two observers/galaxies

$$\vec{v}_A = H_0 \cdot \vec{r}_A \qquad \vec{v}_B = H_0 \cdot \vec{r}_B, \tag{2.118}$$

$$\vec{v}_{BA} = \vec{v}_B - \vec{v}_A = H_0\vec{r}_B - H_0\vec{r}_A = H_0(\vec{r}_B - \vec{r}_A). \tag{2.119}$$

In a homogeneous universe every particle moving with the substratum has a purely radial velocity proporcional to its distance from the observer. (jav: si $v = H_0 r^2$?)

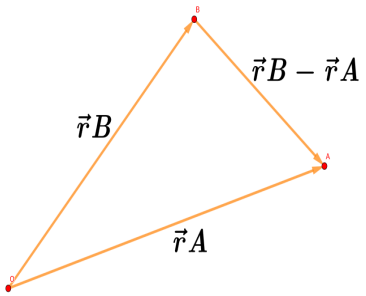

2.6.4 Integrales

```
In [1]: import numpy as np
        from sympy import *
        from gravipy import *
```

$$D = \int_0^R \frac{a}{(a^2 - \rho^2)^{\frac{1}{2}}} d\rho$$

```
In [11]: init_printing()

         a, rho, R = symbols ('a, \\rho, R', positive=True) #Asignamos nuestros simbolos a las varia
         e = Rational(1,2) #Al no poder poner el simbolo 1/2, utilizamo esta forma para poder poner

         D = a / (a**2 - rho**2)**e #La funcion que vamos a integrar

         integrate(D,(rho,0,R))
         #integrate(D,rho)
```

Out[11]:

$$a \operatorname{asin}\left(\frac{R}{a}\right)$$

$$C = \int_0^{2\pi} R d\phi$$

In [5]:
```
phi = symbols ('\\phi')

C = R

integrate(C,(phi,0,2*pi))
```

Out[5]:

$$2\pi R$$

$$A = \int_0^{2\pi} \int_0^{R} \frac{a}{(a^2-\rho^2)^{\frac{1}{2}}} \rho d\rho d\phi$$

In [149]:
```
A = a / (a**2 - rho**2)**e*rho

simplify(integrate(A,(rho,0,R),(phi,0,2*pi)))
```

Out[149]:

$$2\pi a\left(-\sqrt{-R^2+a^2}+\sqrt{a^2}\right)$$

$$t = \frac{1}{H_0} \int_0^{a} \left[\frac{x}{\Omega_{m,0}+(1-\Omega_{m,0})x}\right]^{\frac{1}{2}} dx$$

In [42]:
```
H_0, Omega, x, a = symbols ('H_0, \\Omega_{m0}, x, a')

t =  (1/H_0) * (x / (Omega + (1-Omega)*x))**e

t_1 = t.subs(Omega,1)

integrate(t_1,(x,0,a))
```

Out[42]:

$$\frac{2a^{\frac{3}{2}}}{3H_0}$$

In [151]:
```
#Para Omega > 1

H_0, Omega, x, a = symbols ('H_0, \\Omega_{m0}, x, a')
psi = symbols ('psi')

x1 = Omega / (Omega - 1)*sin(psi/2)**2 # con [0/pi] llamamos nuestra variable x1 que es la

t_x1 = (1/H_0) * (x / (Omega + (1-Omega)*x))**e

t = factor(t_x1.subs(x,x1))

t

#integrate(t,(psi,0,pi))
```

Out[151]:

$$\frac{\sqrt{\frac{\sin^2\left(\frac{\psi}{2}\right)}{-\Omega_{m0}\sin^2\left(\frac{\psi}{2}\right)+\Omega_{m0}+\sin^2\left(\frac{\psi}{2}\right)-1}}}{H_0}$$

In [154]:
```
# Para Omega < 1
H_0, Omega, x, a = symbols ('H_0, \\Omega_{m0}, x, a')
psi = symbols ('psi')

x2 =  Omega / (1 - Omega) *sinh (psi/2)**2

t_x2 = (1/H_0) * (x / (Omega + (1-Omega)*x))**e

t = factor(t_x2.subs(x,x2))

t

#integrate(t,(psi,0,pi))
```

Out[154]:

$$\frac{\sqrt{\frac{\sinh^2\left(\frac{\psi}{2}\right)}{-\Omega_{m0}\sinh^2\left(\frac{\psi}{2}\right)-\Omega_{m0}+\sinh^2\left(\frac{\psi}{2}\right)+1}}}{H_0}$$

$$t = \frac{1}{H_0}\int_0^a \frac{x}{\sqrt{\Omega_{r,0}+(1-\Omega_{r,0})x^2}}$$

In [126]:
```
H_0, Omega_r0, x, a = symbols ('H_0, \\Omega_{r0}, x, a')

t = 1/H_0* x/sqrt((Omega_r0 + (1 - Omega_r0)*x**2))

t_1 = t.subs(Omega_r0,1)

integrate(t_1,(x,0,a))
```

Out[126]:

$$\frac{a^2}{2H_0}$$

In [156]:
```
# Para Omega < 1

H_0, Omega_r0, x, a = symbols ('H_0, \\Omega_{r0}, x, a')

t = 1/H_0* x/sqrt((Omega_r0 + (1 - Omega_r0)*x**2))

integrate(t,(x,0,a))
```

Out[156]:

$$-\frac{\sqrt{\Omega_{r0}}\sqrt{1+\frac{a^2\,\mathrm{polar\_lift}\,(-\Omega_{r0}+1)}{\Omega_{r0}}}}{H_0\,(\Omega_{r0}-1)}+\frac{\sqrt{\Omega_{r0}}}{H_0\,(\Omega_{r0}-1)}$$

$$t=\frac{1}{H_0}\int_0^a \frac{x}{\sqrt{\Omega_{m,0}x+\Omega_{r,0}}}dx$$

In [144]:
```
H_0, Omega_m, Omega_r, x, a = symbols ('H_0, \\Omega_{m0}, \\Omega_{r0} x, a')

#haciendo
y = Omega_m * x + Omega_r

t = 1/H_0 * (x/(sqrt(y)))

t_1 = simplify(integrate(t,(x,0,a)))

factor (t_1)
```

Out[144]:

$$\frac{2\sqrt{\Omega_{r0}}\left(\Omega_{m0}a\sqrt{\frac{\Omega_{m0}a}{\Omega_{r0}}+1}-2\Omega_{r0}\sqrt{\frac{\Omega_{m0}a}{\Omega_{r0}}+1}+2\Omega_{r0}\right)}{3H_0\Omega_{m0}^2}$$

$$t=\frac{1}{H_0}\int_0^a\sqrt{\frac{x}{1-\Omega_{\Lambda,0}+\Omega_{\Lambda,0}x^3}}dx$$

In [191]:
```
H_0, Omega_l, x, a , y = symbols ('H_0, \\Omega_{\\Lambda0},x, a ,y')


t = 1/H_0*sqrt(x/(1-Omega_l + Omega_l * x**3))

#Haciendo

y2 = x**3*abs(Omega_l)/(1-Omega_l)

Ht = 2/(3*(abs(Omega_l)))*1/(sqrt(1 + y**2))

integrate(Ht,(y,0,y2))
```

Out[191]:

$$\frac{2\,\mathrm{asinh}\left(\frac{x^3|\Omega_{\Lambda0}|}{-\Omega_{\Lambda0}+1}\right)}{3\,|\Omega_{\Lambda0}|}$$

In [192]:
```
H_0, Omega_l, x, a , y = symbols ('H_0, \\Omega_{\\Lambda0},x, a ,y')


t = 1/H_0*sqrt(x/(1-Omega_l + Omega_l * x**3))

#Haciendo

y2 = x**3*abs(Omega_l)/(1-Omega_l)

Ht = 2/(3*(abs(Omega_l)))*1/(sqrt(1 - y**2))

integrate(Ht,(y,0,y2))
```

Out[192]:

$$\frac{2\,\mathrm{asin}\left(\frac{x^3|\Omega_{\Lambda0}|}{-\Omega_{\Lambda0}+1}\right)}{3\,|\Omega_{\Lambda0}|}$$

In [ ]:

2.7 The Friedmann-Lemaître equations

The Friedmann equation describes the expansion of the Universe, and is therefore the most important equation in cosmology. Let us derive the equations by using Newton's theory and after that through Einstein theory.

Example 2.7.1: The Friedmann equation

Let us consider an observer in a uniform expanding medium with mass m and density ρ. Then, the total mass $M = 4\pi\rho r^3/3$ contributes to a force, see Figure 2.16

$$F = \frac{GMm}{r^2} = \frac{4\pi G\rho r m}{3}.$$

Our particle has a gravitational potential energy

$$V = -\frac{GMm}{r} = -\frac{4\pi G\rho r^2 m}{3},$$

with the velocity of the particle $\dot{r}$ giving the kinetic energy

$$T = \frac{1}{2}m\dot{r}^2.$$

Energy conservation for that particle $U = T + V$, where U is a constant

$$U = \frac{1}{2}m\dot{r}^2 - \frac{4\pi}{3}G\rho r^2 m,$$

using comoving coordinates $\vec{r} = R(t)\vec{x}$ (r the physical coordinates and x the fix location), then

$$U = \frac{1}{2}m\dot{R}^2x^2 - \frac{4\pi}{3}G\rho R^2x^2 m,$$

if we multiply for $2/mR^2x^2$ and rearranging, we have

$$\frac{\dot{R}^2}{R^2} = \frac{8\pi G}{3}\rho - \frac{kc^2}{R^2},$$

where $kc^2 = -2U/mx^2$. k is just a constant unchanging with either space or time, often called the curvature.

- $k > 0$- the expansion will at some time, halt and reverse itself.
- $k < 0$- the expansion will continue forever.
- $k = 0$- the expansion of the universe will slow down, but only halt at $t = \infty$.

Example 2.7.2: Evolution of the density

From thermodynamics second law $dE + PdV = TdS$ and using $E = mc^2$,

$$\begin{aligned} E &= \frac{4\pi}{3}R^3\rho c^2, \\ \rightarrow \quad \frac{dE}{dt} &= 4\pi R^2\rho c^2\frac{da}{dt} + \frac{4\pi}{3}R^3\frac{d\rho}{dt}c^2, \end{aligned}$$

and for the volume change

$$\frac{dV}{dt} = 4\pi R^2\frac{da}{dt},$$

assuming a reversible expansion $dS = 0$, we get the fluid equation

$$\dot{\rho} + 3\frac{\dot{R}}{R}\left(\rho + \frac{p}{c^2}\right) = 0.$$

The first term in the parenthesis corresponds to the dilution because the volume has increased, while the second is the loss of energy because the pressure has done work as the Universe's volume increased (gravitational potential energy).

Example 2.7.3: The accelerated equation

Differentiating the Friedmann equation, we have

$$2\frac{\dot{R}}{R}\frac{R\ddot{R} - \dot{R}^2}{R^2} = \frac{8\pi G}{3}\dot{\rho} + \frac{2kc^2\dot{R}}{R^3},$$

using $\dot{\rho}$

$$\begin{aligned} \frac{\ddot{R}}{R} - \left(\frac{\dot{R}}{R}\right)^2 &= -4\pi G\left(\rho + \frac{p}{c^2}\right) + \frac{kc^2}{R^2}, \\ \frac{\ddot{R}}{R} &= -\frac{4\pi G}{3}\left(\rho + \frac{3p}{c^2}\right). \end{aligned}$$

independent of the constant k.

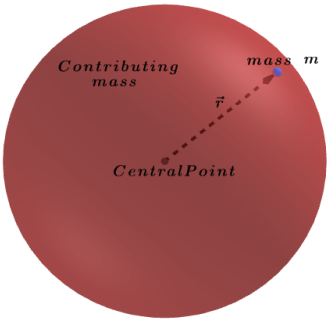

Figure 2.16: Figure of a mass in a solid gravity sphere.

Once we have specified the metric that describes the homogeneous and isotropic expanding universe, the evolution of both the scale factor and matter density follows from Einstein's equations :

$$G_{\mu\nu} \equiv R_{\mu\nu} - \frac{1}{2} g_{\mu\nu} R = \kappa_0 \, T_{\mu\nu}. \tag{2.120}$$

As we have seen previously $G_{\mu\nu}$ is the *Einstein metric tensor*, the *Ricci tensor* $R_{\mu\nu}$ is a combination of first and second derivatives of the metric $g_{\mu\nu}$, and its trace is defined by the *Ricci scalar* $R \equiv g^{\mu\nu} R_{\mu\nu}$; G is the Newton's constant and $\kappa_0 = 8\pi G/c^4$. On the right hand side, the energy-momentum tensor $T_{\mu\nu}$ contains the constituents of the universe. An acceptable modification to Einstein's equations is the introduction of a Lorentz-invariant constant-term $\Lambda g_{\mu\nu}$ into the field equations:

$$R_{\mu\nu} - \frac{1}{2} g_{\mu\nu} R + \Lambda g_{\mu\nu} = \kappa_0 \, T_{\mu\nu}, \tag{2.121}$$

where Λ is called the *cosmological constant* and its value, according to astrophysical observations, is $\Lambda \sim 10^{-52}\mathrm{m}^{-2}$ [21, 103]; we will see more about this component in subsequent sections. Equation (2.121) is in general a complicated set of coupled quasilinear second-order partial differential equations for the ten elements of the metric $g_{\mu\nu}$. Nevertheless, they may exhibit simple analytical solutions in the presence of generic symmetries, for instance, under the assumption of the FRW metric. Considering $g_{\mu\nu}$ in the form of (2.64), the Christoffel symbols

$$\begin{aligned}
\Gamma^0{}_{ij} &= R^2 H g_{ij}, \qquad \Gamma^i{}_{0j} = \Gamma^i{}_{j0} = H\delta^i_j, \\
\Gamma^1{}_{11} &= \frac{kr}{1-kr^2}, \qquad \Gamma^1{}_{22} = -r(1-kr^2), \qquad \Gamma^1{}_{33} = -r(1-kr^2)\sin\theta, \\
\Gamma^2{}_{33} &= -\sin\theta\cos\theta, \qquad \Gamma^2{}_{12} = \Gamma^2{}_{21} = \Gamma^3{}_{13} = \Gamma^3{}_{31} = \frac{1}{r}, \qquad \Gamma^3{}_{23} = \Gamma^3{}_{32} = \cot\theta.
\end{aligned}$$

and the non-vanishing curvature terms are given by

$$R_{00} = -3\frac{\ddot{R}}{R} = -3(\dot{H} + H^2), \tag{2.122}$$

$$R_{ij} = \left[\frac{\ddot{R}}{R} + 2\left(\frac{\dot{R}}{R}\right)^2 + \frac{2c^2k}{R^2}\right] g_{ij}, \tag{2.123}$$

$$R = 6\left[\frac{\ddot{R}}{R} + \left(\frac{\dot{R}}{R}\right)^2 + \frac{c^2k}{R^2}\right], \tag{2.124}$$

and the Einstein tensor

$$G^0_0 = -3\left[\left(\frac{\dot{R}}{R}\right)^2 + \frac{c^2k}{R^2}\right], \tag{2.125}$$

$$G^i_j = -\left[2\frac{\ddot{R}}{R} + \left(\frac{\dot{R}}{R}\right)^2 + \frac{c^2k}{R^2}\right]\delta^i_j. \tag{2.126}$$

where an overdot indicates again derivative with respect to cosmic time t ($\dot{\cdot} \equiv d/dt$).

HW: Compute R and G

HW: Compute the Kretschmann scalar for a FRW spacetime.

The geometry of the space-time is determined by equations (2.125)-(2.126), then to solve Einstein's equations we just need to specify the matter content under consideration.

2.8 The Energy-momentum tensor

The energy-momentum is divided in the following components:

$$T^{\mu\nu} = \begin{bmatrix} T^{00} & \vdots & T^{i0} \\ \cdots & \vdots & \cdots\cdots \\ T^{0j} & \vdots & T^{ij} \end{bmatrix}.$$

- T^{00}- total energy density.
- T^{i0} - energy flux ($\times c^{-1}$) in the i-direction.

- T^{0j} - momentum density ($\times c$) in the j-direction.
- T^{ij} - momentum flow (random thermal motions).
  - T^{ii} - Isotropic pressure in the i-direction.
  - T^{ij} $(i \neq j)$ viscous stresses.

Because we seek for a $T_{\mu\nu}$ consistent with the requirements of homogeneity and isotropy, we need the following to be satisfied:

- Isotropy requires that the mean values of the 3-vector vanish, i.e. $T^{0i} = T^{0j} = 0$.
- T^{ij} at any point (more specifically at $x = 0$) be proportional to δ_{ij} and hence to g_{ij} $(= R^2\delta_{ij}$ at $x = 0)$, then

$$T_{ij}(x = 0) \propto \delta_{ij} \propto g_{ij}(x = 0). \tag{2.127}$$

- Homogeneity requires that the proportionality coefficient be only a function of time

$$T_{00} = \rho(t), \quad \pi_i \equiv T_{i0} = 0, \quad T_{ij} = p(t)g_{ij}(t, \vec{x}). \tag{2.128}$$

$$T^{\mu}_{\nu} = g^{\mu\lambda}T_{\lambda\nu} = \begin{pmatrix} \rho & 0 & 0 & 0 \\ 0 & -p & 0 & 0 \\ 0 & 0 & -p & 0 \\ 0 & 0 & 0 & -p \end{pmatrix}, \tag{2.129}$$

where ρ is the energy density and p the isotropic pressure of the fluid, both of them measured by an observer in a local inertial frame in which the fluid is at rest. This is the stress-energy tensor of a *perfect-fluid* as seen by a comoving observer.

More generally

$$T^{\mu\nu} = \left(\frac{p}{c^2} + \rho\right) u^{\mu}u^{\nu} - pg^{\mu\nu}, \tag{2.130}$$

in the rest frame, where the 4-velocity of the fluid between the fluid and the observer is given by u^{μ}. For a comoving observer $u^{\mu} = (1, 0, 0, 0)$, the energy-momentum tensor hence reduces to $T^{\mu}_{\nu} = \mathrm{diag}(\rho, g^{ii}p)$. Thus, Einstein's equations for a perfect fluid in a FRW background provide two independent expressions (time-time and space-space components), which together yield to the *Friedmann* and *acceleration* equations:

$$G^0_0 \quad \Rightarrow \quad \left(\frac{\dot{R}}{R}\right)^2 = \frac{8\pi G}{3}\rho - \frac{k}{R^2} + \frac{1}{3}\Lambda c^2, \tag{2.131}$$

$$G^i_j \quad \Rightarrow \quad \frac{\ddot{R}}{R} = -\frac{4\pi G}{3}\left(\rho + \frac{3p}{c^2}\right) + \frac{1}{3}\Lambda c^2. \tag{2.132}$$

The cosmological equations, in which $R(t)$ is computed under the aforementioned conditions, are known as the Friedmann-Lemaître-Robertson-Walker equations; we simply refer to them as Friedmann equations.

Another equation of interest is the conservation of the energy-momentum tensor, $\nabla_\mu T^\mu_\nu = \partial_\mu T^\mu_\nu + \Gamma^\mu_{\mu\lambda} T^\lambda_\nu - \Gamma^\lambda_{\mu\nu} T^\mu_\lambda = 0$, which leads to the *continuity equation*:

$$\dot{\rho} + 3\frac{\dot{R}}{R}\left(\rho + \frac{p}{c^2}\right) = 0. \tag{2.133}$$

In order to solve the full set of cosmological equations, we still need to specify an extra condition, for instance the pressure for every kind of material the universe is filled with. The usual, and well-founded, assumption is that there is a pressure contribution associated to each energy density, so that $p \equiv p(\rho)$. Such a relationship is known as the *equation-of-state*. The Friedmann equation (2.131), the energy-momentum conservation (2.133), and the equation-of-state $p = p(\rho)$ are therefore the fundamental expressions that describe the dynamics of a homogeneous and isotropic universe.

2.8.1 Cosmic Inventory

In order to understand the dynamical properties of the universe, we first need to bear in mind the whole content of it. Let us focus on single-barotropic perfect-fluids that satisfy, in general, a time-dependent equation-of-state $w(z)$, of the form

$$p = c^2 w(z) \rho. \tag{2.134}$$

For any component, with constant w, the continuity equation (2.133) can be easily integrated to give [1]

$$\rho \propto R^{-3(1+w)}. \tag{2.136}$$

Moreover, in a universe dominated by the energy density ρ, the Friedmann equation leads to the time evolution of the scale factor:

$$R(t) \propto t^{2/3(1+w)}, \qquad \forall \quad w \neq -1, \tag{2.137}$$

or, in conformal time (Eqn. 2.71):

$$R(\eta) = \eta^{2/(1+3w)}, \qquad \forall \quad w \neq -1. \tag{2.138}$$

[1] For a more general description of $w(a)$, the evolution of the energy density is given by

$$\rho \propto \exp[-3X(a)], \qquad \text{with} \qquad X(a) = \int_1^a [1 + w(a')] d\ln a'. \tag{2.135}$$

That is, the evolution of a universe filled with a given perfect fluid is known once its equation-of-state is specified. The standard Λ-Cold Dark Matter model (ΛCDM) relies upon four main ingredients, described by radiation (photons, massless neutrinos), matter (baryons), the inclusion of a dark matter component (DM) and vacuum energy (Λ). The behaviour of each of these components is summarised as follows:

Radiation

This relativistic component dominates during the earliest stages of the universe. Radiation is characterised by an associated pressure $p_{\rm r} = \rho_{\rm r}/3$[1], with an associated equation-of-state $w_{\rm r} = 1/3$. The evolution of its energy-density and scale factor are thus given by

$$\rho_{\rm r}(t) = \rho_{\rm r,0}\left[\frac{R(t)}{R_0}\right]^{-4}, \qquad \text{and} \qquad R(t) \propto t^{1/2}. \tag{2.139}$$

On the other hand, the energy density of the blackbody radiation

$$\rho_r(T) = \alpha T^4, \tag{2.140}$$

where α is the Stefan-Boltzmann constant. If the present day temperature is pin-up to be $T_0 = 2.726K$ then the number density of radiation today is $n_{\gamma,0} \simeq 4\times 10^8 m^{-3}$ (see more about them in the next section). On the other hand, comparing eqns. (2.139) and (2.140) we have that the universe was denser and hotter in the past

$$T \propto R^{-1}. \tag{2.141}$$

The big bang is somehow explain:

$$t \to 0, \qquad R \to 0, \qquad \rho \to \infty, \qquad T \to \infty. \tag{2.142}$$

Extrapolating our assumptions, at the beginning of the universe ($t \to 0$), the universe was denser and hotter concentrated in a minusculous tiny region.

The total radiation energy-density ρ_r in the universe may be written as the sum of two main contributions: photons (γ) and massless neutrinos (ν):

$$\rho_{\rm r}(t) = \rho_\gamma(t) + \rho_\nu(t). \tag{2.143}$$

[1] we'll obtain this result with statistical mechanics in the following sections.

Photons - Primordial photons play a key role in observational cosmology as they constitute the cosmic microwave background radiation we nowadays observe, as we shall see in more detail in Sections 15.0.1 and 17.2.1.

Massless Neutrinos - Neutrinos are very weakly interacting leptons, which come in three types or 'flavours': electron, muon, and tau; all of them with an associated antiparticle. The amount of massless neutrinos in the cosmic background (estimated from theoretical arguments) is given by

$$\rho_\nu = N_{\rm eff} \times \frac{7}{8} \times \left(\frac{4}{11}\right)^{4/3} \rho_\gamma, \tag{2.144}$$

where $N_{\rm eff}$ is the effective number of neutrino species; note that $N_{\rm eff} = 3.046$ for the standard neutrino species [92]. Nevertheless, several experiments suggest they do have a very small mass. For instance experiments detecting atmospheric neutrinos, solar neutrinos, also reactor neutrinos and accelerator beam neutrinos. Cosmological observations have also provided limits on the neutrino mass; some reviews in the subject can be found in: Dolgov [34], Elgarøy and Lahav [39], Hannestad [49], Lesgourgues and Pastor [74].

Matter

Any type of material with negligible pressure is often referred as 'dust'. It is represented by an equation-of-state $w_{\rm m} = 0$, with energy-density given by

$$\rho_{\rm m}(t) \propto R^{-3}, \qquad \text{and} \qquad R(t) \propto t^{2/3}. \tag{2.145}$$

that is, the dilution of the energy-density is because the expansion of the volume $V \propto R^3$.

Combining expressions in (2.145) we have

$$H = \frac{\dot{R}}{R} = \frac{2}{3t}. \tag{2.146}$$

that is, the universe expands forever but with a decreasing rate. Notice that $t_0 = \frac{2}{3}\frac{1}{H_0}$ and using the Hubble parameter we have that the age of the Universe with content purely giving in the form of matter is $t_0 = 9.3$ Gyrs. This type of universe is called *Einstein de-Sitter Universe*. The total matter content of the universe comes in several forms. In addition to the familiar baryonic matter, observations of the Large-Scale Structure (LSS) suggest that most of the galactic content is in the form of non-baryonic matter, called *Dark-Matter*. The total matter density may be expressed as the sum of baryonic (b) and dark-matter (dm) contributions:

$$\rho_{\rm m}(t) = \rho_{\rm b}(t) + \rho_{\rm dm}(t). \tag{2.147}$$

Baryons - make up the familiar matter of our universe (protons and neutrons). Since the charge of the universe is neutral, there must be equal number of protons and electrons (charged leptons). An elaborated review of Big Bang Nucleosynthesis (BBN) is given by Steigman [125] (see also next section).

Dark matter - The existence of non-baryonic dark matter has been inferred from its gravitational manifestations through the flat rotation curves of galaxies, the mass-to-light ratios in clusters of galaxies, and gravitational lensing of background sources. An extended discussion of the current status of particle dark matter, including experimental evidence and theoretical motivations, is presented by Bertone et al. [14], Sellwood and Kosowsky [120].

Vacuum

If the cosmological constant term is moved to the right-hand-side on Einstein's equations, it can be associated to the *vacuum energy-density*, given by

$$\rho_\Lambda \equiv \frac{\Lambda c^2}{8\pi G}. \tag{2.148}$$

At future cosmic times, while the matter and radiation density dilute away, the vacuum energy-density remains with the same constant value ρ_Λ. The vacuum energy can be modelled as a perfect fluid with negative pressure equal to $p_\Lambda = -\rho_\Lambda$, which corresponds to an equation-of-state $w_\Lambda = -1$: a De-Sitter Universe. For a review about the cosmological constant term see e.g. Carroll [21], Padmanabhan [103], Peebles and Ratra [104]. The cosmological constant is also seen as the simplest form of a more generic *'dark energy'* component, commonly considered as the main candidate to explain the current acceleration of the universe. We shall see in Chapter **??** that $w_{\rm DE}(a)$ evolving in time provides a slightly better description for the current observational data.

Curvature

The contribution of the spatial curvature can be considered as any other energy component by defining a fictitious energy density:

$$\rho_k \equiv -\frac{3kc^2}{8\pi G} R^{-2}. \tag{2.149}$$

This energy-density is described by an equation-of-state $w_k = -1/3$, for which the scale factor evolves proportionally to the cosmic time $a \propto t$. The general behaviour of the curvature term is easily understood if we rewrite the Friedmann equation, with a vanished cosmological constant, in the following way

$$\left(\frac{\dot{R}}{R}\right)^2 = \frac{8\pi G}{3}(\rho + \rho_k). \tag{2.150}$$

For a positive density contribution ρ, the universal expansion can only be stopped if the universe is closed $k > 0$ ($\rho_k < 0$), otherwise it will expand forever.

Missing matter

If the Friedmann equation is written in terms of the present energy-density components, we have

$$\left(\frac{\dot{R}}{R}\right)^2 = \frac{8\pi G}{3}\left[\rho_{\mathrm{r},0}\left(\frac{R}{R_0}\right)^{-4} + \rho_{\mathrm{m},0}\left(\frac{R}{R_0}\right)^{-3} + \rho_{k,0}\left(\frac{R}{R_0}\right)^{-2} + \rho_{\Lambda,0}\left(\frac{R}{R_0}\right)^{-0}\right]. \tag{2.151}$$

Notice that the right-hand-side can be seen as a power series expansion, however with a missing component with contribution R^{-1}. To complete the series, we include this term and named it as the *missing-energy* component [131], for which its energy-density satisfies

$$\rho_X(t) = \rho_{X,0}\left[\frac{R}{R_0}\right]^{-1}, \qquad \text{and} \qquad R \propto t^2. \tag{2.152}$$

The missing-energy component has therefore an equation-of-state $w_X = -2/3$, and behaves similarly to domain walls [12, 134]. We explain it in more detail about this new term in Chapter **??**.

A summary of the main components of the universe, along with their behaviour, is shown in Table 2.2. Before solving the cosmological equations for the whole mixture of perfect-fluid components, we include some essential notation:

Density parameter: We also introduce the ratio of the energy-density relative to the critical density $\rho_{\mathrm{c}} \equiv 3H^2/8\pi G$, as the dimensionless density parameter:

$$\Omega_i(t) \equiv \frac{\rho_i(t)}{\rho_{\mathrm{c}}(t)}, \tag{2.153}$$

where the index 'i' labels a single type of component, such as matter, radiation, etcetera. The present critical density is $\rho_{\mathrm{c},0} = 1.88h^2 \times 10^{-22}$ gcm^{-3}.

component	Ω_i	w_i	$\rho(R)$	$R(t)$	$H(t)$
radiation	$\Omega_{\rm r}$	1/3	$\propto R^{-4}$	$\propto t^{1/2}$	1/2t
matter	$\Omega_{\rm m}$	0	$\propto R^{-3}$	$\propto t^{2/3}$	2/3t
curvature	Ω_k	-1/3	$\propto R^{-2}$	$\propto t$	1/t
missing matter	Ω_X	-2/3	$\propto R^{-1}$	$\propto t^2$	2/t
cosmological constant	Ω_Λ	-1	$\propto R^0$	$\propto \exp(\sqrt{\frac{\Lambda}{3}}t)$	const

Table 2.2: Constituents of the universe and their cosmological parameters: density parameter Ω_i, equation-of-state parameter w_i; and their behaviour: density evolution $\rho(R)$, scale factor $R(t)$, Hubble parameter $H(t)$. (jav: agregar comoving quantities, $r:\eta, dm:\eta^2, \Lambda:-\eta^{-1}$)

2.8.2 The cosmological field equations

We have computed the evolution of the scale factor for a universe made up by single-independent fluids: radiation, matter, vacuum, spatial curvature, vacuum energy and missing energy. To make the basic Friedmann models more realistic, we need to take into account the whole mixture of these components. Suppose that within the mixture, the distinct fluids do not interact with each other but only through their mutual gravitation (perfect fluids). The total energy-momentum tensor of a multiple-component fluid is thus given by

$$T^{\mu\nu} = \sum_i (T^{\mu\nu})_i, \tag{2.154}$$

where i labels the sum over various constituents, each of them individually modelled as a single perfect-fluid with $p_i = w_i\rho_i$. Using the definitions introduced above, the Friedmann equations (2.131) and (2.132) for a multi-fluid universe are now written in the following way

$$\left(\frac{H}{H_0}\right)^2 = \sum_i \Omega_{i,0}\left(\frac{R}{R_0}\right)^{-3(1+w_i)} + \Omega_{k,0}\left(\frac{R}{R_0}\right)^{-2}, \tag{2.155}$$

$$\dot{H} + H^2 = -\frac{4\pi G}{3}\sum_i \rho_i(1+3w_i) = \frac{R\ddot{R}}{\dot{R}^2}. \tag{2.156}$$

The density parameters at any given time are

$$\Omega_i = \Omega_{i,0}\left(\frac{H_0}{H}\right)^2\left(\frac{R}{R_0}\right)^{-3(1+w_i)}. \tag{2.157}$$

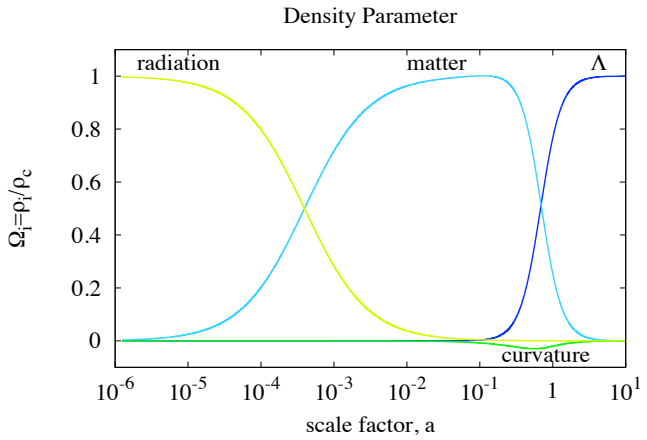

Figure 2.17: The evolution of density parameters $\Omega_i(a)$ are seen as a succession of several epochs, each of them dominated by different components: radiation, matter, curvature and cosmological constant.

Therefore, these equations, at any cosmic time, can be written in the elegant forms:

$$\Omega_T \equiv \sum_i \Omega_i + \Omega_\Lambda = 1 - \Omega_k, \tag{2.158}$$

$$q = \frac{1}{2}\sum_i \Omega_i(1+3w_i). \tag{2.159}$$

In particular, the curvature density-parameter $\Omega_k = -kc^2/H^2R^2$, determines the normalisation of the scale factor (2.66), or *curvature radius*:

$$R_0 = H_0^{-1}\sqrt{-kc^2/\Omega_{k,0}} = \frac{cH_0^{-1}}{\sqrt{|\Omega_{k,0}|}}. \tag{2.160}$$

In a universe with positive curvature, R_0 is just the radius of the 3-sphere. Notice that we can go back and for on the scale factors $a \leftrightarrow R$ from Eqn. (2.66), thus from now on, and for simplicity, we shall use the normalised scale factor a. On the other hand, we notice that the matter distribution (2.158) clearly determines the spatial geometry of the universe: $\Omega_T < 1$ (open), $\Omega_T = 1$ (flat) and $\Omega_T > 1$ (closed).

The Friedmann equations have exact solutions in just a few simple cases, for instance in a universe modelled by perfect-fluids. For this particular case, the density parameters and their dependence on the scale factor are plotted in Figure 2.17. In this Figure, the cosmic evolution of the different constituents are seen as a succession of several epochs, each of them

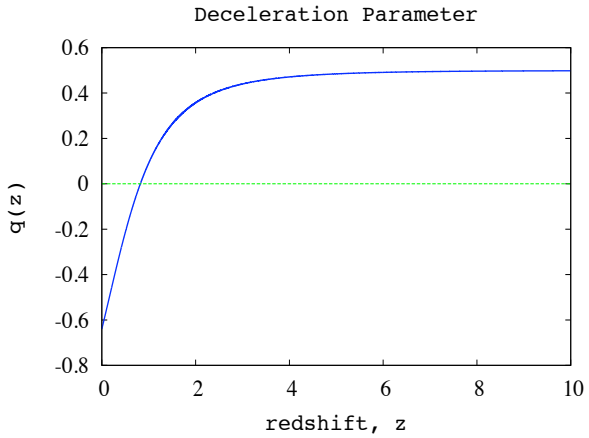

Figure 2.18: Deceleration parameter $q(z)$ as a function of redshift z for a multi-fluid universe. Notice that the universe is currently accelerating ($q(z=0) < 0$).

corresponding to a different perfect-fluid. At the earliest stages, radiation dominates because of its behaviour $\rho_{\rm r} \propto a^{-4}$. Then, at $a_{\rm eq} \approx 4.2 \times 10^{-5} h^{-2}$, the radiation contribution equals that of matter, which starts dominating afterwards. It is noticeable that the curvature term is almost negligible due to the initial conditions taken (see Section 17.4). Finally, the cosmological constant term dominates over the late-time evolution of the universe, and remains so for all time due to its constant energy-density behaviour.

From expression (2.159), we observe that the sign of $(1 + 3w_i)$ determines whether the universe is accelerating ($q < 0$) or decelerating ($q > 0$). If the major contribution comes from a fluid(s) with $w_i > -1/3$ the expansion of the universe will gradually slow-down due to the action of gravity. On the other hand, if $w_i < -1/3$ the pressure component acts as a 'repulsive' term leading to an accelerated expansion. For instance the cosmological constant term, which dominates over the dynamics of the universe at low-redshift, is considered the principal responsible for the present accelerated expansion of the universe, seen in Figure 2.18.

2.9 Scalar Fields

$$S = \int d^4x \sqrt{-g} \left[\frac{1}{2} \partial_\mu \phi \partial^\mu \phi - V(\phi) \right]. \tag{2.161}$$

The corresponding field equation for ϕ is obtained from the Euler-Lagrange equations and

reads

$$\Box^2\phi + \frac{dV}{d\phi} = 0. \tag{2.162}$$

$$T_{\mu\nu} = \partial_\mu\phi\partial_\nu\phi - g_{\mu\nu}\,[\frac{1}{2}\partial_\sigma\phi\partial^\sigma\phi - V(\phi)]. \tag{2.163}$$

$$T_{00} = \rho_\phi = \frac{1}{2}\dot{\phi}^2 + V(\phi) + \frac{1}{2}(\vec{\nabla}\phi)^2, \tag{2.164}$$

$$T_{ii} = p_\phi = \frac{1}{2}\dot{\phi}^2 - V(\phi) - \frac{1}{6}(\vec{\nabla}\phi)^2, \tag{2.165}$$

From the structure of the effective energy-density and pressure, the Friedmann and the acceleration equations for a homogeneous single-scalar field become

$$H^2 = \frac{8\pi G}{3}\left[\frac{1}{2}\dot{\phi}^2 + V(\phi)\right], \tag{2.166}$$

$$\frac{\ddot{a}}{a} = -\frac{8\pi G}{3}\left[\dot{\phi}^2 - V(\phi)\right]. \tag{2.167}$$

with an analogous equation of state

$$w_\phi = \frac{\dot{\phi}^2 - 2V(\phi)}{\dot{\phi}^2 + 2V(\phi)}. \tag{2.168}$$

Therefore, the inflationary condition to be satisfied is $\dot{\phi}^2 \ll V(\phi)$, which is easily fulfilled with a suitable flat potential. Inflation is driven by the vacuum energy of the inflaton field $p_\phi \approx -\rho_\phi$.

2.10 World Models

https://www.youtube.com/watch?v=Y-dMtbHQVI0

Let us take the equation for the total density (2.158) $\Omega_T + \Omega_k = 1$ and the equation for acceleration (2.159) $q = \frac{1}{2}\sum_i \Omega_i(1+3w_i)$. There are some lines useful to draw in order to identify the type of Universe we live on:

- *Open-closed line* $(k=0)$

$$\Omega_{\Lambda,0} = 1 - \Omega_{m,0}. \tag{2.169}$$

- *Accelerating-decelerating line* $(q=0)$

$$\Omega_{\Lambda,0} = \frac{1}{2}\Omega_{m,0}. \tag{2.170}$$

- *Expand-forever-recollapse* & *big bang - no big bang*, it requires a little more work.

In general

$$\dot{a}^2 = a^2 H_0^2(\Omega_{r,0}a^{-4} + \Omega_{m,0}a^{-3} + \Omega_{k,0}a^{-2} + \Omega_{\Lambda,0}) \tag{2.171}$$

with the condition (2.158) $1 = \Omega_r + \Omega_m + \Omega_k + \Omega_\Lambda$ for all time, in particular for $a = 1$. The FRW Universes dominated by matter and vacuum energy are named as **Lemaitre models**. From the Figure 2.19 we have that (considering present data): we live in a nearly flat accelerating universe that presents a big bang in the past and will expand forever in the future.

Cosmological models with zero cosmological constant ($\Omega_{\Lambda,0} = 0$), and strictly non-zero matter or radiation density, are known as the **Friedmann models**.

Dust only Friedmann models ($\Omega_{r,0} = 0$, $\Omega_{k,0} = 1 - \Omega_{m,0}$)

From the equation (2.171), we have

$$\dot{a}^2 = H_0^2(\Omega_{m,0}a^{-1} + 1 - \Omega_{m,0}) \qquad \rightarrow \qquad t = \frac{1}{H_0}\int_0^a \left[\frac{x}{\Omega_{m,0} + (1-\Omega_{m,0})x}\right]^{1/2} dx. \tag{2.172}$$

- $\Omega_{m,0} = 1$ $(k=0)$ - **Einstein de-Sitter model**

$$a(t) = \left(\frac{3}{2}H_0 t\right)^{2/3}. \tag{2.173}$$

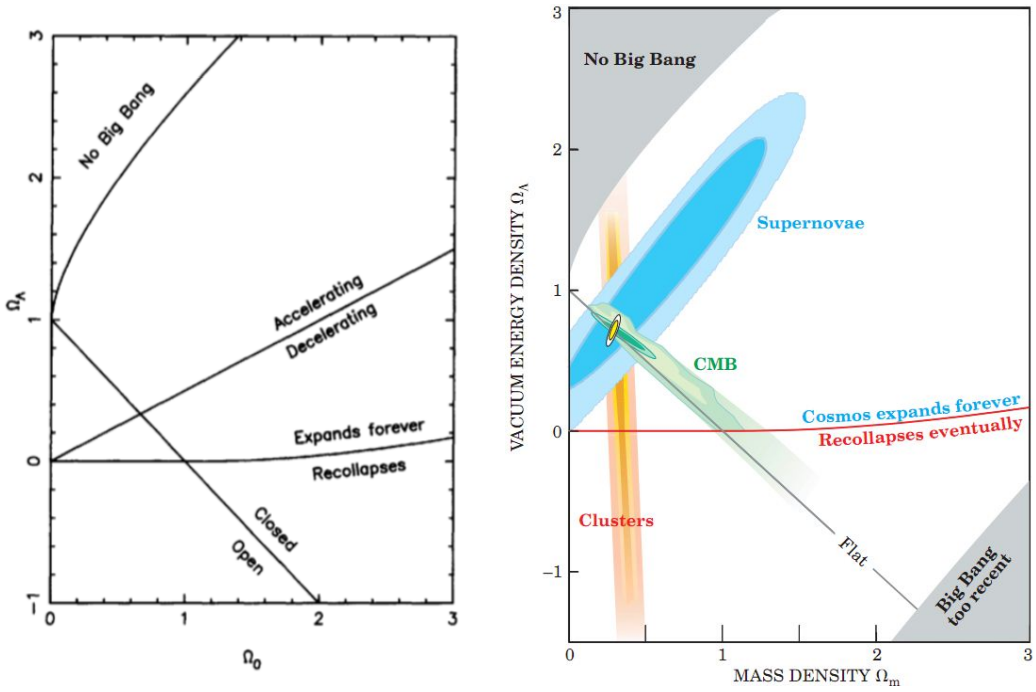

Figure 2.19: (jav: I'll do it later)

- $\Omega_{m,0} > 1$ $(k = 1)$, we write

$$x = \left[\frac{\Omega_{m,0}}{\Omega_{m,0} - 1} \sin^2 \psi/2\right], \qquad \psi = [0, \pi], \tag{2.174}$$

and we have

$$a(t) = \frac{\Omega_{m,0}}{2(\Omega_{m,0} - 1)}(1 - \cos\psi), \qquad t = \frac{\Omega_{m,0}}{2H_0(\Omega_{m,0} - 1)^{3/2}}(\psi - \sin\psi), \tag{2.175}$$

where the first term represents the expression for a cycloid, see Figure 2.20.

- $\Omega_{m,0} < 1$ $(k = -1)$, we write

$$x = \left[\frac{\Omega_{m,0}}{1 - \Omega_{m,0}} \sinh^2 \psi/2\right], \qquad \psi = [0, \pi]. \tag{2.176}$$

and we have

$$a(t) = \frac{\Omega_{m,0}}{2(1 - \Omega_{m,0})}(\cosh\psi - 1), \qquad t = \frac{\Omega_{m,0}}{2H_0(1 - \Omega_{m,0})^{3/2}}(\sinh\psi - \psi). \tag{2.177}$$

Radiation only $(\Omega_{m,0} = 0,\ \Omega_{k,0} = 1 - \Omega_{r,0})$

$$\dot{a}^2 = H_0^2(\Omega_{r,0}a^{-2} + 1 - \Omega_{r,0}) \qquad \rightarrow \qquad t = \frac{1}{H_0}\int_0^a \left[\frac{x}{\sqrt{\Omega_{r,0} + (1 - \Omega_{r,0})x^2}}\right] dx. \tag{2.178}$$

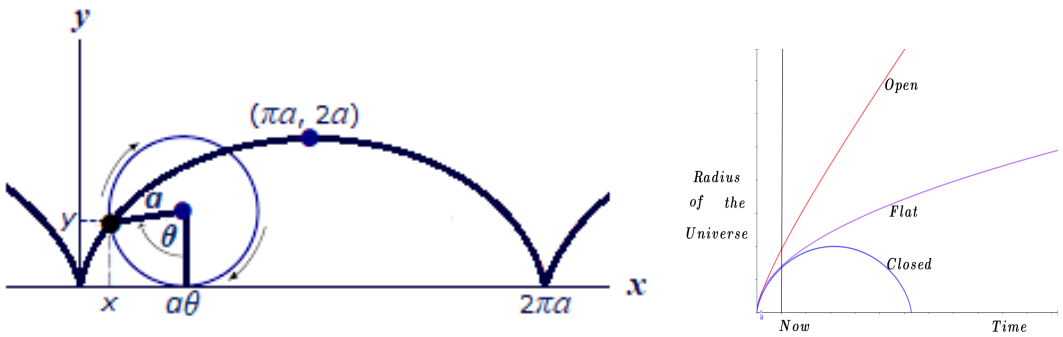

Figure 2.20: (jav: Figure of the universe)

- $\Omega_{r,0} = 1$ $(k = 0)$

$$a(t) = (2H_0 t)^{1/2}. \tag{2.179}$$

- $\Omega_{r,0} < 1$ $(k = -1)$ & $\Omega_{r,0} > 1$ $(k = 1)$

$$a(t) = (2H_0 \Omega_{r,0}^{1/2} t)^{1/2} \left(1 + \frac{1 - \Omega_{r,0}}{2\Omega_{r,0}^{1/2}} H_0 t\right)^{1/2}. \tag{2.180}$$

Spatially flat ($\Omega_{k,0} = 0$, $\Omega_{m,0} + \Omega_{r,0} = 1$)

$$\dot{a}^2 = H_0^2(\Omega_{m,0} a^{-1} + \Omega_{r,0} a^{-2}) \qquad \rightarrow \qquad t = \frac{1}{H_0} \int_0^a \left[\frac{x}{\sqrt{\Omega_{m,0} x + \Omega_{r,0}}}\right] dx, \tag{2.181}$$

haciendo $y = \Omega_{m,0} x + \Omega_{r,0}$

$$H_0 t = \frac{2}{3\Omega_{m,0}^2} \left[(\Omega_{m,0} a + \Omega_{r,0})^{1/2} (\Omega_{m,0} a - 2\Omega_{r,0}) + 2\Omega_{r,0}^{3/2}\right]. \tag{2.182}$$

Cannot be easily inverted to give $a(t)$. Nevertheless $t = \frac{2}{3} a^{3/2}$ for matter only, and $t = \frac{1}{2} a^2$ for radiation, as expected.

Lemaitre models ($\Omega_{\Lambda,0} \neq 0$) but $\Omega_{r,0} = 0$

- Spatially flat $(\Omega_{m,0} + \Omega_{\Lambda,0} = 1)$

$$\dot{a}^2 = H_0^2[(1 - \Omega_{\Lambda,0}) a^{-1} + \Omega_{\Lambda,0} a^2] \qquad \rightarrow t = \frac{1}{H_0} \int_0^a \sqrt{\frac{x}{(1 - \Omega_{\Lambda,0}) + \Omega_{\Lambda,0} x^3}} dx, \tag{2.183}$$

writing $y^2 = x^3 |\Omega_{\Lambda,0}| / (1 - \Omega_{\Lambda,0})$, we have then

$$H_0 t = \frac{2}{3\sqrt{|\Omega_{\Lambda,0}|}} \int_0^{\sqrt{a^3 |\Omega_{\Lambda,0}| / (1 - \Omega_{\Lambda,0})}} \frac{dy}{\sqrt{1 \pm y^2}}, \tag{2.184}$$

with solutions

$$H_0 t = \frac{2}{3\sqrt{|\Omega_{\Lambda,0}|}} f(x) = \begin{cases} \sinh^{-1}[\sqrt{a^3|\Omega_{\Lambda,0}|(1-\Omega_{\Lambda,0})}], & \Omega_{\Lambda,0} > 0. \\ . & \\ \sin^{-1}[\sqrt{a^3|\Omega_{\Lambda,0}|(1-\Omega_{\Lambda,0})}], & \Omega_{\Lambda,0} < 0. \end{cases} \tag{2.185}$$

- Arbitrary spatial curvature ($\Omega_{k,0} = 1 - \Omega_{m,0} - \Omega_{\Lambda,0}$)

$$\dot{a}^2 = H_0^2(\Omega_{m,0}a^{-1} + \Omega_{\Lambda,0}a^2 + \Omega_{k,k}). \tag{2.186}$$

Quite complicated, but it may have solutions by using elliptical functions to get

$$a(t) = \left(\frac{3}{2}H_0\sqrt{\Omega_{m,0}t}\right)^{3/2} \quad \text{small t, radiation domination.} \tag{2.187}$$

$$a(t) \propto \exp\left(H_0\sqrt{\Omega_{\Lambda,0}}t\right) \quad \text{large t, } \Lambda \text{ domination.} \tag{2.188}$$

De-Sitter model ($\Omega_{m,0} = 0,\ \Omega_{r,0} = 0,\ \Omega_{\Lambda,0} = 1 \quad \rightarrow \quad k = 0$)

Not a true model but interesting to study, specially during inflation, and as we shall see in Dark Energy domination

$$\left(\frac{\dot{a}}{a}\right)^2 = H_0^2, \tag{2.189}$$

wit solutions of the form

$$a(t) = \exp[H_0(t - t_0)] = \exp[\sqrt{\Lambda/3}c(t - t_0)]. \tag{2.190}$$

Anti de-Sitter space (negative cosmological constant?).

Einstein static Universe

Before the discovery of the expansion, Einstein introduced the cosmological constant Λ to get $\dot{a} = \ddot{a} = 0$ which has the following implications

$$4\pi G\rho_{m,0} = \Lambda c^2 = \frac{c^2 k}{a^2}, \tag{2.191}$$

from the first equality (using the acceleration equation) we have that $\rho_{m,0} = 2\rho_{\Lambda,0}$ and $\Lambda > 0$, and from the second (using the Friedmann equation) we have that $k = 1$. However this type of universe is an unstable one.

2.11 Distances and Horizons

Now we have all the components of the universe and its dynamics, let's see how they may affect the distances in the universe.

The **particle horizon** is the distance light could have travelled since the origin of the universe. Regions further apart could never have been causally connected. In a time dt light travels a comoving distance $d\chi = cdt/R$, thus the total comoving distance travelled since the big-bang corresponds to,

$$\chi_{\rm p} \equiv c \int_0^t \frac{dt}{R(t)}. \tag{2.192}$$

considering

$$dz = d(1+z) = d\left(\frac{R_0}{R}\right) = -\frac{R_0}{R^2} dR = -\frac{R_0}{R^2}\dot{R}dt = -(1+z)H(z)dt, \tag{2.193}$$

therefore,

$$\chi_{\rm p} = \frac{c}{R_0}\int_0^R \frac{dR}{R^2 H(R)} = \frac{c}{R_0}\int_z^\infty \frac{dz}{H(z)}. \tag{2.194}$$

We must know how $H(z)$ varies with z, which requieres knowledge of the evolution of the scale factor. No information could have propagated further than $\chi_{\rm p}$ on the comoving grid since the beginning of time [33].

Moreover, by changing the order of integration of (2.194), we can also define the *comoving distance* $d_{\rm c}$, or **event horizon**, as the distance light could have travelled between a source at scale factor R and an observer today [33], as

$$\chi_{\rm e} = c\int_t^{t_0} \frac{dt}{R(t)} = \frac{c}{R_0}\int_0^z \frac{dz}{H(z)}. \tag{2.195}$$

Considering the FRW metric in terms of the conformal time (2.72), the distance multiplying the solid angle provides the *metric distance*

$$d_{\rm m} = S_k(\chi). \tag{2.196}$$

In a flat universe ($k = 0$) the metric distance is equal to the comoving distance χ. We emphasize that the comoving distance $d_{\rm c}$ and the metric distance $d_{\rm m}$ are not observables.

A related concept is the *proper distance* $d_{\rm p}$ corresponding to the particle horizon:

$$d_{\rm p}(t) \equiv cR(t)\int_0^t \frac{dt}{R(t)} = R(t)\chi_{\rm p}(t). \tag{2.197}$$

Regions separated by distances greater that the proper distance $d_{\rm p}$ are not causally connected. Furthermore, the *Hubble radius* or *Hubble distance* is defined by

$$d_{\rm H}(t) = cH^{-1}(t). \tag{2.198}$$

The Hubble distance $d_{\rm H}(t)$, often described simply as the *'horizon'* and corresponds to the typical length-scale over which physical processes in the universe operate coherently. It is also the length-scale at which general-relativistic effects become important; on scales much less than $d_{\rm H}(t)$ (within the horizon), Newtonian theory is often sufficient to describe the effects of gravitation [56].

We also introduce the *comoving Hubble distance* as:

$$\chi_{\rm H} = \frac{d_{\rm H}(t)}{R(t)} = \frac{c}{H(t)R(t)} = \frac{c}{\dot{R}(t)}, \tag{2.199}$$

which gives the χ-coordinate corresponding to the Hubble distance.

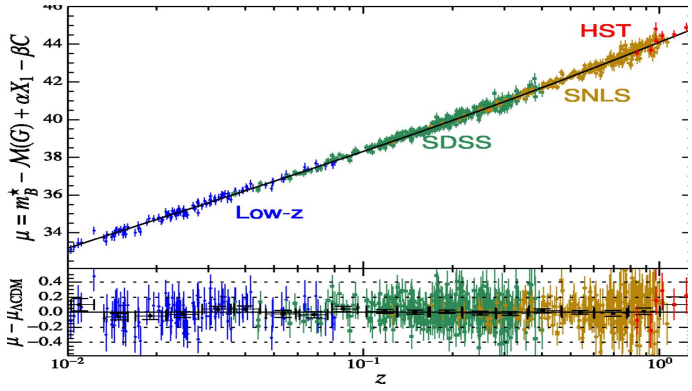

Figure 2.21: Supernovae

A classical way of measuring distances in astronomy is to measure the flux from an object of known luminosity, for example from Supernovae Type Ia (SNe Ia). Let us consider the observed flux F_o at a distance d_L from an emitting source of known luminosity L_e (J s^{-1}):

$$F_o = \frac{L_e}{4\pi d^2}. \tag{2.200}$$

The quantity

$$d_L = \left(\frac{L_e}{4\pi F_o}\right)^{1/2} \tag{2.201}$$

is called the **luminosity distance** of the source.
In a FRW Universe, the proper area of this sphere is

$$A = 4\pi R^2(t_0) S_k^2(\chi). \tag{2.202}$$

The photon frequency received by an observer is redshifted by a factor

$$\frac{\nu_0}{\nu_e} = \frac{R(t_e)}{R(t_0)} = \frac{1}{1+z},$$

and also the rate of the photons that fall into the detector is also reduced by the same factor. Therefore, the observed flux will be

$$F(t_0) = \frac{L(t_e)}{4\pi[R_0 S_k(\chi)]^2} \frac{1}{(1+z)^2}.$$

Then, the *luminosity distance* d_L in terms of measurable quantities is

$$d_L(z) \equiv (1+z) R_0 S_k(\chi). \tag{2.203}$$

The distance-redshift relation is, in fact, one of the most important cosmological tests. This is because given the observables $H_0, \Omega_{i,0}$ and the expression (2.203) we can compute the luminosity distance to an object at any redshift z. Conversely, for a population of standard candles with absolute magnitude M, and apparent magnitude m, we can measure the object's distance modulus μ at a given redshift z, defined by

$$\mu \equiv m - M = 5 \log_{10} \left(\frac{d_L(z)}{1\text{Mpc}} \right) + 25. \tag{2.204}$$

Then, the relationship of μ with redshift allows us to estimate the luminosity distance and thereby constrain the cosmological parameters, as we will see in Chapter 17.

Another classical distance measurement in astronomy is to measure the angle $\delta\theta$ subtended by an object of known physical size l. The *angular distance* is then defined as

$$d_A = l/\delta\theta.$$

From the angular part of the FRW metric, we have

$$l = R(t_e) S(\chi) \delta\theta$$

so that

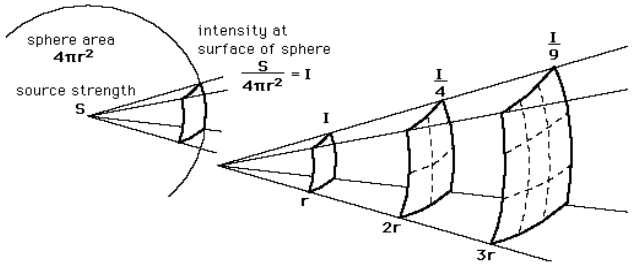

Figure 2.22: (jav: caption)

$$d_A = R(t_e)S(\chi) = R(t_0)\frac{R(t_e)}{R(t_0)}S(\chi) = \frac{R(t_0)S(\chi)}{1+z}.$$

Thus the angular distance is given by

$$d_{\rm A} \equiv \frac{R_0 S_k(\chi)}{(1+z)}, \tag{2.205}$$

or the comoving angular distance

$$d_{\rm M} = R_0 S_k(\chi). \tag{2.206}$$

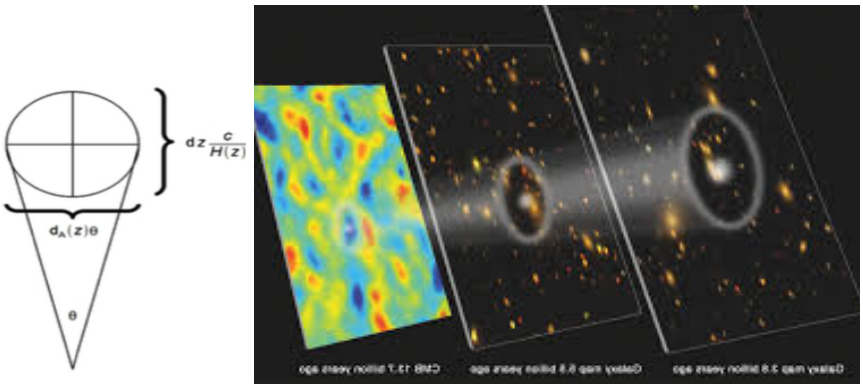

Figure 2.23: (jav: caption)

Curvature affects $D_M(z)$ both through its influence on $H(z)$ and through the geometrical factor. The luminosity distance (relevant to supernovae) is related to the angular distance by

$d_L = d_M(1+z)$.

Hubble tension: https://arxiv.org/pdf/2012.13932.pdf

Graduated paper, Fig 4: https://arxiv.org/pdf/2108.09239.pdf

If redshift-space distortions are weak, which is a good approximation for luminous galaxy surveys after reconstruction, but not for the LyaF, then the constrained quantity is the volume averaged distance

$$d_V(z) = [z d_H(z) d_M^2(z)]^{1/3}. \tag{2.207}$$

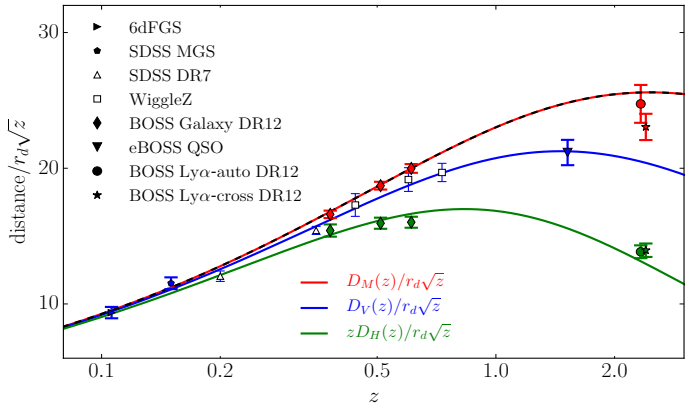

Figure 2.24: (jav: see: https://arxiv.org/pdf/1411.1074.pdf)

Figure 2.25 sketches the distances d_c, d_L and d_A in terms of redshift. It is worthwhile noticing that for small scales, all these distance measures coincide

$$d \simeq \frac{z}{H_0}, \tag{2.208}$$

where the linear evolution of distance with redshift is referred as the *Hubble law* [59].

2.11.1 Look-back time

A general expression for the look-back time

$$t_0 - t = \int_t^{t_0} dt = \int_0^z \frac{dz}{(1+z)H(z)} = \tag{2.209}$$

t emitted, and t_0 received.

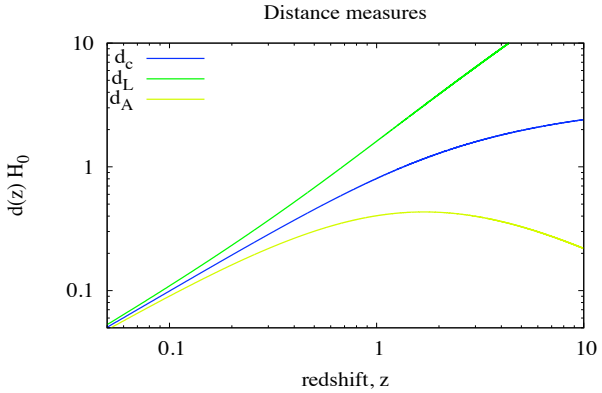

Figure 2.25: Comoving distance d_c, luminosity distance d_L, and angular distance d_A for a universe filled with the same constituents as in Figure 2.17. (jav: Add a dash line with different components. Use python)

$\Omega_{m,0}$	$\Omega_{\Lambda,0}$	H_0=50	70	90
1.0	0.0	13.1	9.3	7.2
0.3	0.0	15.8	11.3	8.8
0.3	0.7	18.9	13.5	10.5

Table 2.3: Age of the Universe (Gyr). Fijar parametros, usar w0=-1.5, -1, -0.5, wa=-0.5, 0, 0.5

$$t_0 - t = \int_0^z \frac{d\bar{z}}{(1+\bar{z})H(\bar{z})} \tag{2.210}$$

$$= \frac{1}{H_0}\int_{(1+z)^{-1}}^1 \frac{xdx}{\sqrt{\Omega_{m,0}x + \Omega_{r,0} + \Omega_{\Lambda,0}x^4 + \Omega_{k,0}x^2}} \tag{2.211}$$

The oldest star in globular clusters $t_{\rm star} \approx 11.5 \pm 1.3$ Gys, hence $t_0 > t_{\rm star}$.

2.11.1.1 Alternatives to the ΛCDM model

The ΛCDM model has had great success in modeling a wide range of astronomical observations. However, it is in apparent conflict with some observations on small-scales within galaxies (e.g. cuspy halo density profiles, overproduction of satellite dwarfs within the Local Group, amongst many others, see for example [**? ?**]). In addition, all attempts to detect WIMPs either directly in the laboratory, or indirectly by astronomical signals of distant objects have failed so far. Also, a large range of the particle parameters – predicted to be detectable – have thereby been

ruled out. For some of these reasons, it seems necessary to explore alternatives to the standard ΛCDM model. With this in mind, several alternatives have been suggested. For instance the Scalar Field Dark Matter (SFDM) model proposes the dark matter is a spin 0 bosson particle [**? ? ? ? ?**]; or the Self Interacting Dark Matter, as its name states, it relies on the cold dark matter to be made of self interacting particles [**?**]. On the other hand, in order to explain the accelerated expansion of the universe there exist different modifications to the theory of General Relativity, i.e. $f(R)$ theories [42**?**], braneworld models [**? ?**]. There are also several candidates to be the dark energy of the universe – alternatives to the cosmological constant –, i.e. scalar fields (quintessence, K-essence, phantom, quintom, non-minimally coupled scalar fields [**? ? ?**] ; or many more alternatives i.e. anisotropic universes [**? ? ?**]. Finally, if the dark energy is assumed to be a perfect fluid, then one of the most popular time-evolving parameterization for its equation of state consists of expanding ω in a Taylor series, for example the Chevallier-Polarski-Linder (CPL) $\omega = \omega_0 + \omega_a (1 - a)$, with two free parameters ω_0, ω_a [26, 87]. It may also be expanded into Fourier series [**?**] or many more Bayesian approaches have been suggested to account for a dynamical dark energy [**?**].

3

Inflation

Even though the Hot Big Bang model possesses a strong observational support, there are still certain inconsistencies or unexplained features to deal with: the flatness, horizon and monopole problems, amongst many others. The *inflationary model* offers the most elegant way so far proposed to solve these problems and therefore to understand why the universe is so remarkably in agreement with the standard cosmology. This model was initially introduced by Guth [48], followed by Linde [84]. For an extended review we refer to the textbooks Liddle and Lyth [81], Linde [85], Mukhanov [98]; and papers: Baumann [13], Liddle [77], Lyth and Riotto [88], Olive [101], Riotto [116]. The inflationary universe, Alan Guth, The first three minutes, Steven Weinberg, Endless Universe, P Steinhardt and N Turok. Let us examine some of the problems of the Hot Big Bang model.

3.0.1 Shortcomings of the Hot Big Bang

Flatness problem

HW: Show that a flat universe is an *unstable* fixed point if the strong energy condition is satisfied. hint: Show that the density parameter evolves with the scale factor a as:

$$\frac{d\Omega}{d\ln R} = (1+3w)\Omega(\Omega-1) \tag{3.1}$$

The Friedmann equation (2.158) can be seen in the following form

$$\Omega_T - 1 = \frac{kc^2}{(RH)^2}. \tag{3.2}$$

Written in this way, we notice that $\Omega_T = 1$ is a very special case. If at the beginning the universe was perfectly flat, then it remains so for all time. Nevertheless, a flat geometry is an unstable critical situation, that is, for even a tiny deviation from it, Ω_T would have evolved quite differently and very quickly the universe would become more curved. This can be seen as a consequence of RH being a decreasing function of time during radiation or matter domination epoch. We observe from (3.2) and Table 2.2 that:

$$\begin{aligned} |\,\Omega_T - 1\,| \quad &\propto t \qquad \text{radiation domination,} \\ |\,\Omega_T - 1\,| \quad &\propto t^{2/3} \qquad \text{dust domination.} \end{aligned}$$

Since the present age of the universe is estimated to be $t_0 \simeq 10^{17}\,\text{sec}$ [72], from the above equations we can deduce the required value of $|\,\Omega_T - 1\,|$ at different early-times in order to obtain the correct value of spatial-geometry at present time $|\,\Omega_{T,0} - 1\,|$. For instance, let us consider some particular epochs:

- Decoupling ($t \simeq 10^{13}\,\text{sec}$), we would need $|\,\Omega_T - 1\,| \leq 10^{-3}$.
- Nucleosynthesis ($t \simeq 1\,\text{sec}$), we would need $|\,\Omega_T - 1\,| \leq 10^{-16}$.
- Planck epoch ($t \simeq 10^{-43}\,\text{sec}$), we would need $|\,\Omega_T - 1\,| \leq 10^{-64}$.

Consequently, at early times $|\,\Omega_T - 1\,|$ had to be fine-tuned extremely close to zero in order to reach its actual observed value [67].

Figure 3.1: (jav: Figure that Ω_k drives away from a=1)

Horizon problem

The *horizon problem* is one of the most important problems within the Big Bang model, as it refers to the communication between different regions of the universe. The age of the universe

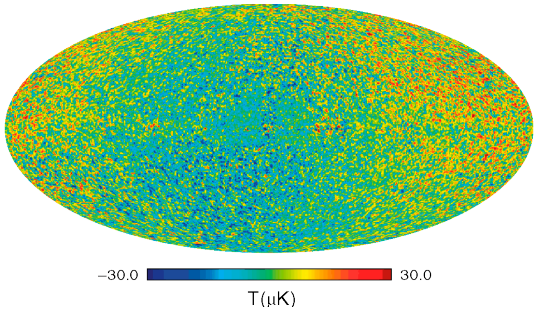

Figure 3.2: Temperature fluctuations observed in the CMB measured by the WMAP-7 experiment. The colour scale represents temperature fluctuations: from -30μK to 30μK. Figure reprinted from [72]. (jav: use an updated figure)

is finite and hence even light should have only travelled a finite distance by any given time. According to the standard cosmology, photons decoupled from the rest of the components at temperatures about $T_{\rm dec} \approx 0.3\,eV$ ($z_{\rm dec} \approx 1100$), from this time on photons free-streamed and travelled basically uninterrupted until reach us, giving rise to the region known as the *observable universe*. This spherical surface at which decoupling process occurred is called the *surface of last scattering*. The primordial photons are responsible for the CMB radiation we observe today. Looking at their fluctuations is thus analogous to taking a snapshot of the universe at that time (about $t_{\rm dec} \approx 380,000$ years after the Big Bang), as seen in Figure 3.2.

Figure 3.2 shows light seen in all directions of sky. These primordial photons have nearly the same temperature $T_{\rm cmb} = 2.725$ K plus small fluctuations (about one part in one hundred thousand). Being at the same temperature is a property of thermal equilibrium, hence observations are easily explained if different regions of the sky have been able to interact and moved towards thermal equilibrium before decoupling. Oddly, the comoving horizon over which causal interactions occurred before photons decoupled was significantly smaller than the comoving distance that radiation travelled after decoupling. This means that photons coming from sky regions separated by more than the horizon scale at last scattering, typically about 1°, would not have been able to interact and establish thermal equilibrium before decoupling. Therefore, the Big Bang model by itself does not offer an explanation of why temperatures seen in opposite directions of the sky are so nearly the same; the homogeneity must have been part of the initial conditions.

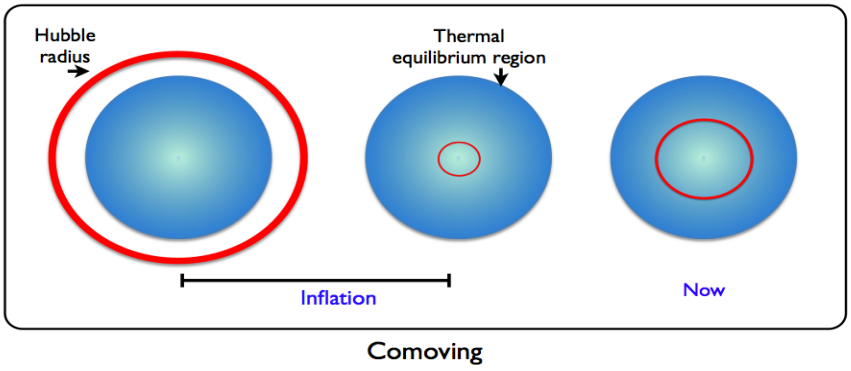

Figure 3.3: Schematic behaviour of the comoving Hubble radius during the Inflationary period (sketched by the red circle). (jav: Now should be CMB, check notes)

Monopole problem

The *monopole problem* was initially the motivation to develop the Inflationary cosmology [47]. The monopole, and other relics, are components of the universe that are expected to emerge as a consequence of unified models. From particle physics models, monopoles would have a mass of 10^6 orders the proton mass. Hence, based on their non-relativistic character, a crude calculation predicts an extremely high abundance at present time, $\Omega_{\mathrm{M},0} \simeq 10^{16}$ [29]. According to this prediction, the universe would be dominated by magnetic monopoles, in contrast with current observations: no one has found any monopole yet [5]. (jav: add textures, string, etc...)

3.0.2 Cosmological Inflation

Inflation is defined as the epoch in the evolution of the universe in which decreases the comoving horizon (comoving Hubble radius) or equivalently the scale factor is quickly accelerated in just a fraction of a second:

$$\text{INFLATION} \iff \frac{d}{dt}\left(\frac{1}{RH}\right) < 0, \tag{3.3}$$

$$\iff \ddot{R} > 0, \tag{3.4}$$

$$\iff \rho + 3p < 0, \tag{3.5}$$

$$\iff \epsilon \equiv -\frac{\dot{H}}{H^2} < 1. \tag{3.6}$$

HW: Probe the equivalence amongst the above relations.

The first term corresponds to the comoving Hubble radius (2.199), which is interpreted as the observable universe becoming smaller during the inflationary period (sketched by the red circle in Figure 3.3). This process allowed our present observable universe to lie within a region located well inside the Hubble radius early on during inflation [81].

Accelerated expansion:

Shrinking the comoving Hubble radius implies an accelerated expansion.

$$\frac{d}{dt}(RH)^{-1} = \frac{d}{dt}(\dot{R})^{-1} = -\frac{\ddot{R}}{\dot{R}^2} < 0 \quad \rightarrow \quad \ddot{R} > 0. \tag{3.7}$$

Slowly-varying Hubble parameter:

We introduce the fractional change of the Hubble parameter per e-fold ϵ, as

$$\frac{d}{dt}(RH)^{-1} = -\frac{\dot{R}H + R\dot{H}}{(RH)^2} = -\frac{1}{R}(1-\epsilon). \tag{3.8}$$

where the last term is defined as follows

$$\epsilon \equiv -\frac{\dot{H}}{H^2} = -\frac{d\ln H}{d\ln R} = -\frac{d\ln H}{dN} < 1. \tag{3.9}$$

where $dN \equiv d\ln R = Hdt$ defines de number of e-folds of the inflationary expansion. This represents that the fractional change of the Hubble parameter per e-fold is small, so the last term tell us that if ϵ is small, then inflation happens. The case $\epsilon = 0$ describes a de-Sitter space (H=constant). We want inflation to last for a sufficiently long time, then we introduce

$$\eta \equiv \frac{d\ln\epsilon}{dN} = \frac{\dot{\epsilon}}{H\epsilon} \tag{3.10}$$

therefore if ϵ needs to remain small for a sufficiently large number of Hubble times, then η should be a small quantity (we'll show that later) (jav: η here or better use conformal time as τ?)

$$|\eta| \ll 1. \tag{3.11}$$

Accelerated expansion:

From the acceleration equation, we can write the condition for inflation in terms of the required material to drive the expansion:

$$\epsilon = -\frac{\dot{H}}{H^2} = \frac{3}{2}\left(1+\frac{p}{\rho}\right) < 1 \quad \rightarrow \quad w = \frac{p}{\rho} < -\frac{1}{3}. \tag{3.12}$$

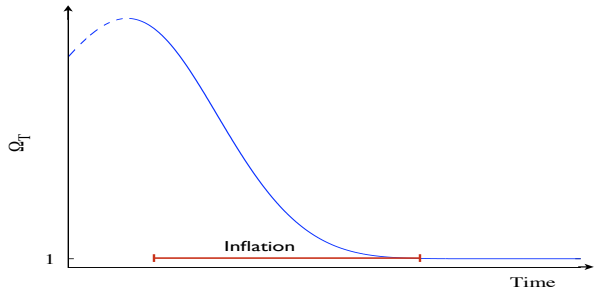

Figure 3.4: Evolution of the density parameter Ω_T, during the inflationary period. Ω_T is driven towards unity.

If this brief period of accelerated expansion occurred, then it is possible that the aforementioned problems of the Big Bang can be solved. However, because in standard physics it is commonly assumed ρ as positive, then to satisfy the acceleration condition it is necessary for the overall pressure to have $p < -\rho/3$.

Nonetheless, neither a radiation nor a matter dominated epoch satisfies such condition. A typical solution would be a universe dominated by a cosmological constant Λ at the earliest stages. As we have shown in Table 2.2, a cosmological constant leads to an exponential expansion, a *de Sitter stage*, and hence the condition (3.4) would be naturally fulfilled. Let us postpone for a bit the problem of finding a component which may satisfy this inflationary condition, and look what happens when a general solution is considered.

Flatness solution

If somehow there was an accelerated expansion, $1/(RH)$ tends to decrease with time, and hence from the expression (3.2), Ω_T is driven towards the unity rather than away from it. In this sense, inflation magnifies the curvature radius of the universe, so locally the universe seems to be flat with great precision, as shown in Figure 3.4. Then, we may ask ourselves by how much should $1/(RH)$ decrease. If the inflationary period started at time $t = t_i$ and ended approximately at the beginning of the radiation dominated era ($t = t_f$), then

$$\mid \Omega_T(10^{-34}\text{sec}) - 1 \mid_{t=t_f} \sim 10^{-54},$$

and

$$\frac{\mid \Omega_T - 1 \mid_{t=t_f}}{\mid \Omega_T - 1 \mid_{t=t_i}} = \left(\frac{R_i}{R_f}\right)^2 \equiv e^{-2N}. \tag{3.13}$$

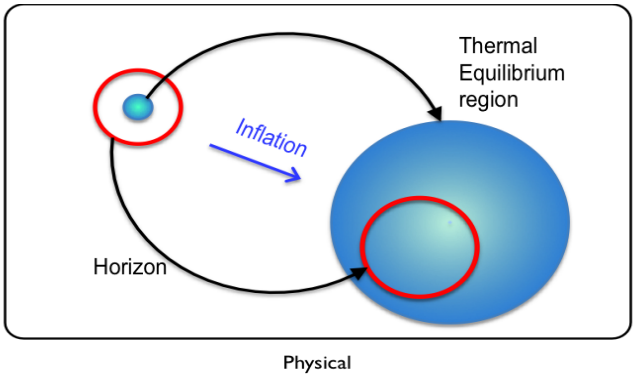

Figure 3.5: Physical evolution of the observable universe during the inflationary period.

So, the required condition to reproduce the value of $\Omega_{T,0}$ today is that inflation lasted for at least $N \equiv \ln R \gtrsim 50$, then Ω_T will be extraordinarily close to one that we still observe it today.

Horizon problem

During inflation the universe expanded drastically and there was a reduction in the comoving Hubble length. That is, a tiny region located inside the Hubble radius evolved and constituted our present observable universe, as seen in Figure 3.5, which represents the physical process of Figure 3.3. Scales that were outside the horizon at CMB decoupling were in fact inside the horizon before inflation. The region of space corresponding to the observable universe therefore was in thermal equilibrium before inflation and the uniformity of the CMB is essentially explained.

Monopole problem

The monopole problem is partially solved by noticing that during the inflationary epoch the universe led to a dramatic expansion over which the density of the unwanted particles were diluted away. Generating enough expansion, the dilution made sure that particles stayed completely out of our observable universe, making pretty difficult to localise any single monopole.

3.0.3 Single-field Inflation

As we have pointed out, a period of accelerated expansion can be created by a cosmological constant Λ, and hence solve the aforementioned problems. After a brief period of time, however, inflation must end and its energy be converted into conventional matter/radiation; this process is called *reheating*. In a universe dominated by a cosmological constant, the reheating process

is seen as Λ decaying into conventional particles. Nevertheless, claiming that Λ is able to decay is still a naive way to face the problem. On the other hand, scalar fields (spin-0 particles) can behave like a *dynamical cosmological constant*. There currently exists a broad diversity of models suggested to give rise the Inflationary period, see for instance [86, 88, 101]. Here, we limit ourselves to single scalar-field models based on general gravity, i.e. derived from the Einstein-Hilbert action. (jav: later present BD models, Higgs and so on) (jav: scalar field models, inflaton, curvaton, quintessence).

Let us consider a scalar field minimally coupled to gravity, with an arbitrary potential $V(\phi)$, specified by the action (jav: check Riotto for signature) (jav: Include the E-L equations for Scalar fields)

$$S = \int d^4x \sqrt{-g} \left[\frac{1}{2} \partial_\mu \phi \partial^\mu \phi - V(\phi) \right]. \tag{3.14}$$

From the action, the Euler-Lagrange equations with a FLRW universe ($\sqrt{-g} = R^3$) lead to the Klein-Gordon equation.

HW: obtener KG

$$\ddot{\phi} + 3H\dot{\phi} - \nabla^2\phi + V_{,\phi} = 0, \tag{3.15}$$

where the second term is referred as the friction due to the expansion.
The energy-momentum tensor corresponding to this scalar field is given by

$$T_{\mu\nu} = \partial_\mu \phi \partial_\nu \phi - g_{\mu\nu} \left[\frac{1}{2} \partial_\sigma \phi \partial^\sigma \phi - V(\phi) \right]. \tag{3.16}$$

By comparing (3.16) to the energy-momentum tensor of perfect fluids (2.130), one can identify an associated energy-density ρ_ϕ and pressure p_ϕ for the scalar-field. In a FRW background, they are found to be

$$T_{00} = \rho_\phi = \frac{1}{2}\dot{\phi}^2 + V(\phi) + \frac{1}{2}(\nabla\phi)^2, \tag{3.17}$$

$$T_{ii} = p_\phi = \frac{1}{2}\dot{\phi}^2 - V(\phi) + \frac{1}{6}(\nabla\phi)^2, \tag{3.18}$$

with its corresponding equation-of-state $p_\phi = w_\phi \rho_\phi$.

HW: Get ρ_ϕ and p_ϕ.

To provide a better understanding of the inflaton field, ϕ can be split up as

$$\phi(t, \mathbf{x}) = \phi(t) + \delta\phi(t, \mathbf{x}), \tag{3.19}$$

where $\phi(t)$ is considered a classical field, that is, the mean value of the inflaton field on the homogeneous and isotropic state; whereas $\delta\phi(t, \mathbf{x})$ describes the quantum fluctuations around $\phi(t)$ (we will see more about perturbations of the field $\delta\phi$ in Section **??**). The evolution equation for the background field ϕ is thus given by

$$\ddot{\phi} + 3H\dot{\phi} + \frac{dV}{d\phi} = 0. \tag{3.20}$$

From the structure of the effective energy-density and pressure, the Friedmann and the acceleration equations for a homogeneous single-scalar field become

$$H^2 = \frac{8\pi G}{3}\left[\frac{1}{2}\dot{\phi}^2 + V(\phi)\right], \tag{3.21}$$

$$\frac{\ddot{a}}{a} = -\frac{8\pi G}{3}\left[\dot{\phi}^2 - V(\phi)\right]. \tag{3.22}$$

with an analogous equation of state

$$w_\phi = \frac{\dot{\phi}^2 - 2V(\phi)}{\dot{\phi}^2 + 2V(\phi)}. \tag{3.23}$$

Therefore, the inflationary condition to be satisfied is $\dot{\phi}^2 \ll V(\phi)$, which is easily fulfilled with a suitable flat potential. Inflation is driven by the vacuum energy of the inflaton field $p_\phi \approx -\rho_\phi$.

(jav: If I use Friedmann and acceleration with p_ϕ and ρ_ϕ, combine them we get KG equation.)

3.0.4 Slow-Roll Inflation

HW: show that $\dot{H} = -4\pi G\dot{\phi}^2$.

By Substituting $\dot{H}$ into ϵ (Eqn. 3.9), we have

$$\epsilon = \frac{4\pi G\dot{\phi}^2}{H^2} = 3\left(\frac{\frac{\dot{\phi}^2}{2}}{\frac{\dot{\phi}^2}{2} + V(\phi)}\right) \tag{3.24}$$

Therefore, Inflation ($\epsilon \ll 1$) occurs when the kinetic energy $\frac{1}{2}\dot{\phi}^2$ makes a small contribution to the total energy $\dot{\phi}^2 \ll H^2 \sim \rho_\phi$, or equivalently $\dot{\phi}^2 \ll V(\phi)$.

Also, the acceleration of the scalar field has to be small or analogously the friction term in the KG equation is dominated by the cosmological expansion. By differentiating the above expression, $\dot{\phi}^2 \ll H^2$, we have

$$\begin{aligned} 2\dot{\phi}\ddot{\phi} &\ll 2H\dot{H} \sim -2H\dot{\phi}^2 \\ &\rightarrow \left|\frac{\ddot{\phi}}{H\dot{\phi}}\right| \ll 1. \end{aligned} \tag{3.25}$$

Then, we define the dimensionless acceleration per Hubble time.

$$\delta \equiv -\frac{\ddot{\phi}}{H\dot{\phi}}, \tag{3.26}$$

to get (3.10)

$$\begin{aligned} \dot{\epsilon} &= 8\pi G\left(\frac{\dot{\phi}\ddot{\phi}}{H^2} - \frac{\dot{\phi}^2\dot{H}}{H^3}\right), \\ \rightarrow \eta &= \frac{\dot{\epsilon}}{H\epsilon} = 2\left(\frac{\ddot{\phi}}{H\dot{\phi}} - \frac{\dot{H}}{H^2}\right) = 2(\epsilon - \delta), \end{aligned} \tag{3.27}$$

therefore, the slow-roll parameters

$$\{\epsilon, |\delta|\} \ll 1 \qquad \text{imply} \qquad \{\epsilon, |\eta|\} \ll 1. \tag{3.28}$$

So far, no approximations have been made.

3.0.5 Slow-Roll approximation

Based on the single scalar-field approach, it is useful to suggest a model starting with a nearly flat potential, i.e. initially satisfies the condition $\dot{\phi}^2 \ll V(\phi)$ (and its derivative $\ddot{\phi} \ll V_{,\phi}$). In this case the field is slowly rolling down on its potential; such an approximation is called *slow-roll inflation* [80, 82]. The equations of motion (3.20) and (3.21), under the slow-roll approximation, then become

$$\begin{aligned} \epsilon \ll 1 \qquad &\rightarrow \qquad \frac{1}{2}\dot{\phi}^2 \ll V(\phi) \sim H^2, \\ &\text{therefore} \qquad H^2 \simeq \frac{8\pi G}{3}V(\phi). \end{aligned} \tag{3.29}$$

$$\begin{aligned} |\delta| \ll 1 \qquad &\rightarrow \qquad \left|\frac{\ddot{\phi}}{H\dot{\phi}}\right| \ll 1 \\ &\text{therefore} \qquad 3H\dot{\phi} \simeq -\frac{dV}{d\phi}, \end{aligned} \tag{3.30}$$

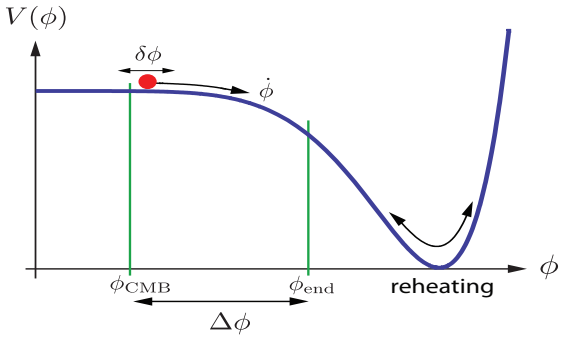

Figure 3.6: Schematic Inflationary process followed by a reheating epoch. Figure reprinted from [13].

The inflationary process can be summarised as an accelerated universe which takes place when the kinetic part of the inflaton field is subdominant over the potential $V(\phi)$ term. Then, when both quantities become comparable inflation ends giving rise to the *reheating process*. Figure 3.6 displays the schematic behaviour of the inflationary process. Also, the slow-roll approximation is consistent if the slope and curvature of the potential are small: $V_{,\phi}, V_{,\phi\phi} \ll V$. Thus, it is now useful to introduce the potential slow-roll parameters $\epsilon_{\rm v}$ and $\eta_{\rm v}$ in the following way [80]:

Combining the above equations, (3.24 and 3.29), we have

$$\epsilon = \frac{4\pi G\dot{\phi}^2}{H^2} \simeq \frac{1}{16\pi G}\left(\frac{V_{,\phi}}{V}\right)^2 \equiv \epsilon_{\rm v}(\phi), \tag{3.31}$$

and combining equations (3.9) and (3.26), with the differential of (3.30), it yields to

$$\epsilon + \delta = -\frac{\dot{H}}{H^2} - \frac{\ddot{\phi}}{H\dot{\phi}} \simeq \frac{1}{8\pi G}\frac{V_{,\phi\phi}}{V} \equiv \eta_{\rm v}(\phi),, \tag{3.32}$$

which define the *potential slow-roll parameters*; where $\epsilon_{\rm v}$ measures the slope of the potential and $\eta_{\rm v}$ its curvature

$$\epsilon_{\rm v}(\phi) \equiv \frac{1}{16\pi G}\left(\frac{V_{,\phi}}{V}\right)^2, \qquad |\eta_{\rm v}(\phi)| \equiv \frac{1}{8\pi G}\frac{|V_{,\phi\phi}|}{V}. \tag{3.33}$$

Equations (3.29) and (3.30) are in agreement with the slow-roll approximation when the following conditions hold

$$\epsilon_{\rm v}(\phi) \ll 1, \quad |\,\eta_{\rm v}(\phi)\,| \ll 1. \tag{3.34}$$

However, these conditions are necessary but not sufficient since even if the potential is flat, it may happen that the scalar field has a large velocity. Hence, one should also consider that the

condition $\dot{\phi}^2 \ll V(\phi)$ holds. Notice that ϵ and η are often called the *Hubble slow-roll parameters*, and during the slow-roll approximation these are related by

$$\epsilon_{\rm v} \simeq \epsilon, \qquad \eta_{\rm v} \simeq 2\epsilon - \frac{1}{2}\eta. \tag{3.35}$$

Within these approximations, it is straightforward to find out the scale factor R between the beginning (t_i) and end (t_e) of inflation, defined by $\epsilon(t_i) = \epsilon(t_e) \equiv 1$. Then, the e-fold number is

$$N_{tot} \equiv \int_{R_i}^{R_e} d\ln a = \int_{t_i}^{t_e} H(t)dt, \tag{3.36}$$

in slow-roll

$$Hdt = \frac{H}{\dot{\phi}}d\phi \simeq -3\frac{H^2}{V_{,\phi}}d\phi \simeq -8\pi G\frac{V}{V_{,\phi}}d\phi = \sqrt{8\pi G}\frac{d\phi}{\sqrt{2\epsilon_{\rm v}}},$$

and therefore

$$N_{tot} = \sqrt{8\pi G}\int_{\phi_i}^{\phi_e}\frac{d\phi}{\sqrt{2\epsilon_{\rm v}}}. \tag{3.37}$$

An estimate of the e-folds number $N(k)$ is given by [81]:

$$N(k) = 62 - \ln\frac{k}{a_0 H_0} + \text{corrections},$$

where the comoving wavenumber k is evaluated at the crossing Hubble radius during inflation. The last 'corrections' is a small term related with energy scales during the inflationary process. The precise value for the second quantity depends on the model as well as normalisation factors, however it does not present any significant change to the total amount of e-folds. Therefore, the value of the e-folds number is ranged to 50-70 [88].

The potential that describes a massive scalar field is given by:

$$V(\phi) = \frac{1}{2}m^2\phi^2. \tag{3.38}$$

Considering the slow-roll approximation, equations (3.29) and (3.30) become:

$$\begin{aligned} H^2 &\simeq \frac{4\pi G}{3}m^2\phi^2, \\ 3H\dot{\phi} &\simeq -m^2\phi. \end{aligned}$$

Thus, the dynamics of this type of model is described by

$$\begin{aligned} \phi(t) &= \phi_i - \frac{m}{\sqrt{12\pi G}}\, t, \\ R(t) &= R_i \exp\left[m\sqrt{\frac{4\pi G}{3}}\left(\phi_i t - \frac{m}{\sqrt{48\pi G}} t^2\right)\right], \end{aligned} \tag{3.39}$$

where ϕ_i and R_i represent the initial conditions at a given initial time $t = t_i$. The slow-roll parameters for this particular potential are computed from equations (3.33)

$$\epsilon_{\rm v} = \eta_{\rm v} = \frac{1}{4\pi G}\frac{1}{\phi^2}, \tag{3.40}$$

that is, an inflationary epoch takes place whilst the condition $|\phi| > 1/\sqrt{4\pi G} = \sqrt{2}M_{pl} \equiv \phi_e$[1] is satisfied, and the total amount that lapses during this accelerated period is encoded on the e-folds number

$$N = 2\pi G\left[\phi^2 - \phi_e^2\right] = 2\pi G\phi^2 - \frac{1}{2}. \tag{3.41}$$

The field value N e-folds before the end of inflation, to the scales relevant for the CMB is

$$\phi_{60} \sim 15 M_{pl}. \tag{3.42}$$

The steps shown before might, in principle, apply to any inflationary single-field model. That is, the general information we need to characterised cosmological inflation is specified by its potential.

[1] where $M_{pl}^2 = \frac{1}{8\pi G}$.

4

Thermal history of the Universe

Introduction

Does antimatter feel gravitational interaction in the same way than ordinary matter does? Even though this question might be in principle easy to answer with the obvious response: It does, since if they are massive, they must feel the gravitational interaction in the same way ordinary matter do. Nevertheless, there is still no experimental evidence to determine how antiparticles behave according to the gravitational interaction. In this paper some theoretical ideas and experimental attempts to answer this question are discussed.

Attraction under gravitational interaction

The first idea that someone might conjecture is that the behaviour of antimatter under the gravitational interaction shall be the same than the ordinary matter, i.e., an attractive behaviour among particles. This idea has been supported by arguing that otherwise (repulsion) it would violate CPT invariance (a fundamental symmetry of every physical theory) since C-symmetry does not modify the gravitational behaviour (mass) of particles/antiparticles. Moreover, energy conservation would not be hold leading to vacuum instability because in the case that matter and antimatter responded oppositely to a gravitational field, one could take advantage of the fact that no energy would be needed to move a pair particle-antiparticle. However all these ideas were later turned down in 1991[**?**].

Repulsion under gravitational interaction

In contrast, due to no experimental evidence has been found to confirm that antimatter should act attractively, some ideas have been proposed to support the thought that antimatter with repulsive behaviour should be valid. Therefore, one main idea in this direction is distinguished and was formulated by Kowitt's [**?**]. Inpired by Dirac's ideas about his propose of a particles sea, Kowitt proposed that a positron should act as hole within the sea of electrons of negative energy but possitive mass. Notice that this entails a modification on how C-inversion acts on particles/antiparticles,i.e., this would imply that a positron has positive energy but negative gravitational mass leading to gravitational repulsion.

Experimental tests

Since at high energies (small distances) the gravity is negligible, it is difficult to directly observe gravitational forces at the particle level, for instance, electromagnetic force dominates over the gravitational one for charged particles since this latter is much more weaker at these scales. However, some experiments such as cold neutral anti-hydrogen experiments have been realised [**?**], taking advantage of the fact that anti-hydrogen is electrically neutral, which open the possibility of a direct measurement about the attractive/repulsive nature of antimatter, however no overwhelming results were obtained. Therefore, some recent experiments with a better accuracy have been done recently in this direction [**?**], with the goal in mind of finding a definitive answer about this dilemma.

Conclusion

Since no experimental evidence about the nature of antimatter under gravitational interaction has been found, some ideas arguing a repulsive/attractive behaviour of antiparticles have been discussed. Finally, the ultimate theory describing antiparticles gravitational nature is still unclear and will be determined until overwhelming experimental evidence is found.

Hoyle-Narlikar theory of gravity

In cosmology, some alternatives to the Big Bang Theory of the evolution of the universe have been proposed. Among these alternative one can find the steady state model where the density of matter in the expanding universe remains unchanged due to a continuous creation of matter. Then, the Hoyle-Narikar theory of gravity is based upon this idea, and will be discussed on this paper.

Once we know what the Mach's principle says, we can define the Hoyle-Narlikar model as [6] a Machian and conformal theory of gravity proposed by Fred Hoyle and Jayant Narlikar that originally fits into the quasi-steady state model of the universe. This theory can be derived from the action

$$S = \sum_a \sum_b \int \int G(a,b)\, da\, db \quad , a \neq b.$$

where $G(a,b)$ is the Green function that holds the equation:

$$\Box G(x,y) + \frac{1}{6} R G(x,y) = \frac{\delta(x-y)}{\sqrt{-g}},$$

where g is the determinant of the spacetime metric.

On the other hand, although the Einstein's theory of relativity has been very successful, one can realise that since it does not provide boundary conditions, a whole family of possible solutions to describe our Universe is in general possible. In contrast, in the Hoyle-Narlikar theory of gravity one can find exactly that, a boundary condition. Interestingly, S. Hawking showed [**?**] that this boundary condition prohibits the existence of a solution type FLRW that is the best model that we have so far to describe our Universe. However, at that time the accelerating expansion of the universe was unknown, and this may allow the existence of such solutions. Furthermore, recently it has been shown[**?**] that in the limit of a smooth fluid model of particle distribution constant in time and space, the model can be reduced to Einstein's general relativity, and thus, FLRW Universe can be recovered.

Conclusion

The main ideas and features of the Hoyle-Narlikar theory of gravity have been discussed. Despite this model can recover Einstein's theory of gravity at a certain limit, perhaps the main problem

is still its nature as a quasi-steady state model, since these kind of models do not fit into the observational data of WMAP [**?**], and thus, its approach as a phenomenological model is still no viable.

Intro: we first considered the homogeneous and isotropic universe, and now we take care about its composition, that is, how the components form.
Some books: The first three minutes, Weinberg's. Baryogenesis, James M. Cline. Baryogenesis, Csaba Balazs (2014). The early universe, Turner.

4.1 History

Highly Speculative.

- $T \sim 10^{19}$GeV, $t \sim 10^{-43}$sec.
  Strings?, quantum gravity?, super gravity?, quantum birth of the Universe?.
  At these temperatures the Energy density is so high that the classical treatment of GR is no longer reliable, and perhaps the necessity of a *Quantum theory of Gravity*.

- $T \sim 10^{16}$GeV, $t \sim 10^{-38}$sec.
  Grand Unified Theories (GUT) phase transition occurs.
  Strong and electroweak interactions are indistinguishable.

- $T \sim 10^{14}$GeV, $t \sim 10^{-34}$sec.
  Inflation, Monopoles.
  Baryogenesis: Origin of matter-antimatter asymmetry.
  Relativistic QFT requires the existence of antiparticles $e^+ + e^- \to \gamma + \gamma$.

- $T \sim 10^{12}$GeV, $t \sim 10^{-30}$sec.
  Peccei-Quinn phase transition. Why QCD does not break CP-symmetry?.

- LHC - 13 TeV (Energies that can be reach).

- $T \sim 100$GeV, $t \sim 10^{-10}$sec.
  Electroweak phase transition.
  Particles receive their masses through the Higgs mechanism.

- $T \sim 10's - 100's$GeV, $t \sim 10^{-8}$sec.
  If dark matter is composed of SUper SYmmetric (SUSY) particles or WIMPs, this is when their interactions freeze out and their cosmological abundance is fixed.

- $T \sim 100 - 300$MeV, $t \sim 10^{-5}$sec.
  Quark-hadron phase transition.

This is when quarks and gluons first become bound into neutrons and protons (baryons - 3 quarks, mesons $\rightarrow q + \bar{q}$).

This is also when axions are produced (if they exist and are the dark matter) – Pretty sure this must have happened.

- $T \sim 0.1 - 10$MeV, $t \sim$ secs-mins.
  Big Bang Nucleosynthesis (BBN) ocurred.
  n^o and p^+ first combine to form D, ${}^3He$,${}^4He$,${}^7Li$.
  The theory agrees very impressively with observations.

- $T \sim 0.8$MeV, $t \sim 1000$sec.
  Neutrino decoupling.
  Neutrino only interacts with the primordial plasma through weak interaction.

- $T \sim 3$eV, $t \sim 10^{4-5}$yrs.
  Before the matter radiation equality $\rightarrow$ energy density is dominated by radiation.
  Perturbations in the dark-matter density can begin to grow.

- $T \sim$eV, $t \sim 400'000$yrs.
  Recombination: $e^- + p^+ \rightarrow H + \gamma$.
  e^- and p^+ combine to form hydrogen atoms.
  CMB and γ decouple $\rightarrow$ photons are tightly coupled to the baryon fluid through Thompson scattering from free e^-. CMB observations.

- $T \sim 10^{1-2}$eV, $t \sim$ millions of years.
  Baryon drag ends $\rightarrow$ baryons are still coupled to the CMB photons so perturbations in the baryon cannot grow.

- $T \sim 10^{-3}$eV, $t \sim 10^9$yrs.
  The first stars and (small) galaxies begin to form.

- $T \sim 0.33$meV, $t \sim 9$Gyr.
  Dark energy-matter equality.

- $T \sim 10^{-4}$eV, $t \sim 10^{10}$yrs.
  Baryons and CMB are entirely decoupled.
  Stars and galaxies have been around for a long time.
  Clusters of galaxies ($\sim$ 1000s) are becoming common.

- Dark Energy domination.

Event	time t	redshift z	temperature T
Inflation	10^{-34} s (?)	–	–
Baryogenesis	?	?	?
EW phase transition	20 ps	10^{15}	100 GeV
QCD phase transition	20 μs	10^{12}	150 MeV
Dark matter freeze-out	?	?	?
Neutrino decoupling	1 s	6×10^9	1 MeV
Electron-positron annihilation	6 s	2×10^9	500 keV
Big Bang nucleosynthesis	3 min	4×10^8	100 keV
Matter-radiation equality	60 kyr	3400	0.75 eV
Recombination	260–380 kyr	1100–1400	0.26–0.33 eV
Photon decoupling	380 kyr	1000–1200	0.23–0.28 eV
Reionization	100–400 Myr	11–30	2.6–7.0 meV
Dark energy-matter equality	9 Gyr	0.4	0.33 meV
Present	13.8 Gyr	0	0.24 meV

Figure 4.1: Thermal History of the Universe (jav: redo this figure)

4.1.1 The Hot Big Bang

The key to understand the thermal history of the universe is the comparison between the rate of interactions Γ and the rate of expansion H. When $\Gamma \gg H$, that is, when the time-scale of particle interactions t_c is much smaller than the characteristic expansion time-scale t_H, such that

$$t_c \equiv \frac{1}{\Gamma} \quad \ll \quad t_H \equiv \frac{1}{H}. \tag{4.1}$$

Therefore, local thermal equilibrium is then reached before the effect of expansion becomes relevant.

As the universe cools down, the rate of interactions may decrease faster than the expansion rate. When $t_c \sim t_H$ is reach, particles decouple from the thermal bath. Different particles may decouple at different times depending of its features, as we shall see below.

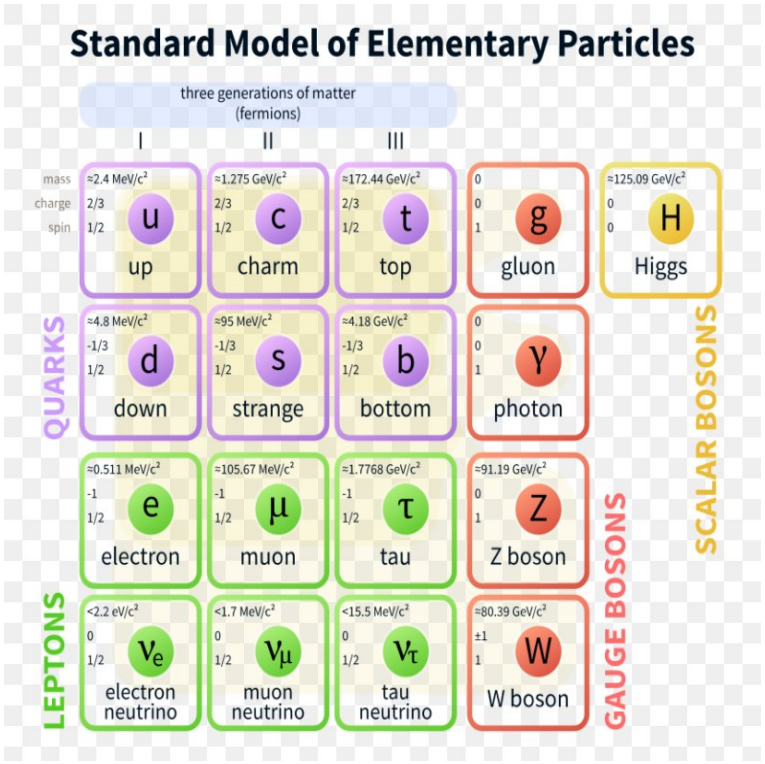

Figure 4.2: Thermal History of the Universe (jav: redo this figure)

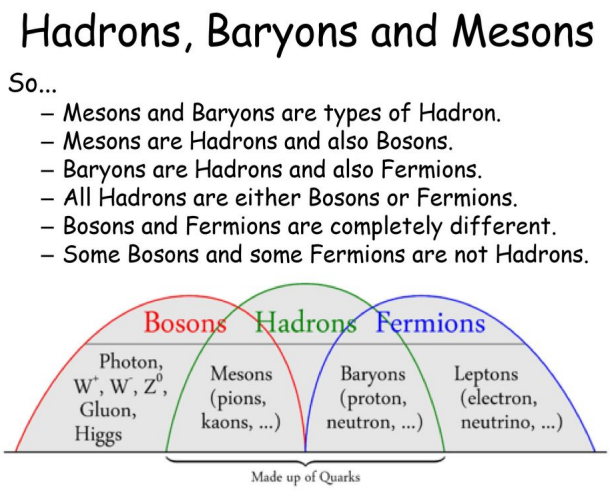

Figure 4.3: Thermal History of the Universe (jav: redo this figure)

4.1.2 Local Thermal equilibrium

Standard model $\gtrapprox$ 100GeV.

The rate of particle interactions can be defined as

$$\Gamma \equiv n\sigma v. \tag{4.2}$$

where

- n: number density of particles.
- σ: interaction cross section.
- v: average velocity of the particles.

For such temperatures ($T \geq 100$GeV), particles are ultra-relativistic $\rightarrow v \sim 1$. The particle mass can be ignored and therefore $n \sim T^3$. Interactions are mediated by *gauge bosons*, which are massless $\rightarrow$ the cross sections for strong and electroweak interactions is (jav: Feymann diagram, explain)

$$\sigma \sim \frac{\alpha^2}{T^2}, \tag{4.3}$$

where $\alpha \equiv \frac{g_A^2}{4\pi}$ is the generalized structure constant associated with the gauge boson A. Then

$$\Gamma = n\sigma v \sim T^3 \times \frac{\alpha^2}{T^2} = \alpha^2 T, \tag{4.4}$$

compare to the Hubble rate $H \sim \sqrt{\rho}/M_{Pl}$ with $\rho \sim T^4$,

$$H \sim \frac{T^2}{M_{Pl}^2}, \tag{4.5}$$

Then

$$\frac{\Gamma}{H} \sim \frac{\alpha^2 M_{Pl}}{T} \sim \frac{10^{16} GeV}{T}, \tag{4.6}$$

with $\alpha \sim 0.01$. Below $T \sim 10^{16}$GeV but above 100GeV the condition is therefore satisfied, and hence the standard model is in thermal equilibrium.

4.1.3 Equilibrium Thermodynamics

From CMB we observe that the early universe was in local thermal equilibrium.

Statistical mechanics: Turning the microscopic laws to understanding the macroscopic world, and its description is based on the *distribution function* $f(\vec{x}, \vec{p}, t)$:

- homogeneity $\rightarrow$ f independent of position $\vec{x}$.
- isotropy $\rightarrow$ momentum dependence is only in terms of its magnitude $p = |\vec{p}|$.

Therefore the particle density in phase space is then the density of states times the distribution function

$$\frac{g}{(2\pi)^3} \times f(p), \tag{4.7}$$

where g are the internal degrees of freedom (i.e. spin). The number density of particles (in real space) is then

$$n = \frac{g}{(2\pi)^3} \int d^3p f(p). \tag{4.8}$$

The energy density of a gas of particles assume that the particles in the early universe were weakly interactions $\rightarrow$ ignore interactions densities. Using $E(p) = \sqrt{m^2 + p^2}$, we get

$$\rho = \frac{g}{(2\pi)^3} \int d^3p f(p) E(p), \tag{4.9}$$

$$P = \frac{g}{(2\pi)^3} \int d^3p f(p) \frac{p^2}{3E}. \tag{4.10}$$

A system is said to be in *kinetic equilibrium* if the particles exchange energy and momentum efficiently. In this case, they can be differentiated by the Fermi-Dirac (+) and Bose-Einstein (-) distributions a temperature T

$$f(p) = \frac{1}{e^{(E-\mu)/T} \pm 1}, \tag{4.11}$$

where μ is the chemical potential. At low temperatures $(E - \mu) > T$ both reduce to Maxwell-Boltzmann distribution

$$f(p) \approx e^{-(E-\mu)/T}. \tag{4.12}$$

If a specie i is in chemical equilibrium, then its chemical potential μ_i is related to the chemical potential μ_j of the other species it interacts with. *Chemical equilibrium* implies that

$$\mu_1 + \mu_2 = \mu_3 + \mu_4. \tag{4.13}$$

Since the number of photons is not conserved (i.e. double compton $e^- + \gamma \rightleftharpoons e^- + \gamma + \gamma$) (jav: Compton is the Thompson low energy limit) hence $\mu_\gamma = 0$ and then if the chemical potential of a particle X is μ_X and the corresponding anti-particle $\bar{X}$ is $\mu_{\bar{X}} = -\mu_X$, then

$$X + \bar{X} \rightleftharpoons \gamma + \gamma. \tag{4.14}$$

Therefore *thermal equilibrium* is achieved for species that are both in kinetic and chemical equilibrium, that is, they share a common temperature $T_i = T$ ('Temperature of the Universe').

4.1.4 Densities and Pressure

Combining the previous equations, using that μ can be neglected (for now), we have

$$n = \frac{g}{2\pi^2}\int_0^\infty dp \frac{p^2}{\exp[\sqrt{p^2+m^2}/T]\pm 1}, \tag{4.15}$$

$$\rho = \frac{g}{2\pi^2}\int_0^\infty dp \frac{p^2\sqrt{p^2+m^2}}{\exp[\sqrt{p^2+m^2}/T]\pm 1}, \tag{4.16}$$

$$P = \frac{g}{6\pi^2}\int_0^\infty dp \frac{p^4(p^2+m^2)^{-1/2}}{\exp[\sqrt{p^2+m^2}/T]\pm 1} \tag{4.17}$$

These integrals have to be evaluated numerically, however in the (ultra) relativistic and non-relativistic limits, we can get analytical results. Some useful integrals:

$$\int_0^\infty d\xi \frac{\xi^n}{e^\xi - 1} = \zeta(n+1)\Gamma(n+1), \tag{4.18}$$

$$\int_0^\infty d\xi \xi^n e^{-\xi^2} = \frac{1}{2}\Gamma\left(\frac{1}{2}(n+1)\right), \tag{4.19}$$

with $\zeta(z)$ is the Riemann zeta-function, and

$$\frac{1}{e^\xi+1} = \frac{1}{e^\xi-1} - \frac{2}{e^{2\xi-1}} \tag{4.20}$$

In the relativistic limit ($T \gg m$)

Homework

$$n = \frac{\zeta(3)}{\pi^2} g T^3 \begin{cases} 1 & \text{bosons} \\ \frac{3}{4} & \text{fermions,} \end{cases} \tag{4.21}$$

$$\rho = \frac{\pi^2}{30} g T^4 \begin{cases} 1 & \text{bosons} \\ \frac{7}{8} & \text{fermions,} \end{cases} \tag{4.22}$$

$$P = \frac{\rho}{3}. \tag{4.23}$$

using the current temperature of the Universe $T_0 = 2.73$K.

$$n_{\gamma,0} = \frac{2\zeta(3)}{\pi^2} T_0^3 \approx 410 \text{ photons cm}^{-3}$$

$$\rho_{\gamma,0} = \frac{\pi^2}{15} T_0^4 \approx 4.6\times 10^{-34} \text{g cm}^{-4} \quad \rightarrow \quad \Omega_{\gamma,0} h^2 \approx 2.5\times 10^{-5}.$$

If we add the chemical potential, the excess of fermion species over its antiparticle, assuming $\mu_+ = -\mu_-$ ($X + \bar{X} \rightleftharpoons \gamma + \gamma$). The net particle number for $T \gg m$ (an exact result) is

Homework

$$\begin{aligned} n - \bar{n} &= \frac{g}{2\pi^2}\int_0^\infty dp p^2 \left(\frac{1}{e^{(p-\mu)/T}+1} - \frac{1}{e^{(p+\mu)/T}+1}\right) \\ &= \frac{1}{6\pi^2} g T^3 \left[\pi^2\left(\frac{\mu}{T}\right) + \left(\frac{\mu}{T^3}\right)^3\right]. \end{aligned} \tag{4.24}$$

The non-relativistic limit ($m \gg T$)

Homework

$$n = g\left(\frac{mT}{2\pi}\right)^{3/2} e^{-m/T}. \tag{4.25}$$

massive particles are exponentially rare at low temperature ($T \ll m$). In this limit $E(p) = \sqrt{p^2+m^2} \approx m$ and from the expressions (4.15) and (4.16) we have $\rho \approx mn$

$$P = nT \ll nm = \rho, \tag{4.26}$$

therefore $P \ll \rho$, non-relativistic gas of particles behaves as a pressurless matter or *dust*. $P = nT$ - ideal gas law (or $PV = Nk_BT$), and adding the chemical potential

$$n = g\left(\frac{mT}{2\pi}\right)^{3/2} e^{-(m-\mu)/T}, \tag{4.27}$$

$$n - \bar{n} = 2g\left(\frac{mT}{2\pi}\right)^{3/2} e^{-m/T} \sinh\left(\frac{\mu}{T}\right), \tag{4.28}$$

the excess of fermion species in the non-relativistic limit (compared to the relativistic limit) the n^o, e^-, p^+ fall exponentially (are *Boltzmann supressed*) as the temperature drops below the mass of the particle.

Interpretation of the annihilation of $X + \bar{X}$: At high energies the annihilation occurred but they are balanced by $X, \bar{X}$ production. At low temperatures the thermal particle energies are not sufficient for pair production.

4.1.5 Effective number of Relativistic Species

Let us consider the temperature of the photon gas as T. Then, the total radiation density is the sum over the energy densities of all relativistic species

$$\rho_r = \sum \rho_i = \frac{\pi^2}{30} g_*(T) T^4, \tag{4.29}$$

where $g_*(T)$ is the effective number of relativistic degrees of freedom at temperature T. There are two contributions:

- Relativistic species not in thermal equilibrium with photons $T_i \neq T \gg m_i$

$$g_*^{dec}(T) = \sum_{i=b} g_i \left(\frac{T_i}{T}\right)^4 + \frac{7}{8} \sum_{i=f} g_i \left(\frac{T_i}{T}\right)^4. \tag{4.30}$$

- Relativistic species in thermal equilibrium with photons, $T_i = T \gg m_i$

$$g_*^{ther}(T) = \sum_{i=b} g_i + \frac{7}{8} \sum_{i=f} g_i. \tag{4.31}$$

- At $T \gtrapprox$100 GeV, all particles of the Standard model are relativistic

$$g_b = 28, g_f = 90 \rightarrow g_* = g_b + \frac{7}{8} g_f = 106.75 \tag{4.32}$$

- As the temperature T drops, various species become non-relativistic and annihilate

- The heaviest particles (top q)[1] annihilate first at $T \sim$ 30GeV ($\frac{1}{6} m_t$), and the effective number of relativistic species is reduced

$$g_* = 106.75 - \frac{7}{8} \times 12 = 96.25. \tag{4.33}$$

- $W^{\pm}, Z^0$, Higgs boson (Gauge bosons) annihilate next, $T \sim$ 10GeV

$$g_* = 96.25 - (1 + 3 \times 3) = 86.25. \tag{4.34}$$

- b quarks follow

$$g_* = 86.25 - \frac{7}{8} \times 12 = 75.75. \tag{4.35}$$

[1] top q decays (99.8%) into W-boson, bottom, and less likely into strange or down. Its mean lifetime is about $\sim 5 \times 10^{-25}$s.

Quarks	t	174.2 ± 3.3GeV	$\bar{t}$	spin=$\frac{1}{2}$	$g = 2 \cdot 2 \cdot 3 = 12$	
	b	4.20 ± 0.07GeV	$\bar{b}$	3 colors		
	c	1.25 ± 0.09GeV	$\bar{c}$			
	s	95 ± 25MeV	$\bar{s}$			
	d	3–7MeV	$\bar{d}$			
	u	1.5–3.0MeV	$\bar{u}$			
						72
Gluons	8 massless bosons			spin=1	$g = 2$	16
Leptons	τ^-	1777.0 ± 0.3MeV	τ^+	spin=$\frac{1}{2}$	$g = 2 \cdot 2 = 4$	
	μ^-	105.658MeV	μ^+			
	e^-	510.999keV	e^+			
						12
	ν_τ	< 18.2MeV	$\bar{\nu}_\tau$	spin=$\frac{1}{2}$	$g = 2$	
	ν_μ	< 190keV	$\bar{\nu}_\mu$			
	ν_e	< 2 eV	$\bar{\nu}_e$			
						6
Electroweak gauge bosons	W^+	80.403 ± 0.029GeV		spin=1	$g = 3$	
	W^-	80.403 ± 0.029GeV				
	Z^0	91.1876 ± 0.0021GeV				
	γ	0 $(< 6 \times 10^{-17}$eV)			$g = 2$	
						11
Higgs boson (SM)	H^0	> 114.4GeV		spin=0	$g = 1$	1
						$g_f = 72 + 12 + 6 = 90$
						$g_b = 16 + 11 + 1 = 28$

Figure 4.4: Thermal History of the Universe (jav: redo this table)

- and finally c, τ quarks

$$g_* = 75.75 - \frac{7}{8} \times (12 + 4) = 61.75. \tag{4.36}$$

- Before strange annihilate the matter undergoes to the QCD phase transition $T \sim 150$MeV. quarks combine into baryons (p^+, n^0) and mesons (pions). All particles except pions $(\pi^\pm, \pi^0)$ are non-relativistic below T_{QCD} phase transition. Thus the only particle species left are pions, e^-, μ, ν, γ, therefore

$$g_* = \underbrace{2}_{\gamma} + 3 + \frac{7}{8} \times (4 + 4 + 6) = 17.25. \tag{4.37}$$

- Next, e^- & e^+ annihilate and we need the Entropy.

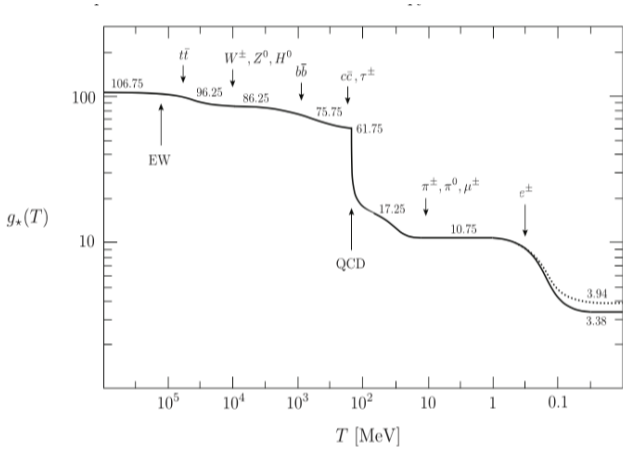

Figure 4.5: Thermal History of the Universe (jav: redo this figure)

4.1.6 Conservation of Entropy

It is useful to track a conserved quantity. To a good approximation we can therefore treat the expansion of the universe as adiabatic, so the total entropy stays constant [even beyond the equilibrium].

Homework

$$\frac{\partial P}{\partial T} = \frac{\rho + P}{T} \tag{4.38}$$

Consider the second law of Thermodynamics

$$TdS = dU + PdV, \tag{4.39}$$

Using $U = \rho V$

$$\begin{aligned} dS &= \frac{1}{T}\left(d[(\rho+P)V] - VdP\right) && (4.40)\\ &= \frac{1}{T}d\left[(\rho+P)V\right] - \frac{V}{T^2}(\rho+P)dT && (4.41)\\ &= d\left(\frac{\rho+P}{T}V\right) && (4.42) \end{aligned}$$

Let us show the conservation of entropy

$$\begin{aligned} \frac{dS}{dt} &= \frac{d}{dt}\left[\frac{\rho+P}{T}V\right] && (4.43)\\ &= \frac{V}{T}\left[\frac{d\rho}{dt} + \frac{1}{V}\frac{dV}{dt}(\rho+P)\right] + \frac{V}{T}\left[\frac{dP}{dt} - \frac{\rho+P}{T}\frac{dT}{dt}\right] = 0 && (4.44) \end{aligned}$$

The first term in equation resembles the continuity equation, while the second term is given by the homework. We just showed the conservation of entropy whilst in equilibrium.

It is convenient to work with the entropy density $s = S/V$. From dS we see that

$$s = \frac{\rho + P}{T}, \tag{4.45}$$

from ρ and P, we have (jav: still in relativistic limit)

$$s = \sum \frac{\rho_i + P_i}{T_i} \equiv \frac{2\pi^2}{45} g_{*S}(T) T^3 \tag{4.46}$$

4.1.7 Effective number of degrees of freedom in entropy

$$g_{*S}(T) = g_{*S}^{th}(T) + g_{*S}^{dec}(T), \tag{4.47}$$

notice that in thermal equilibrium

$$g_{*S}^{th}(T) = g_{*}^{th}(T), \tag{4.48}$$

for decoupled species

$$g_{*S}^{dec}(T) \equiv \sum_{i=b} g_i \left(\frac{T_i}{T}\right)^3 + \frac{7}{8} \sum_{i=f} g_i \left(\frac{T_i}{T}\right)^3 \neq g_{*}^{dec}(T). \tag{4.49}$$

Conservation of entropy has two consequences

1. The number of particles in a comoving volume is ($N \equiv Vn$) is proportional to the number density n_i divided by the entropy density $N_i \equiv \frac{n_i}{s}$. If no particles are produced or destroy (with $s \propto a^{-3}$) then $n_i \propto a^{-3}$ and N_i is constant. i.e. baryon number after baryogenesis

$$\frac{n_B}{s} \equiv \frac{(n_b - n_{\bar{b}})}{s}$$

2. It implies

$$g_{*S}(T) T^3 a^3 = const, \qquad \text{or} \qquad T \propto g_{*S}^{-1/3} a^{-1}. \tag{4.50}$$

Away from the particle mass thresholds g_{*S} is approximately constant and hence $T \propto a^{-1}$, as expected.

In the previous eq use $T \propto g_{*S}^{-1/3} a^{-1}$ into the Friedmann equation (jav: planck mass)

$$H = \frac{1}{a}\frac{da}{dt} \simeq \left(\frac{\rho_r}{3M_P^2}\right)^{1/2} \simeq \frac{\pi}{3}\left(\frac{g_*}{10}\right)^{1/2}\frac{T^2}{M_P}, \tag{4.51}$$

for a radiation dominated universe $a \propto t^{1/2}$ and for $T \propto t^{-1/2}$.

$$\frac{T}{1MeV} \simeq 1.5 g_*^{-1/4}\left(\frac{1sec}{t}\right)^{1/2} \tag{4.52}$$

The temperature of the Universe one second after the Big Bang was about 1MeV.

4.1.8 Neutrino decoupling

Neutrinos are coupled to the thermal bath via weak interactions processes like

$$\nu_e + \bar{\nu_e} \rightleftharpoons e^+ + e^-, \tag{4.53}$$

$$e^- + \bar{\nu_e} \rightleftharpoons e^- + \bar{\nu_e}. \tag{4.54}$$

The cross section for these interactions $\sigma \sim G_F^2 T^2$ and hence $\Gamma \sim G_F^2 T^5$. As the temperature decrease, the interaction rate dropped much more rapidly than the Hubble rate $H \sim T^2/M_P$ (jav: Mp)

$$\frac{\Gamma}{H} \sim \left(\frac{T}{1MeV}\right)^3. \tag{4.55}$$

Neutrinos decoupled around 1MeV (more accurately $T_{dec} \sim 0.8$MeV).

After decoupling, neutrinos move freely along geodesics and preserve the relativistic Fermi-Dirac distribution. The neutrino number density (and particle number conservation) requires $n_\nu \propto a^{-3}$ and therefore $T_\nu \propto a^{-1}$.

4.1.9 Electron-Positron Annihilation

Shortly after neutrinos decouple, T drops below the electron mass and electron positron annihilation occurs:

$$e^+ + e^- \rightleftharpoons \gamma + \gamma. \tag{4.56}$$

The energy density and entropy of the electron and positron are transferred to the photons, therefore the photons are thus 'heated'.

Consider the change in the effective number of degrees of freedom in entropy

$$g_{*S}^{th} = \begin{cases} 2 + \frac{7}{8} \times 4 & T \gtrsim m_e \\ 2 & T < m_e \end{cases} \tag{4.57}$$

in equation $g_{*S}^{th}(aT_\gamma)^3$ remains constant, therefore aT_γ increases after $e^+ + e^-$ annihilation by a factor $\left(\frac{4}{11}\right)^{1/3}$, while aT_ν remains the same. Hence, the temperature of neutrinos after the $e^+ + e^-$ annihilation is slightly lower

$$T_\nu = \left(\frac{4}{11}\right)^{1/3} T_\gamma. \tag{4.58}$$

For $T \ll m_e$, the effective number of relativistic species (in energy density and entropy)

$$g_* = 2 + \frac{7}{8} \times 2N_{\rm eff} \left(\frac{4}{11}\right)^{4/3} = 3.36 \tag{4.59}$$

$$g_{*S} = 2 + \frac{7}{8} \times 2N_{\rm eff} \left(\frac{4}{11}\right) = 3.94 \tag{4.60}$$

with $N_{\rm eff}$ is the effective number of neutrino species. It explains the previous plot.

If neutrino decoupling was instantaneous, then $N_{\rm eff} = 3$. Also that neutrino spectrum after decoupling deviates slightly from Fermi-Dirac distribution $N_{\rm eff} = 3.046$. Planck satellite constraints are $N_{\rm eff} = 3.36 \pm 0.34$.

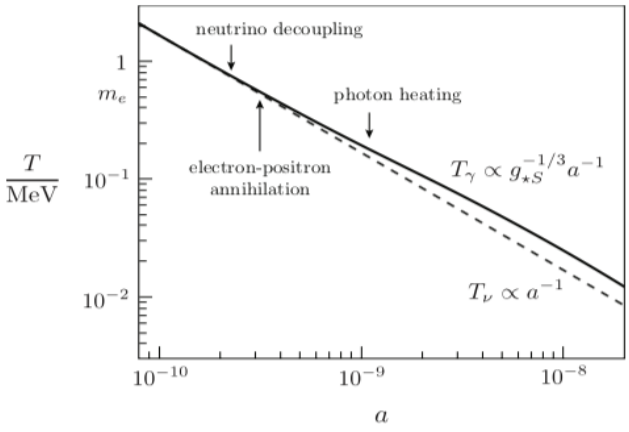

Figure 4.6: Thermal History of the Universe (jav: redo this fig)

4.1.10 Cosmic Neutrino Background

$$T_\nu = \left(\frac{4}{11}\right)^{1/3} T_\gamma \tag{4.61}$$

holds until the present day. $T_{\nu,0} = 1.95K = 0.17$meV, lower than the CMB.

The number density of neutrinos is

$$n_\nu = \frac{3}{4} N_{\rm eff} \times \frac{4}{11} n_\gamma, \tag{4.62}$$

using $n_{\gamma,0}$ implies 112 neutrinos cm^{-3} per flavour. If neutrinos are massless

$$\rho_\nu = \frac{7}{8} N_{\rm eff} \left(\frac{4}{11}\right)^{4/3} \rho_\gamma \rightarrow \Omega_\nu h^2 \approx 1.7 \times 10^{-5}. \tag{4.63}$$

however, neutrino oscillation experiments show that ν do have mass and the minimum $\sum m_{\nu,i} >$ 60meV. Massive neutrinos behave as radiation like particles in the early universe, and as matter-like particles in the late universe.

For massive neutrinos

$$\Omega_\nu h^2 \approx \frac{\sum m_{\nu,i}}{94eV}. \tag{4.64}$$

Observation of the CMB, SNIa constrain $\sum m_{\nu,i} < 1eV$, 25 times the energy density of photons but still subdominant $0.001 < \Omega_\nu < 0.02$ (jav: [?]).

Once Big Bang Nucleosynthesis is over, at time $t \sim 300s$ and temperature $T \sim 8 \times 10^8 K$, the Universe is a thermal bath of photons, protons, electrons, in addition to neutrinos and the unknown dark matter particle(s). The energy density is dominated by the relativistic component, photons and neutrinos.

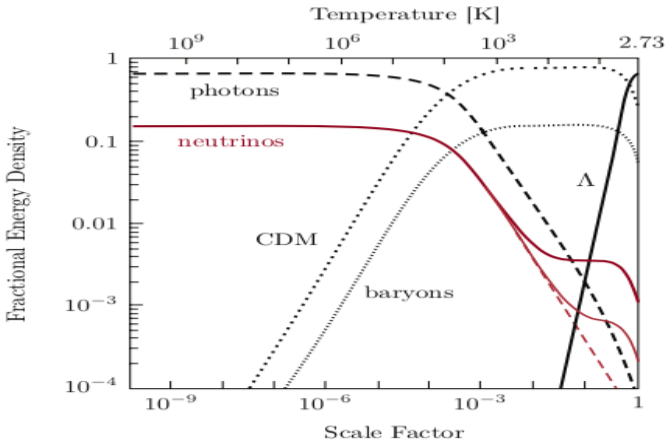

Figure 4.7: Thermal History of the Universe (jav: redo this fig)

5

Beyond the Equilibrium

(jav: add Boltzmann figure)

5.1 Recombination

An important event in the history of the early universe is the formation of the first atoms. At temperatures above about 1 eV, the universe still consisted of a plasma of free electrons and nuclei. Photons were tightly coupled to the electrons via Compton scattering, which in turn strongly interacted with protons via Coulomb scattering. There was very little neutral hydrogen. When the temperature became low enough, the electrons and nuclei combined to form neutral atoms (recombination), and the density of free electrons fell sharply. The photon mean free path grew rapidly and became longer than the horizon distance. The photons decoupled from the matter and the universe became transparent. Today, these photons form the cosmic microwave background.

5.1.1 Saha Equilibrium

Let us start at $T >$1eV, when baryons and photons were still in equilibrium through electromagnetic reactions such as

$$e^- + p^+ \rightleftharpoons H + \gamma. \tag{5.1}$$

Since $T < m_i$, $i = \{e, p, H\}$, we have the following equilibrium abundaces

$$n_i = g_i \left(\frac{m_i T}{2\pi}\right)^{3/2} \exp\left(\frac{\mu_i - m_i}{T}\right), \tag{5.2}$$

where $\mu_p + \mu_e = \mu_H$.

Consider the ratio

$$\left(\frac{n_H}{n_e n_p}\right)_{eq} = \frac{g_H}{g_e g_p}\left(\frac{m_H}{m_e m_p}\frac{2\pi}{T}\right)^{3/2} e^{m_p+m_e-m_H/T}, \tag{5.3}$$

we can use $m_H \approx m_p$ (but the difference $B_H \equiv m_p + m_e - m_H = 13.6\text{eV}$, the binding energy of Hydrogen). Also, the degrees of freedom $g_p = g_e = 2, g_H = 4$, and considers the universe is electrically neutral, hence $n_e = n_p$, therefore

$$\left(\frac{n_H}{n_e^2}\right)_{eq} = \left(\frac{2\pi}{m_e T}\right)^{3/2} e^{B_H/T}. \tag{5.4}$$

We wish to follow the *free electron fraction* defined as the ratio

$$X_e \equiv \frac{n_e}{n_b}, \tag{5.5}$$

where n_b is the baryon density

$$n_b = \eta n_\gamma = \eta \times \frac{2\zeta(3)}{\pi^2} T^3, \tag{5.6}$$

and η is the *baryon-to-photon ratio*, $\eta = 5.5 \times 10^{-10}(\Omega_b h^2/0.020)$.

The total baryon number density $n_b \approx n_p + n_H = n_e + n_H$, hence

$$\left(\frac{1-X_e}{X_e^2}\right)_{\text{eq}} = \frac{n_H}{n_e^2} n_b. \tag{5.7}$$

We arrive at the so-called Saha equation

$$\left(\frac{1-X_e}{X_e^2}\right)_{\text{eq}} = \frac{2\zeta(3)}{\pi^2}\eta\left(\frac{2\pi T}{m_e}\right)^{3/2} e^{B_H/T}. \tag{5.8}$$

Fig. (5.1) shows the redshift evolution of the free electron fraction as predicted both by the Saha approximation and by a more exact numerical treatment (see below). The Saha approximation correctly identifies the onset of recombination, but it is clearly insufficient if the aim is to determine the relic density of electrons after freeze-out.

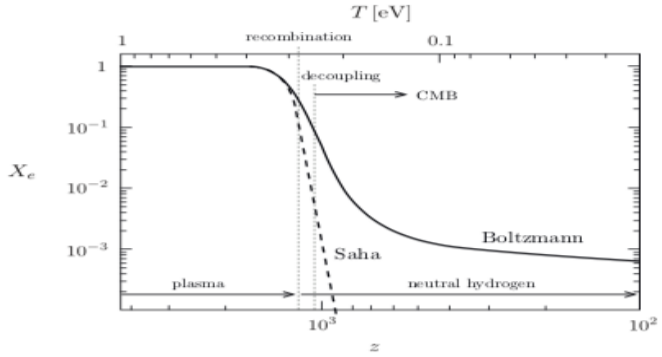

Figure 5.1: Free electron fraction as a function of redshift. (jav: redo)

5.1.2 Hydrogen Recombination

Let us define the recombination temperature $T_{\rm rec}$ as the temperature where $X_e = 10^{-1}$, i.e. when 90% of the electrons have combined with protons to form hydrogen. We find

$$T_{\rm rec} \approx 0.3eV \simeq 3600K. \tag{5.9}$$

Using $T_{\rm rec} = T_0(1 + z_{\rm rec})$, with $T_0 = 2.7$K, gives the redshift of recombination,

$$z_{\rm rec} \approx 1320. \tag{5.10}$$

Since matter-radiation equality is at $z_{\rm eq} \simeq 3500$, we conclude that recombination occurred in the matter-dominated era. Using $a(t) = (t/t_0)^{2/3}$, we obtain an estimate for the time of recombination

$$t_{\rm rec} = \frac{t_0}{(1 + z_{\rm rec})^{3/2}} \sim 290\ 000yrs. \tag{5.11}$$

Recombination was not an instantaneous process but proceeded relatively quickly nevertheless, with the fractional ionisation decreasing from $X = 0.9$ to $X = 0.1$ over a time interval $\Delta t \sim$ 70 000yrs. With the number density of free electrons dropping rapidly, the time when photons and baryons decoupled follows soon.

5.2 Photon Decoupling

Photons are most strongly coupled to the primordial plasma through their interactions with electrons, through Thomson scattering

$$e^- + \gamma \rightleftharpoons e^- + \gamma, \tag{5.12}$$

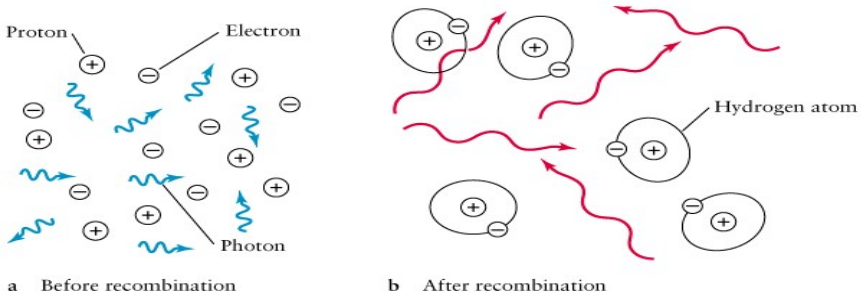

Figure 5.2: Recombination process.

i.e. the elastic scattering of electromagnetic radiation by a free charged particle. Thomson scattering is the low-energy limit of Compton scattering and is a valid description in the regime where the photon energy is much less than the rest-mass energy of the electron. An important feature of Thomson scattering is that it introduces polarization along the direction of motion of the electron

The mean free path for photons (the mean distance travelled between scattering) is

$$\lambda = \frac{1}{n_e \sigma_T}, \tag{5.13}$$

and therefore the interaction rate at which a photon undergoes scattering, given by

$$\Gamma_\gamma \approx n_e \sigma_T, \tag{5.14}$$

decreases as the density of free electrons drops. Where $\sigma_T \approx 2 \times 10^{-3}$ MeV^{-2} is the Thomson cross section. Since $\Gamma_\gamma \propto n_e$, the interaction rate becomes smaller than the expansion rate, and hence photons and electrons decouple roughly when

$$\Gamma_\gamma(T_{\rm dec}) \sim H(T_{\rm dec}), \tag{5.15}$$

$$\Gamma_\gamma(T_{\rm dec}) = n_b X_e(T_{\rm dec}) \sigma_T = \frac{2\zeta(3)}{\pi^2} \eta \sigma_T X_e(T_{\rm dec}) T_{\rm dec}^3. \tag{5.16}$$

and

$$H(T_{\rm dec}) = H_0\sqrt{\Omega_m}\left(\frac{T_{\rm dec}}{T_0}\right)^{3/2}. \tag{5.17}$$

we get

$$X_e(T_{\rm dec})T_{\rm dec}^{3/2} \sim \frac{\pi^2}{2\zeta(3)}\frac{H_0\sqrt{\Omega_m}}{\eta\sigma_T T_0^{3/2}}. \tag{5.18}$$

Using the Saha equation for $X_e(T_{\rm dec}) \sim 0.01$, we find

$$T_{\rm dec} \sim 0.27eV. \tag{5.19}$$

The redshift and time of decoupling are

$$z_{\rm dec} \sim 1100, \qquad t_{\rm dec} \sim 380\ 000 \text{ yrs}. \tag{5.20}$$

After decoupling the photons stream freely (their mean free path becomes very much longer): the Universe is now transparent to radiation. Observations of the cosmic microwave background today allow us to probe the conditions at last-scattering.

5.3 Last Scattering

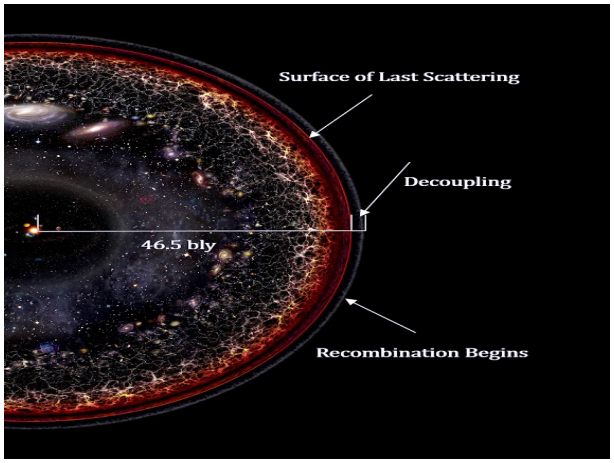

Figure 5.3: A summary of possible geometries. (jav: redo this figure)

After their last scattering off an electron, photons were able to travel unimpeded through the Universe. These are the Cosmic Microwave Background photons we receive today, still with their blackbody distribution, now redshifted by a factor of 1100. They constitute a last

scattering surface, or more appropriately a last scattering layer, since (obviously) not all photons underwent their last scattering simultaneously.

Of course, there is nothing special about this particular surface, other than it happens to be at the right distance for the photons to have reached us today. There are photons originating at every point, and observers in different parts of the Universe will see photons originating from different large spheres, of the same radius, centred on their location.

6

Big-Bang Nucleosynthesis

Big-Bang Nucleosynthesis refers to how the light elements like H, He and Li were synthesized in the Big Bang. In particular, the ratio of the density of helium to hydrogen

$$\frac{n_{He}}{n_H} \sim \frac{1}{16} \tag{6.1}$$

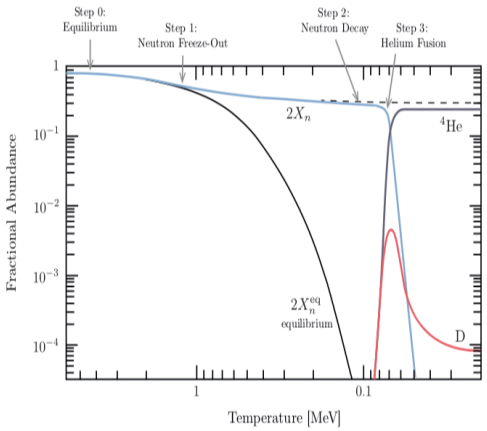

Figure 6.1: Helium production in the Universe

Step 0: Equilibrium Abundances

No elements heavier than Helium are produced. We need to track hydrogen, helium and isotopes: deuterium, tritium and ^{3}He.

At temperatures of order $T \approx 0.1$ Mev only free protons and neutrons exist $\rightarrow$ we need to solve for the neutron/proton ratio and use it for the synthesis of Deuterium, Helium, etc.

The Relative abundances of n^o and p^+

In the early universe, n^o and p^+ are coupled by weak interactions

$$\begin{aligned} n + \nu_{e^-} &\longleftrightarrow p^+ + e^- \\ n + e^+ &\longleftrightarrow p^+ + \bar{\nu}_{e^-} \end{aligned}$$

taking into account that μ_{e^-} and μ_ν are negligibly small, we have that $\mu_n = \mu_p$ and therefore

$$\left(\frac{n_n}{n_\rho}\right)_{eq} = \left(\frac{m_n}{m_p}\right)^{3/2} e^{-(m_n - m_p)/T}. \tag{6.2}$$

A fair assumption is the mass of neutron are comparable with the mass of the proton $m_n \sim m_p$ to get

$$\left(\frac{n_n}{n_p}\right)_{eq} = e^{-Q/T} \tag{6.3}$$

with $Q \equiv m_n - m_p$=1.3MeV, the bounding energy of hydrogen.

Therefore, for temperatures $T \gg 1MeV$ there are as many neutrons as protons. and for $T < 1MeV$ the neutron fractions gets smaller.

Next, Deuterium (isotope of hydrogen, with one p^+ and one n^o)

$$\begin{aligned} n + p^+ &\longleftrightarrow D + \gamma \\ \mu_n + \mu_p &= \mu_D \end{aligned}$$

$$\left(\frac{n_D}{n_n n_p}\right)_{eq} = \frac{3}{4}\left(\frac{m_D}{m_n m_p}\frac{2\pi}{T}\right)^{3/2} e^{-(m_D - m_n - m_p)/T} \tag{6.4}$$

using that the internal degrees of freedom ($g_D = 3$, $g_p = g_n = 2$), $2m_n \approx 2m_p \approx 1.9$ GeV and in the exponential binding energy of deuterium is given by$B_D \equiv m_n + m_p - m_D = 2.22$ MeV.

$$\left(\frac{n_D}{n_p}\right)_{eq} = \frac{3}{4} n_n^{eq}\left(\frac{4\pi}{m_p T}\right)^{3/2} e^{B_D/T} \tag{6.5}$$

To get an order of magnitude

$$n_n \sim n_b = \eta\ n_\gamma = \eta \frac{2\zeta(3)}{\pi^2} T^3 \tag{6.6}$$

$$\Rightarrow \quad \left(\frac{n_D}{n_p}\right)_{eq} \approx \eta \left(\frac{T}{m_p}\right)^{3/2} e^{B_D/T} \tag{6.7}$$

$\eta \rightarrow$ inhibits the production of deuterium until T drops well beneath the binding energy B_D (approximately up to $T \sim 0.1$MeV)

Step 1 Neutron Freeze-out

All neutrons incorporate into ^4He

Thermal equilibrium happend until $T_{dec} \sim 0.8$ MeV, where neutrinos decouple and then on we need $\rightarrow$ Boltzmann eqn.

Define the neutron fraction as $X_n \equiv \frac{n_n}{n_n + n_p}$

$$X_n^{eq}(T) = \frac{e^{-Q/T}}{1 + e^{-Q/T}} \tag{6.8}$$

Therefore,

$$\begin{aligned} &X_n^{eq}(0.8MeV) = 0.17 \\ &X_n^{\infty} \sim X_n^{eq}(0.8MeV) \sim \frac{1}{6} \end{aligned} \tag{6.9}$$

Step 2 Neutron decay

At temperatures $T > 0.2MeV$ ($t \sim 100$ sec) the lifetime of the neutron becomes important. Take the freeze-out abundance by an exponential decay factor

$$X_n(T) = X_n^{\infty} e^{-t/\tau_n} = \frac{1}{6} e^{-t/\tau_n} \qquad (\tau_n = 886.7 \pm 0.8 sec) \tag{6.10}$$

Step 3 Helium Fusion

The Universe is mostly made of p^+ and n^o and heavier nuclei have to be built sequentially from lighter nuclei in two-particle reactions.

First Deuterium

$$n + p^{+} \quad \longleftrightarrow \quad D + \gamma \tag{6.11}$$

Only when D is available can helium be formed (as long as enough free neutrons are available)

$$D + p^{+} \quad \longleftrightarrow \quad {}^{3}He + \gamma \tag{6.12}$$

$$D + {}^{3}He \quad \longleftrightarrow \quad {}^{4}He + p^{+} \tag{6.13}$$

• Abundance cannot be formed until sufficient deuterium has become available →, this effect is known as the *Deuterium bottle neck*. Only when there is enough Deuterium → the Helium is produced.

When Nucleosynthesis happened

When the Deuterium fraction in equation would be of order are i.e $(n_D/p)_{eq} \sim 1$, that is (using Eqn. (6.7))

$$T_{nuc} \sim 0.06MeV, \qquad \left(\frac{T}{1MeV}\right) \simeq 1.5 g_{*}^{-1/4} \left(\frac{1sec}{t}\right)^{1/2} \tag{6.14}$$

with $g_{*} = 3.38$

$$\Rightarrow \quad t_{nuc} = 120sec \left(\frac{0.1MeV}{T_{nuc}}\right)^{2} \sim 330sec \tag{6.15}$$

and from Eqn. (6.10)

$$X_n(t_{nuc}) \sim \frac{1}{8}. \tag{6.16}$$

Helium is produced almost immediately after deuterium, since two n^o go into one nucleus of the ${}^{4}He$

$$n_{He} = \frac{1}{2} n_n(t_{nuc}) \qquad \text{or} \tag{6.17}$$

$$\frac{n_{He}}{n_H} = \frac{n_{He}}{n_p} \simeq \frac{\frac{1}{2}X_n(t_{nuc})}{1 - X_n(t_{nuc})} \sim \frac{1}{2} X_n(t_{nuc}) \sim \frac{1}{16} \tag{6.18}$$

sometime as the mass fraction of Helium

$$\frac{4 n_{He}}{n_H} \sim \frac{1}{4}. \tag{6.19}$$

6.1 BBN as a Probe of BSM physics

The Helium mass fraction depends on several inputs parameters.

- g_* - The number of relativistic degrees of freedom determines H during the radiation era, therefore, $H \propto g_F^{1/2}$ and hence affects the freeze-out temperature.

$$G_F^2 T_F^5 \sim \sqrt{G_N g_*} T_F^2 \qquad \Rightarrow \qquad T_F \propto g_*^{1/6} \tag{6.20}$$

  $\Rightarrow$ increasing g_* increases T_F (weak force?)

  $\Rightarrow$ increases the n/p ratio at freeze-out

  $\Rightarrow$ increases the final helium abundance

- τ_n - Large neutron lifetime (15 mins 881.5 sec) would reduce the amount of neutron decay after freeze-out.

  $\Rightarrow$ increases the final helium abundance.

- Q Larger mass difference $(m_n - m_p)$ decreases the n/p ratio at freeze-out

  $\Rightarrow$ decreases the final helium abundance.

- η - The amount fo helium increases with increasing η as nucleosynthesis starts earlier for large baryon density.

- G_N - increasing the strength of gravity increases the freeze-out temperature $T \propto G_N^{1/6}$.

  $\Rightarrow$ increases the final helium abundance.

- G_F - increasing the weak force, decrease the freeze-out temperature $T_f \propto G_F^{-2/3}$.

  $\Rightarrow$ decrease the final helium abundance.

Changing the input, would change the predictions of BBN : BBN is a probe of fundamental physics.

6.2 Light Element Synthesis

The couple Boltzmann equation have to be solved numerically

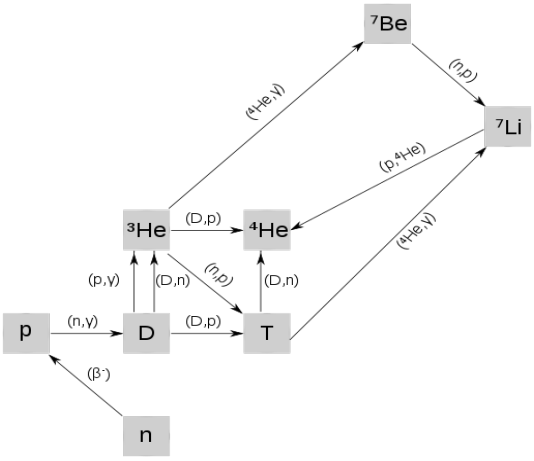

Figure 6.2: Helium production in the Universe

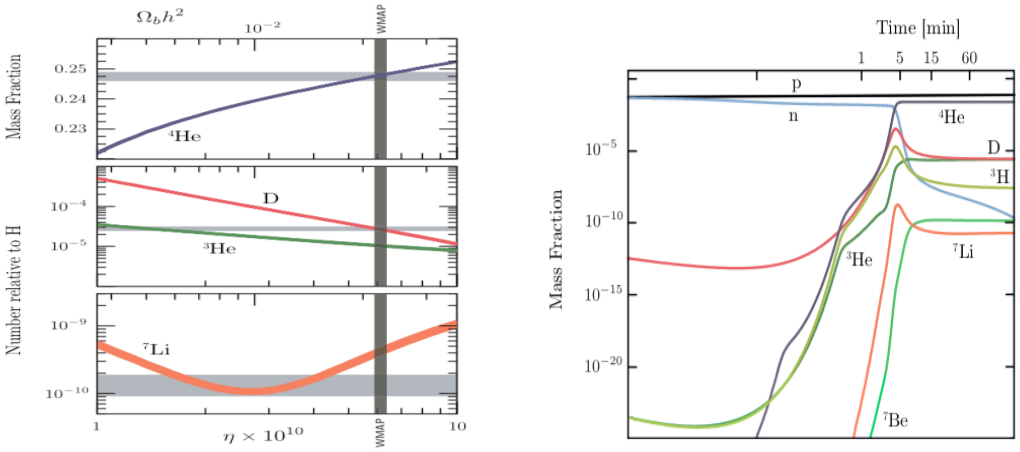

Figure 6.3: Helium production in the Universe

7

The Perturbed Universe

Introduction

As in many other areas oh physics, perturbation theory has been a powerful tool to aboard several problems such as calculations of the power spectra of the cosmic microwave background (CMB), recombination and so on, where the most relevant terms are linear [**?**]. Therefore, several approaches to perturbation theory in cosmology have been proposed, and in this paper the Lagrangian perturbation theory is discussed and contrasted with the Eulerian perturbation theory.

Eulerian perturbation theory

In comoving coordinates, the characteristic equation for this formalism is given by

$$\partial_t^2\delta + 2\frac{\dot{a}}{a}\partial_t\delta = \frac{1}{a^2}\nabla[(1+\delta)\nabla\phi] + \frac{1}{a^2}\partial_\alpha\partial_\beta\left[\frac{P^{\alpha\beta}}{\rho_b} + (1+\delta)v^\alpha v^\beta\right]. \tag{7.1}$$

where $\delta \equiv \rho/\overline{\rho} - 1$, with ρ the particles density. Also, v is the mean velocity of a space phase element, ϕ is a solution for the Poisson's equation, and $P^{\alpha\beta}$ is called the pressure tensor. Then, in the Eulerian regime

$$\delta \ll 1 \quad \text{and} \quad \left(\frac{vt}{d}\right)^2 \approx \delta \ll 1,$$

where d is for the coherence length of the perturbation and t its dynamical time, $t \approx (G\rho)^{-1/2}$. Furthermore, In linear perturbation theory the fluid equations assume the form

$$\partial_t\delta + \nabla\cdot\mathbf{v}a = 0 \quad \& \quad \partial_t^2\delta + 2\frac{\dot{a}}{a}\partial_t\delta = \frac{\nabla^2 p}{\rho_b a^2} + 4\pi G\rho_b\delta.$$

with a the scale FLRW scale factor.

Lagrangian perturbation theory

This approach to perturbation theory was proposed by Moutarde *et al* in 1991 [**?**]. And as in the Eulerian case, this formalism is written in comoving coordinates, and the equivalent characteristic equation (7.1) is given by

$$J(\tau, \mathbf{q})\nabla_x \ddot{x} = \beta(\tau)[J(\tau, \mathbf{q}) - 1], \tag{7.2}$$

with x the particles position and $\mathbf{q}$ the corresponding momentum. $J^{-1} = \delta - 1$ and $\beta = \frac{6}{\tau^2 + \Omega(k)}$. Notice that for any solution of (7.2), a divergence-free displacement field can be added, and this composition will be a solution as well. Then, in order to take this fact into account the following constraint is imposed

$$\nabla_x \times \dot{\mathbf{x}} = 0.$$

Finally, the equation to solve is obtained through $\Gamma \equiv \ddot{\mathbf{x}}$ as function of $\mathbf{q}$ as

$$\nabla_x \Gamma = J(\tau, \mathbf{q})^{-1} \sum_{i,j} \Gamma_{i,j} A_{ji},$$

where the A_{ij} are the cofactors of J.

Conclusion

An overview on the Lagrangian perturbation theory has been presented. In comparison with the Eulerian case, perturbative solutions are obtained by means of an iterative procedure. But in contrast, the expansion concerns the particles displacement field itself. Moreover, from Lagrangian perturbation theory is expected that its approach to non-linear regime might lead to finally understand deeply higher regimes. Then, it is hoped to obtain new and more precise results from this perturbation theory formalism in the future.

The homogeneous and isotropic model provides an accurate description of the physical properties of the universe on large scales: the expansion history and the evolution of its energy content. Nevertheless, at small scales homogeneity and isotropy are no longer valid approximations, and therefore we have to make use of a more complex theory to describe, for instance, the temperature anisotropies observed in the CMB and the matter distribution. We have seen that the temperature of the photons in the CMB presents small anisotropies compared to the background temperature $\Delta T/\bar{T} \sim 10^{-5}$. This tiny value supports the use of linear perturbation theory to predict accurately its statistical distribution. The idea of perturbation theory

is straightforward: perturb the metric and the stress-energy tensor in the Einstein's equations about the background and, to first order, drop products of small quantities. Then solve the coupled system of equations

$$\delta G_{\mu\nu} = 8\pi G \delta T_{\mu\nu}. \tag{7.3}$$

This section is aimed to present an outline of linear perturbation theory, but for an extended review, we refer to Bardeen [10], Dodelson [33], Hu and Dodelson [57], Kodama and Sasaki [66], Liddle and Lyth [81], Ma and Bertschinger [89], Mukhanov [98], Mukhanov et al. [99]; special attention is paid to the papers written by Challinor [24], Doran [36], Durrer [38], Knobel [65], Kurki-Suonio [70].

An outline of the theoretical concepts revised in this chapter is displayed in Figure 7.1 . The quantities shown in the bottom panel will allow us to establish the connection with current and future cosmological observations, as we shall see in the next chapter.

7.1 Newtonian Perturbation Theory

On scales well inside the Hubble radius and when describing non-relativistic matter, Newtonian gravity is an adequate approximation of GR in cosmology.

Consider an ideal, self-gravitating non-relativistic fluid described by ρ, $P \ll \rho$, $\vec{u}$, $\vec{r}$ (vector position), t.

$$Continuity \quad : \quad \partial_t \rho + \nabla_{\vec{r}} \cdot (\rho \vec{u}) = 0, \qquad \text{(energy density conservation)}, \tag{7.4}$$

$$Euler \quad : \quad \partial_t \vec{u} + \vec{u} \cdot \nabla_{\vec{r}} \vec{u} = -\frac{1}{\rho} \nabla_{\vec{r}} \rho - \nabla_r \Phi, \qquad \text{(momentum conservation)}, \tag{7.5}$$

where $g = -\nabla_r \Phi$ is gravitational aceleration and $\partial_t \vec{u} + \vec{u} \cdot \nabla_r \vec{u}$ convective derivate (follows the fluid element as it moves).

$$Poisson : \qquad \nabla^2_{\vec{r}} \Phi = 4\pi G \rho, \tag{7.6}$$

and $\nabla^2_{\vec{r}} \Phi$ is the gravitational potential $\nabla^2_{\vec{r}} \Phi = 4\pi G \rho - \Lambda$.

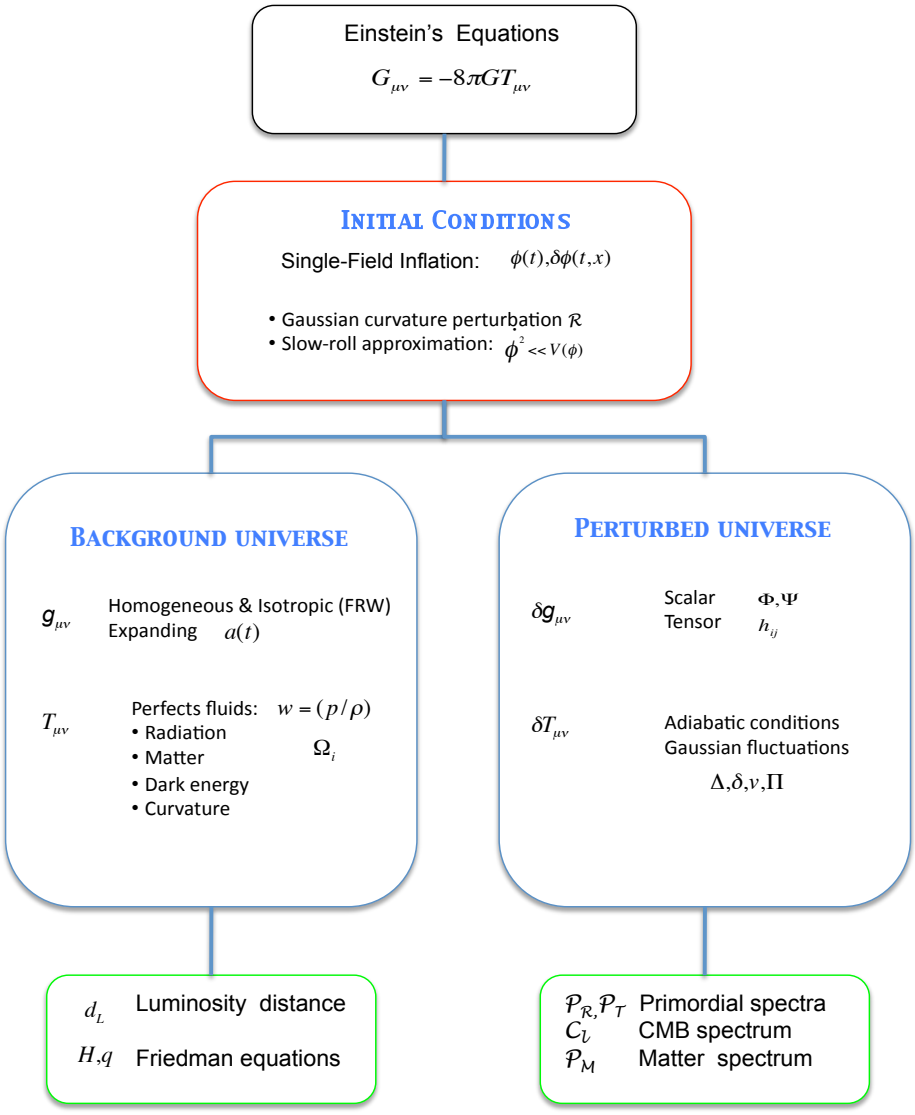

Figure 7.1: Outline of the theoretical concepts reviewed throughout this chapter.

7.1.1 Perturbation analysis

$$\rho \rightarrow \bar{\rho}(t) + \delta\rho \equiv \bar{\rho}(1+\delta). \tag{7.7}$$

$$P \rightarrow \bar{P}(t) + \delta P. \tag{7.8}$$

$$u \rightarrow a(t)H(t)\vec{x} + \vec{v}. \tag{7.9}$$

$$\Phi \rightarrow \bar{\Phi}(\vec{x}, t) + \phi. \tag{7.10}$$

$$\tag{7.11}$$

where we have introduced the density contrast δ as the fractional overdensity $= \delta\rho/\bar{\rho}$ density perturbation, and ϕ as the perturbed gravitational potential.

0-order

Consider a uniform expanding ball of fluid satisfying Hubble's law $\vec{u} = H(t)\vec{r}$ (from the perspective of the fluid equations).

Taking $\Phi = 0$ at $\vec{r} = 0$, we have from the Poisson equation

$$\frac{\partial}{\partial r}\left(r^2 \frac{\partial \Phi}{\partial r}\right) = (4\pi G\rho - \Lambda)r^2, \tag{7.12}$$

$$\frac{\partial \Phi}{\partial r} = \frac{1}{3}(4\pi G\rho - \Lambda)r, \tag{7.13}$$

$$\Rightarrow \Phi = \frac{1}{6}(4\pi G\rho - \Lambda)r^2. \tag{7.14}$$

The Euler equation becomes

$$\frac{\partial H}{\partial t}\vec{r} + H^2\vec{r}\cdot\nabla_{\vec{r}}\vec{r} = -\frac{1}{3}(4\pi G\rho - \Lambda)\vec{r}, \tag{7.15}$$

$$\Rightarrow \frac{\partial H}{\partial t} + H^2 = \frac{1}{3}(\Lambda - 4\pi G\rho), \tag{7.16}$$

with $\vec{r}\cdot\nabla_{\vec{r}}\vec{r} = \vec{r}$. This is the Newtonian limit of one of Friedmann equations.

The continuity equation

$$\partial_t\rho + \nabla_{\vec{r}}\cdot[\rho(t)H(t)\vec{r}] = 0, \tag{7.17}$$

$$\partial_t\rho + 3\rho H = 0, \tag{7.18}$$

$$\frac{1}{\rho}\frac{\partial \rho}{\partial t} + \frac{3}{a}\frac{\partial a}{\partial t} = 0 \qquad \Rightarrow \rho \propto a^{-3}. \tag{7.19}$$

the dilution of the mass density by expansion, (7.16) y (7.19) have a first integral (exact) given by

$$-K = a^2\left(H^2 - \frac{8\pi G}{3}\rho - \frac{1}{3}\Lambda\right). \tag{7.20}$$

HW: Show K is a constant, hence a solution

$$\begin{aligned} -\frac{\partial K}{\partial t} &= 2a^2 H\left(H^2 - \frac{8\pi G}{3}\rho - \frac{1}{3}\Lambda\right) + a^2\left(2H\frac{\partial H}{\partial t} - \frac{8\pi G}{3}\frac{\partial \rho}{\partial t}\right) \\ &= a^2\left[2H^3 - \frac{16\pi G}{3}H\rho - \frac{2}{3}H\Lambda + 2H\left(-H^2 - \frac{4\pi G}{3}\rho + \frac{1}{3}\Lambda\right) + 8\pi G H\rho\right] \\ &= 0. \end{aligned}$$

Therefore,

$$H^2 - \frac{K}{a^2} = \frac{1}{3}(8\pi G\rho - \Lambda), \tag{7.21}$$

the intrinsic curvature of the surfaces of homogeneity .

Comoving coordinates

The position $\vec{r} = a(t)\vec{x}$, has velocity $\frac{d\vec{r}}{dt} = H(t)\vec{r}$, with $\vec{x}$ the comoving spatial coordinates

$$\left(\frac{\partial}{\partial t}\right)_{\vec{r}} = \left(\frac{\partial}{\partial t}\right)_{\vec{x}} + \left(\frac{\partial \vec{x}}{\partial t}\right)_{\vec{r}} \cdot \nabla_{\vec{x}} \tag{7.22}$$

$$= \left(\frac{\partial}{\partial t}\right)_{\vec{x}} - H(t)\vec{x}\cdot\nabla. \tag{7.23}$$

∇ is the gradient respect to $\vec{x}$ at fixed t and $\nabla_{\vec{r}} = a^{-1}\nabla$.

The velocity field

$$\vec{u} = \frac{d\vec{r}}{dt} = \frac{d(a\vec{x})}{dt} = aH\vec{x} + a\frac{d\vec{x}}{dt}, \tag{7.24}$$

the second term in the r.h.s. defines the peculiar velocity, which describes changes in the co-moving coordinates of fluid elements in time.

1st order

The continuity equation (on new coordinate system)

$$\left[\frac{\partial}{\partial t} - H\vec{x}\cdot\nabla\right][\bar{\rho}(1+\delta)] + \frac{1}{a}\nabla\cdot[\bar{\rho}(1+\delta)(Ha\vec{x}+\vec{v})] = 0, \tag{7.25}$$

(jav: falta un paso)

$$\underbrace{\partial_t\bar{\rho} + 3\rho H}_{0th-order} + \underbrace{(\partial_t\rho + 3\bar{\rho}H)\delta + \bar{\rho}\partial_t\delta + \frac{\bar{\rho}}{a}\nabla\cdot\vec{v}}_{1st-order} + \underbrace{\frac{\bar{\rho}}{a}(\vec{v}\cdot\nabla\delta + \delta\nabla\cdot\vec{v})}_{2nd-order} = 0, \tag{7.26}$$

In linear perturbation theory

$$\partial_t\delta + \frac{1}{a}\nabla\cdot\vec{v} = 0. \tag{7.27}$$

Homework

$$\partial_t\vec{v} + H\vec{v} = -\frac{1}{a\bar{\rho}}\nabla\delta\rho - \frac{1}{a}\nabla\phi. \tag{7.28}$$

$$\nabla^2\Phi = 4HGa^2\bar{\rho}\delta. \tag{7.29}$$

Scalar/vector descomposition

We can always decompose the vector $\vec{\mathrm{v}}$ as

$$\vec{\mathrm{v}} = \underbrace{\nabla v}_{scalar} + \underbrace{\vec{\mathrm{v}}_\perp}_{vector}, \tag{7.30}$$

where $\nabla\cdot\vec{\mathrm{v}}_\perp = 0$.

From the continuity equation, the vector part of $\vec{\mathrm{v}}$ does not lead to *clumping* of the matter.

• Since $\nabla\times\vec{\mathrm{v}} = \nabla\times\vec{\mathrm{v}}_\perp$, $\vec{\mathrm{v}}_\perp$ describes the vorticity of the fluid. In linear theory, the escalar and vector parts decouple.

• From perturbed Euler equation, take curl

$$\nabla\times\partial_t\vec{\mathrm{v}} = \partial_t(\nabla\times\vec{\mathrm{v}}_\perp) = -H\nabla\times\vec{\mathrm{v}}_\perp. \tag{7.31}$$

where the first equality uses the continuity equation, and from the second one we have that $\nabla \times \vec{v}_\perp$ decays as $1/a$ in a expanding universe.

Recalling $\nabla_r = a^{-1}\nabla$, the physical vorticity $\nabla_r \times \vec{u} = a^{-1}\nabla \times \vec{v}_\perp$, then the vorticity falls as $1/a^2$, therefore **vector modes can be neglected**. For initial conditions from *inflation*, vector modes are *not excited* in the first place.

7.2 The Jean's length

The time derivate of the perturbed continuity equation (7.27)

$$\partial_t^2 \delta - \frac{1}{a} H \nabla \cdot \vec{v} + \frac{1}{a} \nabla \cdot \partial_t \vec{v} = 0, \tag{7.32}$$

using Euler (7.28) and Poisson (7.29)

$$\partial_t^2 \delta - \frac{1}{a} H \nabla \cdot \vec{v} - \frac{1}{a} \nabla \cdot \left(H \vec{v} + \frac{1}{a\bar{\rho}} \nabla \delta P + \frac{1}{a} \nabla \phi \right) = 0 \tag{7.33}$$

$$\Rightarrow \quad \partial_t^2 \delta - \frac{2}{a} H \nabla \vec{v} - \frac{1}{a^2 \bar{\rho}} \nabla^2 \delta P - \frac{1}{a^2} \nabla^2 \phi = 0 \tag{7.34}$$

$$\Rightarrow \quad \partial_t^2 \delta + 2H \partial_t \delta - 4\pi G \bar{\rho} \delta - \frac{1}{a^2 \bar{\rho}} \nabla^2 \delta P = 0. \tag{7.35}$$

The fundamental equation for the growth of structure in Newtonian theory. It shows the general competition between infall by gravitational attraction ($4\pi G \bar{\rho} \delta$) and pressure ($\nabla^2 \delta P$)

- Consider a barotropic fluid $P = P(\rho)$

$$\Rightarrow \quad \delta P = \frac{\partial P}{\partial \rho} \bar{\rho} \delta \equiv c_s^2 \bar{\rho} \delta, \tag{7.36}$$

where c_s^2 is the sound speed

If we Fourier expanding $\nabla^2 \to -k^2$

$$\partial_t^2 \delta + 2H \partial_t \delta + \left(\frac{c_s^2 k^2}{a^2} - 4\pi G \bar{\rho} \right) \delta = 0. \tag{7.37}$$

$$w^2 = \frac{c_s^2 k^2}{a^2} - 4\pi G \bar{\rho}. \tag{7.38}$$

(jav: add three cases, static w/o gravity, static w/ gravity and expanding)

Damped oscillator (in a expanding universe)

Provided that $\frac{c_s^2 k^2}{a^2} > 4\pi G\bar{\rho}$.

$\Rightarrow$ The Pressure support gives rise to acoustic oscillator (sound waves) in the fluid.

• However for $\frac{c_s^2 k^2}{a^2} < 4\pi G\bar{\rho}$ the system is unstable

proper wavelength $\lambda = 2\pi a/k$, $\lambda_J \equiv c_s^2\sqrt{\frac{\pi}{G\bar{\rho}}}$

perturbations with $\lambda > \lambda_J$ are gravitational unstable (experience power low-growth)

perturbations with $\lambda < \lambda_J$ pressure supports oscillations (fluctuations oscillate with decreasing amplitude)

8

Applications to cold-Dark matter

8.1 Solutions in a Einstein -de Sitter phase ($\bar{P} \approx 0,\ k = \Lambda = 0$)

Large scales

After matter-radiation equality, before dark energy dominates

$\Rightarrow$ Einstein -de Sitter model $P \approx 0$ and zero curvature or Λ

The fractional overdensity in the baryons δ_b approaches the CDM δ_c, and the matter behaves like a single pressure-free fluid whit a total density contrast

$$\delta_m = \frac{\bar{\rho}_b \delta_b + \bar{\rho_c} \delta_c}{\bar{\rho}_b + \bar{\rho_c}} \approx \delta_c \tag{8.1}$$

$c_s = 0$ for linearized CDM fluctuation $k << a^2$

Since $H^2 \propto \bar{\rho} \propto a^{-3}$, $a \propto t^{2/3} \Rightarrow H = \frac{2}{3t}$ and $4\pi G\bar{\rho} = \frac{2}{3t^2}$

• Scales of cosmological interest are much larger than Jean's scale ($k^2 \ll a^2$) for baryons and CDM fluctuations

$$\Rightarrow \quad \partial_m^2 \delta_m + \frac{4}{3t}\partial_t \delta_m - \frac{2}{3t^2}\delta_m = 0 \tag{8.2}$$

assuming $\delta_m \sim t^p$ we get that $\delta_m \propto t^{-1} \propto a^{-3/2}$, and $\delta_m \propto t^{2/3} \propto a$. The growing-mode $\rightarrow$ grows like scale factor.

In expanding universe $\rightarrow$ power law-growth of δ. Exponential growth predicted in a non-expanding universe (middle term cancels out)

• **The Poisson equation**

The gravitational potential is constant

$$-k^2\phi = 4\pi G \underbrace{\bar{\rho}}_{a^{-3}} \underbrace{\delta}_{a} a^2 = constant \tag{8.3}$$

for δ_r we need relativistic perturbation theory.

8.2 The Meszaros effect

CDM grows only logarithmically on scales inside the sound horizon during radiation domination

$$\partial_t^2 \delta_i + 2H\partial_t \delta_i - 4\pi G \sum_j \bar{\rho}_j \delta_j - \frac{1}{a^2 \bar{\rho}_i} \nabla^2 \delta P_i = 0 \tag{8.4}$$

$\nabla^2 \delta P_i$ we shall shows he properly when we develop relativistic perturbation theory

for CDM

$$\partial_t^2 \delta_c + 2H\partial_t \delta_c - 4\pi G \sum_j \bar{\rho}_j \delta_j = 0 \tag{8.5}$$

$$\partial_t^2 \delta_c + \frac{1}{t}\partial_t \delta_c - 4\pi G \bar{\rho}_c \delta_c = 0 \tag{8.6}$$

$a \propto t^{1/2}$, $H = \frac{1}{2t}$

$$\partial_t^2 \delta_c \sim H^2 \delta_c \sim \frac{8\pi G}{3} \bar{\rho}_r \delta_c \gg 4\pi G \bar{\rho}_c \delta_c \tag{8.7}$$

since $\bar{\rho}_r \gg \bar{\rho}_c$ during radiation domination

$$\partial_t^2 \delta_c + \frac{1}{t}\partial_t \delta_c = 0 \tag{8.8}$$

$\delta_c = constant$, $\delta_c \propto \ln t$

The effectively unclustered radiation reduces the growth of δ_c to only log
Need to wait until matter-domination so the DM density fluctuations grow significantly.

8.3 Late-time suppression of structure formation by Λ

Dark matter doesn't cluster

$$\partial_t^2 \delta_m + 2H\partial_t \delta_m - 4\pi G \bar{\rho}_m \delta_m = 0 \tag{8.9}$$

when dominates $a \propto e^{t\sqrt{\Lambda/3}}$, $H \simeq constant$, and $4\pi G\bar{\rho}_m \ll H^2 \sim \left(\frac{\Lambda}{3}\right) \sim \frac{8\pi G \rho_\Lambda}{3}$

$$\Rightarrow \quad \partial_t^2 \delta_m + 2H\partial_t \delta_m \simeq 0 \tag{8.10}$$

$\delta_m = constant$, $\delta_m \propto e^{-2t\sqrt{\Lambda/3}} \propto a^{-2}$, Λ suppresses the growth of structure [matter fluctuations]

Gravitational potential

$$-k^2\phi = 4\pi G \underbrace{\bar{\rho}}_{a^{-3}} \delta a^2 \quad \propto a^{-1} \tag{8.11}$$

This affects the integrated Sachs-Wolfe effect as we shall see later.

8.4 Evolution of baryon fluctuations after decoupling

The coupled dynamics of the baryon and CDM fluids after decoupling

$$\partial_t^2 \delta_b + \frac{4}{3t}\partial_t \delta_b = 4\pi G(\bar{\rho}_c \delta_b + \bar{\rho}_c \delta_c) \tag{8.12}$$

$$\partial_t^2 \delta_c + \frac{4}{3t}\partial_t \delta_c = 4\pi G(\bar{\rho}_c \delta_b + \bar{\rho}_c \delta_c) \tag{8.13}$$

substituting $\Delta \equiv \delta_c - \delta_b$, we have

$$\partial_t^2 \Delta + \frac{4}{3t}\partial_t \Delta = 0 \tag{8.14}$$

which has solutions $\Delta = constan$ or $\Delta \propto t^{-1/3}$ while δ_m has solutions t^{-1}, $t^{2/3}$, therefore

$$\frac{\delta_c}{\delta_b} = \frac{\bar{\rho}_m \delta_m + \bar{\rho}_b \Delta}{\bar{\rho}_m \delta_m - \bar{\rho}_c \Delta} \rightarrow \frac{\delta_m}{\delta_m} = 1. \tag{8.15}$$

9

Relativistic Perturbation Theory

Scales larger than the Hubble radius and for relativistic fluids (Newton is inadequate), basic idea:

- Perturb the metric
- Perturb the stress-energy tensor in Einstein equations
- For linear perturbations, drop products of small quantities

$$\delta G_{\mu\nu} = 8\pi G \delta T_{\mu\nu} + \Lambda \delta g_{\mu\nu}. \tag{9.1}$$

9.1 Perturbed Spacetime

$$g_{\mu\nu} = \bar{g}_{\mu\nu} + \delta g_{\mu\nu}, \tag{9.2}$$

where the background metric corresponds to the spatially-flat FRW metric

$$ds^2 = a^2(\eta)(d\eta^2 - \delta_{ij} dx^i dx^j) = a^2 \eta_{\mu\nu} dx^\mu dx^\nu, \tag{9.3}$$

with Friedmann equations, in conformal time

$$\mathcal{H}^2 = \frac{1}{3} a^2 (8\pi G \rho + \Lambda) \tag{9.4}$$

$$\dot{\mathcal{H}} = \frac{1}{6} a^2 [2\Lambda - 8\pi G(\rho + 3P)] \tag{9.5}$$

with $\mathcal{H}' \equiv \partial_\eta a/a = aH$. The most general perturbation to the background metric is (jav: why?)

$$ds^2 = a^2(\eta)\left\{(1+2\psi)d\eta^2 - 2B_i dx^i d\eta - [(1-2\phi)\delta_{ij} + 2E_{ij}]dx^i dx^j\right\}. \tag{9.6}$$

- ϕ, ψ are scalar functions of η and x^i

- B_i transforms like a three-vector

$$x^i \to x'^i, \quad B_i \to \frac{\partial x^j}{\partial x'^i} B_j. \tag{9.7}$$

- E_{ij} is symmetric ($E_{ij} = E_{ji}$) and trace-free ($\delta^{ij}E_{ij} = 0$) three-tensor

$$x^i \to x'^j, \quad E_{ij} \to \frac{\partial x^k}{\partial x'^i}\frac{\partial x^l}{\partial x'^j} E_{kl}. \tag{9.8}$$

latin indices on spatial vectors and tensors are raised and lowered with $\delta_{ij} \to B^i = \delta^{ij}B_j$, $E^i_j = \delta^{ik}E_{kj}$.

9.2 Scalar, vector and tensor decomposition

$$B_i = \underbrace{\partial_i B}_{\text{scalar}} + \underbrace{B_i^T}_{\text{vector}}. \tag{9.9}$$

The vector part is transverse (divergence free) $\delta^{ij}\partial_j B_i^T = 0$.

$$E_{ij} = \underbrace{\partial_{<i}\partial_{j>}E}_{\text{scalar}} + \underbrace{\partial_{(i}E_{j)}^T}_{\text{vector}} + \underbrace{E_{ij}^T}_{\text{tensor}}. \tag{9.10}$$

$$\partial_{<i}\partial_{j>}E \equiv \partial_i\partial_j E - \frac{1}{3}\delta_{ij}\nabla^2 E \qquad trace-free \tag{9.11}$$

E_{ij}^T is symmetric, trace-free and transverse $\partial^i E_{ij} = 0$.

$\delta^{ik}\partial_k E_{ij}^T = 0$ traceless, E_i^T is transverse $\partial^i E_i^T = 0$ (divergence-free).

For E_{ij}

- Scalar - one degree of freedom $E(\vec{x}, \eta)$, and they are ψ, ϕ, E, B

- Vector - two degrees of freedom, E_i^T - three components, but one constraint (divergence-vanishes) (they are E_i, B_i).
- Tensors - two degrees fo freedom, E_{ij}^T - five components but $\delta^{ij}\partial_k, E_{ij}^T$ are three constraints.

Total 4 + 4 + 2 = 10 degrees of freedom (Number of equations we need, - minus the coordinates)

9.3 Orthogornal frame vectors

To construct explicity an orthonormal frame of 4 vectors $(E_0)^\mu$ and $(E_i)^\mu$ in the perturbed metric

- Timelike $(E_0)^\mu$ - the 4 velocity u^μ of an observer at rest relative to the coordinate system

$$g_{\mu\nu}u^\mu u^\nu = 1 \qquad \bar{g}_{\mu\nu}\bar{u}^\mu\bar{u}^\nu = 1 \tag{9.12}$$

$$\delta g_{\mu\nu}\bar{u}^\mu u^\nu + 2\bar{u}_\mu \delta u^\mu = 0 \tag{9.13}$$

$(E_0)^\mu \sim u^\mu \qquad ? \to u^\mu = a^{-1}\delta^0_\mu \qquad \delta g_{00} = 2a^2\psi \qquad \to \delta u^0 = -\psi a^{-1}$

$(E_0)^\mu = a^{-1}\delta^\mu_0(1-\psi) \quad$ Since $g_{\mu\nu}(E_0)^\mu(E_0)^\nu = a^{-2}(1-2\psi)g_{00} = a^{-2}(1-2\psi)a^2(1+2\psi) = 1$

- Spacelike

$$(E_i)^\mu = a^{-1}[B_i\delta^\mu_0 + (1+\phi)\delta^\mu_i - E^j_i\delta^\mu_j] \tag{9.14}$$

$$g_{\mu\nu}(E_0)^\mu(E_i)^\nu = a^{-1}(1-\psi)g_{0\nu}(E_i)^\nu \tag{9.15}$$

$$= a^{-2}(1-\psi)[g_{00}B_i + g_{0i}(1+\phi) - g_{0j}E^j_i] \tag{9.16}$$

$$= B_i - B_i = 0 \tag{9.17}$$

Homework

$$g_{\mu\nu}(E_i)^\mu(E_j)^\nu = -\delta_{ij} \tag{9.18}$$

9.4 Matter perturbations

• Metric perturbations

$$ds^2 = a^2(\eta)\left\{(1+2\psi)d\eta^2 - 2B_i dx^i d\eta - [(1-2\phi)\delta_{ij} + 2E_{ij}]dx^i dx^j\right\}. \tag{9.19}$$

• Orthonormal frame vectors

$$(E_0)^\mu = a^{-1}(1-\psi)\delta_0^\mu - timelike. \tag{9.20}$$

$$(E_i)^\mu = a^{-1}[B_i\delta_0^\mu + (1+\phi)\delta_i^\mu - E_i^j\delta_j^\mu] - Spacelike. \tag{9.21}$$

In a orthonormal frame

$$T^{\hat{0}\hat{0}} = \bar{\rho}(\eta) + \delta\rho \quad energydensity \tag{9.22}$$

$$T^{\hat{0}\hat{i}} = q^i \quad momentumdensity \tag{9.23}$$

$$T^{\hat{i}\hat{j}} = [\bar{P}(\eta) + \delta P]\delta^{ij} - \Pi^{ij} \quad fluxof3momentum \tag{9.24}$$

where Π^{ij} is the trace-free anisotropic stress

If there're several contributions $T_{\mu\nu} = \sum_I T^I_{\mu\nu}$

$$\delta\rho = \sum \delta\rho_I, \quad \delta P = \sum \delta P_I, \quad q^i = \sum \delta q_I^i, \quad \Pi^{ij} = \sum_I \Pi_I^{ij} \tag{9.25}$$

SVT descomposition q_i,Π_{ij}

• Construct the coordinate components of $T^{\mu\nu}$, in terms of $T^{\mu\nu} = (E_\alpha)^\mu(E_\beta)^\nu T^{\hat{\alpha}\hat{\beta}}$

we can derive the above expressions by using

$$\bar{T}^{\mu}_{\nu} = (\bar{\rho} + \bar{P})\bar{U}^{\mu}\bar{U}^{\nu} - \bar{P}\delta^{\mu}_{\nu} \tag{9.26}$$

with

$$T^{\mu}_{\nu} = \bar{T}^{\mu}_{\nu} + \delta T^{\mu}_{\nu} \tag{9.27}$$

$$\delta T^{\nu}_{\mu} = (\delta\rho + \delta P)\vec{U}^{\mu}\vec{U}_{\nu} + (\vec{\rho}\vec{P})(\delta U^{\mu}U_{\nu} + U^{\mu}\delta U_{\nu}) - \delta P\delta^{\mu}_{\nu} - \Pi^{\mu}_{\nu}$$

$$\begin{aligned} T^{00} &= (E_0)^0(E_0)^0T^{\hat{0}\hat{0}} + 2(E_0)^0(E_i)^0T^{\hat{0}\hat{i}} + (E_i)^0(E_j)^0T^{\hat{i}\hat{j}} && (9.28)\\ &= a^{-2}(1-2\psi)\bar{\rho}(1+\delta) + \mathcal{O}(2) + \mathcal{O}(2) && (9.29)\\ &= a^{-2}\bar{\rho}(1+\delta-2\psi) && (9.30) \end{aligned}$$

$$\begin{aligned} T^{0i} &= (E_0)^0(E_0)^iT^{\hat{0}\hat{0}} + (E_0)^0(E_j)^iT^{\hat{0}\hat{j}} + (E_j)^0(E_0)^iT^{\hat{0}\hat{j}} + (E_j)^0(E_k)^iT^{\hat{j}\hat{k}} && (9.31)\\ &= 0 + a^{-2}\delta^i_j q^j + 0 + a^{-2}B_j\delta^i_k\bar{P}\delta^{jk} && (9.32)\\ &= a^{-2}(q^i + \bar{P}B^i) && (9.33) \end{aligned}$$

$$\begin{aligned} T^{ij} &= (E_0)^i(E_0)^jT^{\hat{0}\hat{0}} + (E_0)^i(E_k)^jT^{\hat{0}\hat{k}} + (E_k)^i(E_0)^jT^{\hat{k}\hat{0}} + (E_k)^i(E_l)^jT^{\hat{k}\hat{l}} && (9.34)\\ &= 0 + 0 + 0 + a^{-2}[(1+\phi)\delta^i_k - E^i_k][(1+\phi)\delta^j_l - E^j_l][(\bar{P}+\delta P)\delta^{kl} - \Pi^{kl}] && (9.35)\\ &= a^{-2}[\bar{P}\delta^{ij} + (2\bar{P}\phi + \delta P)\delta^{ij} - 2\bar{P}E^{ij} - \Pi^{ij}] && (9.36) \end{aligned}$$

things look neater (in mixed coordinate components)

$$\begin{aligned} T^0_0 &= g_{\mu 0}T^{0\mu} = g_{00}T^{00} + g_{0i}T^{0i} && (9.37)\\ &= a^2(1+2\psi)a^{-2}\bar{\rho}(1-2\psi+\delta)\mathcal{O}(2) && (9.38)\\ &= \bar{\rho}(1+\delta) && (9.39) \end{aligned}$$

Homework:

$$T^i_0 = q^i$$

$$T^i_j = -(\bar{P} + \delta P)\delta^i_j + \Pi^i_j$$

The stress-energy tensor for a perfect fluid is

$$T^\mu_\nu = (\rho + P)u^\mu u_\nu - P\delta^\mu_\nu \tag{9.40}$$

$u^\mu = \frac{dx^\mu}{d\tau}$ τ proper time (jav: use t as proper time)

$g_{\mu\nu}u^\mu u^\nu = 1 \quad \Rightarrow$

$$\begin{aligned} 1 &= g_{\mu\nu}\frac{dx^\mu}{d\tau}\frac{dx^\nu}{d\tau} && (9.41)\\ &= g_{\mu\nu}\left(\frac{d\eta}{d\tau}\right)^2\frac{dx^\mu}{d\eta}\frac{dx^\nu}{d\eta} && (9.42)\\ &= \left(\frac{d\eta}{d\tau}\right)^2(g_{00} + 2g_{0i}\frac{dx^i}{d\eta} + g_{ij}\frac{dx^i}{d\eta}\frac{dx^j}{d\eta}) && (9.43) \end{aligned}$$

where $u^i = \frac{dx^i}{d\eta}$ is the coordinate velocity - small perturbation.

$$\Rightarrow \quad 1 = \left(\frac{d\eta}{d\tau}\right)^2 g_{00} = a^2(1+2\psi)\left(\frac{d\eta}{d\tau}\right)^2$$

at linear order

$$\frac{d\eta}{d\tau} = \frac{1}{a}(1-\psi) \tag{9.44}$$

the fluids 4 velocity $u^\mu = a^{-1}[1-\psi, v^i]$

and

$$u_0 = g_{00}u^0 + g_{0i}u^i = a^2(1+2\psi)a^{-1}(1-\psi) + \mathcal{O}(2) = a(1+\psi) \tag{9.45}$$

$$u_i = g_{i0}u^0 + g_{ij}u^j = -a^2B_ia^{-1} - a^2\delta_{ij}a^{-1}v^j = -a(B_i + v_i) \tag{9.46}$$

Peculiar velocity of the matter

$$q^i = T^i_0 = (\rho + P)a^{-1}v^i a(1+\psi) = (\rho + P)v^i \tag{9.47}$$

9.5 The gauge problem

The metric perturbations aren't uniquely defined, but depend on our choice of coordinates or the *gauge choice*.

• We implicitly chose a *specific time slicing* of the spacetime and *specific spatial coordinate* on these slides.

⇒ Making a different choice of coordinates, can change the values of the perturbation variables and may even introduce fictitious perturbations

i.e **FRW spacetime**

change the spatial coordinates

$$x^i \to \tilde{x}^i + \xi^i(\eta, x) \tag{9.48}$$

$$\Rightarrow dx^i = d\tilde{x}^i - \partial_\eta \xi^i d\eta - \partial_k \xi^i d\tilde{x}^k \tag{9.49}$$

$\frac{\partial}{\partial\eta} = \bullet$ equiv. $\frac{\partial}{\partial\tau} = '$ η,τ conform $\dot{\xi}_i \equiv \partial_\eta \xi_i$ and $ds^2 = a^2(d\eta^2 - \delta_{ij} dx^i dx^j)$

and

$$ds^2 = a^2(\eta)[d\eta^2 - 2\dot{\xi}_i d\tilde{x}^i d\eta - (\delta_{ij} + 2\partial_{(i}\xi_{j)}) d\tilde{x}^i d\tilde{x}^j] \tag{9.50}$$

we *apparently have introduced* the metric perturbation, but these are just *fictitious gauge modes*, that can be removed by going back to the old coordinates.

Similar, we can change our time slicing $\eta \to \eta + \xi^0(\eta, \vec{x})$

$$\rho(\eta) \to \rho(\eta + \xi^0(\eta, \vec{x})) = \bar{\rho}(\eta) + \dot{\bar{\rho}}\xi^0. \tag{9.51}$$

even in an unperturbed universe, a change of the coordinate can introduce a fictitious density perturbation.

Therefore, we need a more physical way to identify true perturbations → define them in such a way the don't chance under change coordinates.

9.6 Gauge transformations

Consider small changes in coordinates $x^\mu \to \tilde{x}^\mu \equiv x^\mu + \xi^\mu(\eta, \vec{x})$

$$\tilde{\eta} = \eta + T(\eta, x^i) \qquad \tilde{x}^i = x^i + L^i(\eta, x^j).$$

For a scalar field Φ (i.e. inflation), the new perturbation at the same event is ($\bar{\Phi}$ is homogeneous)

$$\begin{aligned} \delta\tilde{\Phi} &= \Phi - \bar{\Phi}(\tilde{\eta}) && (9.52)\\ &= \Phi - \bar{\Phi}(\eta + T) && (9.53)\\ &= \Phi - \bar{\Phi}(\eta) - T\dot{\bar{\Phi}}. && (9.54) \end{aligned}$$

to first order

$$\delta\tilde{\Phi} = \delta\Phi - T\dot{\bar{\Phi}}. \tag{9.55}$$

For metric perturbations

$\bar{g}_{\mu\nu}$ is the metric in the background

$$\begin{aligned} \delta\tilde{g}_{\mu\nu} &= \tilde{g}_{\mu\nu} - \bar{g}_{\mu\nu}(\tilde{\eta}, \tilde{x}^i) && (9.56)\\ &= \frac{\partial x^\alpha}{\partial \tilde{x}^\mu}\frac{\partial x^\beta}{\partial \tilde{x}^\nu} g_{\alpha\beta} - \bar{g}_{\mu\nu}(\tilde{\eta}, \tilde{x}^i) && (9.57)\\ &= \frac{\partial x^\alpha}{\partial \tilde{x}^\mu}\frac{\partial x^\beta}{\partial \tilde{x}^\nu}[\delta g_{\alpha\beta} + \bar{g}_{\alpha\beta}(\eta, x^i)] - \bar{g}_{\mu\nu}(\tilde{\eta}, \tilde{x}^i) && (9.58)\\ &= \delta g_{\mu\nu} + \left(\frac{\partial x^\alpha}{\partial \tilde{x}^\mu}\frac{\partial x^\beta}{\partial \tilde{x}^\nu} - \delta^\alpha_\mu\delta^\beta_\nu\right)\bar{g}_{\alpha\beta}(\eta, x^i) - T\dot{\bar{g}}_{\mu\nu}(\eta, x^i) - L^i\partial_i\bar{g}_{\mu\nu}(\eta, x^i) && (9.59) \end{aligned}$$

to linear order, we need to know this, the inverse of $\frac{\partial \tilde{x}^\mu}{\partial x^\alpha}$

The matrix of derivates

$$\frac{\partial \tilde{x}^\alpha}{\partial x^\mu} = \begin{pmatrix} \partial\tilde{\eta}/\partial\eta & \partial\tilde{\eta}/\partial x^i \\ \partial\tilde{x}^i/\partial\eta & \partial\tilde{x}^i/\partial x^j \end{pmatrix} = \begin{pmatrix} 1+\dot{T} & \partial_i T \\ \dot{L}^i & \delta^i_j + \partial_j L^i \end{pmatrix} \tag{9.60}$$

inverse of matrix with form $1+\Delta$, is $1-\Delta$ to first order in Δ

$$\frac{\partial x^\alpha}{\partial \tilde{x}^\mu} = \begin{pmatrix} \partial\eta/\partial\tilde{\eta} & \partial\eta/\partial\tilde{x}^i \\ \partial x^i/\partial\tilde{\eta} & \partial x^i/\partial\tilde{x}^j \end{pmatrix} = \begin{pmatrix} 1-\dot{T} & -\partial_i T \\ -\dot{L}^i & \delta^i_j - \partial_j L^i \end{pmatrix} \tag{9.61}$$

Substitute

$$\delta\tilde{g}_{00} = \delta g_{00} + \left(\frac{\partial x^\alpha}{\partial\tilde{\eta}}\frac{\partial x^\beta}{\partial\tilde{\eta}} - \delta^\alpha_0\delta^\beta_0\right)\bar{g}_{\alpha\beta} - T\dot{\bar{g}}_{00} - L^i\partial_i\bar{g}_{00} \tag{9.62}$$

$$\begin{aligned} 2a^2\tilde{\psi} &= 2a^2\psi + \left(\frac{\partial\eta}{\partial\tilde{\eta}}\frac{\partial\eta}{\partial\tilde{\eta}} - 1\right)\bar{g}_{00} + 2\frac{\partial\eta}{\partial\tilde{\eta}}\frac{\partial x^i}{\partial\tilde{\eta}}\bar{g}_{0i} + \frac{\partial x^i}{\partial\tilde{\eta}}\frac{\partial x^j}{\partial\tilde{\eta}}\bar{g}_{ij} - T\partial_\eta a^2 & (9.63)\\ &= 2a^2\psi - 2\dot{T}a^2 + \mathcal{O}(2) + \mathcal{O}(2) - 2T\mathcal{H}a^2 & (9.64)\end{aligned}$$

$$\tilde{\psi} = \psi - \dot{T} - \mathcal{H}T \tag{9.65}$$

Tarea

$$\begin{aligned}\tilde{\phi} &= \phi + \mathcal{H}T + \frac{1}{3}\partial_i L^i & (9.66)\\ \tilde{B}_i &= B_i + \partial_i T - \dot{L}_i & (9.67)\\ \tilde{E}_{ij} &= E_{ij} - \partial_{<i}L_{j>} & (9.68)\end{aligned}$$

9.7 Gauge invariant perturbations

SVT - decomposition

only the scalar modes

$$\tilde{\eta} = \eta + T, \qquad \tilde{x}^i = x^i + \delta^{ij}\partial_j L \tag{9.69}$$

$$\begin{aligned}\tilde{\psi} &= \psi - \dot{T} - \mathcal{H}T & (9.70)\\ \tilde{\phi} &= \phi + \mathcal{H}T + \frac{1}{3}\nabla^2 L & (9.71)\\ \tilde{B} &= B + T - \dot{L} & (9.72)\\ \tilde{E} &= E - L & (9.73)\end{aligned}$$

4 functional degrees of freedom , and 2 gauge functions (T and L) $\Rightarrow$ construct two gauge invariant quantities (do not change under gauge transformation)

Bardeen variables

$$\Psi \equiv \psi + \mathcal{H}(B - \dot{E}) + \dot{B} - \ddot{E} \tag{9.74}$$

$$\Phi \equiv \phi - \mathcal{H}(B - \dot{E}) + \frac{1}{3}\nabla^2 E \tag{9.75}$$

$$\Phi_i \equiv \dot{E}_i - B_i \tag{9.76}$$

Tarea: show that Φ, Ψ, Φ_i don't change under a coordinate transformation

9.7.1 Gauge fixing

An alternative solution to the gauge problem is to **fix the gauge** and keep track of all perturbations i.e. use the freedom of T and L to set two scalar metric perturbations to zero

Newtonian gauge (conformal)

$$E = B = 0 \tag{9.77}$$

$$ds^2 = a^2(\eta)[(1 + 2\psi)d\eta^2 - (1 - 2\phi)\delta_{ij}dx^i dx^j] \tag{9.78}$$

$$\Psi = \psi, \qquad \Phi = \phi \qquad \text{Bardeen potentials} \tag{9.79}$$

The physics appears simple since

- hypersurfaces of constant time are orthogonal to the observers at rest ($B = 0$)
- induced geometry of the constant-time hypersurfaces is isotropic ($E = 0$)
- in the absence of anisotropic stress $\Psi = \Phi$
- Similarity of the metric to the usual weak-field limit of GR about Minkowski
- Ψ plays the role of the gravitational potential (will see)

Therefore, preferred gauge for studying the formation of large-scale structures and CMB anisotropies

Spatially flat gauge

$$\phi = E = 0$$

Convenient for computing inflationary perturbations. Fluctuations in the inflation field

Synchronous gauge

$$\psi = B = 0$$

See Ma and Betschinger.

9.8 Perturbations of the Stress-Energy tensor

Repeat the analysis (more convenient with mixed components)

$$\begin{aligned} \delta\tilde{T}^{\mu}_{\nu} &= \frac{\partial\tilde{x}^{\mu}}{\partial x^{\alpha}}\frac{\partial x^{\beta}}{\partial\tilde{x}^{\nu}}T^{\alpha}_{\beta} - \bar{T}^{\mu}_{\nu}(\eta + T, x^i + L^i) && (9.80)\\ &= \delta T^{\mu}_{\nu} + \left(\frac{\partial\tilde{x}^{\mu}}{\partial x^{\alpha}}\frac{\partial x^{\beta}}{\partial\tilde{x}^{\nu}} - \delta^{\mu}_{\alpha}\delta^{\beta}_{\nu}\right)\bar{T}^{\alpha}_{\beta} - T\dot{\bar{T}}^{\mu}_{\nu} - L^i\partial_i\bar{T}^{\mu}_{\nu} && (9.81)\end{aligned}$$

for $T^0_0 = \bar{\rho} + \delta\rho$

$$\begin{aligned} \delta\tilde{\rho} &= \delta\rho + \left(\frac{\partial\tilde{\eta}}{\partial x^{\alpha}}\frac{\partial x^{\beta}}{\partial\tilde{\eta}} - \delta^0_{\alpha}\delta^{\beta}_0\right)\bar{T}^{\alpha}_{\beta} - T\dot{\bar{\rho}} - L^i\partial_i\bar{\rho} && (9.82)\\ &= \delta\rho + \left(\frac{\partial\tilde{\eta}}{\partial\eta}\frac{\partial\eta}{\partial\tilde{\eta}} - 1\right)\bar{\rho} - \frac{\partial\tilde{\eta}}{\partial x^i}\frac{\partial x^j}{\partial\tilde{\eta}}\bar{\rho}\delta^i_j - T\dot{\bar{\rho}} && (9.83)\\ &= \delta\rho + [(1+\dot{\bar{T}})(1-\dot{\bar{T}}) - 1]\bar{\rho} - \mathcal{O}(2) - T\dot{\bar{\rho}} && (9.84)\end{aligned}$$

$$\delta\tilde{\rho} = \delta\rho - T\dot{\bar{\rho}} \quad (9.85)$$

Tarea

$$\begin{aligned} \delta\tilde{P} &= \delta P - T\dot{\bar{P}} && (9.86)\\ \tilde{q}^i &= q^i + (\bar{\rho} + \bar{P})\dot{L}^i && (9.87)\\ \tilde{\Pi}^i_j &= \Pi^i_j && (9.88)\end{aligned}$$

9.9 Gauge invariant perturbations

one useful combination

$$\bar{\rho}\Delta \equiv \delta\rho + \dot{\bar{\rho}}(v+B) \tag{9.89}$$

$$= \delta\rho - 3\mathcal{H}(\bar{\rho}+\bar{p})(B+v) \tag{9.90}$$

where $q_i = (\bar{\rho}+\bar{p})\partial_i v$, Δ comoving-gauge density perturbation

Exercise Δ is gauge-invariant

9.10 Gauge fixing

Define the gauge in the matter sector.

9.10.1 Uniform density gauge

Use the freedom in the time-slicing to set the total density perturbation to zero

$$\delta\rho = 0$$

9.10.2 comoving gauge

Scalar momentum density to vanish

$$q = 0$$

naturally connected to the inflationary initial conditions.

9.11 Adiabatic fluctuations

• Simple inflation models predict initial fluctuations that are adiabatic.

⇒ Energy densities of all species are constant on hypersurfaces and all species have the same peculiar velocities.

The quantity

$$\frac{\delta\rho_I}{\bar{\rho}_I + \bar{P}_I} - \frac{\delta\rho_J}{\bar{\rho}_J + \bar{P}_J} \tag{9.91}$$

is gauge invariant since $\delta\tilde{\rho}_I \rightarrow \delta\rho_I - T\dot{\bar{\rho}}_I$, I and J labelled the species, and $\dot{\bar{\rho}}_J = -3\mathcal{H}(\bar{\rho} + \bar{P})[= -(1+w_i)\rho_i]$

Moreover, it vanished for adiabatic fluctuations since then all $\delta\rho_J = 0$, in a gauge for which the constant-time hypersurfaces coincide with those of uniform total density

$$\delta = \frac{\delta\rho_I}{\dot{\bar{\rho}}_I} = \frac{\delta\rho_J}{\dot{\bar{\rho}}_J} \qquad \Rightarrow \qquad \frac{\delta_I}{1+w_I} = \frac{\delta_J}{1+w_J} \qquad \text{for all species I and J} \tag{9.92}$$

δ_J is the fractional density contrast

$$\delta_J \equiv \frac{\delta\rho_J}{\bar{\rho}_J} \tag{9.93}$$

For adiabatic perturbations, matter ($w_m \approx 0$), radiation ($w_r = \frac{1}{3}$) obey $\delta_r = \frac{4}{3}\delta_m$ and the total density perturbation

$$\delta\rho_{tot} = \bar{\rho}_{tot}\delta_{tot} = \sum_I \bar{\rho}_I\delta_I \tag{9.94}$$

is dominated by the especies that is dominated in the background since all the δ_I are comparable

9.12 Isocurvature fluctuations

Adibatic perturbations correspond to a change in the total energy density

Isocurvature perturbation only correspond to perturbation betwen the different components

$$\delta_{IJ} \equiv \frac{\delta_I}{1+w_I} - \frac{\delta_J}{1+w_J} \tag{9.95}$$

single-field inflation predicts that the primordial perturbations are purely adiabatic $\delta_{IJ} = 0$

10

Linerised Evolution Equations

The perturb Einstein equations $\delta G_{\mu\nu} = 8\pi G \delta T_{\mu\nu}$

- We can use two gauge function T y L to set the metric perturbations E y B to zero

10.1 Conformal Newtonian Gauge

$$ds^2 = a^2[(1+2\psi)d\eta^2 - (1-2\phi)\delta_{ij}dx^i dx^j] \tag{10.1}$$

$\phi = \Phi$ and $\psi = \Psi$

Perturbed connections coefficients

we first require

$$\Gamma^{\mu}_{\nu\rho} = \frac{1}{2}g^{\mu k}(\partial_\nu g_{k\rho} + \partial_\rho g_{k\nu} - \partial_k g_{\nu\rho}) \tag{10.2}$$

with inverse

$$g^{\mu\nu} = \frac{1}{a^2}\begin{pmatrix} 1-2\psi & 0 \\ 0 & -(1-2\phi)\delta^{ij} \end{pmatrix} \tag{10.3}$$

$$\Gamma^0_{00} = \frac{1}{2}g^{00}(2\partial_\eta g_{00} - \partial_\eta g_{00}) \quad (10.4)$$
$$= \frac{1}{2}g^{00}\partial_\eta g_{00} \quad (10.5)$$
$$= \frac{1}{2a^2}(1-2\psi)\partial_\eta[a^2(1+2\psi)] \quad (10.6)$$
$$= \mathcal{H} + \dot{\psi} \quad (10.7)$$

Homework

$$\Gamma^0_{0i} = \partial_i\psi \quad (10.8)$$
$$\Gamma^i_{00} = \delta^{ij}\partial_j\psi \quad (10.9)$$
$$\Gamma^0_{ij} = \mathcal{H}\delta_{ij} - [\dot{\phi} + 2\mathcal{H}(\phi+\psi)]\delta_{ij} \quad (10.10)$$
$$\Gamma^i_{j0} = \mathcal{H}\delta^i_j - \dot{\phi}\delta^i_j \quad (10.11)$$
$$\Gamma^i_{jk} = -2\delta^i_{(j}\delta_{k)}\phi + \delta_{jk}\delta^{il}\partial_l\phi \quad (10.12)$$

10.2 Perturbed Stress-Energy Conservation

$G_{\mu\nu} = 8\pi G T_{\mu\nu} + \Lambda g_{\mu\nu}$ implies conservation of energy and momentum via the contracted Bianchi identify

$$\nabla^\mu G_{\mu\nu} = 0 \qquad \rightarrow \qquad \nabla^\mu T_{\mu\nu} = 0 \quad (10.13)$$

it's more convenient to work with the mixed components

$$\nabla_\mu T^\mu_{\ \nu} = 0 \qquad or \qquad \partial_\mu T^\mu_\nu + \Gamma^\mu_{\mu\rho}T^\rho_\nu - \Gamma^\rho_{\mu\nu}T^\mu_\rho = 0 \quad (10.14)$$

Continuity equation

the $\nu = 0$ component

$$\partial_0 T^0_{\ 0} + \partial_i T^i_{\ 0} + \Gamma^\mu_{\mu 0}T^0_{\ 0} + \underbrace{\Gamma^\mu_{\mu i}T^i_{\ 0}}_{\mathcal{O}(2)} - \Gamma^0_{00}T^0_{\ 0} - \underbrace{\Gamma^0_{i0}T^i_{\ 0}}_{\mathcal{O}(2)} - \underbrace{\Gamma^i_{00}T^0_{\ i}}_{\mathcal{O}(2)} - \Gamma^i_{j0}T^j_{\ i} = 0 \quad (10.15)$$

subs. the perturbed stress-energy tensor and connection coefficients

$$\partial_\eta(\bar{\rho}+\delta\rho) + \partial_i q^i + (\mathcal{H}+\dot{\psi}+3\mathcal{H}-3\dot{\phi})(\bar{\rho}+\delta\rho) - (\mathcal{H}+\dot{\psi})(\bar{\rho}+\delta\rho) - (\mathcal{H}-\dot{\phi})\delta^i_j[-(\bar{P}+\delta P)\delta^j_i + \Pi^j_i] = 0 \quad (10.16)$$

$$\Rightarrow \dot{\bar{\rho}} + \partial_\eta \delta\rho + \partial_i q^i + 3\mathcal{H}(\bar{\rho} + \delta\rho) - 3\bar{\rho}\dot{\phi} + 3\mathcal{H}(\bar{P} + \delta P) - 3\bar{P}\dot{\phi} = 0 \tag{10.17}$$

the zero part

$$\dot{\bar{\rho}} + 3\mathcal{H}(\bar{\rho} + \bar{P}) = 0 \tag{10.18}$$

the first order part

$$\partial_\eta \delta\rho + \partial_i q^i - 3(\bar{\rho} + \bar{P})\dot{\phi} + 3\mathcal{H}(\delta\rho + \delta P) = 0 \tag{10.19}$$

- $\partial_i q^i$ - describes changes due to the local fluid flow because peculiar velocity
- $3\mathcal{H}$ - dilution due to the background expansion
- $\dot{\phi}$ - density changes caused by perturbations to the local expansion rate $(1 - \phi)a$ is the local scale factor

$\delta \equiv \frac{\delta\rho}{\bar{\rho}}$ - fractional overdensity
$q^i = (\bar{\rho} + \bar{P})u^i$ in terms of the peculiar velocity

$$\dot{\delta} + \left(1 + \frac{\bar{P}}{\bar{\rho}}\right)(\partial_i u^i - 3\dot{\phi}) + 3\mathcal{H}\left(\frac{\delta P}{\delta\rho} - \frac{\bar{P}}{\bar{\rho}}\right)\delta = 0 \tag{10.20}$$

relativistic version of the continuity equation, $limitP << \rho \rightarrow$ recover the Newtonian continuity equation in conformal time

$$\dot{\delta} + \partial_i u^i - 3\dot{\phi} = 0 \tag{10.21}$$

but with a general-relastivistic correction [small on sub-horizon sacales $k >> \mathcal{H}$]

10.3 Euler equation

$\nu = i$

$$\partial_\mu T^\mu_{\ i} + \Gamma^\mu_{\mu\rho} T^\rho_{\ i} - \Gamma^\rho_{\mu i} T^\mu_{\ \rho} = 0 \tag{10.22}$$

$$\partial_\eta T^0_{\ i} + \partial_j T^j_{\ i} + \Gamma^\mu_{\mu 0} T^0_{\ i} + \Gamma^\mu_{\mu j} T^j_{\ i} - \Gamma^0_{0i} T^0_{\ 0} - \Gamma^0_{ji} T^j_{\ 0} - \Gamma^j_{0i} T^j_{\ 0} - \Gamma^j_{ki} T^k_{\ j} = 0 \tag{10.23}$$

we have not written down explicitly before

$$\begin{aligned} T^0_{\ i} &= g_{i\mu}T^{0\mu} = g_{i0}T^{00} + g_{ij}T^{0j} \\ &= 0 - a^2(1-2\phi)\delta_{ij}a^{-2}q^i \\ &= -q^i \end{aligned} \tag{10.24}$$

then becomes

$$\begin{aligned} -\dot{q}_i + \partial_j[-(\bar{P} \ &+ \ \delta P)\delta^j_i + \Pi^j_i] - 4\mathcal{H}q_i - (\partial_j\psi - 3\partial_j\phi)\bar{P}\delta^j_i - \partial_i\psi\bar{\rho} \\ &- \ \mathcal{H}\delta_{ij}q^j + \mathcal{H}\delta^j_i q_j + \underbrace{(-2\delta^j_{(i}\partial_{k)}\phi + \delta_{ki}\delta^{il}\partial_l\phi)}_{-3\partial_i\phi\bar{P}}\bar{P}\delta^k_j = 0 \end{aligned} \tag{10.25}$$

$$\Rightarrow \qquad -\dot{q}_i - \partial_i\delta P + \partial_j\Pi^j_i - 4\mathcal{H}q_i - (\bar{\rho}+\bar{P})\partial_i\psi = 0 \tag{10.26}$$

using $q_i = (\bar{\rho}+\bar{P})v_i$, the relativistic version of the Euler equation

$$\dot{v}_i + \frac{1}{\bar{\rho}+\bar{P}}\partial_i\delta P - \frac{1}{\bar{\rho}+\bar{P}}\partial_i\Pi^j_i + \mathcal{H}v_i + \frac{\dot{\bar{P}}}{\bar{\rho}+\bar{P}}v_i + \partial_i\psi = 0 \tag{10.27}$$

- $\mathcal{H}v_i$ - redshifting of peculiar velocities
- $\dot{\bar{P}}/\dot{\bar{\rho}}$ - small corrections for relativistic fluids
- $\dot{\bar{P}}/\dot{\bar{\rho}} = c_s^2$ for adiabatic fluctuations

we just need the gravitational potentials ψ and ϕ to the close the system of equations

10.4 Perturbed Einstein equations

We requiere the Einstein tensor $G_{\mu\nu} = R_{\mu\nu} - \frac{1}{2}Rg_{\mu\nu}$ so we need Ricci $R_{\mu\nu}$ tensor and scalar R

$$R_{\mu\nu} = \partial_\rho\Gamma^\rho_{\mu\nu} - \partial_\nu\Gamma^\rho_{\mu\rho} + \Gamma^\alpha_{\mu\nu}\Gamma^\rho_{\alpha\rho} - \Gamma^\alpha_{\mu\rho}\Gamma^\rho_{\nu\alpha} \tag{10.28}$$

for 00:

$$R_{00} = \partial_\rho\Gamma^\rho_{00} - \partial_\eta\Gamma^\rho_{0\rho} + \Gamma^\alpha_{00}\Gamma^\rho_{\alpha\rho} - \Gamma^\alpha_{0\rho}\Gamma^\rho_{0\alpha} \tag{10.29}$$

the terms with $\rho = 0$ cancel

$$
\begin{aligned}
R_{00} &= \partial_i\Gamma^i_{00} - \partial_\eta\Gamma^i_{0i} + \Gamma^\alpha_{00}\Gamma^i_{\alpha i} - \Gamma^\alpha_{0i}\Gamma^i_{0\alpha} && (10.30)\\
&= \partial_i\Gamma^i_{00} - \partial_\eta\Gamma^i_{0i} + \Gamma^0_{00}\Gamma^i_{0i} + \underbrace{\Gamma^j_{00}\Gamma^i_{ji}}_{\mathcal{O}(2)} - \underbrace{\Gamma^0_{0i}\Gamma^i_{00}}_{\mathcal{O}(2)} - \Gamma^j_{0i}\Gamma^i_{0j} \\
&= \nabla^2\psi - 3\partial_\eta(\mathcal{H} - \dot\phi) - 3(\mathcal{H} + \dot\psi)(\mathcal{H} - \dot\phi) - (\mathcal{H} - \dot\phi)^2\delta^j_i\delta^i_j && (10.31)\\
R_{00} &= -3\dot{\mathcal{H}} + \nabla^2\psi + 3\mathcal{H}(\dot\phi + \dot\psi) + 3\ddot\phi && (10.32)
\end{aligned}
$$

Homework

$$R_{0i} = 2\partial_i\dot\phi + 2\mathcal{H}\partial_i\psi \qquad (10.33)$$

$$
\begin{aligned}
R_{ij} &= [\dot{\mathcal{H}} + 2\mathcal{H}^2 - \ddot\phi + \nabla^2\phi - 2(\dot{\mathcal{H}} + 2\mathcal{H}^2)(\phi + \psi) - \mathcal{H}\dot\psi - 5\mathcal{H}\dot\phi]\delta_{ij} \\
&+ \partial_i\partial j(\phi - \psi) && (10.34)
\end{aligned}
$$

Ricci scalar

$$R = g^{00}R_{00} + \underbrace{2g^{0i}R_{0i}}_{=0} + g^{ij}R_{ij} \qquad (10.35)$$

$$
\begin{aligned}
a^2R &= (1 - 2\psi)R_{00} - (1 + 2\phi)\delta^{ij}R_{ij} && (10.36)\\
&= (1 - 2\psi)[-3\dot{\mathcal{H}} + \nabla^2\psi + 3\mathcal{H}(\dot\phi + \dot\psi) + 3\ddot\phi] && (10.37)\\
&\quad - \underbrace{\delta^{ij}\delta_{ij}}_{3}(1 + 2\phi)[\dot{\mathcal{H}} + 2\mathcal{H}^2 - \ddot\phi + \nabla^2\phi && (10.38)\\
&\quad -2(\dot{\mathcal{H}} + 2\mathcal{H}^2)(\phi + \psi) - \mathcal{H}\dot\psi - 5\mathcal{H}\dot\phi] - (1 + 2\phi)\nabla^2(\phi - \psi) && (10.39)
\end{aligned}
$$

simplifying to linear order

$$a^2R = -6(\dot{\mathcal{H}} + \mathcal{H}^2) + 2\nabla^2\psi - 4\nabla^2\phi + 12(\dot{\mathcal{H}} + \mathcal{H}^2)\psi + 6\ddot\phi + 6\mathcal{H}(\dot\psi + 3\dot\phi) \qquad (10.40)$$

the Einstein tensor 00:

$$
\begin{aligned}
G_{00} &= R_{00} - \frac{1}{2}g_{00}R && (10.41)\\
&= -3\dot{\mathcal{H}} + \nabla^2\psi + 3\mathcal{H}(\dot\phi + \dot\psi) + 3\ddot\phi + 3(1 + 2\psi)(\dot{\mathcal{H}} + \mathcal{H}^2) && (10.42)\\
&\quad -\frac{1}{2}[2\nabla^2\psi - 4\nabla^2\phi + 12(\dot{\mathcal{H}} + \mathcal{H}^2)\psi + 6\ddot\phi + 6\mathcal{H}(\dot\psi + 3\dot\phi)] && (10.43)\\
G_{00} &= 3\mathcal{H}^2 + 2\nabla^2\phi - 6\mathcal{H}\dot\phi && (10.44)
\end{aligned}
$$

since $g_{0i} = 0$ (newtonian)

$$G_{0i} = 2\partial_i\dot{\phi} + 2\mathcal{H}\partial_i\psi \tag{10.45}$$

$$\begin{aligned} G_{ij} &= R_{ij} - \frac{1}{2}g_{ij}R & (10.46)\\ &= [\dot{\mathcal{H}} + 2\mathcal{H}^2 - \ddot{\phi} + \nabla^2\phi - 2(\dot{\mathcal{H}} + 2\mathcal{H})(\phi + \psi) - \mathcal{H}\dot{\psi} - 5\mathcal{H}\dot{\phi}]\delta_{ij} & (10.47)\\ &\quad +\partial_i\partial_j(\phi - \psi) - 3(1 - 2\phi)(\dot{\mathcal{H}} + \mathcal{H}^2)\delta_{ij} & (10.48)\\ &\quad +\frac{1}{2}[2\nabla^2\psi - 4\nabla^2\phi + 12(\dot{\mathcal{H}} + \mathcal{H}^2)\psi + 6\ddot{\phi} + 6\mathcal{H}(\dot{\psi} + 3\dot{\phi})]\delta_{ij} & (10.49) \end{aligned}$$

this neates up

$$\begin{aligned} G_{ij} &= -(2\dot{\mathcal{H}} + \mathcal{H}^2)\delta_{ij} + [\nabla^2(\psi - \phi) + 2\ddot{\phi} + 2(2\dot{\mathcal{H}} + \mathcal{H}^2)(\phi + \psi)\\ &\quad +2\mathcal{H}\dot{\psi} + 4\mathcal{H}\dot{\phi}]\delta_{ij} + \partial_i\partial_j(\phi - \psi) & (10.50) \end{aligned}$$

10.5 Einstein equations

00:

$$G_{00} = 8\pi G T_{00} + \Lambda g_{00} \tag{10.51}$$

$$\begin{aligned} 3\mathcal{H}^2 + 2\nabla^2\phi - 6\mathcal{H}\dot{\phi} &= 8\pi G(g_{00}T^0_{\ 0} + g_{0i}T^i_{\ 0}) + \Lambda a^2(1 + 2\psi) & (10.52)\\ &= 8\pi G a^2\bar{\rho}(1 + 2\psi)(1 + \delta) + \Lambda a^2(1 + 2\psi) & (10.53) \end{aligned}$$

zero-order

$$\mathcal{H}^2 = \frac{8\pi G}{3}a^2\bar{\rho} + \frac{1}{3}\Lambda a^2 \tag{10.54}$$

first order

$$\begin{aligned} \nabla^2\phi &= (8\pi G a^2\bar{\rho} + \Lambda a^2)\psi + 3\mathcal{H}\dot{\phi} + 4\pi G a^2\bar{\rho}\delta & (10.55)\\ \nabla^2\phi &= 3\mathcal{H}(\dot{\phi} + \mathcal{H}\psi) + 4\pi G a^2\bar{\rho}\delta & (10.56) \end{aligned}$$

oi

$$G_{0i} = 8\pi G T_{0i} + \Lambda g_{0i} \tag{10.57}$$

$$\begin{aligned} T_{0i} &= g_{0\mu} g_{i\nu} T^{\mu\nu} && (10.58)\\ &= g_{00} g_{ij} T^{0j} \qquad (g_{0i} = 0) \\ &= -a^2(1+2\psi)a^2(1-2\phi)\delta_{ij}a^{-2}q^j && (10.59)\\ &= -a^2 q_i && (10.60) \end{aligned}$$

$$\Rightarrow \partial_i \dot{\phi} + \mathcal{H}\partial_i\psi = -4\pi G a^2 q_i \qquad with \quad q_i = (\bar{\rho} + \bar{P})\partial_i v \tag{10.61}$$

$$\dot{\phi} + \mathcal{H}\psi = -4\pi G a^2 (\bar{\rho} + \bar{P}) v \tag{10.62}$$

using G_{00}

$$\Rightarrow \nabla^2 \phi = 4\pi G a^2 [\bar{\rho}\delta - 3\mathcal{H}(\bar{\rho} + \bar{P})v] \tag{10.63}$$

$[\bar{\rho}\delta - 3\mathcal{H}(\bar{\rho} + \bar{P})v]$ poisson with source density

$\bar{\rho}\Delta \equiv [\bar{\rho}\delta - 3\mathcal{H}(\bar{\rho} + \bar{P})(B + v)]$ the gauge-invariant variable ($B = 0$), since $B = 0$ in the conformal newtonian gauge.

• introduce comoving hypersurfaces-orthogonal to the wordlines of a set of observers comoving with the total matter

In the comoving gauge ($q^i = 0, B_i = 0$), Δ is the fractional overdensity

ij

$$\begin{aligned} G_{ij} &= 8\pi G T_{ij} + \Lambda g_{ij} \\ &= 8\pi G g_{ik} g_{jl} T^{kl} - a^2 \Lambda (1-2\phi)\delta_{ij} \\ &= 8\pi G a^4 (1-2\phi)^2 \delta_{ik}\delta_{jl} a^{-2} [\bar{P}\delta^{kl} + (2\bar{P}\phi - \delta P)\delta^{kl} - \Pi^{kl}] - a^2\Lambda(1-2\phi)\delta_{ij} \\ &= 8\pi G a^2 (1-4\phi)[\bar{P}\delta_{ij} + (2\bar{P}\phi + \delta P)\delta_{ij} - \Pi_{ij}] + a^2\Lambda(1-2\phi)\delta_{ij} \\ &= a^2(8\pi G\bar{P} - \Lambda)\delta_{ij} + a^2[8\pi G(\delta\rho - 2\bar{P}\phi) + 2\Lambda\phi]\delta_{ij} - 8\pi G a^2 \Pi_{ij} \end{aligned} \tag{10.64}$$

using G_{ij} to zero order

$$2\dot{\mathcal{H}} + \mathcal{H}^2 = -a^2(8\pi G\bar{P} - \Lambda) \tag{10.65}$$

the second Friedmann equation.

The first order

$$\begin{aligned} [\nabla^2(\psi-\phi) + 2\ddot{\phi} + 2(2\dot{\mathcal{H}} + \mathcal{H}^2)(\phi+\psi) + 2\mathcal{H}\dot{\psi} + 4\mathcal{H}\dot{\phi}]\delta_{ij} + \partial_i\partial_j(\phi-\psi) \\ = a^2[8\pi G(\delta P - 2\bar{P}\phi) + 2\Lambda\phi]\delta_{ij} - 8\pi G a^2 \Pi_{ij} \end{aligned} \tag{10.66}$$

• consider first the trace-free part

$$\partial_{<i}\partial_{j>}(\phi - \psi) = -8\pi G a^2 \Pi_{ij} \tag{10.67}$$

in the absence of anisitropic stress $\phi = \psi$ so there's only one gauge-invariant degree of freedom in the metric (Π_{ij} neutrino decoupling - or not a perfect fluid.)

• the trace part $\delta^{ij}/3$

$$\begin{aligned} \nabla^2(\psi-\phi) + 2\ddot{\phi} + 2(2\dot{\mathcal{H}} + \mathcal{H}^2)(\phi+\psi) + 2\mathcal{H}\dot{\psi} + 4\mathcal{H}\dot{\phi} + \frac{1}{3}\nabla^2(\phi-\psi) \\ = 8\pi G a^2 \delta P - 2a^2(8\pi G\bar{P} - \Lambda)\phi \end{aligned} \tag{10.68}$$

using zero order

$$\ddot{\phi} + \frac{1}{3}\nabla^2(\psi-\phi) + 2\dot{\mathcal{H}} + \mathcal{H}^2)\psi + \mathcal{H}\dot{\phi} + 2\mathcal{H}\dot{\phi} = 4\pi G a^2 \delta P \tag{10.69}$$

10.5.1 Conserved curvature perturbation

An important quantity conserved on super Hubble scales for adiabatic scalar fluctuation irrespective of $w(z)$: the comoving curvature perturbation.

$\Rightarrow$ Perturbation to the intrinsic curvature scalar of comoving hypersurfaces ($q^i = 0$) allows to match the perturbations from inflation to those in the radiation dominated universe on large scales without needing to know the details of the reheating phase at the end inflation.

• work out the intrinsic curvature of surfaces fo constant time

- The induced metric γ_{ij} (just the spatial part)

$$\gamma_{ij} \equiv a^2[(1-2\phi)\delta_{ij} + 2E_{ij}] \tag{10.70}$$

$$^{(3)}\Gamma^i_{jk} = \frac{1}{2}\gamma^{il}(\partial_j\gamma_{kl} + \partial_k\gamma_{jl} - \partial_l\gamma_{jk}) \tag{10.71}$$

inverse $\gamma^{ij} = a^{-2}[(1+2\phi)\delta^{ij} - 2E^{ij}]$ we need Γ to zero order, γ_{ij} are first order perturbations

$$\begin{aligned} ^{(3)}\Gamma^i_{jk} &= \delta^{il}\partial_j(-\phi\delta_{kl} + E_{kl}) + \delta^{il}\partial_k(-\phi\delta_{jl} + E_{jl}) - \delta^{il}\partial_l(-\phi\delta_{jk} + E_{jk}) \\ &= -(2\delta^i_{(j}\partial_{k)}\phi - \delta^{il}\delta_{jk}\partial_l\phi) + (2\partial_{(j}E^i_{k)} - \delta^{il}\partial_l E_{jk}) \end{aligned} \tag{10.72}$$

The intrinsic curvature is the associated Ricci scalar

$$^{(3)}R = \gamma^{ik}\partial^{(3)}_l\Gamma^l_{ik} - \gamma^{ik}\partial^{(3)}_k\Gamma^l_{il} + \underbrace{\gamma^{ik(3)}\Gamma^{l(3)}_{ik}\Gamma^m_{lm}}_{=0}\underbrace{-\gamma^{ik(3)}\Gamma^{m(3)}_{il}\Gamma^l_{km}}_{=0} \tag{10.73}$$

to first-order

$$a^{2\,(3)}R = \delta^{ik}\partial_l{}^{(3)}\Gamma^l_{ik} - \delta^{ik}\partial_k{}^{(3)}\Gamma^l_{il} \tag{10.74}$$

$$\begin{aligned} \text{first term} &= -\delta^{ik}(2\delta^l_{(i}\partial_{k)}\phi - \delta^{il}\delta_{ik}\partial_j\phi) + \delta^{ik}(2\partial_{(i}E^l_{k)} - \delta^{jl}\partial_j E_{ik}) \\ &= -2\delta^{kl}\partial_k\phi + 3\delta^{jl}\partial_j\phi + 2\partial_i E^{il} - \delta^{jl}\partial_j(\underbrace{\delta^{ik}E_{ik}}_{=0}) \\ &= \delta^{kl}\partial_k\phi + 2\partial_k E^{kl} \end{aligned} \tag{10.75}$$

$$\begin{aligned} \text{second term} &= -\delta^l_l\partial_i\phi - \delta^l_i\partial_l\phi + \partial_i\phi + \partial_l E^l_i + \partial_i E^l_l - \partial_l E^l_i \\ &= -3\partial_i\phi \end{aligned} \tag{10.76}$$

$$\begin{aligned} a^{2(3)}R &= \partial_l(\delta^{kl}\partial_k\phi + 2\partial_k E^{kl}) + 3\delta^{ik}\partial_k\partial_i\phi \\ &= \nabla^2\phi + 2\partial_i\partial_j E^{ij} + 3\nabla^2\phi \\ &= 4\nabla^2\phi + 2\partial_i\partial_j E^{ij} \end{aligned} \tag{10.77}$$

vector and tensor perturbations are zero. Scalar perturbations, $E_{ij} = \partial_{<i}\partial_{j>}E$

$$\begin{aligned} \partial_i\partial_j E^{ij} &= \delta^{il}\delta^{jm}\partial_i\partial_j(\partial_l\partial_m E - \frac{1}{3}\delta_{lm}\nabla^2 E) \\ &= \nabla^2\nabla^2 E - \frac{1}{3}\nabla^2\nabla^2 E = \frac{2}{3}\nabla^4 E \end{aligned} \tag{10.78}$$

$$a^{2(3)}R = 4\nabla^2(\phi + \frac{1}{3}\nabla^2 E) \tag{10.79}$$

$-(\phi + \nabla^2 E/3) \equiv$ curvature perturbation

and the comoving curvature perturbation $\mathcal{R}$ evaluated in the comoving gauge ($B_i = 0 = q^i$), to form a gauge-invariant combination that equals $\mathcal{R}$ in the comoving gauge

Homework: $\mathcal{R} = -\phi - \frac{1}{3}\nabla^2 E + \mathcal{H}(B + v)$ is a gauge-invariant expression

10.5.2 A conservation law

$\mathcal{R}$ is conserved on large scales for adiabatic perturbations. In the conformal newtonian gauge

$$\mathcal{R} = -\phi + \mathcal{H}v \tag{10.80}$$

using Einstein 0i

$$\mathcal{R} = -\phi - \frac{\mathcal{H}(\dot{\phi} + \mathcal{H}\psi)}{4\pi G a^2(\bar{\rho} + \bar{P})} \tag{10.81}$$

$$\begin{aligned} -4\pi G a^2(\bar{\rho} + \bar{P})\dot{\mathcal{R}} &= 4\pi G a^2(\bar{\rho} + \bar{P})\dot{\phi} + \dot{\mathcal{H}}(\dot{\phi} + \mathcal{H}\psi) + \mathcal{H}(\ddot{\phi} + \dot{\mathcal{H}}\psi + \mathcal{H}\dot{\psi}) \\ &\quad - \frac{\mathcal{H}(\dot{\phi} + \mathcal{H}\psi)}{(\bar{\rho} + \bar{P})}(2\mathcal{H}(\bar{\rho} + \bar{P}) + \dot{\bar{\rho}} + \dot{\bar{P}}) \end{aligned} \tag{10.82}$$

using $\dot{\bar{\rho}} = -3\mathcal{H}(\bar{\rho} + \bar{P})$

$$\begin{aligned} &= 4\pi G a^2(\bar{\rho} + \bar{P})\dot{\phi} + \dot{\mathcal{H}}(\dot{\phi} + \mathcal{H}\psi) + \mathcal{H}(\ddot{\phi} + \dot{\mathcal{H}}\psi + \mathcal{H}\dot{\psi}) \\ &\quad -\mathcal{H}(\dot{\phi} + \mathcal{H}\psi)\left[2\mathcal{H} - 3\mathcal{H}\left(1 + \frac{\dot{\bar{P}}}{\dot{\bar{\rho}}}\right)\right] \end{aligned} \tag{10.83}$$

in $\dot{\bar{P}}$ use Poisson, and $\mathcal{H}^2 - \dot{\mathcal{H}} = 4\pi G a^2(\bar{\rho} + \bar{P})$

$$\begin{aligned} -4\pi G a^2(\vec{\rho} + \vec{P})\dot{\mathcal{R}} &= (\mathcal{H}^2 - \dot{\mathcal{H}})\dot{\phi} + \dot{\mathcal{H}}(\dot{\phi} + \mathcal{H}\psi) + \mathcal{H}(\ddot{\phi} + \dot{\mathcal{H}}\psi + \mathcal{H}\dot{\psi}) \\ &\quad - \mathcal{H}^2(\dot{\phi} + \mathcal{H}\psi) + \frac{\mathcal{H}\dot{\bar{P}}}{\dot{\bar{\rho}}}(\nabla^2\phi - 4\pi G a^2\bar{\rho}\delta) \end{aligned} \tag{10.84}$$

adding and subtracting $4\pi G a^2 \mathcal{H}\delta P$

$$\begin{aligned} -4\pi G a^2(\bar{\rho} + \bar{P})\dot{\mathcal{R}} &= \mathcal{H}[\ddot{\phi} + \mathcal{H}\dot{\psi} + 2\mathcal{H}\dot{\phi} + (2\dot{\mathcal{H}} + \mathcal{H}^2)\psi - 4\pi G a^2\delta P] \\ &\quad + 4\pi G a^2\mathcal{H}\underbrace{\left(\delta P - \frac{\dot{\bar{P}}}{\dot{\bar{\rho}}}\bar{\rho}\delta\right)}_{\delta P_{nad}} + \frac{\mathcal{H}\dot{\bar{P}}}{\dot{\bar{\rho}}}\nabla^2\phi \end{aligned} \tag{10.85}$$

with δP_{nad}, the non-adiabatic pressure perturbation. It is gauge invariant since $\delta P \quad \to \quad \delta P - T\dot{\bar{P}}, \qquad \delta\rho \quad \to \quad \delta\rho - T\dot{\bar{\rho}}$

it vanished for a baryonic equation of state $P = P(\rho)$ more generally, it vanished for adiabatic fluctuations. Using the trace-part fo the ij Einstein equation

$$-4\pi G a^2(\bar{\rho} + \bar{P})\dot{\mathcal{R}} = \frac{1}{3}\mathcal{H}\nabla^2(\phi - \psi) + 4\pi G a^2\mathcal{H}\delta P_{nad} + \frac{\mathcal{H}\dot{\bar{P}}}{\dot{\bar{\rho}}}\nabla^2\phi \tag{10.86}$$

if δP_{nad} vanishes, the $RHS \sim \mathcal{H}k^2\phi \sim \mathcal{H}k^2\mathcal{R}$

$$\Rightarrow \qquad \frac{\dot{\mathcal{R}}}{\mathcal{H}} \sim \left(\frac{k}{\mathcal{H}}\right)^2 \mathcal{R} \qquad \frac{d\ln\mathcal{R}}{d\ln a} \sim \left(\frac{k}{\mathcal{H}}\right)^2 \tag{10.87}$$

$\mathcal{R}$ doesn't evalue on super-Hubble scales $k << \mathcal{H}$

$\mathcal{R}$ at horizon crossing during inflation survives unaltered until later times.

10.6 Summary

Newtonian Gauge, no-anisotropic stress, $\Psi = \Phi$

metric : $ds^2 = a^2(\eta)\left[(1+2\phi)d\eta^2 - (1-2\phi)\delta_{ij}dx^i dx^j\right]$

Einstein:

$$\nabla^2\phi - 3\mathcal{H}(\dot{\phi} + \mathcal{H}\phi) = 4\pi G a^2 \delta\rho \tag{10.88}$$

$$\dot{\phi} + \mathcal{H}\phi = -4\pi G a^2(\bar{\rho} + \bar{P})v \tag{10.89}$$

$$\ddot{\phi} + 3\mathcal{H}\dot{\phi} + (2\dot{\mathcal{H}} + \mathcal{H}^2) = 4\pi G a^2 \delta P \tag{10.90}$$

using the comoving gauge density contrast

$$\nabla^2\phi = 4\pi G a^2 \vec{\rho}\Delta \tag{10.91}$$

Conservation:

$$\dot{\delta} + 3\mathcal{H}\left(\frac{\delta P}{\delta\rho} - \frac{\bar{P}}{\bar{\rho}}\right)\delta = -\left(1 + \frac{\bar{P}}{\bar{\rho}}\right)(\nabla\cdot\bar{v} - 3\dot{\phi}) \tag{10.92}$$

$$\dot{v} + 3\mathcal{H}\left(\frac{1}{3} - \frac{\dot{\bar{P}}}{\dot{\bar{\rho}}}\right)v = -\frac{\nabla\delta P}{\bar{\rho} + \bar{P}} - \nabla\phi \tag{10.93}$$

$$\mathcal{R} = -\phi - \frac{\mathcal{H}(\dot{\phi} + \mathcal{H}\phi)}{4\pi G a^2(\bar{\rho} + \bar{P})} \tag{10.94}$$

doesn't evolve on super-Hubble scales $k << \mathcal{H}$

Adiabatic perturbations

11

Initial conditions

Inflation sets the initial conditions up [for those superhorizon modes]

Spectrum of inflation for the curvature perturbation $\mathcal{R}$ $\leftrightarrow$ The gravitational potential Φ, in the Newtonian gauge $\phi = \psi$

$$\mathcal{R} = -\phi - \frac{2}{3(1+w)}\left(\frac{\phi'}{\mathcal{H}} + \phi\right), \tag{11.1}$$

w is the equation of state for the background.

Adiabatic perturbations and constant equation $w \approx c_s^2$ for a single component

$$\phi'' + 3(1+w)\mathcal{H}\phi' + wk^2\phi = 0. \tag{11.2}$$

Homework: Derive the above relation

11.0.1 Super horizon limit

Consider scales $k \ll \mathcal{H}$, which means drop the last term in order to get

$$\phi'' + 3(1+w)\mathcal{H}\phi' = 0, \tag{11.3}$$

where the growing-mode solution is $\phi = constant$, independent of w (for $w = constant$).

Meaning: The gravitational potential is frozen outside the horizon during both radiation and matter eras.

From the Poisson equation

$$\delta = -\frac{2}{3}\frac{k^2}{\mathcal{H}^2}\phi - \frac{2}{\mathcal{H}}\phi' - 2\phi \qquad \left[\frac{3}{2}\mathcal{H}^2 = 4\pi G a^2 \bar{\rho}\right], \tag{11.4}$$

on super horizon scales $k \ll \mathcal{H}$ and $\phi \approx constant$,

$$\delta \approx -2\phi = constant, \tag{11.5}$$

primordial gravitational potential $\Rightarrow$ δ is also frozen on super-horizon scales.

For adiabatic initial conditions

$$\delta_m = \frac{3}{4}\delta_r \approx -\frac{3}{2}\phi_{rad}, \tag{11.6}$$

($\delta_r \approx \delta$ during radiation era). On super horizon scales, the density perturbations are therefore simply proportional to the curvature perturbations set up by inflation.

Radiation to matter transition

Exploit the conservation or $\mathcal{R}$ on super-Hubble scales $k \ll \mathcal{H}$

$$\mathcal{R} = -\frac{5+3w}{3+3w}\phi, \tag{11.7}$$

(super horizon) relating fluctuations the CMB to primordial fluctuation.
Considering $w = \frac{1}{3}$, $w = 0$

$$\mathcal{R} = -\frac{3}{2}\phi_{rad} = -\frac{5}{3}\phi_{mat} \quad \Rightarrow \quad \phi_{mat} = \frac{9}{10}\phi_{rad}. \tag{11.8}$$

ϕ decreases by a factor of 9/10 in the transition from radiation dominated to matter dominated.

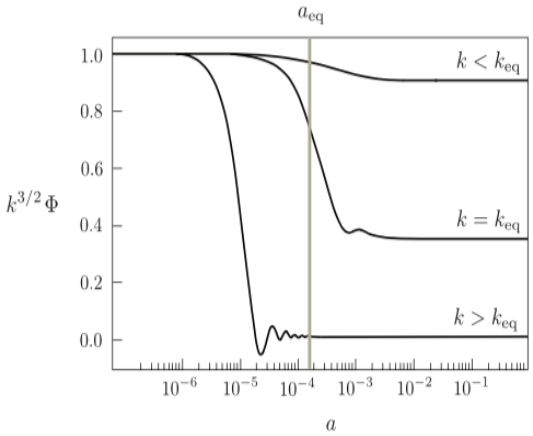

Figure 11.1: Evolution of perturbations.

11.1 Evolution fo fluctuations

• Gravitational potential (10.90)

- Radiation Era

$$\delta P = \frac{\delta\rho}{3}, \quad \mathcal{H}^2 \propto a^{-2}, \quad a \propto \eta, \quad \mathcal{H} = \frac{1}{\eta} \tag{11.9}$$

$$\phi'' + \frac{3}{\eta}\phi' - \frac{1}{\eta^2}\phi = \frac{4\pi G a^2 \bar{\rho}}{3}\delta_r. \tag{11.10}$$

using Einstein 00

$$\begin{aligned} &\phi'' + \frac{3}{\eta}\phi' - \frac{1}{\eta^2}\phi = \frac{1}{3}\nabla^2\phi - \frac{1}{\eta}\left(\phi' + \frac{1}{\eta}\phi\right) \\ &\Rightarrow \phi'' + \frac{4}{\eta}\phi' - \frac{1}{3}\nabla^2\phi = 0 \\ &\phi'' + \frac{4}{\eta}\phi' + \frac{k^2}{3}\phi = 0 \end{aligned} \tag{11.11}$$

damped wave equation with propagation speed $\frac{1}{\sqrt{3}}$.
Now, using $\phi = u(x)/x$ and $x = k\eta/\sqrt{3}$, we have

$$u'' + \frac{2}{x}u' + \left(1 - \frac{2}{x^2}\right)u = 0, \tag{11.12}$$

with solutions

$$\phi(x) = A_k \frac{J_1(x)}{x} + B_k \frac{n_1(x)}{x}. \tag{11.13}$$

Where the Bessel and Neumann are described by

$$J_1(x) = \frac{\sin x}{x^2} - \frac{\cos x}{x} = \frac{x}{3} + \mathcal{O}(x^3), \tag{11.14}$$

$$n_1(x) = -\frac{\cos x}{x^2} - \frac{\sin x}{x} = -\frac{1}{x^2} + \mathcal{O}(x^3), \tag{11.15}$$

however, the Neumann blows up for small x (early times) : hence reject that solution.

The proportionality constant A_k can be found by matching the solutions to the primordial value of the potential

$$\phi_k(0) = -\frac{2}{3}\mathcal{R}_k(0), \tag{11.16}$$

and therefore

$$\phi_k(\eta) = -2\mathcal{R}_k(0)\left(\frac{\sin x - x\cos x}{x^3}\right) \qquad \text{all scales} \tag{11.17}$$

- Outside the sound horizon $x = \frac{1}{\sqrt{3}}k\eta \ll 1 \quad \Rightarrow \quad \phi = constant.$

- On subhorizon scales $x \gg 1$ [use that $J_\ell(x) \sim \frac{1}{x}\sin\left(x - \frac{\ell\pi}{3}\right)$] to get

$$\phi_k(\eta) = 6\mathcal{R}_k(0)\frac{\cos\left(\frac{1}{\sqrt{3}}k\eta\right)}{(k\eta)^2}. \tag{11.18}$$

During the radiation era, subhorizon modes of ϕ oscillate with $f = \frac{1}{\sqrt{3}}k$ and amplitude that decays as $\eta^{-2} \propto a^{-2}$.

11.2 Matter era

$w = 0$

$$\phi'' + \frac{6}{\eta}\phi = 0, \tag{11.19}$$

$$\phi = \begin{cases} constant \\ \\ \eta^{-5} \propto a^-5/2 \end{cases} \tag{11.20}$$

$\phi = cons$ is frozen on all scales during matter domination.

11.3 Radiation

11.3.1 Evolution of perturbations

Radiation era (radiation perturbations)

$$\delta_r = -\frac{2}{3}(k\eta)^2\phi - 2\eta\phi' - 2\phi \tag{11.21}$$

$$\Delta_r = -\frac{2}{3}(k\eta)^2\phi. \tag{11.22}$$

(using $\Delta = \nabla^2\phi/4\pi G a^2\rho, 3/2\mathcal{H}^2 = 4\pi G a^2\rho, \mathcal{H} \propto 1/\eta \propto 1/a$).

Outside the horizon ($k\eta \ll 1$) $\delta_r = -2\phi$ and is constant, Δ_r grows as $\eta^2 \propto a^2$.

Inside the horizon ($k\eta \gg 1$)

$$\delta_r \approx \Delta_r = -\frac{2}{3}(k\eta)^2\phi = 4\mathcal{R}(0)\cos\left(\frac{1}{\sqrt{3}}k\eta\right), \tag{11.23}$$

oscillates w/constant amplitude and $4\mathcal{R}(0)$ is the solution $\delta_r'' - \frac{1}{3}\nabla^2\delta_r = 0$.

Matter era

Radiation perturbations are subdominant

On sub-horizon

$$\left.\begin{aligned}\delta_r' &= -\tfrac{4}{3}\nabla\cdot\vec{v}_r \\ v_r' &= -\tfrac{1}{4}\nabla\delta_r - \nabla\phi\end{aligned}\right\} \delta_r'' - \frac{1}{3}\nabla^2\delta_r = \frac{4}{3}\nabla^2\phi = cons \tag{11.24}$$

is an harmonic oscillator w/constant driving force, the acoustic oscillator $\rightarrow$ give rise to the peaks in the CMB spectrum.

Dark matter

Early times ($r + m$) (no baryons)

$$\mathcal{H}^2 = \frac{\mathcal{H}_0^2\Omega_m^2}{\Omega_r}\left(\frac{1}{y} + \frac{1}{y^2}\right) \qquad y \equiv \frac{a}{a_{eq}}. \tag{11.25}$$

- Subhorizon scales

$$\left.\begin{array}{c} \delta_m' = -\nabla \cdot \vec{v}_m \\ \vec{v}_m{}' = -\mathcal{H}\vec{v}_m - \nabla\phi \end{array}\right\} \delta_m'' + \mathcal{H}\delta_m' = \nabla^2\phi. \tag{11.26}$$

(only sourced by matter fluctuations)

$$\delta_m'' + \mathcal{H}\delta_m' - 4\pi G a^2 \bar{\rho}_m \delta_m \approx 0. \tag{11.27}$$

can be written as the Meszaros equation

$$\frac{d^2\delta_m}{dy^2} + \frac{2+3y}{2y(1+y)}\frac{d\delta_m}{dy} - \frac{3}{2y(1+y)}\delta_m = 0 \tag{11.28}$$

with solutions.

$$\delta_m \propto \begin{cases} 2+3y \\ (2+3y)\ln\left(\frac{\sqrt{1+y}+1}{\sqrt{1+y}-1}\right) - 6\sqrt{1+y} \end{cases} \tag{11.29}$$

- For $y \ll 1$ (RD) $\Rightarrow$ $\delta_m \propto \ln y \propto \ln a$

- For $y \gg 1$ (MD) $\Rightarrow$ $\delta_m \propto y \propto a$

	$\mathcal{R}D$			mD	
		ϕ	$\delta_m(\Delta_m)$	ϕ	$\delta_m(\Delta_m)$
$k >> k_{eq}$	super	constant	constant (a^2)	-	-
	sub	a^{-2}	$\ln a$	constant	a
$k << k_{eq}$	super	constant	constant (a^2)	constant	constant (a)
	sub	-	-	constant	a

Intermediate times

From the gravitational potential

$$\Delta m = \frac{\nabla^2\phi}{4\pi G a^2 \bar{\rho}} \propto \begin{cases} a \\ a^{-\frac{3}{2}} \end{cases} \tag{11.30}$$

Late times $(m + \Lambda)$

$$\nabla^2\phi = 4\pi G a^2 \bar{\rho}_m \Delta,$$

pressure fluctuations are neligable

$$\phi'' + 3\mathcal{H}\phi' + (2\mathcal{H}' + \mathcal{H}^2)\phi = 0$$

since $a^2\bar{\rho}_m \propto a^{-1}$, $\phi \propto \Delta_m/a$

$$\partial_\eta^2\left(\frac{\Delta_m}{a}\right) + 3\mathcal{H}\partial_\eta\left(\frac{\Delta_m}{a}\right) + (2\mathcal{H}' + \mathcal{H}^2)\left(\frac{\Delta_m}{a}\right) = 0 \tag{11.31}$$

$$\Delta_m'' + \mathcal{H}\Delta_m' + (\mathcal{H}' - \mathcal{H}^2)\Delta_m = 0 \qquad \text{w/Friedmann} \tag{11.32}$$

$$\Delta_m'' + \mathcal{H}\Delta_m' - 4\pi G a^2\bar{\rho}_m\Delta_m = 0 \qquad \text{valid on all scales} \tag{11.33}$$

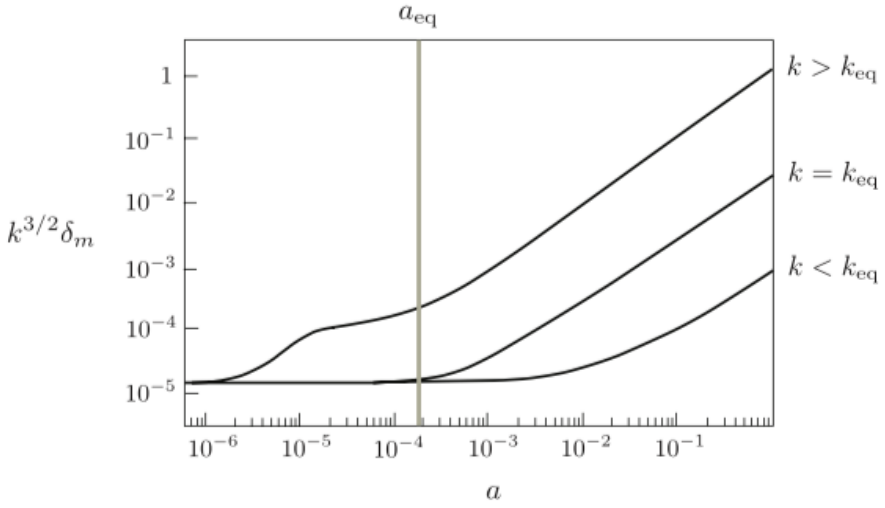

Figure 11.2: Evolution of perturbations.

Baryons

- Before decoupling.

$z > z_{dec} \approx 1100$, photons and baryons are coupled strongly to each other via Compton scattering

$$v_\gamma = v_b, \qquad \delta_\gamma = \frac{4}{3}\delta_b.$$

The pressure of the photons supports oscillations on small scales

- After decoupling

$$\delta_b' + \mathcal{H}\delta_b' = 4\pi G a^2(\bar{\rho}_b\delta_b + \bar{\rho}_c\delta_c)$$
$$\delta_c' + \mathcal{H}\delta_c' = 4\pi G a^2(\bar{\rho}_b\delta_b + \bar{\rho}_c\delta_c)$$
$$\bar{\rho}_m\delta_m = \bar{\rho}_b\delta_b + \bar{\rho}_c\delta_c$$

Define $D \equiv \delta_b - \delta_c$, subtracting

$$D'' + \frac{2}{\eta}D' = 0 \qquad D \propto \begin{cases} constant \\ \\ \eta^{-1} \end{cases}$$

while δ_m

$$\delta_m'' + \frac{2}{\eta}\delta_m' - \frac{6}{\eta^2}\delta_m = 0 \qquad \delta_m \propto \begin{cases} \eta^2 \\ \\ \eta^{-3} \end{cases}$$

since

$$\frac{\delta_b}{\delta_c} = \frac{\bar{\rho}_m\delta_m + \bar{\rho}_c D}{\bar{m}\delta_m - \bar{\rho}_b D} \quad \rightarrow \quad \frac{\delta_m}{\delta_m} = 1 \tag{11.34}$$

δ_b approaches δ_c.

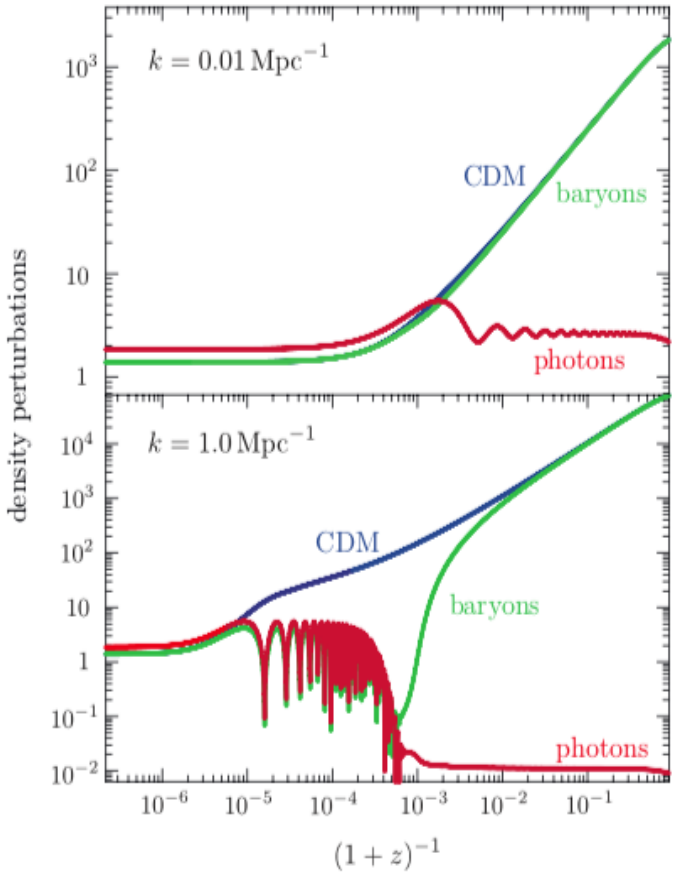

Figure 11.3: Evolution of perturbations.

12

Initial conditions from inflation

From quantum to classical

$$\delta\Phi(t,\bar{x}) \equiv \Phi(t,\vec{x}) - \bar{\Phi}(t). \tag{12.1}$$

• Quantum fluctuations induce a non-zero variance in the amplitudes of these oscillations

$$\left\langle |\delta\Phi_k|^2 \right\rangle \equiv \left\langle 0|\delta\Phi_k|^2 0 \right\rangle. \tag{12.2}$$

• Then inflationary expansion stretches these fluctuations to super horizon scales.

• At horizon crossing, $k = aH$, switch from inflation fluctuations $\delta\Phi$ to fluctuations in the conserved curvature perturbation $\mathcal{R}$. [In spatially flat gauge $\phi = E = 0$].

$$\mathcal{R} = -\phi - \frac{1}{3}\nabla^2 E + \mathcal{H}(B+v) \quad \longrightarrow \mathcal{H}(B+v) \quad \text{zero curvature gauge}$$
$$\text{recall} \quad \delta T^0_j = -(\bar{\rho}+\bar{p})\partial_j(B+v)$$

compare to the stress tensor of a scalar field

$$\delta T^0_j = g^{0\mu}\partial_\mu\Phi\partial_j\delta\Phi = g^{00}\partial_0\bar{\Phi}\partial_j\delta\Phi = \frac{\bar{\Phi}'}{a^2}\partial_j\delta\Phi$$
$$B + v = -\frac{\delta\Phi}{\bar{\Phi}'}$$
$$\mathcal{R} = -\frac{\mathcal{H}}{\bar{\Phi}'}\delta\Phi. \tag{12.3}$$

For the Unperturbed FRW metric

$$S = \int d\eta d^3x \left[\frac{1}{2}a^2\left(\Phi'^2 - (\nabla\Phi)^2\right) - a^4 V(\Phi)\right], \tag{12.4}$$

in the background $\Phi = \bar{\Phi}(\eta)$ is homogeneous

Fluctuations in Φ: $\Phi = \bar{\Phi} + \frac{u}{a}$ where $u = a\delta\Phi$

expanding the fluctuations in u, the term in square brackets becomes

$$\underbrace{a\bar{\Phi}'u'}_{\delta^{(1)}} - \underbrace{a'\bar{\Phi}'u}_{\delta^{(1)}} + \frac{1}{2}u'^2 - u'u\mathcal{H} + \frac{1}{2}u^2\mathcal{H}^2 - \frac{1}{2}(\nabla u)^2 - \underbrace{a^3 u V_{,\Phi}}_{\delta^{(1)}} - \frac{1}{2}a^2u^2V_{,\Phi\Phi}. \tag{12.5}$$

Looking only the terms marked with $\delta^{(1)}$, the first term can be integrated by parts and dropping the boundary term, we have

$$\delta^{(1)} = -\int d\eta d^3x \left[(\bar{\Phi}'a)' + a'\bar{\Phi}' + a^3V_{,\Phi}\right] u \tag{12.6}$$

to then

$$\delta^{(1)} = -\int d\eta d^3x a[\bar{\Phi}'' + 2\mathcal{H}\bar{\Phi}' + a^2V_{,\Phi}]u \tag{12.7}$$

where

$$\bar{\Phi}'' + 2\mathcal{H}\bar{\Phi}' + a^2V_{,\Phi} = 0 \qquad \text{Klein-Gorden for the background field} \tag{12.8}$$

hence, we need to go to the second order in the action

$$\delta^{(2)} = \frac{1}{2}\int d\eta d^3x \left[(u')^2 - (\nabla u)^2 - 2\mathcal{H}uu' + \left(\mathcal{H}^2 - a^2V_{,\Phi\Phi}\right)u^2\right] \tag{12.9}$$

$$uu' = \frac{1}{2}(u^2)'$$

$$\delta^{(2)} = \frac{1}{2}\int d\eta d^3x \left[(u')^2 - (\nabla u)^2 + \left(\frac{a''}{a} - a^2V_{,\Phi\Phi}\right)u^2\right]. \tag{12.10}$$

During slow-roll inflation we have

$$\frac{V_{,\Phi\Phi}}{H^2} \approx \frac{3M_p^2V_{,\Phi\Phi}}{V} = 3\eta_V \ll 1, \tag{12.11}$$

since $a' = a^2H$, $H \sim constant$, deriving

$$\frac{a''}{a} \approx 2a'H = 2a^2H^2 \gg a^2V_{,\Phi\Phi} \tag{12.12}$$

$$\delta^{(2)} = \int d\eta d^3x \frac{1}{2}\left[(u')^2 + \frac{a''}{a}u^2 - (\nabla u)^2\right]. \tag{12.13}$$

Applying $E - L$

$$u'' - \frac{a''}{a}u - \nabla^2 u = 0 \qquad \text{Mukhanov-Sasaki equation.} \tag{12.14}$$

for each Fourier mode

$$u_k'' + \left(k^2 - \frac{a''}{a}\right)u_k = 0. \tag{12.15}$$

12.1 Canonical quantization

Follow the quantization of the harmonic oscillator.

Define the momentum conjugate to u

$$\pi_u \equiv \frac{\partial \mathcal{L}}{\partial \dot{u}} = \dot{u}, \tag{12.16}$$

promote π and u to operator-valued, commutation relations

$$[\hat{u}(\eta, \vec{x}), \hat{\pi}(\eta, \vec{x}')] = i\delta(\vec{x} - \vec{x}') \qquad \text{Heinsenberg picture} \tag{12.17}$$

$$\frac{\partial^2 \hat{u}}{\partial \eta^2} - \frac{a''}{a}\hat{u} - \nabla^2 \hat{u} = 0 \tag{12.18}$$

Quantum oscillators $\hat{a}_k^\dagger$,$\hat{a}_k$ creation and annihilation operators

The general solution to the equation

$$\hat{u}(\eta, x) = \int \frac{d^3k}{(2\pi)^{\frac{3}{2}}}[\hat{a}(k)u_k(\eta)e^{i\bar{k}\cdot x} + \hat{a}^\dagger(\bar{k})u_k^*(\eta)e^{-i\bar{k}\cdot\bar{x}}] \tag{12.19}$$

Fourier

$$\hat{u}(\eta, \vec{k}) = \hat{a}_{\vec{k}}u_k(\eta) + \hat{a}_{\vec{k}}^\dagger u_k^*(\eta). \tag{12.20}$$

12.2 Power spectrum

Power spectrum $P_u(k)$ by computing the two-point correlator of the flied u in Fourier space

$$\left\langle 0|\hat{u}(\eta,\bar{k})\hat{u}^{\dagger}(\eta,\bar{k}^{'})|0\right\rangle = \frac{2\pi^2}{k^3}P_u(k)\delta(\bar{k}-\bar{k}^{'}) \tag{12.21}$$

after some algebra

$$\left\langle 0|\hat{u}(\eta,\bar{k})\hat{u}^{\dagger}(\eta,\bar{k}^{'})|0\right\rangle = |u_k(\eta)|^2\delta(\bar{k}-\bar{k}^{'}) \tag{12.22}$$

the power spectrum is thus $P_u(k) = \frac{k^3}{2\pi^2}|u_k(\eta)|^2$ since $u = a\delta\Phi$

$$P_{\delta\Phi}(k) = \frac{k^3}{2\pi^2}\left|\frac{u_k(\eta)}{a(\eta)}\right|^2 \tag{12.23}$$

we requiere more detailed solutions.

During slow-roll inflation, $H \sim constant$, or H_k for few e-folds, integrating

$$\begin{aligned} \frac{a'}{a} = \mathcal{H} = aH_k \quad &\Rightarrow \quad a = -\frac{1}{H_k\eta} \\ a'' = -\frac{2}{H_k\eta^3} \quad &\Rightarrow \quad \frac{a''}{a} = \frac{2}{\eta^2} \end{aligned} \tag{12.24}$$

$$u_k^{''} + \left(k^2 - \frac{2}{\eta^2}\right)u_k = 0 \tag{12.25}$$

with solutions

$$u_k(\eta) = \frac{e^{-ik\eta}}{\sqrt{2k}}\left(1 - \frac{i}{k\eta}\right) \tag{12.26}$$

few e-folds after Hubble exit (super horizon)

$$u_k(\eta) \approx -\frac{ie^{-ik\eta}}{\eta\sqrt{2k^3}} \quad \Rightarrow \quad \frac{u_k(\eta)}{a(\eta)} \approx \frac{iH_ke^{-ik\eta}}{\sqrt{2k^3}} \tag{12.27}$$

Form the modes that have excited the Hubble radius

$$P_{\delta\Phi}(k) = \left(\frac{H_k}{2\pi}\right)^2 \tag{12.28}$$

A light scalar field in quasi the Sitter spacetime acquires an almost-scale-invariant spectrum of fluctuations

$$\mathcal{P}_{\mathcal{R}}(k) = \left(\frac{\mathcal{H}}{\bar{\Phi}'}\right)^2 P_{\delta\Phi} = \left(\frac{H^2}{2\pi\bar{\Phi}'}\right)^2 \tag{12.29}$$

Using slow-roll

$$H^2 \approx \frac{1}{3M_p^2} V(\bar{\Phi}), \qquad 3H\dot{\bar{\Phi}} = -V_{,\Phi} \tag{12.30}$$

$$\mathcal{P}_{\mathcal{R}}(k) = \left(\frac{H^2}{2\pi\dot{\bar{\Phi}}}\right)^2 \approx \left(\frac{3H^3}{2\pi V_{,\Phi}}\right)^2 = \frac{\left(V/M_p^2\right)^3}{3(2\pi)^2 (V_{,\Phi})^2} = \frac{8}{3}\left(\frac{V^{1/4}}{\sqrt{8\pi}M_p}\right)\frac{1}{\epsilon_V} \tag{12.31}$$

CMB obs. constrain $\mathcal{P}_{\mathcal{R}}(k) \sim 2 \times 10^{-9}$

12.3 Primordial perturbations from inflation

• Slow-roll inflation produces a spectrum of curvature perturbations that is almost scale-invariant (Harrison-Zeldovich)

• We can quantify small departures from scale-invariance

$$P_{\mathcal{R}} = A_s \left(\frac{k}{k_0}\right)^{n_s-1} \tag{12.32}$$

$n_s(k)$ spectral index $n_s(k) - 1 \equiv \frac{d\ln P_R(k)}{d\ln k}$ in terms of the potential

$$\frac{d}{d\ln k} = \frac{dt}{d\ln k}\frac{d\Phi}{dt}\frac{d}{d\Phi} \tag{12.33}$$

at Hubble exit

$$k = aH \Rightarrow \frac{d\ln k}{dt} = H\left(1 + \frac{\partial_t H}{H^2}\right) \tag{12.34}$$

$$\begin{aligned}\frac{\partial_t H}{H^2} &= -\frac{3}{2}\left(\frac{\bar\rho + \bar P}{\bar\rho}\right) \\ &\approx -\frac{3}{2}\frac{(\partial_t\Phi)^2}{V} = -\frac{1}{2}\frac{(3H\partial_t\Phi)^2}{3H^2V} \\ &\approx -\frac{M_p^2}{2}\left(\frac{V_{,\Phi}}{V}\right)^2 = -\epsilon_V, \qquad \frac{d\ln k}{dt} \approx H(1-\epsilon_V)\end{aligned} \tag{12.35}$$

$$\begin{aligned}\frac{d}{d\ln k} &\approx \frac{1}{H}\frac{d\Phi}{dt}\frac{d}{d\Phi} \\ &\approx \underbrace{-\frac{V_{,\Phi}}{3H^2}\frac{d}{d\Phi}}_{\text{1stFriedmann}} \approx \underbrace{-M_p^2\frac{V_{,\Phi}}{V}\frac{d}{d\Phi}}_{\text{2ndFriedmann}} \approx -M_p^2\sqrt{2\epsilon_V}\frac{d}{d\Phi}\end{aligned} \tag{12.36}$$

differenciate the spectrum

$$n_s - 1 = -M_p\sqrt{2\epsilon_V}\frac{d}{d\Phi}(\ln V - \ln\epsilon_V) \tag{12.37}$$

$$- Mp\sqrt{2\epsilon_V}\left(\frac{V_{,\Phi}}{V} - \frac{\epsilon_{V,\Phi}}{\epsilon_V}\right) \tag{12.38}$$

second term

$$\frac{d\ln\epsilon_V}{d\Phi} = 2\left(\frac{V_{,\Phi\Phi}}{V'} - \frac{V_{,\Phi}}{V}\right) \tag{12.39}$$

$$\approx \frac{\sqrt{2}}{M_p}\left(\frac{\eta_V}{\sqrt{\epsilon_V}} - 2\sqrt{\epsilon_V}\right) \tag{12.40}$$

$$n_s - 1 = 2\eta_V(\Phi) - 6\epsilon_V(\Phi) \tag{12.41}$$

$\rightarrow$ $\frac{dn_s}{d\ln k}$ second-order in slow roll (running parameter).

• Gravitational waves from inflation

tensor modes

$$ds^2 = a^2[d\eta^2 - (\delta_{ij} + 2E_{ij}^T)dx^i dx^j] \tag{12.42}$$

E_{ij}^T trace-free and $\delta^{ik}\partial_k E_{ij}^T = 0$

there are two degrees of freedom associated $\rightarrow$ behave like massless scalar fields

$$S^{(2)} = \frac{M_p^2}{8}\int d\eta dx^3 a^2[(E_{ij}^{T'})^2 - (\nabla E_{ij}^T)^2] \tag{12.43}$$

define

$$\frac{M_p^2}{2}aE_{ij}^T \equiv \frac{1}{\sqrt{2}}\begin{pmatrix} f_+ & f_x & 0 \\ f_x & -f_+ & 0 \\ 0 & 0 & 0 \end{pmatrix} \tag{12.44}$$

$$S^{(2)} = \frac{1}{2}\sum_{I=+,x}\int d\eta d^3x[(u_I')^2 - (\nabla u_I)^2 + \frac{a''}{a}u_I^2] \tag{12.45}$$

two copies for the action $u = a\delta\Phi$

$$P_t(k) = \frac{8}{M_p^2}\left(\frac{H_k}{2\pi}\right)^2 \tag{12.46}$$

using the slow-roll inflation

$$P_t(k) \approx \frac{128}{3}\left(\frac{V^{1/4}}{\sqrt{8\pi}M_p}\right)^4 \tag{12.47}$$

defines the tensor-to-scalar ratio

$$r \equiv \frac{P_t(k)}{P_R(k)} \approx 16\epsilon_V$$

$$P_t(k) = A_t \left(\frac{k}{k_0}\right)^{n_t} \tag{12.48}$$

tensor spectral index

$$\begin{aligned} n_t \frac{d\ln P_n(k)}{d\ln k} \approx \frac{d\ln V}{d\ln k} &= -M_p\sqrt{2\epsilon_V}\frac{V_{,\Phi}}{V} \\ &= -M_p\sqrt{2\epsilon_V}\frac{\sqrt{2\epsilon_V}}{M_p} \\ &= -2\epsilon_V \end{aligned} \tag{12.49}$$

Note that $r \approx -8n_t$, the first consistency relation.

12.4 The matter power spectrum

The distribution of matter is a key cosmological observable

MPS $\mathcal{P}_{\Delta m}(\eta;\vec{k})$ is defined by

$$< \Delta_m(\eta,\vec{k})\Delta_m^*(\eta,\vec{k}') > \equiv \frac{2\pi}{k^3}\mathcal{P}_{\Delta_m}(\eta,k)\delta(\bar{k}-\bar{k}') \tag{12.50}$$

is dimensionless, but frequently

$$P_{\Delta_m}(\eta,k) \equiv \frac{2\pi}{k^3}\mathcal{P}_{\Delta_m}(\eta,k). \tag{12.51}$$

• Real-space measures of matter clustering, σ_R

$\rightarrow$ the variance of Δ_m averaged in spheres of radius R, equivalent to the variance of Δ_m convolved with

$$\frac{3\Theta(R-|x|)}{4\pi R^3} \tag{12.52}$$

normalized spherical top hat, which in Fourier space is $W(kR)$

$$W(x) \equiv \frac{3}{x^3}(\sin x - x\cos x) \tag{12.53}$$

$$\sigma_R^2 = \int \frac{d^3\bar{k}}{(2\pi)^3}W^2(kR)P_{\Delta_m}(k). \tag{12.54}$$

Historically $R = 8h^{-1}$ MPc is chosen

Makes the scale at which perturbation theory breaks down and non-linear effects become important.

Whre lineal perturbation holds

$$\Delta_m(\eta, \bar{k}) = T(\eta, k)\mathcal{R}(0, \bar{k}). \tag{12.55}$$

$T(\eta, k)$ transfer function that relates the primordial curvature perturbation to the comoving matter perturbation. [Sometimes you will find it as $\delta(k, \eta) \sim \phi_p D_1(\eta) T(k)$, with the growth function

$$D_1(a) \propto H(a) \int^a \frac{da}{(aH(a))^3}. \tag{12.56}$$

The primordial curvature power spectrum is almost scale-free so it contributes with a factor of k^{-3}.

- First $k < k_{eq}$.

Relates relate Δ_m to ϕ via the poisson equation

$$\begin{aligned} &\Delta_m \sim k^2\phi \qquad \left[\phi(\eta, \bar{k}) = -\frac{3}{5}\mathcal{R}(0, \bar{k}) \qquad \text{matter domination}\right] \\ &\Rightarrow \quad T(\eta, k) \propto k^2 \\ &\qquad P_{\Delta m}(k) \propto \frac{k^4}{k^3} \propto k \qquad \text{on large scales.} \end{aligned}$$

- For $k > k_{eq}$

The newtonian-gauge δ_c is constant in time until horizon entry $\delta_c(0, \bar{k}) \propto \phi(0, \bar{k}) \propto \mathcal{R}(0, \bar{k})$.

Then, the Meszaros effect operates inside the horizon and δ_c grows logarithmically with proper time

$$\frac{\delta_c(t_{eq}, k)}{\delta_c(0, \bar{k})} \sim 1 + \ln\left(\frac{t_{eq}}{t_k}\right) \tag{12.57}$$

at time of horizon entry $a(t_k)H(t_k) = k$ and $a \propto t^{1/2}$ in radiation domination $\Rightarrow t_k \propto \frac{1}{k^2}$

$$\begin{aligned} &\sim 1 + 2\ln\left(\frac{k}{k_{eq}}\right) \qquad k > k_{eq} \\ T(\eta, k) &\propto \ln\left(\frac{k}{k_{eq}}\right) \\ P_{\Delta_m} &\propto k^{-3}\ln^2\left(\frac{k}{k_{eq}}\right) \qquad k >> k_{eq} \end{aligned} \tag{12.58}$$

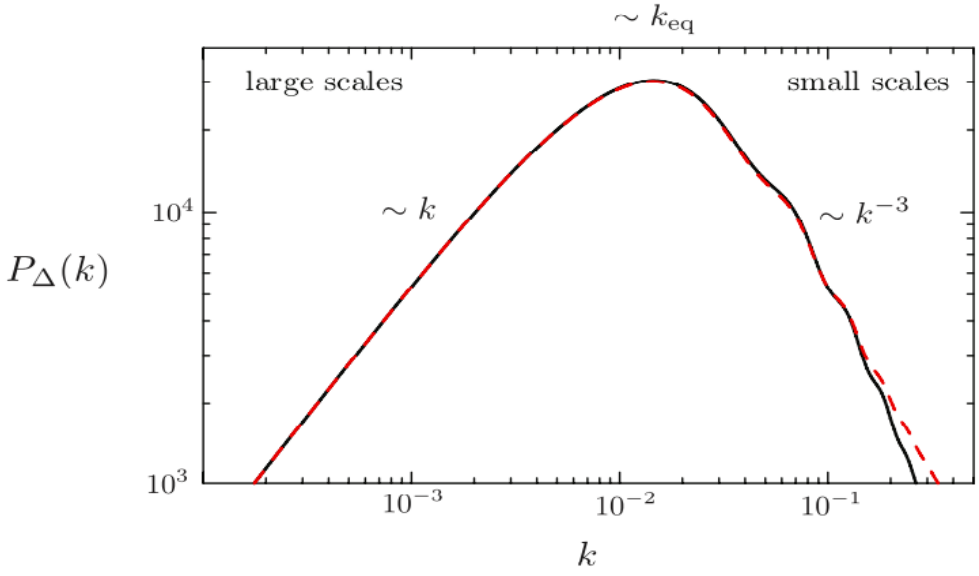

Figure 12.1: Evolution of perturbations.

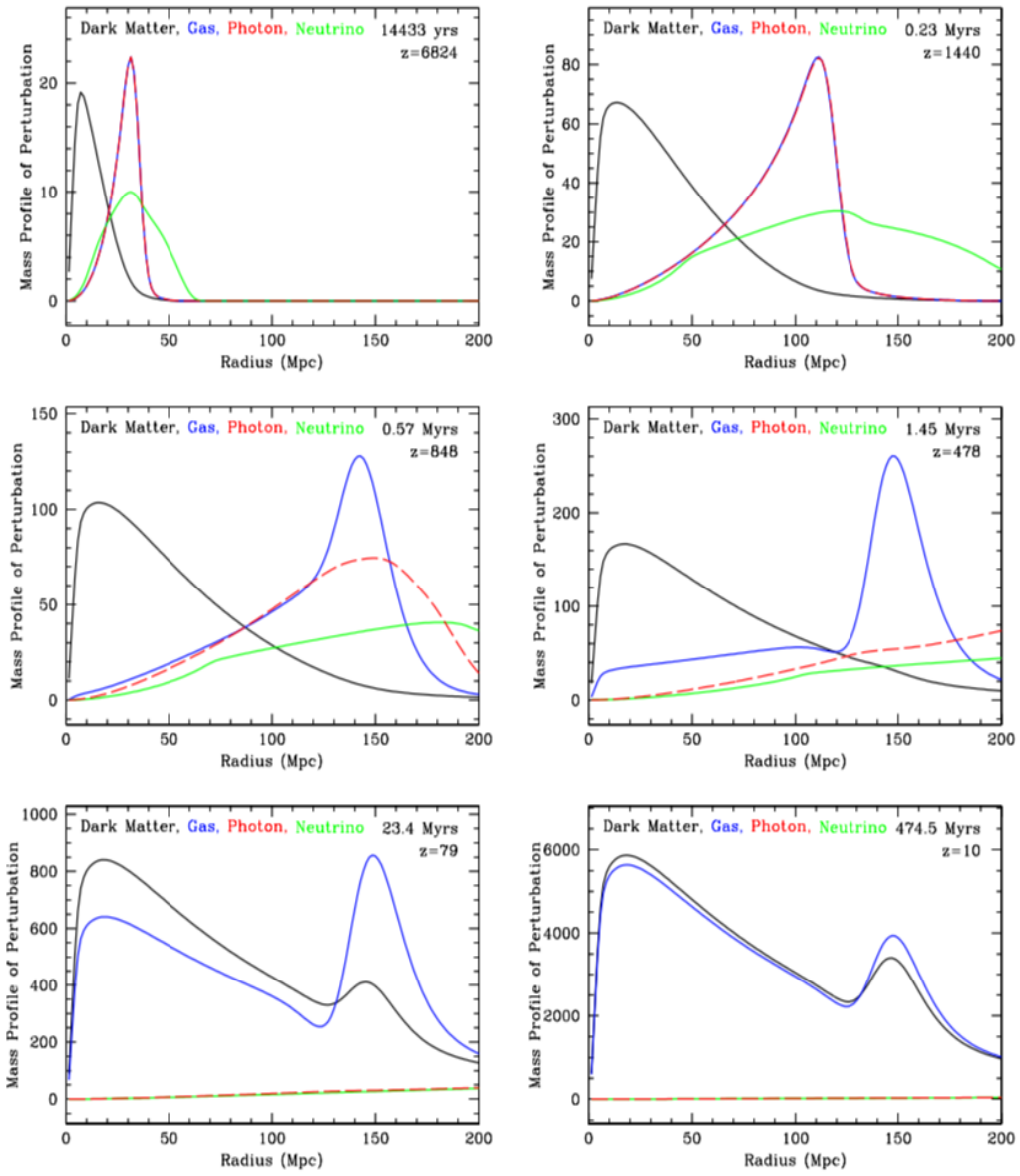

Figure 12.2: Evolution of perturbations.

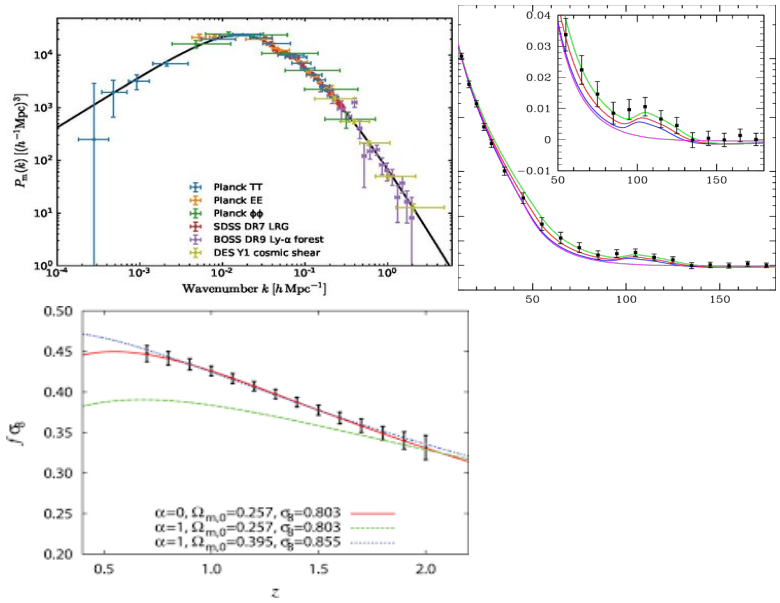

Figure 12.3: Evolution of perturbations.

13

CMB

1. Cosmic Microwave Background – Observational cosmology, history.
   Recombination, Decoupling, Last Scattering – Pettini
   Black body radiation

2. Stats
   Perturbations
   Acoustic peaks
   Polarization, Tensor perturbations

3. Observations
   Physical Implications, Cosmology
   Codes
   What else, Non-gaussianity, Primordial Gravitational waves

The cosmic microwave background (CMB) is the thermal radiation left over from the "Big Bang", also known as "relic radiation". It is fundamental to observational cosmology because it is the oldest light in the universe, dating to the epoch of recombination. With a traditional optical telescope, the space between stars and galaxies (the background) is completely dark. However, a sufficiently sensitive radio telescope shows a faint background glow, almost exactly the same in all directions, that is not associated with any star, galaxy, or other object. This glow is strongest in the microwave region of the radio spectrum.
The CMB is a snapshot of the oldest light in our Universe, imprinted on the sky when the Universe was just 380,000 years old. It shows tiny temperature fluctuations that correspond to

regions of slightly different densities, representing the seeds of all future structure: the stars and galaxies of today.

13.1 Isotropic CMB

The Cosmic Microwave Background radiation was discovered in 1965 by two American radio astronomers, Arno Penzias and Robert Wilson, while trying to identify sources of noise in microwave satellite communications at Bell Laboratories in New Jersey. Their discovery was announced alongside the interpretation of the CMB as relic thermal radiation from the Big Bang by Robert Dicke and collaborators working at the nearby Princeton University. Interestingly, the possibility of a cosmic thermal background were first entertained by Gamow, Alpher and Herman in 1948 as a consequence of Big Bang nucleosynthesis, but the idea was so beyond the experimental

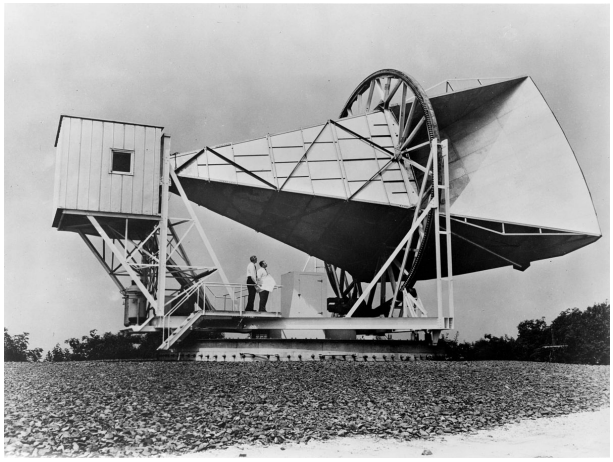

Figure 13.1: Discovery of the CMB.

The original detection by Penzias and Wilson was at a wavelength of 73.5 mm, this being the wavelength of the telecommunication signals they were working with; this wavelength is two orders of magnitude longer than $\lambda_{\text{peak}} = 1.1\text{mm}$ of a $T = 2.7255\text{K}$ blackbody.

At any angular position (θ, ϕ) on the sky, the spectrum of the CMB is a near-perfect blackbody (see Figure 13.2). The CMB is in fact the closest approximation we have to an ideal

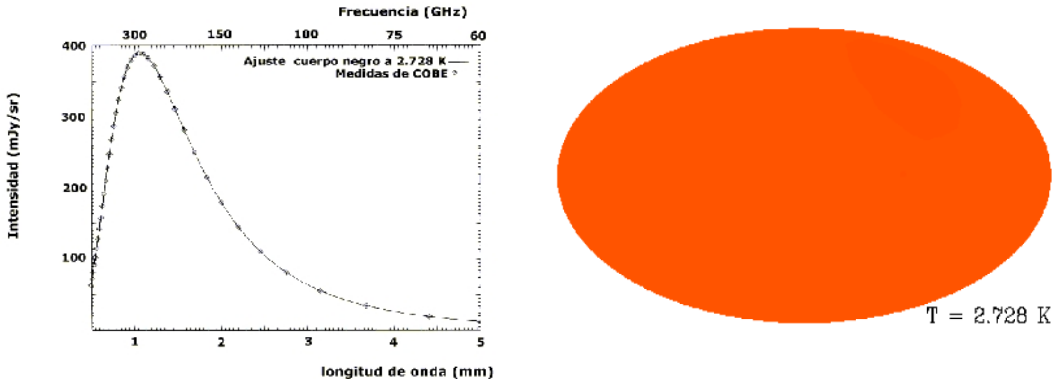

Figure 13.2: Blackbody radiation.

blackbody. With $T(\theta, \phi)$ denoting the temperature at a given point on the sky, the mean temperature averaged over the whole sky is

$$\langle T \rangle = \frac{1}{4\pi} \int T(\theta, \phi) \sin\theta d\theta d\phi = 2.7255 \pm 0.0006K \tag{13.1}$$

The deviations from this mean temperature from point to point on the sky are tiny. Defining the dimensionless T fluctuations:

$$\frac{\delta T}{T}(\theta, \phi) = \frac{T(\theta, \phi) - \langle T \rangle}{\langle T \rangle} \tag{13.2}$$

is found that

$$\left\langle \left(\frac{\delta T}{T} \right) \right\rangle^{1/2} = 1.1 \times 10^{-5} \tag{13.3}$$

Such deviations were first reported in 1992 by the COBE team. Subsequent CMB missions (WMAP and Planck) have significantly improved the angular resolution and precision in the mapping of the CMB sky, as illustrated in Figure 13.3.

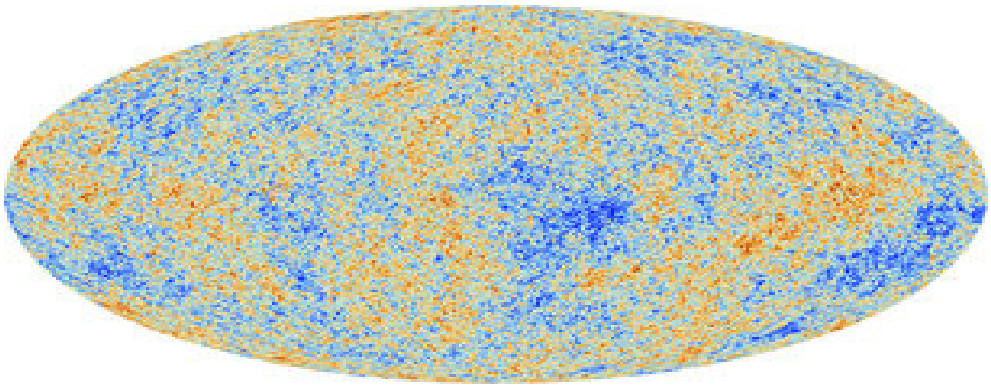

Figure 13.3: CMB seen by Planck.

14

The Boltzmann equation

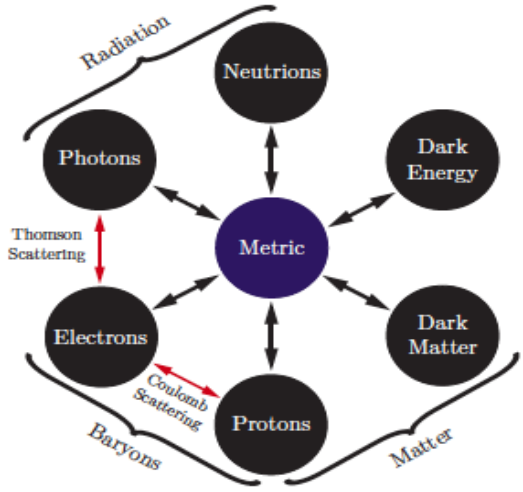

Figure 14.1: Interactions between the different forms of matter in the universe.

The Boltzmann equation

$$\frac{df}{d\eta} = C[f] \tag{14.1}$$

The expansion of the Universe is slow compared to the microwave frequency of the CMB. It is hence adiabatic, as far as the photons are concerned. The distribution function of the cosmic microwave background with temperature $\bar{T}$ is

$$\bar{f} = \left[\exp\left(\frac{E}{\bar{T}}\right) - 1\right]^{-1}. \tag{14.2}$$

We see that $\bar{f}$ depends just upon the energy E of a photon. Writing $T = T_0 a^{-1}$, we see that $\bar{f}$ is a function of aE only:

$$\bar{f}(aE) = \left[\exp\left(\frac{aE}{\bar{T}_0}\right) - 1\right]^{-1}. \tag{14.3}$$

To make the connection, we note that in General Relativity, the energy of a photon is given by

$$E = -u_\mu p^\mu, \tag{14.4}$$

and for observers in the unperturbed background at rest, i.e. $u_\mu = a(1,0,0,0)$, we haven then $E = -a\,p$, where $p \equiv |\mathbf{p}| = \sqrt{p^i p^j \delta_{ij}}$, in the background $p^0 = p$.

Them $\bar{f}$ depends solely of $P = a^2 p$, and therefore use P as an argument for f.

The full distribution function is naively a function of (x^μ, p^μ). Yet, the physics governing the evolution of f respects the mass shell condition $p_\mu p^\mu = m^2$. Therefore, f is a function $f(x^\mu, p^i)$ only. Use p^0 as a function of p^i right from the start. In order to do this, let us split the spatial momentum

$$p^i \equiv p n^i \tag{14.5}$$

into its magnitude p and the unit vector of photon momentum $\mathbf{n}$, so $\delta_{ij} n^i n^j = 1$. Hence, we arrive at our final set of variables for f

$$f = f(\eta, \mathbf{x}, P, \mathbf{n}) \tag{14.6}$$

The complete distribution function for each species can be split into background plus a perturbation part:

$$f(\eta, \mathbf{x}, P, \mathbf{n}) = \bar{f}(P) + F(\eta, \mathbf{x}, P, \mathbf{n}), \tag{14.7}$$

Useful relations, got them from $g_{\mu\nu} p^\mu p^\nu = 0$

$$p^0 = p(1 - \Psi - \Phi) \tag{14.8}$$

$$p_0 = -a^2 p(1 + [\Psi - \Phi]) \tag{14.9}$$

$$p_i = a^2 p n_i (1 - 2\Phi) \tag{14.10}$$

$$\sqrt{-g} = a^4(1 + \Psi - 3\Phi) \tag{14.11}$$

and $\mu = \frac{\mathbf{k}\cdot\mathbf{n}}{k}$, and a useful formula

$$\frac{\partial p}{\partial p^i} = \frac{\partial \sqrt{\delta_{mn} p^m p^n}}{\partial p^i} = \frac{1}{2}\frac{2p_i}{p} = n_i \tag{14.12}$$

14.1 Collisionless Part

The evolution of perturbations in the universe is quantified by the Boltzmann equation:

$$\left(\frac{\partial f}{\partial \eta}\right)_P + \frac{\partial f}{\partial x^i}\frac{\partial x^i}{\partial \eta} + \frac{\partial f}{\partial P}\frac{\partial P}{\partial \eta} + \frac{\partial f}{\partial n^i}\frac{\partial n^i}{\partial \eta} = C[f, G], \tag{14.13}$$

which relates the effects of gravity on the photon distribution function f to the rate of interactions with other species, given by the *collision term* $C[f, G]$. The previous distribution applies to polarization as well by simply replacing $F \to G$ (we use G to denote the linear polarization distribution function) and $\bar{f} = \bar{f}' \to 0$

On the Boltzmann equation the last term vanishes, because it is of second order in perturbation theory: $\bar{f}$ does not depend on n^i and hence $\partial f/\partial n^i$ is a perturbation. In addition $\partial n^i/\partial \eta$, is a change in photon direction that can only come from a spatially inhomogeneous scattering process. So all in all the last term is of second order and we can safely discard it.

The most difficult term is the third one.

$$\frac{\partial P}{\partial \eta} = \frac{\partial}{\partial \eta} a^2 p \tag{14.14}$$

$$= 2\frac{\dot{a}}{a} a^2 p + a^2 \frac{\partial p}{\partial \eta} \tag{14.15}$$

and using the equation

$$\frac{\partial p}{\partial \eta} = \frac{\partial p}{\partial p^i}\frac{\partial p^i}{\partial \eta} = n^i \frac{\partial p^i}{\partial \eta} \tag{14.16}$$

The third term can be computed from the geodesic equation

$$p^0 \frac{\partial p^i}{\partial \eta} + \Gamma^i_{\alpha\beta} p^\alpha p^\beta = 0 \tag{14.17}$$

then

$$n_i \frac{\partial p^i}{\partial \eta} = -(p^0)^{-1} n_i \Gamma^i_{\alpha\beta} p^\alpha p^\beta \tag{14.18}$$

Collecting all the terms, we have

$$n_i \Gamma^i_{\beta\gamma} p^\beta p^\gamma = 2\frac{a'}{a} p^0 p + p^2 \left[i\mu k(\Psi - \Phi) - 2\Phi'\right] \tag{14.19}$$

$$\frac{\partial f}{\partial P}\frac{\partial P}{\partial \eta} = -P\bar{f}_{,P}\{i\mu k[\Phi + \Psi] + 2\Phi'\}, \tag{14.20}$$

and the spatial part

$$\frac{\partial f}{\partial x^i}\frac{\partial x^i}{\partial \eta} = i\mu k F(\eta, \mathbf{x}, P, \mathbf{n}). \tag{14.21}$$

Collecting the terms involving the background only

$$\left(\frac{\partial f}{\partial \eta}\right)_P = 0 \tag{14.22}$$

The change in a distribution function of massless particles which depends solely on P is zero: the preservation of the background black body spectrum.

As far as the perturbed distribution is concerned, it is much more exciting:

$$\left(\frac{\partial F}{\partial \eta}\right)_P + i\mu k F - P\bar{f}_{,P}\{i\mu k[\Phi + \Psi] + 2\Phi'\} = C[f, G] \tag{14.23}$$

Finally, making the substitution $F \to G$, $\bar{f}' \to 0$, we get the simple evolution equation for the linear polarization G

$$\left(\frac{\partial G}{\partial \eta}\right)_P + i\mu k G = C_G[f, G] \tag{14.24}$$

where $C_G[f, G]$ is the collision term for G.

14.1.1 Perturbed temperature

Writing the temperature function T in terms of the photon *brightness temperature perturbation* $\Delta \equiv \Delta T/\bar{T}$, we have

$$T(\eta, \mathbf{x}, \mathbf{n}) = \bar{T}(\eta)[1 + \Delta(\eta, \mathbf{x}, \mathbf{n})], \tag{14.25}$$

$$\begin{aligned} f = \bar{f}\left(\frac{P}{1+\Delta}\right) &= \bar{f} + \frac{\partial \bar{f}}{\partial P}\left[\frac{P}{1+\Delta} - P\right] \\ &= \bar{f} + \frac{\partial \bar{f}}{\partial P} P\left(\frac{1}{1+\Delta} - 1\right) \\ &= \bar{f} + \frac{\partial \bar{f}}{\partial P} P(1 - \Delta - 1) \\ &= \bar{f} - \frac{\partial \bar{f}}{\partial P} P\Delta \end{aligned} \tag{14.26}$$

and therefore F and Δ are connected via

$$F(\eta, \mathbf{x}, P, \mathbf{n}) = -P\frac{\partial \bar{f}}{\partial P}\Delta(\eta, \mathbf{x}, \mathbf{n}). \tag{14.27}$$

So,

$$G(\eta, \mathbf{x}, P, \mathbf{n}) = -P\frac{\partial \bar{f}}{\partial P}\mathcal{Q}(\eta, \mathbf{x}, \mathbf{n}). \tag{14.28}$$

Then, the simplify Boltzmann equation becomes

$$\Delta' + ik\mu\Delta = -i\mu k[\Phi + \Psi] - 2\Phi' + \hat{C}[f, G] \tag{14.29}$$

where $\hat{C}[f, G] \equiv C[f, G]/(P\bar{f}_{,P})$

14.2 The Collision Term from Compton Scattering

The dominant term for the coupling of photons to the baryons is via inverse Compton scattering

$$e^-(\mathbf{q}) + \gamma(\mathbf{p}) \rightleftharpoons \mathbf{e}^-(\mathbf{q}') + \gamma(\mathbf{p}') \tag{14.30}$$

where we are interested how the photon distribution as a function of momentum p changes [Thomson scattering is the low-energy limit of Compton scattering]. The amplitude can be calculated from the Feynman rules.

$$C[f, G] = an_e\sigma_T\bar{f}_{,P}P\left\{i\mu v_b + \Delta(\eta, \mathbf{x}, \mathbf{n}) - \frac{1}{4}\int_{-1}^{1}\Delta(\eta, \mathbf{x}, \mathbf{n}')[P_2(\lambda)P_2(\mu) + 2]d\lambda \right. \tag{14.31}$$

$$\left. -\frac{1}{4}\int_{-1}^{1}\mathcal{Q}(\eta, \mathbf{x}, \mathbf{n}')P_2(\mu)[-2\sqrt{6\pi}5_2Y_2^0(\lambda)]d\lambda\right\} \tag{14.32}$$

The expansion of the temperature perturbation (Δ) and polarisations (Q and U), in terms of the spherical harmonics $Y_l^m(\mathbf{n})$, are

$$\Delta(\eta, \mathbf{x}, \mathbf{n}) = \sum_l (-i)^l\Delta_l(k, \eta)P_l(\hat{\mathbf{k}}\cdot\mathbf{n}), \tag{14.33}$$

$$(Q \pm iU)(\eta, \mathbf{x}, \mathbf{n}) = \sum_{l=2}(-i)^l(E_l^0 \pm iB_l^0)\sqrt{\frac{4\pi}{2l+1}}\,{}_{\mp 2}Y_l^0(\mathbf{n}), \tag{14.34}$$

where E and B are the electric and magnetic modes and the P_l's represent the Legendre polynomials. So

$$C[f, G] = an_e\sigma_T\bar{f}_{,P}P\left\{i\mu v_b + \Delta(\eta, \mathbf{k}, \mathbf{n}) + \frac{1}{10}\Delta_2P_2(\mu) - \Delta_0 - \frac{\sqrt{6}}{10}[E_2 - \Delta_2]\right\} \tag{14.35}$$

The Boltzmann equation thus yields to the evolution equation of temperature perturbations [36]:

$$\Delta' + ik\mu\Delta + \kappa'\Delta = -i\mu k[\Phi + \Psi] - 2\Phi' + \kappa'\left\{\frac{1}{4}\delta_\gamma - \Phi - i\mu v_b + \frac{1}{10}P_2(\mu)[\sqrt{6}E_2 - \Delta_2]\right\}. \quad (14.36)$$

$$Q' + ik\mu Q + \kappa' Q = \frac{\kappa'}{10}\{P_2(\mu) - 1\}\left[\sqrt{6}E_2 - \Delta_2\right]. \quad (14.37)$$

Note that the temperature perturbation $\Delta(\mathbf{n})$ is a function of either $\Delta(\eta, \mathbf{x}, \mathbf{n})$ or, in Fourier space, $\Delta(\eta, \mathbf{k}, \mathbf{n})$; $\kappa' \equiv an_e\sigma_T$ is the differential optical depth and $\mu = k^{-1}\mathbf{k}\cdot\mathbf{n}$ the direction cosine.

We have use the expressions for the first few moments of the distribution function

$$T^\mu_\nu = \int \sqrt{-g}\frac{p^\mu p_\nu}{|p_0|} f(p, x) d^3p \quad (14.38)$$

$$\delta = 4\Phi + \frac{1}{\pi}\int \Delta(\mathbf{n})\mathbf{d\Omega} \quad (14.39)$$

We notice that (14.36) is not manifestly gauge-invariant, however by defining the gauge invariant temperature perturbation $\mathcal{M} = \Delta + 2\Phi$, and its multipole decomposition

$$\mathcal{M}(\eta, \mathbf{x}, \mathbf{n}) = \sum_l (-i)^l \mathcal{M}_l(\eta, \mathbf{k}) P_l(\mathbf{n}), \quad (14.40)$$

the evolution equation (14.36), in gauge-invariant components, becomes:

$$\mathcal{M}' + ik\mu\mathcal{M} + \kappa'\mathcal{M} = i\mu k[\Phi - \Psi] + \kappa'\left\{\frac{1}{4}D_g^\gamma - i\mu v_b + \frac{1}{10}P_2(\mu)\left[\sqrt{6}E_2 - \mathcal{M}_2\right]\right\}. \quad (14.41)$$

The procedure is as follows: For each Legendre polynomials P_l

- replace $\mathcal{M}(\eta, \mu)$ by its multipole expansion
- multiply by $P_l(\mu)$
- integrate both l.h.s. and r.h.s. of the new equation over μ : $\int_{-1}^{1} d\mu$
- use the orthogonality relation $\int_{-1}^{1} d\mu P_l(\mu)P_n(\mu) = 2\delta_{ln}/(2l+1)$

After integrating (14.41) for each l and applying orthogonality relations of the Legendre polynomials, the hierarchy for $\mathcal{M}$ is hence given by [58]:

$$\mathcal{M}_0' = -\frac{k}{3}V_\gamma, \tag{14.42}$$

$$\mathcal{M}_1' = \kappa'(V_b - V_\gamma) + k(\Psi - \Phi) + k\left(\mathcal{M}_0 - \frac{2}{5}\mathcal{M}_2\right), \tag{14.43}$$

$$\mathcal{M}_2' = -\kappa'(\mathcal{M}_2 - \mathcal{C}) + k\left(\frac{2}{3}V_\gamma - \frac{3}{7}\mathcal{M}_3\right), \tag{14.44}$$

$$\mathcal{M}_l' = -\kappa'\mathcal{M}_l + k\left(\frac{l}{2l-1}\mathcal{M}_{l-1} - \frac{l+1}{2l+3}\mathcal{M}_{l+1}\right), \quad l > 2, \tag{14.45}$$

and similarly for the polarisation

$$E_2' = -\frac{k\sqrt{5}}{7}E_3 - \kappa'(E_2 + \sqrt{6}\mathcal{C}), \tag{14.46}$$

$$E_l' = k\left(\frac{{}_2\kappa_l}{2l-1}E_{l-1} - \frac{{}_2\kappa_{l+1}}{2l+3}E_{l+1}\right) - \kappa' E_l, \quad l > 2. \tag{14.47}$$

Here $\mathcal{C} = \mathcal{M}_2 - \sqrt{6}E_2/10$ and ${}_2\kappa_l = \sqrt{l^2-4}$ are combinatorial factors.

Massless neutrinos follow the same multipole hierarchy as $\mathcal{M}$, however without polarisation and Thompson scattering. Hence, the perturbed neutrino distribution $\mathcal{N}$ satisfies [36]:

$$\mathcal{N}_0' = -\frac{k}{3}V_\nu, \tag{14.48}$$

$$\mathcal{N}_0' = k(\Psi - \Phi) + k\left(\mathcal{N}_0 - \frac{2}{5}\mathcal{N}_2\right), \tag{14.49}$$

$$\mathcal{N}_l' = k\left(\frac{l}{2l-1}\mathcal{N}_{l-1} - \frac{l+1}{2l+3}\mathcal{N}_{l+1}\right), \quad l > 1. \tag{14.50}$$

For completeness, we quote the hierarchy for the tensor multipoles, temperature $\tilde{\Delta}_l^T$, polarisation $\tilde{\Delta}_l^P$ and cross-correlation $\tilde{\Delta}_l^{T,P}$ [36, 136]:

$$\tilde{\Delta}_0^T = -k\tilde{\Delta}_1^T - \kappa'[\tilde{\Delta}_0^T - \psi] - h', \tag{14.51}$$

$$\tilde{\Delta}_0^P = -k\tilde{\Delta}_2^T - \kappa'[\tilde{\Delta}_1^T + \psi], \tag{14.52}$$

$$\tilde{\Delta}_l^{T,P} = \frac{k}{2l+1}\left[l\tilde{\Delta}_{l-1}^{T,P} - (l+1)\tilde{\Delta}_{l+1}^{T,P}\right] - \kappa'\tilde{\Delta}_l^{T,P}; \quad l \geq 1, \tag{14.53}$$

where h is the longitudinal-scalar part of tensor decomposition in (**??**), and ψ is given by

$$\psi = \frac{1}{10}\tilde{\Delta}_0^T + \frac{1}{7}\tilde{\Delta}_2^T + \frac{3}{70}\tilde{\Delta}_4^T - \frac{3}{5}\tilde{\Delta}_0^P + \frac{6}{7}\tilde{\Delta}_2^P - \frac{3}{70}\tilde{\Delta}_4^P. \tag{14.54}$$

The Boltzmann hierarchy is nowadays solved numerically with software packages such as CMBFAST [119] to produce the CMB spectrum. Also, a widely used implementation is the

CAMB code [76], often embedded in the analysis package CosmoMC. Different codes have also been implemented to compute the CMB spectrum, i.e. CMBEASY is fully object oriented C++ [35], CLASS is written in C [73], and CMBquick is written in Mathematica, but is unavoidably slow [109].

14.3 The Line of Sight Strategy

So usually, we are interested in $\mathcal{M}(\eta_0, \mu)$. It turns out that there is a clever way to obtain this that even highlights the different contributions towards the final anisotropy. Let us develop this Line of Sight strategy. Inspecting, one notices that the l.h.s can be written as

$$e^{-i\mu k\eta} e^{-\kappa(\eta)} \dot{L} \tag{14.55}$$

where

$$L \equiv e^{i\mu k\eta} e^{\kappa(\eta)} \mathcal{M} \tag{14.56}$$

Hence, the Boltzmann equation translates into

$$\dot{L} = e^{i\mu k\eta} e^{\kappa(\eta)} \left[i\mu k(\Phi - \Psi) + \kappa' \left(\frac{1}{4} D_g^\gamma - i\mu V_b - \frac{1}{2}(3\mu^2 - 1)\mathcal{C} \right) \right] \tag{14.57}$$

and integrated over conformal time

$$L(\eta_0) = \int_0^{\eta_0} d\eta e^{i\mu k\eta} e^{\kappa(\eta)} \left[i\mu k(\Phi - \Psi) + \kappa' \left(\frac{1}{4} D_g^\gamma - i\mu V_b - \frac{1}{2}(3\mu^2 - 1)\mathcal{C} \right) \right] \tag{14.58}$$

The photon perturbation today is given by

$$\mathcal{M}(\mu, \eta_0) = \int_0^{\eta_0} d\eta e^{i\mu k(\eta - \eta_0)} e^{\kappa(\eta) - \kappa(\eta_0)} \times \left[i\mu k(\Phi - \Psi) + \kappa' \left(\frac{1}{4} D_g^\gamma - i\mu V_b - \frac{1}{2}(3\mu^2 - 1)\mathcal{C} \right) \right] \tag{14.59}$$

The product $g \equiv \kappa' \exp(\kappa(\eta) - \kappa(\eta_0))$ plays an important role and is called the visibility function. Its peak defines the epoch of recombination.

Each term in the above Equation containing factors of μ, can be integrated by parts, in order to get rid of μ. Applying this procedure to all terms involving μ yields

$$\mathcal{M}(\mu, \eta_0) = \int_0^{\eta_0} e^{\imath\mu k(\eta - \eta_0)} S_T(k, \eta) d\eta \tag{14.60}$$

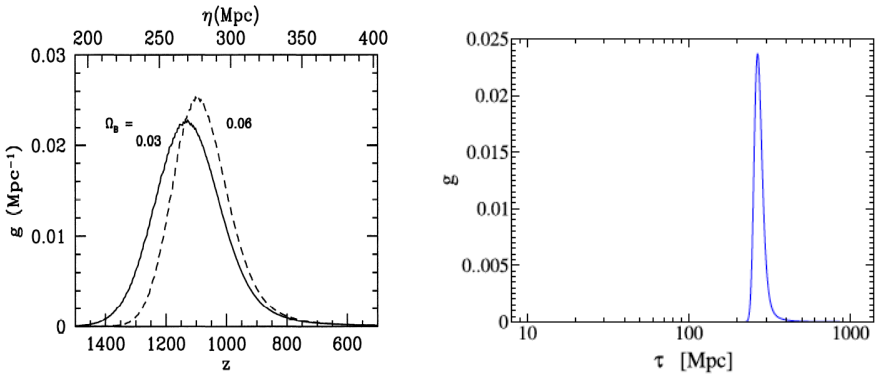

Figure 14.2: Visibility function. Its peak at about $\eta \approx 300$Mpc defines the epoch of last scattering.

where the source is

$$\begin{aligned} S_T &= -e^{\kappa(\eta)-\kappa(\eta_0)}[\Phi' - \Psi'] + g'\left[\frac{V_b}{k} + \frac{3}{k^2}\mathcal{C}'\right] + g''\frac{3}{2k^2}\mathcal{C} \\ &+ g\left[\frac{1}{4}D_g^\gamma + \frac{V_b'}{k} - (\Phi - \Psi) + \frac{\mathcal{C}}{2} + \frac{3}{2k^2}\mathcal{C}''\right], \end{aligned} \tag{14.61}$$

Let us examine in more detail the temperature perturbations. The density contrast D_g^γ is the main contribution, driving the spectrum towards the oscillatory behaviour. It can be seen as an intrinsic temperature variation over the background last-scattering surface: $\delta T/T \propto D_g^\gamma/4$. The Doppler shift, V_b-term, describes the blueshift caused by last scattering electrons moving towards the observer. The term involving time derivatives of the potentials, $(\Phi' - \Psi')$, is known as the *integrated Sachs-Wolfe* effect (ISW) [118]. It describes the change of the CMB photon energy due to the evolution of the potentials along the line of sight. The terms involving $\mathcal{C}$ and its derivatives describe polarisation effects and are far less important than the D_g^γ term. Finally, the $(\Phi - \Psi)$ term arises from the gravitational redshift when climbing out of the potential well at last scattering. The combination $D_g^\gamma/4 - (\Phi - \Psi)$ is known as the *ordinary Sachs-Wolfe effect* (SW). This gives the main contribution on scales that at decoupling were well outside the horizon [24, 36].

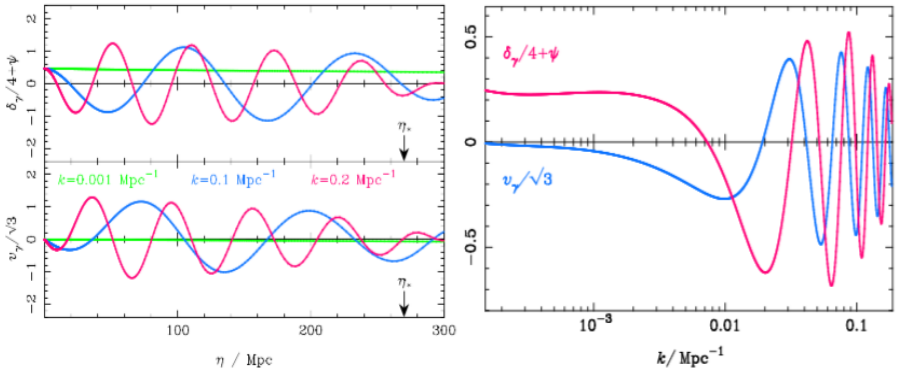
$\delta_\gamma/4+\psi$
$v_\gamma/\sqrt{3}$
k=0.001 Mpc^{-1}
k=0.1 Mpc^{-1}
k=0.2 Mpc^{-1}
η_*
100
200
300
η / Mpc
0.5
0
−0.5
10^{-3}
0.01
0.1
k/ Mpc^{-1}

Figure 14.3

15

Statistics of Random Fields

The density contrast δ, introduced in the previous section, can be considered statistically as a random field with zero mean, $\langle\delta(\mathbf{x})\rangle = 0$. The measure of the clustering degree in the spatial direction $\mathbf{r}$ is determined by the *correlation function* ξ, which is defined as the product of the density contrast at two separate points, $\mathbf{x}$ and $\mathbf{x}+\mathbf{r}$:

$$\xi(r) \equiv \langle\delta(\mathbf{x})\delta(\mathbf{x}+\mathbf{r})\rangle. \tag{15.1}$$

Because of statistical homogeneity and isotropy of a random field, the two-point correlator depends only on the distance $r = |\mathbf{r}|$ between the two points. On the other hand, the amplitude of fluctuations on different lengths are described by the *power spectrum* $\mathcal{P}(k)$, which is simply the inverse Fourier transform of the correlation function ξ:

$$\langle\hat{\delta}(\mathbf{k})\hat{\delta}(\mathbf{k}')\rangle = \frac{2\pi^2}{k^3}\mathcal{P}(k)\delta_D(\mathbf{k}-\mathbf{k}'), \tag{15.2}$$

where $\hat{\delta}$ is the Fourier transform of the density contrast δ. The Dirac's delta distribution δ_D guarantees that modes relative to different wave-numbers are uncorrelated in order to preserve homogeneity; $\mathcal{P}(k)$ has dependency only on the magnitude of the momenta no on $\mathbf{k}$ direction because of isotropy. The normalisation factor $2\pi^2/k^3$ in the definition of the power spectrum is conventional and has the virtue of making $\mathcal{P}(k)$ dimensionless if $\delta(\mathbf{x})$ is.

15.0.1 CMB power spectrum

The primary anisotropies carried out by physical effects before the recombination epoch, encoded in the fractional temperature perturbation, are expanded in terms of the spherical har-

monics on the surface of last scattering by

$$\frac{\Delta T}{\bar{T}}(\eta_0, \mathbf{x_0}, \mathbf{n}) = \sum_{l,m} a_{lm} Y_{lm}(\mathbf{n}), \tag{15.3}$$

where the a_{lm}'s define the multipoles of the CMB anisotropy; $\mathbf{x_0}$ is our position and η_0 the present conformal time. Assuming the $a_{l,m}$'s are Gaussian random fields, the two-point correlator gives

$$\langle a_{lm} a^*_{l'm'} \rangle = C_l \delta_{ll'} \delta_{mm'}. \tag{15.4}$$

The angular *CMB power spectrum* C_l^{TT} is computed through the two-point correlation function (15.1) by

$$C(\theta) \equiv \left\langle \frac{\Delta T(\mathbf{n})}{\bar{T}} \frac{\Delta T(\mathbf{n}')}{\bar{T}} \right\rangle = \sum_l \frac{2l+1}{4\pi} C_l P_l(\mathbf{n} \cdot \mathbf{n}'). \tag{15.5}$$

where $\mathbf{n} \cdot \mathbf{n}' = \cos\theta$, and we have used the addition theorem for spherical harmonics to express the sum of products of Y_{lm}'s in terms of the Legendre polynomials. We consider initial conditions in terms of the conformal Newtonian gauge potential $\Phi_{\rm ini} = \mathcal{R}$. Because the evolution equations for Δ are independent of the direction $\mathbf{k}$, we may write

$$\Delta_l(\eta_0, \mathbf{k}, \mathbf{n}) = \Phi_{\rm ini}(\mathbf{k}) \Delta_l(\eta_0, k, \mathbf{n}). \tag{15.6}$$

Therefore the C_l's are found to be

$$C_l^{XY} = \frac{4\pi}{(2l+1)^2} \int \frac{d^3k}{(2\pi)^3} \, \mathcal{P}_{\mathcal{R}}(k) \, \Delta_l^X(k) \Delta_l^Y(k), \tag{15.7}$$

where X and Y represent the *temperature* (T) and *polarisations* (E or B); $\mathcal{P}_{\mathcal{R}}(k)$ is the power spectrum of the initial curvature perturbations

$$\mathcal{P}_{\mathcal{R}}(k) = A_s \left(\frac{k}{k_0} \right)^{n_s - 1} \tag{15.8}$$

and A_s the initial scalar amplitude, quoted at a reference scale k_0 (one chooses $k_0 = 0.05$Mpc) and the spectrum is a featureless power law with scalar spectral index n_s.

The moments obtained from the line of sight integration method [119], in terms of the spherical Bessel functions j_l, are given by

$$\Delta_l^T = (2l+1) \int d\eta j_l(k[\eta - \eta_0]) S_T(k, \eta), \tag{15.9}$$

$$\Delta_l^E = (2l+1) \sqrt{\frac{(l-2)!}{(l+2)!}} \int_0^{\eta_0} d\eta S_E(k, \eta) j_l(x), \tag{15.10}$$

with the sources

$$\begin{aligned} S_T &= -e^{\kappa(\eta)-\kappa(\eta_0)}[\Phi' - \Psi'] + g'\left[\frac{V_b}{k} + \frac{3}{k^2}\mathcal{C}'\right] + g''\frac{3}{2k^2}\mathcal{C} \\ &+ g\left[\frac{1}{4}D_g^\gamma + \frac{V_b'}{k} - (\Phi - \Psi) + \frac{\mathcal{C}}{2} + \frac{3}{2k^2}\mathcal{C}''\right], \end{aligned} \tag{15.11}$$

$$S_E = \frac{3g\mathcal{C}}{4x^2}, \tag{15.12}$$

where we have used $x \equiv k(\eta_0 - \eta)$ and the visibility function $g \equiv \kappa' \exp(\kappa(\eta) - \kappa(\eta_0))$.

For completeness, we quote the hierarchy for the tensor multipoles, temperature $\tilde{\Delta}_l^T$, polarisation $\tilde{\Delta}_l^P$ and cross-correlation $\tilde{\Delta}_l^{T,P}$ [36, 136]:

$$C_{XY;l}^{\rm tens} = \frac{4\pi}{(2l+1)^2}\int \frac{d^3k}{(2\pi)^3}\,\mathcal{P}_\mathcal{T}(k)\,\Delta_{X;l}^{\rm tens}(k)\Delta_{Y;l}^{\rm tens}(k), \tag{15.13}$$

where $\mathcal{P}_\mathcal{T}(k)$ is the initial tensor power spectrum, and the moments:

$$\Delta_{T;l}^{\rm tens} = \sqrt{\frac{(l+2)!}{(l-2)!}}\int_0^{\eta_0} d\eta S_T^{\rm tens}(k,\eta)\frac{j_l(x)}{x^2}, \tag{15.14}$$

$$\Delta_{E,B;l}^{\rm tens} = \int_0^{\eta_0} d\eta S_{E,B}^{\rm tens}(k,\eta) j_l(x), \tag{15.15}$$

with the sources (using (15.22)):

$$S_T^{\rm tens}(k,\eta) = h'\exp(-\kappa) + g\psi, \tag{15.16}$$

$$\begin{aligned} S_E^{\rm tens}(k,\eta) &= g\left\{\psi - \frac{\psi''}{k^2} + \frac{2\psi}{x^2} - \frac{\psi'}{kx}\right\} \\ &\quad -g'\left\{\frac{2\psi'}{k^2} + \frac{4\psi}{kx}\right\} - 2g''\frac{\psi}{k^2}, \end{aligned} \tag{15.17}$$

$$S_B^{\rm tens}(k,\eta) = g\left\{\frac{4\psi}{x} + \frac{2\psi'}{k}\right\} + 2g'\frac{\psi}{k}. \tag{15.18}$$

$$\tilde{\Delta}_0^T = -k\tilde{\Delta}_1^T - \kappa'[\tilde{\Delta}_0^T - \psi] - h', \tag{15.19}$$

$$\tilde{\Delta}_0^P = -k\tilde{\Delta}_2^T - \kappa'[\tilde{\Delta}_1^T + \psi], \tag{15.20}$$

$$\tilde{\Delta}_l^{T,P} = \frac{k}{2l+1}\left[l\tilde{\Delta}_{l-1}^{T,P} - (l+1)\tilde{\Delta}_{l+1}^{T,P}\right] - \kappa'\tilde{\Delta}_l^{T,P}; \quad l \geq 1, \tag{15.21}$$

where h is the longitudinal-scalar part of tensor decomposition in (**??**), and ψ is given by

$$\psi = \frac{1}{10}\tilde{\Delta}_0^T + \frac{1}{7}\tilde{\Delta}_2^T + \frac{3}{70}\tilde{\Delta}_4^T - \frac{3}{5}\tilde{\Delta}_0^P + \frac{6}{7}\tilde{\Delta}_2^P - \frac{3}{70}\tilde{\Delta}_4^P. \tag{15.22}$$

The slow way would be to get the C_l's directly from the (vast) multipole hierarchy of the photon distribution and the multipole hierarchy up to $l \equiv 3000$. In contrast, the line of sight

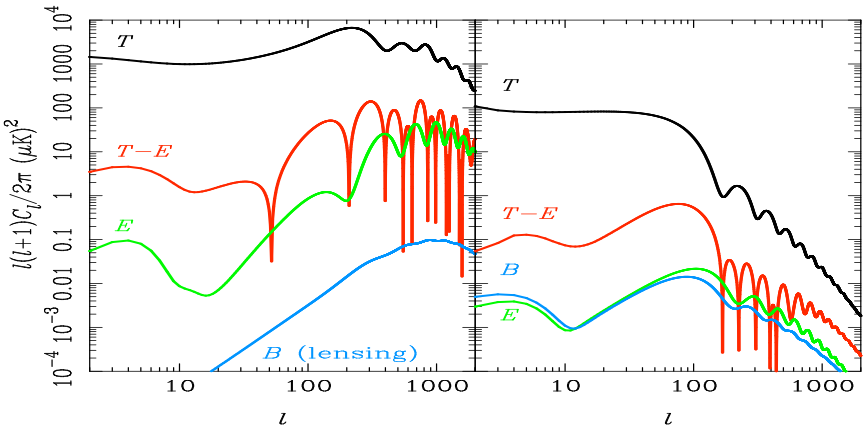

Figure 15.1: CMB spectra for all the contributions: Temperature, E-mode, B-mode and T-E cross-correlation. The left-hand-side displays the scalar perturbations whereas the right-hand-side tensor perturbations (gravitational waves). Figure reprinted from Challinor [25]

integration gets the Δ_l's by folding the source term S with the spherical Bessel functions j_l. While the Bessel functions oscillate rapidly in this convolution, the source term is most of the time rather slowly changing. It thus suffices to calculate the sources at few (cleverly chosen) points and interpolate between.

Figure 15.1 shows the adiabatic CMB spectra for all the contributions: Temperature, E-mode, B-mode and T-E cross-correlation. The left-hand-side of the panel displays the CMB spectra for scalar perturbations, whereas the right-hand-side tensor perturbations (gravitational waves). All of them in units of $l(l+1)/2\pi[\mu K]^2$.

15.1 Codes

The Boltzmann hierarchy is nowadays solved numerically with software packages such as CMB-FAST [119] to produce the CMB spectrum. Also, a widely used implementation is the CAMB code [76], often embedded in the analysis package CosmoMC. Different codes have also been implemented to compute the CMB spectrum, i.e. CMBEASY is fully object oriented C++ [35], CLASS is written in C [73], and CMBquick is written in Mathematica, but is unavoidably slow [109].

1995/ Fortran 77

- COSMICS: Cosmological initial conditions and microwave anisotropy
  * Chung-Pei Ma, Edmund Bertschinger. arXiv:astro-ph/9506072

http://ascl.net/cosmics.html

1996/ Fortran 77

- CMBFAST: A microwave anisotropy code
  * Seljak Uros, Zaldarriaga Matias. arXiv:astro-ph/9603033, arXiv:astro-ph/9704265

http://ascl.net/cmbfast.html

2000/ Fortran 90

- CAMB: Code for Anisotropies in the Microwave Background.
  * Antony Lewis, Anthony Challinor and Anthony Lasenby. arXiv:astro-ph/9911177

http://camb.info/

2003/ C++

- CMBEASY: an Object Oriented Code for the Cosmic Microwave Background
  * Michael Doran arXiv:astro-ph/0302138v2

http://www.thphys.uni-heidelberg.de/ robbers/cmbeasy/index.html

2001

Davis Anisotropy Shortcut (DASh)

DASh incorporates many analytic and semianalytic approximations that have been presented elsewhere in the literature and also some new ones. The Astrophysical Journal, 578:665-674, 2002

TABLE I. Comparison between CMB Codes [a]

	CAMB	CLASS	CMBEASY	CMBquick	CosmoLib [b]
Language	F90	C	C++	Mathematica	F90[c]
gauge [d]	syn.	syn./Newt. [e]	syn./gauge-inv.	Newt.	Newt.
open/close universe	Yes	No	No	No	No
massive neutrinos	Yes	Yes	Yes	Yes	No
tensor perturb.	Yes	Yes	Yes	Yes	Yes
CDM isocurvature mode	Yes	Yes	Yes	Yes	Yes
dark energy perturb.	Yes	Yes	Yes	No	Yes
nonzero $c^2_{a,b}$	Yes	Yes	Yes	No	Yes
dark energy EOS.	constant	$w_0 + w_a(1-a)$	arbitrary	-1	arbitrary
non-smooth primordial power	No	No	No	No	Yes
MCMC driver	Yes	No	Yes	No	Yes
periodic proposal density	No	No	No	No	Yes
data simulation	No	No	No	No	Yes
second-order perturb. [f]	No	No	No	Yes	No [g]

[a] Here we do not include CMBFast, which is no longer supported by its authors or available for download.

http://lambda.gsfc.nasa.gov/toolbox/

Figure 15.2: a

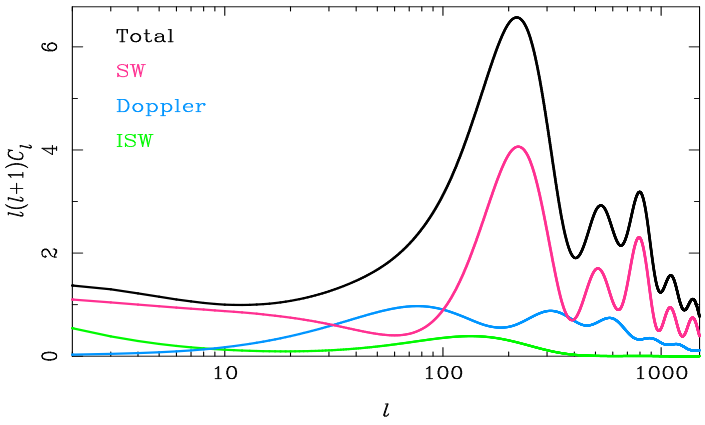

Figure 15.3: Total CMB temperature-spectrum and its different contributions: Sachs-Wolfe (SW) $D_g^\gamma/4 - (\Phi - \Psi)$; Doppler effect V_b^γ; and the integrated Sachs-Wolfe effect (ISW) coming from evolution of the potential along the line of sight. Figure from Challinor [25]

15.2 Description of fluctuations

- The $l = 0$ term of the correlation function (the monopole) vanishes if the mean temperature has been defined correctly.
- The $l = 1$ (the dipole) reflects the motion of the Earth through space. What we are seeing is the effect of the Earth's motion relative to the local comoving frame of reference. The Earth is moving with a velocity $v = 369 kms^{-1}$ towards a point on the boundary of the constellations of Crater and Leo.
- The Sachs-Wolfe effect ($l < 100$) - The gravitational effects are the dominant contributions at large angular scales. $C_l \propto \int d\ln k \mathcal{P}_\mathcal{R}(k) j_l^2(k[\eta - \eta_0])$, and if we make use of the integral

$$\int_0^\infty j_l^2(x)dx = \frac{1}{2l(l+1)} \tag{15.23}$$

and assume a nearly scale-invariant scalar spectrum $n_\mathrm{s} \approx 1$, then

$$\frac{l(l+1)C_l}{2\pi} = \frac{1}{25}A_s \tag{15.24}$$

is approximately constant, shown as a flat plateau at low multipoles. More generally, a primordial spectrum that varies as a power-law in k gives an angular power spectrum going like

$$C_l \sim \frac{\Gamma(l + n_s/2 - 1/2)}{\Gamma(l - n_s/2 + 5/2)} \tag{15.25}$$

- Intermediate scales ($100 < l < 1000$) - Perturbations inside the horizon have evolved causally and produced the anisotropy at the last scattering epoch ($l_{\rm hor} \approx 200$). The balance between the gravitational force and radiation pressure is presented as series of characteristic peaks called *acoustic oscillations*.

- Small scales ($l > 1000$) - The thickness of the last scattering surface leads to a damping of $C_l^T \sim l^{-4}$ at the highest multipoles, commonly called the *Silk effect*. The total mean-squared distance that a photon will have moved by such a random walk by the time η_* is therefore

$$\int_0^{\eta_*} \frac{d\eta'}{a n_e \sigma_T} \sim \frac{1}{k_D^2} \tag{15.26}$$

  which defines a damping scale k_D^{-1}.

  At these scales, important contributions are also provided by secondary anisotropies: gravitational lensing, Rees-Sciama effect (RS), Sunyaev-Zel'dovich effect (SZ), kinetic Sunyaev-Zel'dovich effect, Ostriker-Vishniac effect (OV), foregrounds from discrete sources [1].

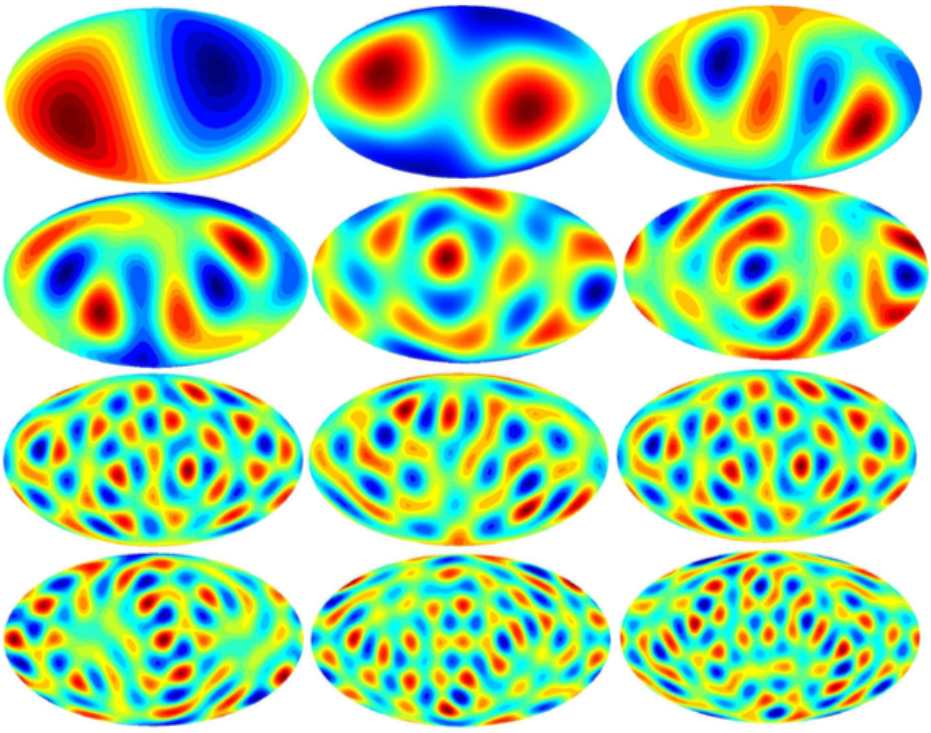

Figure 15.4

16

Bayesian Statistics

Bayesian statistics and MCMC (Markov Chain Monte Carlo) algorithms have found their place in the field of Cosmology. They have become important mathematical and numerical tools, especially in parameter estimation and model comparison. In this paper we review some of the fundamental concepts to understand Bayesian statistics, to then introduce the MCMC algorithms and samplers that allow us to perform the parameter inference procedure. We also provide a general description of the standard cosmological model, known as the ΛCDM model, along with several alternatives to it; and current datasets coming from astrophysical and cosmological observations. Finally, with the tools acquired we use a MCMC algorithm implemented in python -called SimpleMC- to test the cosmological models and find out the combination of parameters that best describes the universe.

16.1 Introduction

The beginning of the standard cosmology as it is known today emerged after 1920 when the Shapley-Curtis debate was carried out [**?**]. This debate was held between the astronomers Harlow Shapley and Heber Curtis, resulting in a revolution for astronomy at that time by reaching an important conclusion: "The universe had a larger scale than the Milky Way". Several observations at that epoch established that the size and dynamics of the cosmos could be explained by Einstein's General Theory of Relativity. In its childhood, cosmology was a speculative science based only on a few data sets, and it was characterized by a dispute between two cosmological models: the steady state model and the Big Bang (BB) theory. It was not until 1990 when the amount of data increased enough to discriminate and rule out compelling

theories, being the BB model awarded as the most accepted theory. During the same decade, David Schramm heralded the "Golden Age of Cosmology" at a National Academy of Sciences colloquium [**?**].

Once the new age of cosmological observations arrived with a large variety of data, it was necessary to confront the cosmological models with such data. This was usually done through statistics. It is important to notice that, since we have only one universe, we cannot rely on a frequentist interpretation of statistics (we are not able to create multiple universes and make a frequentist inference of our models). An alternative interpretation to help us in our task is Bayesian statistics. In Bayesian statistics the probability is interpreted as a "degree of belief" and it may be useful when repetitive processes are complicated to reproduce.

The main aim of this work is to provide an introduction of Bayesian parameter inference and its applications to cosmology. We assume the reader is familiarized with the basic concepts of statistics, but not necessarily with Bayesian statistics. Then, we provide a general introduction to this subject, enough to work out some examples. This review is written in a generic way so the reader interested on the parameter inference may apply the theory to any subject, in particular we put into practice the Bayesian concepts on the cosmology branch of physics.

The paper is organized as follows. We start in Section 17.3 by pointing out the main differences between the Bayesian and Frequentist approaches to statistics. Then, in Section 16.3 we explain the basic and necessary mathematical concepts in Bayesian statistics to perform the parameter estimation procedure for a given model. Once we have the mathematical background, we continue in Section 16.4 with some of the numerical resources available to simplify our task, such numerical tools may become important given the fact that, in general, it is not possible to derive analytical results, specially when a model contains several parameters that need to be confronted with data. We then provide an example of some of these methods and tools applied to the simple problem of fitting a straight line in Section 16.5. In Section **??** we present an introduction to cosmology and applications of the tools given in previous sections in cosmology, then in Section **??** the focus is in some of the codes available to perform this work. Then, in Section **??**, we apply these techniques to constrain the parameter space that describes the standard cosmological model, namely the ΛCDM model, and several alternatives to it. Finally, in Section **??** we present our conclusions.

16.2 Bayesian vs Frequentist statistics

Fundamentally, the main difference between Bayesian and Frequentist statistics is on the definition of probability. From a Frequentist point of view, probability has meaning in limiting cases of repeated measurements

$$P = \frac{n}{N}, \tag{16.1}$$

where n denotes the number of successes and N the total number of trials. Frequentist statistics defines probability as the limit for the number of independent trials going to infinity. Then, **for Frequentist statistics, probabilities are fundamentally related to frequencies of events**. On the other hand, in Bayesian statistics the concept of probability is extended to cover degrees of certainty about a statement. **For Bayesian statistics, probabilities are fundamentally related to our knowledge about an event**.

Here we introduce some key concepts to understand the consequences this difference entails; for an extended review see [**? ? ? ? ?**]. Let x be a random variable related to a particular event and $P(x)$ its corresponding probability distribution, for both cases the same rules of probabilities apply[1]:

$$P(x) \geq 0, \tag{16.2a}$$

$$\int_{-\infty}^{\infty} dx P(x) = 1. \tag{16.2b}$$

For *mutually exclusive* events we have

$$P(x_1 \cup x_2) = P(x_1) + P(x_2), \tag{16.2c}$$

but in general

$$P(x_1 \cup x_2) = P(x_1) + P(x_2) - P(x_1 \cap x_2).$$

These rules are summed up as follow. The first condition (16.2a) is necessary due to the probability of having an event is always positive. The second rule (16.2b) is a normalized relation, which tells us that we are certain to obtain one of the possible outcomes. Now, in the third point (16.2c) we have that the probability of obtaining an observation, from a set of mutually exclusive events, is given by the individual probabilities of each event. Finally, and in

[1] These rules are defined for a continuous variable; however, the corresponding discrete definition can be given immediately by replacing $\int dx \to \sum$.

general, if one event occurs *given* the occurrence of another then the probability that both x_1 and x_2 happen is equal to the probability of x_1 times the probability of x_2 given that x_1 has already happened

$$P(x_1 \cap x_2) = P(x_1)P(x_2|x_1). \tag{16.2d}$$

If two events x_1 and x_2 are mutually exclusive then

$$P(x_1 \cap x_2) = 0 = P(x_2 \cap x_1). \tag{16.3}$$

The rules of probability distributions must be fulfilled by both Frequentist and Bayesian statistics. However, there are some consequences derived by the fact these two scenarios have a different definition of probability, as we shall see.

16.2.1 Frequentist statistics

Any frequentist inferential procedure relies on three basic ingredients: the data, the model and an estimation procedure. The main assumption in Frequentist statistics is that the data has a definite, albeit unknown, underlying distribution to which all inference pertains.

The **data** is a measurement or observation, denoted by X, that can take any value from a corresponding sample space. A **sample space** of an observation X can be defined as a measurable space $(x, \hat{B})$ that contains all values that X can take upon measurement. In Frequentist statistics it is considered that there is a probability function $P_0 : \hat{B} \to [0, 1]$ in the sample space $(x, \hat{B})$ representing the "true distribution of the data"

$$X \sim P_0.$$

Now there is the model. For Frequentist statistics the **model** Q is a collection of probability measurements $P_\theta : \hat{B} \to [0, 1]$ in the sample space $(x, \hat{B})$. The distributions P_θ are called *model distributions*, with θ as the model parameters; in this approach θ is unchanged. A model Q is said to be well-specified if it contains the true distribution of the data P_0, i.e.

$$P_0 \in Q.$$

Finally, we need a point-estimator (or estimator) for P_0. An *estimator* for P_0 is a map $\hat{P} : x \to Q$, representing our "best guess" $\hat{P} \in Q$ for P_0 based on the data X.

Frequentist	Bayesian
Data are a repeatable random sample. There is a frequency.	Data are observed from the realized sample.
Underlying parameters remain constant during this repeatable process.	Parameters are unknown and described probabilistically.
Parameters are fixed.	Data are fixed.

Table 16.1: Main differences between the Bayesian and Frequentist interpretations.

Hence, the Frequentist statistics is based on trying to answer the following questions: "what the data is trying to tell us about P_0?" or "considering the data, what can we say about the mean value of P_0?".

16.2.2 Bayesian statistics

In Bayesian statistics, data and model are two elements of the same space [**?**], i.e. no formal distinction is made between measured quantities X and parameters θ. One may envisage the process of generating a measurement's outcome $Y = y$ as two draws, one draw for Θ (where Θ is a model with associated probabilities to the parameter θ) to select a value of θ and a subsequent draw for P_θ to arrive at $X = x$. This perspective may seem rather absurd in view of the definitions for a Frequentist way of thinking, but in Bayesian statistics where probabilities are related to our own knowledge, it results natural to associate probability distributions to our parameters. In this way an element P_θ of the model is interpreted simply as the distribution of X given the parameter value θ, i.e. as the conditional distribution $X|\theta$.

16.2.3 Comparing both descriptions

Table 16.1 provides a short summary of the most important differences between the two statistics. To understand these differences let us review a typical example. Here we present an experiment and, since we are interested in comparing both descriptions, we show only the basic results from both points of view: Frequentist and Bayesian.

Example.- Let us assume we have a coin that has a probability p to land as heads and a probability $1 - p$ to land as tails. In the process of trying to estimate p (which must be $p = 0.5$

since we have only two possible states) we flip the coin 14 times, obtaining heads in 10 of the trials. Now we are interested in the next two possible events. To be precise: "What is the probability that in the next two tosses we will get two heads in a row?".

- *Frequentist approach.* As mentioned previously, in Frequentist statistics probability is related to the frequency of events, then our best estimate for p is $P(head) = p = \frac{\#\ of\ heads}{\#\ of\ events} = 10/14$. So, the probability of having 2 heads in a row is $P(2heads) = P(head)P(head) \simeq 0.51$.

- *Bayesian approach.* In Bayesian statistics p is not a value, it is a random variable with its own distribution, and it must be defined by the existing evidence. In this example a good distribution for p is a binomial distribution

$$P(D|p) = \binom{14}{10} p^{10}(1-p)^4, \tag{16.4}$$

  where D is our data set (14 trials and 10 successes). Then, by considering a non-informative prior (beforehand we do not know anything about p) and averaging over all possible values of p we have that the probability of having two heads is

$$P(2heads|D) = \frac{B(13,5)}{B(11,5)} = 0.485, \tag{16.5}$$

  where $B(x,y)$ is the beta function. This Bayesian example will be expanded in detail during the following section, but for now we just want to stress out that both approximations arrive at different results.

In the Frequentist approach, since we adopt the probability as a frequency of events (the probability of having a head was fixed by $p = 10/14$), hence the final result was obtained by only multiplying each of these probabilities (since we assume the events are independent of each other). On the other hand, in the Bayesian framework it was necessary to average over all possible values of p in order to obtain a numerical value. However, in both cases, the probability differs from the real one ($P(2heads) = 0.25$) because we don't have enough data for our estimations.

Note: If you are unfamiliar with Bayesian statistics, do not be scared of the last example. In the next section we review the basic concepts and get back to this example to use the new tools learned.

16.3 A first look at Bayesian statistics

Before we start with the applications of Bayesian statistics in cosmology it is necessary to understand the most important mathematical tools in the Bayesian procedure. In this section, we present an informal revision but encourage the reader to look for the formal treatment in the literature, cited in each section.

16.3.1 Bayes theorem, priors, posteriors and all that stuff

When anyone is interested on the Bayesian framework, there are several concepts to understand before presenting the results. In this section we quickly review these concepts and then we take back the example about the coin toss given in the last section.

The Bayes theorem. The Bayes theorem is a direct consequence of the axioms of probability shown in Eqs. (16.2). From Eqn. (16.2d), without loss of generality, it must be fulfilled that $P(x_1 \cap x_2) = P(x_2 \cap x_1)$. In such case the following relation applies

$$P(x_2|x_1) = \frac{P(x_1|x_2)P(x_2)}{P(x_1)}. \tag{16.6}$$

As already mentioned, in the Bayesian framework data and model are part of the same space. Given a model (or hypothesis) H, considering $x_1 \to D$ as a set of data, and $x_2 \to \theta$ as the parameter vector of said hypothesis, we can rewrite the above equation as

$$P(\theta|D, H) = \frac{P(D|\theta, H)P(\theta|H)}{P(D|H)}. \tag{16.7}$$

This last relation is the so-called **Bayes theorem** and the most important tool in a Bayesian inference procedure. In this result, $P(\theta|D, H)$ is called the **posterior** probability of the model. $P(D|\theta, H) \equiv L(D|\theta, H)$ is called the **likelihood** and it will be our main focus in future sections. $P(\theta|H) \equiv \pi(\theta)$ is called the **prior** and expresses the knowledge about the model before acquiring the data. This prior can be fixed depending on either previous experiment results or the theory behind. $P(D|H) \equiv \mathcal{Z}$ is the evidence of the model, usually referred as the **Bayesian Evidence**. We notice that this evidence acts only as a normalizing factor, and is nothing more than the average of the likelihood over the prior

$$P(D|H) = \int d^N\theta P(D|\theta, H)P(\theta|H), \tag{16.8}$$

where N is the dimensionality of the parameter space. This quantity is usually ignored, for practical reasons, when testing the parameter space of a unique model. Nevertheless, the Bayesian

$\lvert\mathcal{B}_{0,1}\rvert$	Odds	Probability	Strength
< 1.0	$< 3:1$	< 0.750	Inconclusive
1.0-2.5	$\sim 12:1$	0.923	Significant
2.5-5.0	$\sim 150:1$	0.993	Strong
> 5.0	$> 150:1$	> 0.993	Decisive

Table 16.2: Jeffreys guideline scale for evaluating the strength of evidence when two models are compared.

evidence plays an important role for selecting the model that best "describes" the data, known as *model selection*. For convenience, the ratio of two evidences

$$K \equiv \frac{P(D|H_0)}{P(D|H_1)} = \frac{\int d^{N_0}\theta_0 \; P(D|\theta_0, H_0)P(\theta_0|H_0)}{\int d^{N_1}\theta_1 \; P(D|\theta_1, H_1)P(\theta_1|H_1)} = \frac{\mathcal{Z}_0}{\mathcal{Z}_1}, \tag{16.9}$$

or equivalently the difference in log evidence $\ln \mathcal{Z}_0 - \ln \mathcal{Z}_1$ if often termed as the **Bayes factor** $\mathcal{B}_{0,1}$:

$$\mathcal{B}_{0,1} = \ln \frac{\mathcal{Z}_0}{\mathcal{Z}_1}, \tag{16.10}$$

where θ_i is a parameter vector (with dimensionality N_i) for the hypothesis H_i and $i = 0, 1$. In Eqn. (16.10), the quantity $\mathcal{B}_{0,1} = \ln K$ provides an idea on how well model 0 may fit the data when is compared to model 1. Jeffreys provided a suitable guideline scale on which we are able to make qualitative conclusions (see Table 17.2).

We can see that Bayes theorem has an enormous implication with respect to a statistical inferential point of view. In a typical scenario we collect some data and hope to interpret it with a given model, however, we usually do the opposite. That is, first we have a set of data and then we can confront a model considering the probability that our model fits the data. Bayes theorem provides a tool to relate both scenarios. Then, thanks to the Bayes theorem, in principle, we are able to select the model that best fits the data.

Example.- We go back to the example shown in the last section: the coin toss. We are interested in the probability of obtaining two heads in a row given the data $P(2heads|D)$ ($D =$ the previous 14 coin tosses acting as data). First of all let us assume that we have a model with parameter p to define the probability of obtaining the two heads given our model $P(2heads|p)$. This parameter will have a probability distribution $P(p|D)$ depending on the data we already

have. Therefore the probability can be obtained by averaging over all the possible parameters with its corresponding density distribution

$$P(2heads|D) = \int_0^1 P(2heads|p)P(p|D)dp. \tag{16.11}$$

For simplicity we do not update p between the two tosses and we assume that both are independent from each other. With this last assumption we have

$$P(2heads|p) = [P(head|p)]^2, \tag{16.12}$$

where $P(head|p)$ is the probability of obtaining a head given our model. We assume a simple description of $P(head|p)$ as

$$P(head|p) = p \quad \Rightarrow \quad P(2heads|p) = p^2. \tag{16.13}$$

On the other hand, notice that we do not know *a priori* the quantity $P(p|D)$ but $P(D|p)$ (i.e. we know the probability of obtaining a dataset by considering a model as correct). A good choice for experiments that have two possible results is a binomial distribution

$$P(x|p,n) = \binom{n}{x} p^x (1-p)^{n-x}, \tag{16.14}$$

with n the number of trials (this case = 14) and x the number of successes (here =10). Hence, we have an expression for $P(D|p)$ [Eqn. (16.4)]. Now we need to compute $P(p|D)$. Using the Bayes formula we have

$$P(p|D) = \frac{P(D|p)P(p)}{P(D)}. \tag{16.15}$$

A very convenient prior distribution for this scenario is the *beta distribution* $Beta(p;a,b)$[2] defined as

$$Beta(p;a,b) = \frac{\Gamma(a+b)}{\Gamma(a)\Gamma(b)} p^{a-1}(1-p)^{b-1}, \tag{16.16}$$

where Γ is the gamma function. So

$$P(p) = Beta(p;a,b). \tag{16.17}$$

We are interested in the explicit form of $P(p|D)$ and in such case we need to compute $P(D)$. Plugging Eqn. (16.4) and Eqn. (16.17) into the integral of Eqn. (16.8) we have

$$P(D) = B(10+a, 4+b) \equiv \frac{\Gamma(10+a)\Gamma(4+b)}{\Gamma((10+a)+(4+b))}, \tag{16.18}$$

[2] It is chosen because it describes several statistical distributions, in particular the normal distribution defined as the non-informative one.

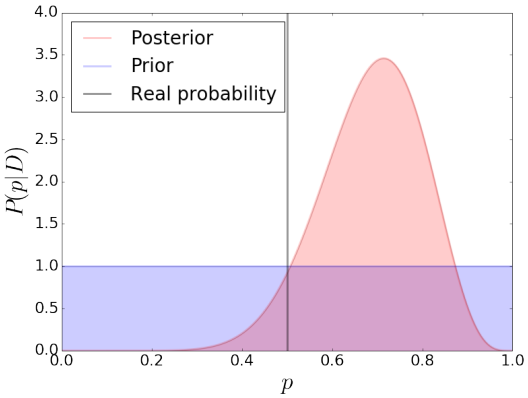

Figure 16.1: The coin example: blue figure displays the prior distribution $P(p)$ which is updated, using the data, to get the posterior distribution $P(p|D)$, (red). The vertical black line corresponds to the real value, $p = 0.5$.

and therefore

$$P(p|D) = \frac{p^{10+a-1}(1-p)^{4+b-1}}{B(10+a, 4+b)}. \tag{16.19}$$

Now we need to know the values of a and b. If we assume that we know nothing about p, then we can assume the prior as an uniform distribution, this means $a = b = 1$. Notice from Fig. 16.1 that our posterior result (Red figure) described by Eqn. (16.19) does not exactly agree with the real value of p (black dashed vertical line). We would expect the posterior distribution be centered at $p = 0.5$ with a very narrow distribution. Nevertheless this value is recovered by increasing the experimental data.

Finally, solving the integral in Eqn. (16.11) using (16.13) and (16.19) we arrive at the result obtained in the previous section

$$P(2heads|D) = \frac{B(13,5)}{B(11,5)} = 0.485. \tag{16.20}$$

16.3.2 Updating the probability distribution

As seen in the coin example, we weren't able to get the real value of p because the lack of enough data. If we want to be closer, we would have to keep flipping the coin until the amount of data becomes sufficient. Let us continue with the example: suppose that after throwing the coin 100 times we obtain, let's say, 56 heads, while after throwing it 500 times we obtain 246 heads. Then, we expect to obtain a thinner distribution with center close to $p = 0.5$ (see Fig.

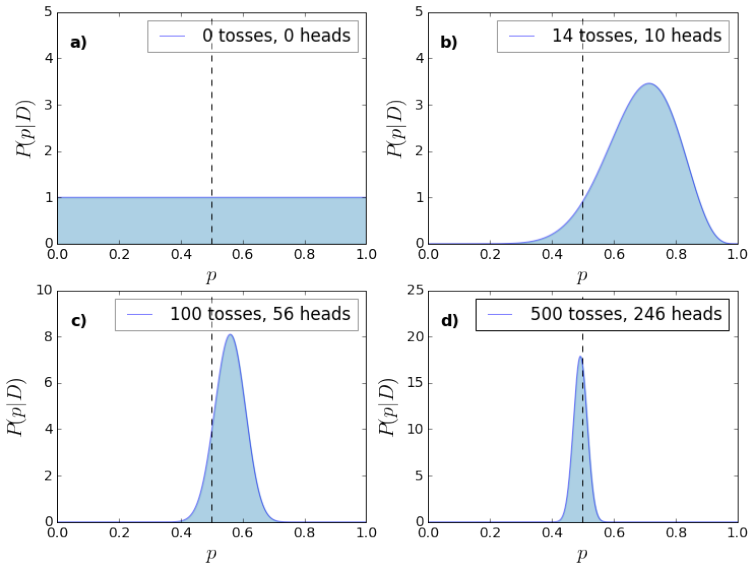

Figure 16.2: Posterior distributions $P(p|D)$, when the data is increased. Notice that while we continue increasing the experimental results, the posterior distribution starts to be more localized near by the real value $p = 0.5$.

16.2). Given this, it is clear that in order to confront a parameter model and be more accurate about the most probable (or "real") value, it is necessary to increase the amount of data (and the precision) in any experiment. That is, if we take into account the 500 tosses – with 246 heads – the previous result is updated to $P(2heads|D) = 0.249$, much closer to the real value.

Then, we have some model parameters that have to be confronted with different sets of data. This can be done in two alternative ways: (a) by considering the sum of all datasets we have; or (b) by taking each data set as the new data, but our prior information updated by the previous information. The important point in Bayesian statistics is that it is indeed equivalent to choose any of these two possibilities. In the coin toss example it means that it is identical to start with the prior given in Fig. 16.2-a and then by considering the 500 datapoints we can arrive at the posterior in Fig. 16.2-d, or similarly start with the posterior shown in Fig. 16.2-c as our prior and consider only the last 400 datapoints to obtain the same posterior, displayed in Fig. 16.2-d.

In fact, if we rewrite Bayes theorem so that all probabilities are explicitly dependent on

some prior information I [**?**]

$$P(\theta|DI,H) = \frac{P(\theta|I,H)P(DI|\theta,H)}{P(D|I,H)}, \tag{16.21}$$

and then we consider a new set of data D', letting the old data become part of the prior information $I' = DI$, we arrive at

$$P(\theta|D'I',H) = \frac{P(\theta|I,H)P(DD'I|\theta,H)}{P(DD'|I,H)} = P(\theta|[DD']I,H), \tag{16.22}$$

where we can explicitly see the equivalence of the two different options.

16.3.3 About the Likelihood

We mentioned that the Bayesian evidence is usually set apart when doing any inference procedure in the parameter space of a single model. Then, without loss of generality, we can fix it to $P(D|H) = 1$. If we ignore the prior[3] we can identify the posterior with the likelihood $P(\theta|D,H) \propto L(D|\theta,H)$ and thus, by maximizing it, we can find the most probable set of parameters for a model given the data. However, having ignored $P(D|H)$ and the prior, we are not able to provide an absolute probability for a given model, but only relative probabilities. On the other hand, it is possible to report results independently of the prior by using the *Likelihood ratio*. The likelihood at a particular point in the parameter space can be compared with the best-fit value, or the maximum likelihood L_{max}. Then, we can say that some parameters are acceptable if the likelihood ratio

$$\Lambda = -2\ln\left[\frac{L(D|\theta,H)}{L_{max}}\right], \tag{16.23}$$

is bigger than a given value.

Let us assume we have a Gaussian posterior distribution, which is single-peaked. We consider that $\hat{\theta}$ is the **mean** of the distribution

$$\hat{\theta} = \int d\theta\theta P(\theta|D,H). \tag{16.24}$$

If our model is well-specified and the expectation value of $\hat{\theta}$ corresponds to the real or most probable value θ_0, we have

$$\langle\hat{\theta}\rangle = \theta_0, \tag{16.25}$$

[3]It is expected that the real value of any given parameter for a large enough dataset is independent of the prior.

then we say that $\hat{\theta}$ is *unbiased*. Considering a Taylor expansion of the *log likelihood* around its maximum

$$\ln L(D|\theta) = \ln L(D|\theta_0) + \frac{1}{2}(\theta_i - \theta_{0i})\frac{\partial^2 \ln L}{\partial\theta_i \partial\theta_j}(\theta_j - \theta_{0j}) + ..., \tag{16.26}$$

where θ_0 corresponds to the parameter vector of the real model. In this manner, we have that the likelihood can be expressed as a multi-variable likelihood given by

$$L(D|\theta) = L(D|\theta_0)\exp\left[-\frac{1}{2}(\theta_i - \theta_{0i})H_{ij}(\theta_j - \theta_{0j})\right], \tag{16.27}$$

where

$$H_{ij} = -\frac{\partial^2 \ln L}{\partial\theta_i \partial\theta_j}, \tag{16.28}$$

is called the **Hessian matrix** and it controls whether the estimates of θ_i and θ_j are correlated. If it is diagonal, these estimates are uncorrelated.

The above expression for the likelihood is a good approximation as long as our posterior distribution possesses a single-peak. It is worth mentioning that, if the data errors are normally distributed, then the likelihood for the data will be a Gaussian function as well. In fact, this is always true if the model is linearly dependent on the parameters. On the other hand, if the data is not normally distributed we can resort to the central limit theorem. In this way, the central limit theorem tell us that the resulting distribution will be best approximated by a multi-variate Gaussian distribution [**?**].

16.3.4 Letting aside the priors

In this section we present an argument for letting aside the prior in the parameter estimation. For this, we follow the example given in [**?**]. In this example there are two people, A and B, that are interested in the measurement of a given physical quantity θ. A and B have different prior beliefs regarding the possible value of θ. This discrepancy could be given by the experience, such as the possibility that A and B have made the same measurement at different times. Let us denote their priors by $P(\theta|I_i)$, $(i = A, B)$, and assume they are described by two Gaussian distributions with mean μ_i and variance Σ_i^2. Now, A and B make a measurement of θ together using an apparatus subject to a Gaussian noise with known variance σ. They obtain the value $\theta_0 = m_1$. Therefore they can write their likelihoods for θ as

$$L(D|\theta, HI) = L_0 \exp\left[-\frac{1}{2}\frac{(\theta - m_1)^2}{\sigma^2}\right]. \tag{16.29}$$

By using the Bayes formula, the posterior of the model A (and B) becomes

$$P(\theta|m_1) = \frac{L(m_1|\theta I_i)P(\theta|I_i)}{P(m_1|I_i)}, \tag{16.30}$$

where we have skipped writing explicitly the hypothesis H and used the notation given in Eqn. (16.21). Then, the posterior of A and B are (again) Gaussian with mean

$$\hat{\mu}_i = \frac{m_1 + (\sigma/\Sigma_i)^2\mu_i}{1 + (\sigma/\Sigma_i)^2}, \tag{16.31}$$

and variance

$$\tau_i^2 = \frac{\sigma^2}{1 + (\sigma/\Sigma_i)^2}, \quad (i = A, B). \tag{16.32}$$

Thus, if the likelihood is more informative than the prior i.e. $(\sigma/\Sigma_i) \ll 1$ the posterior mean of A (and B) will converge towards the measured value, m_1. As more data are obtained one can simply replace the value of m_1 in the above equation by the mean $\langle m \rangle$ and σ^2 by σ^2/N. Then, we can see that the initial prior μ_i of A and B will progressively be overridden by the data. This process is illustrated in Figure 16.3 where the green (red) curve corresponds to the probability distribution of θ for person A (B) and the blue curve corresponds to their likelihood.

16.3.5 Chi-square and goodness of fit

We mentioned the main aim of parameter estimation is to maximize the likelihood in order to obtain the most probable set of model parameters, given the data. If we consider the Gaussian approximation given in Eqn. (16.27) we can see the likelihood will be maximum if the quantity

$$\chi^2 \equiv (\theta_i - \theta_{0i})H_{ij}(\theta_j - \theta_{0j}), \tag{16.33}$$

is minimum. The quantity χ^2 is usually called **chi-square** and is related to the Gaussian likelihood via $L = L_0 e^{-\chi^2/2}$. Then, we can say that maximizing the Gaussian likelihood is equivalent to minimizing the chi-square. However, as we mentioned before, there are some circumstances where the likelihood cannot be described by a Gaussian distribution, in these cases the chi-square and the likelihood are no longer equivalent.

The probability distribution for different values of χ^2 around its minimum, is given by the χ^2 distribution for $v = n - M$ degrees of freedom, where n is the number of independent data points and M the number of parameters. Hence, we can calculate the probability that

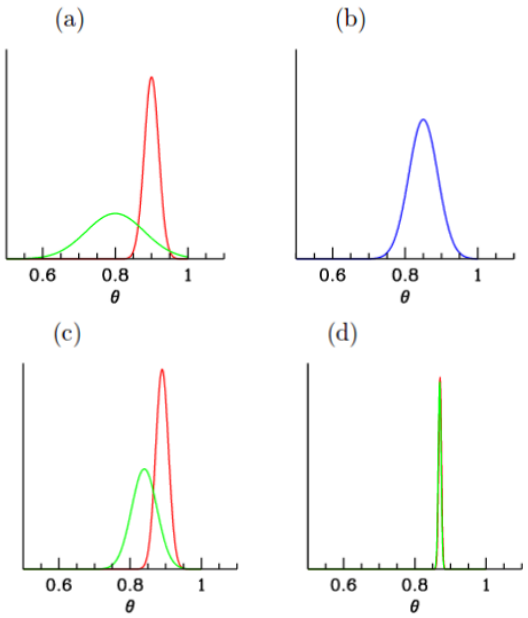

Figure 16.3: Converging views in Bayesian inference (taken from [**?**]). A and B have different priors $P(\theta|I_i)$ for a value θ (panel (a)). Then, they observe one datum with an apparatus subject to a Gaussian noise and they obtained a likelihood $L(\theta; HI)$ (panel (b)), after which their posteriors $P(\theta|m_1)$ are obtained (panel (c)). Then, after observing 100 data, it can be seen how both posteriors are practically indistinguishable (panel (d)).

an observed χ^2 exceeds by chance a value $\hat{\chi}$ for the correct model. This probability is given by $Q(v, \hat{\chi}) = 1 - \Gamma(v/2, \hat{\chi}/2)$ [**?**], where Γ is the incomplete Gamma function. Then, the probability that the observed χ^2 (even the correct model) is less than a given value $\hat{\chi}^2$ is $1 - Q$. This statement is strictly true if the errors are Gaussian and the model is a linear function of the likelihood, i.e., for Gaussian likelihoods.

If we evaluate the quantity Q for the best-fit values (minimum chi-square) we can have a measure of the goodness of fit. If Q is small (small probability) we can interpret it as:

- The model is wrong and can be rejected.
- The errors are underestimated.
- The error measurements are not normally distributed.

On the other hand, if Q is too large there are some reasons to believe that:

- Errors have been overestimated.

		$\Delta\chi^2$		
σ	p	$M=1$	$M=2$	$M=3$
1	68.3%	1.00	2.30	3.53
2	95.4%	4.00	6.17	8.02
3	99.73%	9.00	11.8	14.20

Table 16.3: $\Delta\chi^2$ for the conventional 68.3%, 95.4% and 99.73% as a function of the number of parameters (M) for the joint confidence level.

- Data are correlated or non-independent.
- The distribution is non-Gaussian.

16.3.6 Contour plots and confidence regions

Once the best fit parameters are obtained we would like to know the confidence regions where values could be considered good candidates for our model. The most logical election is to take values inside a compact region around the best fit value. Then, a natural choice are regions with constant χ^2 boundaries. When the χ^2 possesses more than one minimum, it is said that we have non-connected confidence regions, and for multi-variate Gaussian distributions (as the likelihood approximation in Eqn. (16.27)) these are ellipsoidal regions. In this section we exemplify how to calculate the confidence regions, following [**?**].

We consider a little perturbation from the best fit of chi-square $\Delta\chi^2 = \chi^2 - \chi^2_{best}$. Then we use the properties of χ^2 distribution to define confidence regions for variations on χ^2 to its minimum. In Table 16.3 we see the typical 68.3%, 95.4% and 99.73% confidence levels as a function of number of parameters M for the joint confidence level. For Gaussian distributions (as likelihood) these correspond to the conventional 1, 2 and 3 σ confidence levels. As an example we plot in Figure 16.4 the corresponding confidence regions associated to the coin example.

The general recipe to compute constant χ^2 confidence regions is as follows: after finding the best fit by minimizing χ^2 (or maximizing the likelihood) and checking that Q is acceptable for the best parameters, then:

1. Let M be the number of parameters, n the number of data and p be the confidence limit desired.

2. Solve the equation:

$$Q(n-M, min(\chi^2)+\Delta\chi^2) = p. \tag{16.34}$$

3. Find the parameter region where $\chi^2 \leq min(\chi^2)+\Delta\chi^2$. This defines the confidence region.

16.3.7 Marginalization

It is clear that a model may (in general) depend on more than one parameter. However, some of these parameters θ_i may be of less interest. For example, they may correspond to nuisance parameters like calibration factors, or it may be the case that we are interested in only one of the parameter constraints rather than the joint of two or more of them simultaneously. Then we **marginalize** over the uninteresting parameters by

$$P(\theta_1, ..., \theta_j, H|D) = \int d\theta_{j+1}...d\theta_m P(\theta, H|D), \tag{16.35}$$

where m is the total number of parameters in our model and θ_1,...,θ_j denote the parameters we are interested in.

16.3.8 Fisher Matrix

Once we have a dataset it is important to know the accuracy for which we can estimate parameters. Fisher suggested a way 70 years ago [**?**]. In this section we review the main results of his work.

First of all, consider again a Gaussian likelihood. As we notice, the **Hessian matrix** H_{ij} has information on the parameter errors and their covariance. More specifically, when all parameters are fixed except one (e.g. the i-th parameter), its error is $1/\sqrt{H_{ii}}$. These errors are called conditional errors, although they are rarely used.

A quantity to forecast the precision of a model, that arises naturally with Gaussian likelihoods, is the so-called **Fisher information matrix**

$$F_{ij} = -\left\langle \frac{\partial^2 \mathcal{L}}{\partial\theta_i \partial\theta_j} \right\rangle, \tag{16.36}$$

where

$$\mathcal{L} = \ln L. \tag{16.37}$$

It is clear that $F = \langle H \rangle$, where the average is made with observational data.

As we can see from Eqn. (16.2c), for independent data sets the complete likelihood is the product of the likelihoods, and the Fisher matrix is the sum of individual Fisher matrices.

A pedagogical and easy case is having one-parameter θ_i with a Gaussian likelihood. In this scenario

$$\Delta\mathcal{L} = \frac{1}{2}F_{ii}(\theta_i - \theta_{0i})^2, \tag{16.38}$$

when $2\Delta\mathcal{L} = 1$ and identifying the $\Delta\chi^2$ corresponding to 68% confidence level, we notice that $1/\sqrt{F_{ii}}$ yields the $1-\sigma$ displacement for θ_i. In the general case

$$\sigma_{ij}^2 \geq (F^{-1})_{ij}. \tag{16.39}$$

Thus, when all parameters are estimated simultaneously from the data, the marginalized error is

$$\sigma_{\theta_i} \geq (F^{-1})_{ii}^{1/2}. \tag{16.40}$$

The beauty of the Fisher matrix approach is that there is a simple prescription for setting it up by only knowing the model and measurement uncertainties, and under the assumption of a Gaussian likelihood the Fisher matrix is the inverse of the covariance matrix. So, all we have to do is set up the Fisher matrix and then invert it to obtain the covariance matrix (that is, the uncertainties on the model parameters). In addition, its fast calculations also enables one to explore different experimental setups and optimize the experiment.

The main point of the Fisher matrix formalism is to predict how well the experiment will be able to constrain the parameters, of a given model, before doing the experiment and perhaps even without simulating it in any detail. We can then forecast the results of different experiments and look at trade-offs such as precision versus cost. In other words, we can engage in experimental design. The inequality in Eqn. (16.39) is called the Kramer-Rao inequality. One can see that the Fisher information matrix represents a lower bound of the errors. Only when the likelihood is normally distributed, the inequality is transformed into an equality. However as we saw in Sec. 16.3.3 a Gaussian likelihood is only applicable to some circumstances, being generally impossible to be applied, so the key is to have a good understanding of our theoretical model in such a way that we can construct a Gaussian likelihood.

16.3.8.1 Constructing Fisher Matrices: A simple description

Let us construct Fisher matrices in a simple way. Suppose we have a model that depends of N parameters $\theta_1, \theta_2, ..., \theta_N$. We consider M observables $f_1, f_2, ..., f_M$ each one related to the model

parameters by some equation $f_i = f_i(\theta_1, \theta_2, ..., \theta_N)$. Then the elements of the Fisher matrix can be computed as

$$F_{ij} = \sum_k \frac{1}{\sigma_k^2} \frac{\partial f_k}{\partial \theta_i} \frac{\partial f_k}{\partial \theta_j}, \tag{16.41}$$

where σ_k are the errors associated to each observable and we have considered them Gaussianly distributed.

Here, instead of taking the real data values (which could be unknown) it is possible to recreate the data with a fiducial model. The errors associated to the mock data can be taken as the expected experimental errors, and then be possible to calculate the above expression.

To complement the subject, there is also the **Figure of Merit** used by the Dark Energy Task Force (DETF) [**?**] which is defined as the reciprocal of the area in the plane enclosing the 95% confidence limit of two parameters. The larger the figure of merit the greater accuracy one has measuring said parameters. As an example let us take a look at Figure **??** and right panel of Figure **??**, the area of the error ellipse with only Hubble Data (HD) is clearly bigger than the error ellipse using HD plus several data sets. Then, for this case the figure of merit would be bigger than with only HD data since its area is smaller, making it more accurate for measuring the parameters Ω_m and h. The DETF figure of merit can also be used to see how different experiments break degeneracies. It can also be used to predict accuracy in future experiments (experimental design).

16.3.9 Importance Sampling

We call **Importance Sampling** (IS) to different techniques of determining properties of a distribution by drawing samples from another one. The main request of this idea, is that the distribution one samples from should be representative of the distribution of interest (for a larger number of samples). In such case, we should infer different quantities out of it. In this section we review the basic concepts necessary to understand the IS, following [**?**].

Suppose we are interested in computing the expectation value $\mu_f = E_p[f(X)]$, where $f(X)$ is a probability density of a random variable X and the sub-index p means average over the distribution p. Then, if we consider a new probability density $q(x)$ that satisfies $q(x) > 0$ whenever $f(x)p(x) \neq 0$, we can rewrite the mean value μ_f as

$$\mu_f = \int f(x)p(x)dx = \int f(x)\frac{p(x)}{q(x)}q(x)dx = E_q[f(X)w(x)], \tag{16.42}$$

where $w(x) = p(x)/q(x)$, and now we have an average over q. So, if we have a collection of different draws $x^{(1)}, ..., x^{(m)}$ from $q(x)$, we can estimate μ_f using these draws as

$$\hat{\mu}_f = \frac{1}{m}\sum_{j=1}^{m} w(x^{(j)}) f(x^{(j)}). \tag{16.43}$$

If $p(x)$ is known only up to a normalizing constant, the above expression can be calculated as a ratio estimate

$$\hat{\mu}_f = \frac{\sum_{j=1}^{m} w(x^{(j)}) f(x^{(j)})}{\sum_{j=1}^{m} w(x^{(j)})}. \tag{16.44}$$

For the strong law of large numbers, in the limit when $m \to \infty$ we will have that $\hat{\mu}_f \to \mu_f$.

Another useful quantity to compute in Bayesian analysis is the ratio between evidences for two different models

$$\frac{P'(D)}{P(D)} = E\left[\frac{P'(\theta, D)}{P(\theta, D)}\right]_{P(\theta|D)} \simeq \frac{1}{N}\sum_{n=1}^{N} \frac{P'(D|\theta_n)P'(\theta_n)}{P(D|\theta_n)P(\theta_n)}, \tag{16.45}$$

where the samples $\{\theta_n\}$ are drawn from $P(\theta|D)$.

An important result for importance sampling is that, if we have a new set of data which is broadly consistent with the current data (in the sense that the posterior only shrinks), we can make use of importance sampling in order to quickly calculate a new posterior including the new data.

16.3.10 Combining datasets: Hyperparameter method

Suppose we are dealing with multiple datasets $\{D_1, ..., D_N\}$, coming from a collection of different surveys $\{S_1, ..., S_N\}$. Sometimes it is difficult to know, *a priori*, if all our data are consistent with each other, or whether there could be one or more that are likely to be erroneous. If we were sure that all datasets are consistent, then it should be enough to update the probability as seen in Sec. 16.3.2 in order to calculate the new posterior distribution for the parameters we are interested in. However, since there is usually an uncertainty about this, a way to know how useful a data may be is by introducing the **hyperparameter method**. This method was initially introduced by [**? ?**] in order to perform a joint estimation of cosmological parameters from combined datasets. This method may be used as long as every survey is independent from each other. In this section we review the main steps necessary to understand the hyperparameter method. If the reader is interested in a more extended explanation, we

encourage to consult [**? ?**].

The main feature of this process is the introduction of a new set of "hyperparameters" α in the Bayesian procedure to allow extra freedom in the parameter estimation. These hyperparameters are equivalent to nuisance parameters in the sense that we need to marginalize over them in order to recover the posterior distribution, i.e.

$$P(\theta|D,H) = \frac{1}{P(D|H)} \int P(\theta|\alpha,H)P(\alpha|D,H)d\alpha, \tag{16.46}$$

where we have used the Bayes theorem. Now, for the method it is necessary to assume the hyperparameters α and the parameters of interest θ are independent, i.e. $P(\theta,\alpha,H) = P(\alpha)P(\theta,H)$, it is also necessary to assume that each hyperparameter α_k is independent from each other, i.e. $P(\alpha) = P(\alpha_1)P(\alpha_2)...P(\alpha_N)$. In this way we can rewrite the above expression as

$$P(\theta|D,H) = \frac{P(\theta,H)}{P(D|H)} \left[\prod_{k=1}^{N} \int P(D_k|\theta,\alpha_k,H)P(\alpha_k)d\alpha_k \right]. \tag{16.47}$$

Here, the quantity inside the square brackets is the marginalized likelihood over the hyperparameters. We can identify the quantity inside the integration as the individual likelihood $L(D_k|\theta,\alpha_k,H)$, for every α_k and the data set D_k; $P(D|H)$ is the evidence and, similarly to a parameter inference procedure, it works as a normalizing function, i.e. $P(D|H) = \int d\theta P(\theta,H)L(D|\theta,H)$. Notice that, by considering $P(\alpha_k) = \delta(\alpha_k - 1)$, we rely on the standard approach, where no hyperparameters are used.

We add these α_k in order to weight every dataset and take away the data that does not seem to be consistent with other ones. Then, we would like to know whether the data supports the introduction of hyperparameters or not. A way to address this point is given by the Bayesian evidence K defined in Eqn. (16.9). If we consider a Gaussian likelihood with maximum entropy prior, and assuming that in average the hyperparameters' weight are unity, we can rewrite the marginalized likelihood function $L(D|\theta,H_1)$ for model H_1 as

$$P(D|\theta,H_1) = \prod_{k=1}^{N} \frac{2\Gamma(\frac{n_k}{2}+1)}{\pi^{n_k/2}|V_k|^{1/2}} (\chi_k^2+2)^{-(\frac{n_k}{2}+1)}, \tag{16.48}$$

obtaining an explicit functional form for K, given by

$$K = \prod_{k=1}^{N} \frac{2^{n_k/2+1}\Gamma(n_k/2+1)}{\chi_k^2+2} e^{-\chi_k^2/2}. \tag{16.49}$$

Here, χ^2_k is given by (16.33) for every dataset and n_k is the number of points contained in D_k. In equation (16.48) V_k is the covariance matrix for the k-data. Suppose we have two models, one with hyperparameters, called H_1, and a second one without them, called H_0. The Bayesian evidence $P(D|H_i)$ is the key quantity for making a comparison between two different models. In fact, by using the Bayes factor K from Eqn. (16.49) we can estimate the necessity to introduce the hyperparameters to our model using the criteria given in Table 17.2. Notice that, if we have a set of independent samples for H_0, we can compute an estimate for K with the help of equation (16.45).

16.4 Numerical tools

In typical scenarios it results very difficult to compute the posterior distribution analytically. For these cases the numerical tools available play an important role during the parameter estimation task. There exist several options to carry out this work, nevertheless in this section we focus only on the Markov Chain Monte Carlo (MCMC) with the Metropolis Hastings algorithm (MHA). Additionally, in this section we present some useful details we take into account to make more efficient our computation.

16.4.1 MCMC techniques for parameter inference

The purpose of a MCMC algorithm is to build up a sequence of points (called "**chain**") in a parameter space in order to evaluate the posterior of Eqn. (16.7). In this section we review the basic results for this procedure in a simplistic way, but for curious readers it is recommendable to check [**? ? ? ?**] for the Markov chain theory.

A **Monte Carlo** simulation is assigned to algorithms that use random number generators to approximate a specific quantity. On the other hand, a sequence $X_1, X_2, ...$ of elements of some set is a **Markov Chain** if the conditional distribution of X_{n+1} given $X_1, ..., X_n$ depends only on X_n. In other words, a Markov Chain is a process where we can compute subsequent steps based only in the information given at the present. An important property of a Markov Chain is that it converges to a stationary state where successive elements of the chain are samples from the target distribution, in our case it converges to the posterior $P(\theta|D, H)$. In this way we can estimate all the usual quantities of interest out of it (mean, variance, etc).

The combination of both procedures is called a **MCMC**. The number of points required to get good estimates in MCMCs is said to scale linearly with the number of parameters, so this

method becomes much faster than grids as the dimensionality increases.

The target density is approximated by a set of delta functions

$$p(\theta|D,H) \simeq \frac{1}{N}\sum_{i=1}^{N}\delta(\theta-\theta_i), \tag{16.50}$$

being N the number of points in the chain. Then, the posterior mean is computed as

$$\langle\theta\rangle = \int d\theta\theta P(\theta,H|D) \simeq \frac{1}{N}\sum_{i=1}^{N}\theta_i, \tag{16.51}$$

where $\simeq$ follows because the samples θ_i are generated out of the posterior by construction. Then, we can estimate any integrals (such as the mean, variance, etc.) as

$$\langle f(\theta)\rangle \simeq \frac{1}{N}\sum_{i=1}^{N} f(\theta_i). \tag{16.52}$$

As mentioned before, in a Markov Chain it is necessary to generate a new point θ_{i+1} from the present point θ_i. However, as it is expected, we need a criteria for accepting (or refusing) this new point depending on whether it turns out to be better for our model or not. If this new step is worse than the previous one, we may accept it, since it could be the case that, if we only accept steps with better probability, we could be converging into a local maximum in our parameter space and, therefore, not completely mapping all of it. The simplest algorithm that contains all this information in its methodology is known as the Metropolis-Hastings algorithm.

16.4.1.1 Metropolis-Hastings algorithm

In the **Metropolis-Hastings algorithm** [**? ?**] it is necessary to start from a random initial point θ_i, with an associated posterior probability $p_i = p(\theta_i|D,H)$. We need to propose a candidate θ_c by drawing from a **proposal distribution** $q(\theta_i,\theta_c)$ used as a generator of new random steps. Then, the probability of acceptance the new point is given by

$$p(acceptance) = min\left[1, \frac{p_c q(\theta_c,\theta_i)}{p_i q(\theta_i,\theta_c)}\right]. \tag{16.53}$$

If the proposal distribution is symmetric the algorithm is reduced to the *Metropolis algorithm*

$$p(acceptance) = min\left[1, \frac{p_c}{p_i}\right]. \tag{16.54}$$

In this way the complete algorithm can be expressed by the following steps:

1. Choose a random initial condition θ_i in the parameter space and compute the posterior distribution.

2. Generate a new candidate from a proposal distribution in the parameter space and compute the corresponding posterior distribution.

3. Accept (or not) the new point with the help of the Metropolis-Hastings algorithm.

4. If the point is not accepted, repeat the previous point in the chain.

5. Repeat steps 2-4 until you have a large enough chain.

16.4.1.2 A first example of parameter inference

In order to exemplify the numerical tools learned in this section, let us go back to the coin toss example seen in Sec. 16.3.1. Since our main interest is that the reader understands the basic procedure given in this section, let us try to estimate the value of p (or region of values for p) that best matches our data (hence, we assume only the 14 times that the coin was thrown). To calculate the posterior distribution (16.17) we use the MHA.

As mentioned before, we consider a likelihood given by a binomial distribution (16.4) and a normal distributed prior (16.16) ($a = b = 1$). As our first "guess" for p we consider $p_i = 0.1$. We generate a new candidate p_c as $p_c = p_{cu} + G(p_{cu}, \hat{\sigma})$, where $G(p_{cu}, \hat{\sigma})$ is our proposed Gaussian distribution centered at p_{cu} with variance $\hat{\sigma} = 0.1$; p_{cu} is the current value of p, for our first step is $p_{cu} = p_i$. Then, we introduce the MHA in a Python code, as can be seen in Appendix **??**. Our final result, (shown in Fig. 16.4), is a posterior distribution that matches very well with the results calculated analytically (shown in Figure 16.1). Numerically we obtained $p = 0.695^{+0.123}_{-0.107}$, where the upper and lower values for p correspond to the 1σ standard deviation. Notice that we have plotted the width of our 1σ, 2σ and 3σ confidence regions in the same figure.
To complement the example we also show in the right panel of Figure 16.4 the Markov Chain generated by our code where we have considered 5000 steps in our chain. It is easy to see that the chain oscillates with a large amplitude around a middle value. This amplitude is expected because we do not have enough data to constrain more accurately the value of p.

Remark: In appendix **??** we include the MCMC algorithm using an explicit code for the MCMC process. However, in Python there are some modules that can simplify this task. For example, PyMC3 [**?**] is a Python module that implements statistical models and fitting algorithms, including the MCMC algorithm. We use this module at the end of this section by applying the tools already learned.

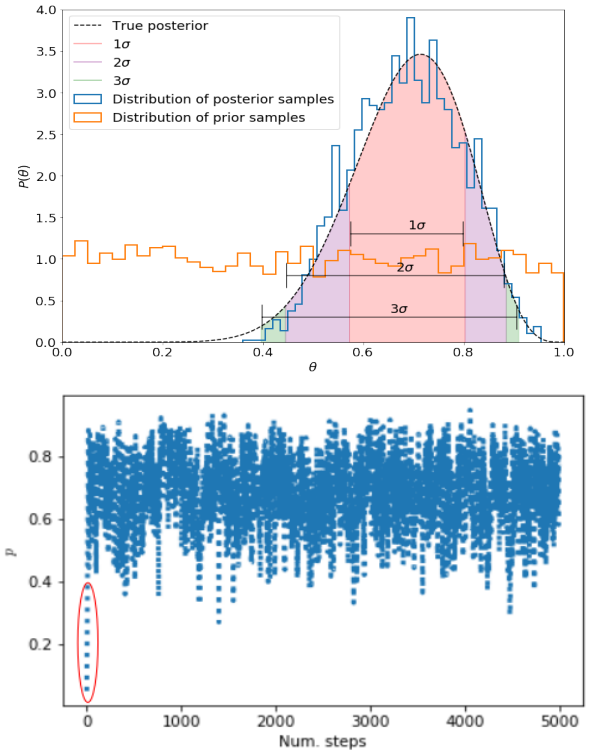

Figure 16.4: Left panel: 1D posterior distribution for our example. We plot the prior distribution (red), true posterior (dashed-black) and the posterior calculated by the MHA (blue). We plot 1,2 and 3σ confidence regions for the estimation of p. Right panel: associated Markov chain. We use $p_i = 0.1$ as our first "guess" for p.

16.4.1.3 Convergence test

It is clear that we need a test to know when our chains have converged. We need to verify that the points in the chain are not converging to a "false convergent point" or to a local maximum point. In this sense, we need that our algorithm takes into account this possible difficulty. The simplest way (the informal way) to know if our chain is converging to a global maximum is by running several chains starting with different initial proposals for the parameters we are interested in. Then, if we see by naked eye, that all the chains seem to converge into a single region of the possible value for our parameter, we may say that our chains are converging to that region.

Taking yet again the example of the coins, we can run several chains for the above example and try to estimate if the value (region) of p that we found is a stationary value. In Figure 16.5 we plot 5 different Markov chains with initial "guess" conditions $p = 0.2, 0.3, 0.5, 0.7, 0.9$. As we

expected from the analytical result, after several steps all the chains seem to concentrate near by the same value.

The convergence method used above is very informal and we would like to have a better way to ensure that our result is correct. The usual test is the *Gelman-Rubin* convergence criterion [**? ?**]. That is, by starting with M chains with very different initial points and N points per chain, if θ_i^j is a point in the parameter space of position i and belonging to the chain j, we need to compute the mean of each chain

$$\langle \theta^j \rangle = \frac{1}{N} \sum_{i=1}^{N} \theta_i^j, \tag{16.55}$$

and the mean of all the chains

$$\langle \theta \rangle = \frac{1}{NM} \sum_{i=1}^{N} \sum_{j=1}^{M} \theta_i^j. \tag{16.56}$$

Then, the chain-to-chain variance B is

$$B = \frac{1}{M-1} \sum_{j=1}^{M} (\langle \theta^j \rangle - \langle \theta \rangle)^2, \tag{16.57}$$

and the average variance of each chain is

$$W = \frac{1}{M(N-1)} \sum_{i=1}^{N} \sum_{j=1}^{M} (\theta_i^j - \langle \theta^j \rangle)^2. \tag{16.58}$$

If our chains converge, W and B/N must agree. In fact we say that the chains converge when the quantity

$$\hat{R} = \frac{\frac{N-1}{N} W + B(1 + \frac{1}{M})}{W}, \tag{16.59}$$

which is the ratio of the two estimates, approaches unity. A typical convergence criteria is when $0.97 < \hat{R} < 1.03$.

16.4.1.4 Some useful details

The proposal distribution. The choice of a proposal distribution q is crucial for the efficient exploration of the posterior. In our example we used a Gaussian-like distribution with a variance (step) $\hat{\sigma} = 0.1$. This value was taken because we initially explored, by hand, different values for $\hat{\sigma}$ and we select the quickest that approaches the analytic posterior distribution of p. However, if the scale of q is too small compared to the scale of the target (in the sense that the typical jump is small), then the chain may take very long to explore the target distribution which implies that the algorithm will be very inefficient. As we can see in Figure 16.6 (left panel), considering

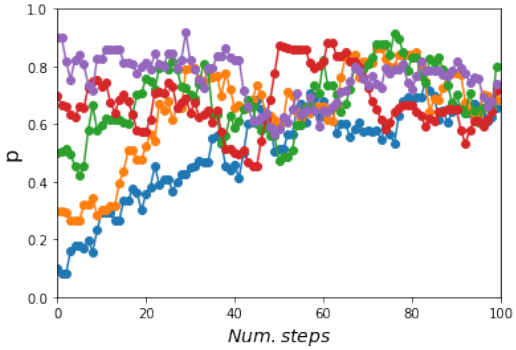

Figure 16.5: Multiple MCMC. We use five Markov Chains to estimate the convergence.

an initial step $p_i = 0.6$ and a variance for the proposal distribution $\hat{\sigma} = 0.002$, the number of points are not enough for the system to move to its "real" posterior distribution. On the other hand, if the scale of q is too large, the chain gets stuck and it does not jump very frequently (right panel of the figure with $\hat{\sigma} = 0.8$) so we will have different "peaks" in our posterior.

In order to fix this issue in a more efficient way, it is recommendable to run an exploratory MCMC, compute the covariance matrix from the samples, and then re-run with this covariance matrix as the covariance of a multivariate Gaussian proposal distribution. This process can be computed a couple of times before running the "real" MCMC.

The burn-in. It is important to notice that at the beginning of the chain we will have a region of points outside the stationary region (points inside the ellipse in the right panel of Figure 16.4). This early part of the chain (called "burn-in") must be ignored, this means that the dependence on the starting point must be lost. Thus, it is important to have a reliable convergence test.

Thinning. There are several Bayesian statisticians that usually thin their MCMC, this means that they do not prefer to save every step given by the MCMC; instead, they prefer to save a new step each time n steps have taken place. An obvious consequence of thinning the chains is that the amount of autocorrelation is reduced. However, as long as the chains are thinned, the precision for the estimated parameters is reduced [**?**]. Thinning the chains can be useful in other kind of circumstances, for example, if we have limitations in memory. Notice that thinning a chain does not yield incorrect results; it yields correct results but less efficient

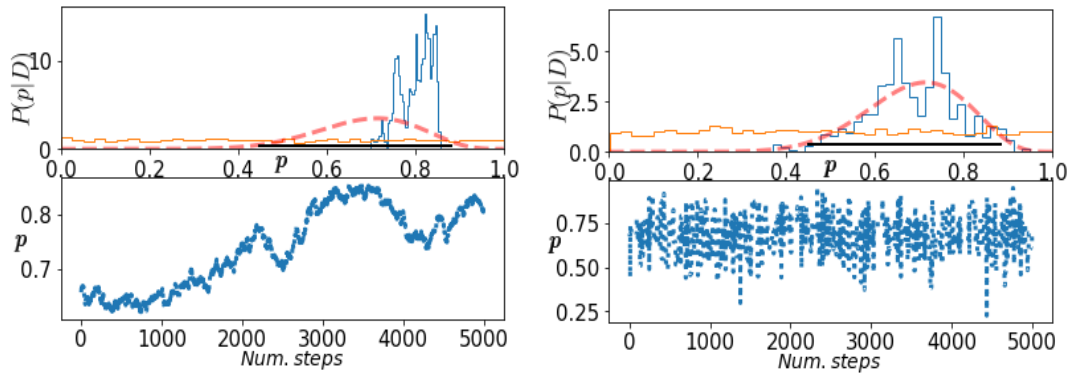

Figure 16.6: Two Markov Chains considering different variance for our Gaussian proposal distribution. Left panel corresponds to $\hat{\sigma} = 0.002$, while right panel corresponds to $\hat{\sigma} = 0.8$.

than using the full chains.

Autocorrelation probes. A complementary way to look for convergence in a MCMC estimation is by looking for the autocorrelation between the samples. The autocorrelation *lag* k is defined as the correlation between every sample and the sample k steps before. It can be quantified as [**?** **?**]

$$\rho_k = \frac{Cov(X_t, X_{t+k})}{\sqrt{Var(X_t)Var(X_{t+k})}} = \frac{E[(X_t - X)(X_{t+k} - X)]}{\sqrt{E[(X_t - X)^2]E[(X_{t+k} - X)^2]}}, \tag{16.60}$$

where X_t is the t-th sample and X is the mean of the samples. This autocorrelation should become smaller as long as k increases (this means that samples start to become independent).

More samplers

Gibbs sampling. The basic idea of the Gibbs sampling algorithm [**?**] is to split the multidimensional θ into blocks and sample each block separately, conditional on the most recent values of the other blocks. It basically breaks a high-dimensional problem into low-dimensional problems.

The algorithm reads as follows:

1. θ consists of k blocks $\theta_1, ..., \theta_k$. Then, at step i
2. Draw θ_1^{i+1} from $p(\theta_1|\theta_2^i, ..., \theta_k^i)$
3. Draw θ_2^{i+1} from $p(\theta_2|\theta_1^{i+1}, \theta_3^i, ..., \theta_k^i)$

4. ...

5. Draw θ_k^{i+1} from $p(\theta_k|\theta_1^{i+1}, \theta_2^{i+1}, ..., \theta_{k-1}^{i+1})$

6. Repeat the above steps for the wished iterations with $i \to i+1$.

The distribution $p(\theta_1|\theta_2, ..., \theta_k) = \frac{p(\theta_1,...,\theta_k)}{p(\theta_2,...,\theta_k)}$ is known as the *full conditional distribution of* θ_1. This algorithm is a special case of MHA where the proposal is always accepted.

Metropolis Coupled Markov Chain Monte Carlo (MC^3). It is easy to see that it could be a little problematic if our likelihood has local maxima. The MC^3 is a modification of the standard MCMC algorithm that consists of running several Markov Chains in parallel to explore the target distribution for different "temperatures". This simplifies the way we sample our parameter space and help us to avoid this local maxima. Here we exemplify the basic idea of this algorithm, however if you are interested in a more extensive explanation, or a modification to make the temperature of the chains dynamical, please consult the reference [**?**].

We consider a tempering version of the posterior distribution $P(\theta, T|D, H)$

$$P(\theta, T|D, H) \propto L(\theta, D)^{1/T} P(\theta, H), \tag{16.61}$$

where L is the likelihood and $P(\theta, H)$ the prior. Notice that, for higher T, individual peaks of L become flatter, making the distribution easier to sample with a MCMC algorithm. Now, we have to run N chains with different temperatures assigned in a ladder $T_1 < T_2 < ... < T_N$, usually taken with a geometrically distributed division, with $T_1 = 1$. The coldest chain T_1 samples the posterior distribution more accurately and behaves as a typical MCMC. Then, we define this chain as the main chain. The rest of the chains are running such that they can cross local maximum likelihoods easier and transport this information to our main chain.

The chains explore independently the landscape for a certain number of generations. Then, in a pre-determined interval, the chains are allowed to "swap" its actual position with a probability

$$A_{i,j} = min\left\{\left(\frac{L(\theta_i)}{L(\theta_j)}\right)^{1/T_j - 1/T_i}, 1\right\}. \tag{16.62}$$

In this way, if a swap is accepted, chains i and j must exchange their current position in the parameter space, then chain i has to be in position θ_j and chain j has to move to position θ_i.

We can see that, since the hottest chain T_{max} can access easier to all the modes of $P(\theta, H, T_{max}|D)$, then it can propagate its position to colder chains, to be precise, it can

propagate its position to the coldest chain $T = 1$. At the same time, the position of colder chains can be propagated to hotter chains, allowing them to explore the entire prior volume.

Affine Invariant MCMC Ensemble Sampler. The main property of this algorithm relies on its invariance under affine transformations. Let's consider a highly anisotropic density

$$p(x_1, x_2) \propto \exp\left(\frac{-(x_1 - x_2)^2}{2\epsilon} - \frac{(x_1 + x_2)^2}{2}\right), \tag{16.63}$$

which is difficult to calculate for small ϵ. But by making the affine transformation

$$y_1 = \frac{x_1 - x_2}{\sqrt{\epsilon}}, \quad y_2 = x_1 + x_2, \tag{16.64}$$

we can rewrite the anisotropic density into the easier problem

$$p(y_1, y_2) \propto \exp\left(\frac{-(y_1^2 + y_2^2)}{2}\right). \tag{16.65}$$

A MCMC sampler has the form $X(t+1) = R(X(t), \psi(t), p)$, where $X(t)$ is the sample after t iterations, R is the sampler algorithm, ψ is the sequence of independent identically distributed random variables and p is the density. A sampler is said to be affine invariant if, for any affine transformation $Ax + b$,

$$R(AX(t) + b, \psi(t), p_{A,b}) = AR(X(t), \psi(t), p) + b. \tag{16.66}$$

There are already several algorithms that are affine invariant, one of the easiest is known as the *stretch move* [**?**]. An algorithm fully implemented in Python under the name **EMCEE** [**?**] is also affine invariant, and there are also some other algorithms that can be found in [**?**].

Even more samplers. The generation of the elements in a Markov chain is probabilistic by construction and it depends on the algorithm we are working with. The MHA is the easiest algorithm used in Bayesian inference. However, there are several algorithms that can help us to fulfill our mission. For instance, some of the most popular and effective ones, are the Hamiltoninan Monte Carlo (see e.g. [**? ?**]) or the Adaptative Metropolis-Hastings (AMH) (see e.g. [**?**]).

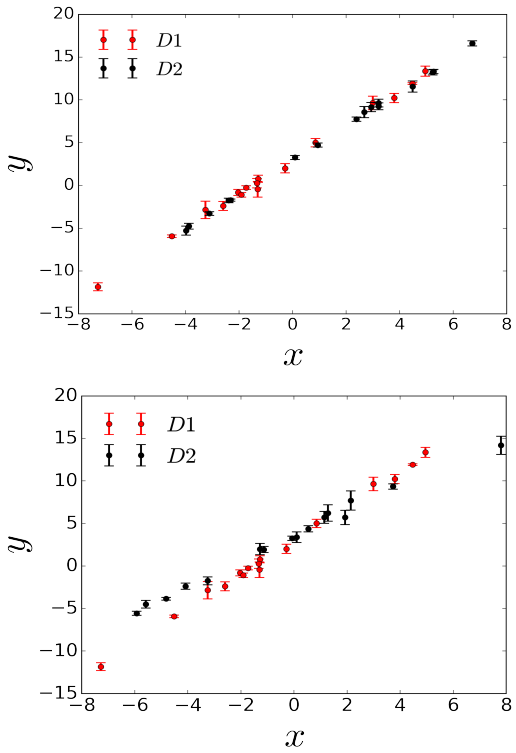

Figure 16.7: Datasets D_1 and D_2 measured by our straight-line theory. Case 1 (left) and case 2 (right).

16.5 Fitting a straight-line

In this section we apply the tools learned so far to the simplest example: fitting a straight-line. That is, we assume that we have a certain theory where our measurements should follow a straight line. Then, in order to apply our techniques, we simulate several datasets along this line. One of the principal topics we want to analyse is the hyperparameter method and how it works, so we will apply our analysis to two different cases (Figure 16.7):

1. Consider two datasets taken from the same straight-line but with different errors.

2. Consider two datasets but now we simulate both of them from different straight-lines and different errors.

In our analysis we used the PyMC3 module implemented in Python. Our complete code can be downloaded from the git repository [**?**]. This code is simple to use and can be modified easily for any model to be tested. We recommend to use the file called "new model" where the reader can find a blank project. Here the data and model can be added up and, by running all the

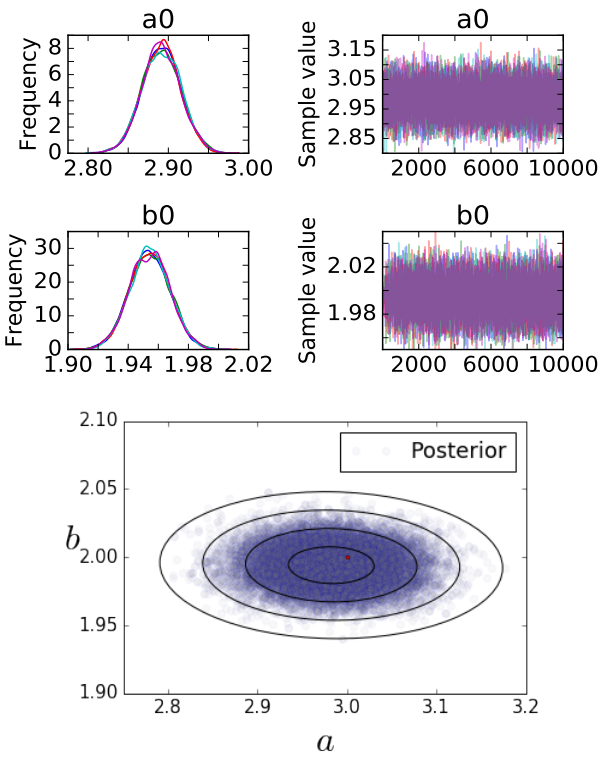

Figure 16.8: Left panel: 1D marginalized posterior distributions for our samples and the Markov chains for model H_0. Right panel: 2D marginalized posterior distributions along with 1-4 confidence regions for our parameters for model H_0. The red point corresponds to the true value.

notebook, obtain all the analysis we present in this section. One can find as well several notes that will help in programming the model with PyMC3, even if the model contains functions that are not defined in PyMC3.

16.5.1 Case 1

In this example we start by considering that our measurements for a given theory (a straight-line $y = a + bx$) are given by the data shown in left panel of Figure 16.7. These two datasets, D1 and D2, were generated from the line $y = 3 + 2x$, adding a gaussian error to each point. For D1 we add an error with a standard deviation $\sigma_1 = 0.3$, while for D2 we use $\sigma_2 = 0.2$. Then, we would like to estimate the parameters of the model, i.e. a and b. We will analyse this data with and without the hyperparameter method and discuss in detail our results.

Without hyperparameters. Model H_0.

Before we make a Bayesian estimation, it is necessary to specify our priors. As we have seen, a good prior is a non informative one. Suppose we only know some limits for a and b (we can see them by eye in our data). Then we consider the flat priors

$$a \propto U[0,5] \quad \text{and} \quad b \propto U[0,3], \tag{16.67}$$

where $U[\alpha,\beta]$ are uniform distributions with lower limit α and upper limit β.

From equation (16.27) we can write our likelihood as

$$L(D;line) \propto \exp\left[-\sum_d \frac{(y_d-y)^2}{2\sigma_d^2}\right], \tag{16.68}$$

where y_d is our data taken from the dataset $D = D_1 + D_2$ and σ_d its errors.

We use the MHA to generate our MCMC. In our analysis we ran 5 chains with 10,000 steps for each one. We ran each chain with a temperature $T = 2$ and we thinned them every 50 steps. The results we obtained correspond to $a = 2.982 \pm 0.047$ and $b = 1.994 \pm 0.013$, and their posterior distributions are plotted in Figure 16.8. Notice that there are some regions where the frequency of events in our sample is increased. So we can say that such parameter regions seem to more likely match the data. Additionally we compute the Gelman-Rubin criterion for each variable in order to verify that our results converged, i.e. for a is 1.000017 and for b is 1.000291. We see that this number is very close to 1, so our convergence criterion is fulfilled. Right panel of Figure 16.8 displays the $1-4\ \sigma$ confidence regions. We also add a point in red to show the real value for our parameters. The real value for a and b are inside of the curve corresponding to one standard deviation of our estimations in the inferential method.

We continue with the autocorrelation plots. As we mentioned, we need these plots to be small as k increases in order to consider that our analysis is converging. We see in Figure 16.9 such plots and notice that our convergence criteria is fulfilled. Then, in Case 1 we can see that the model H_0 looks to be a very good estimation procedure.

With hyperparameters. Model H_1.

Now let us consider the Hyperparameter method. In this case our likelihood can be written as Eq. (16.48). Similarly to the last procedure, we compute the posterior with flat priors and using 5 chains with 10,000 steps for each one, and check for autocorrelations. Our results are as

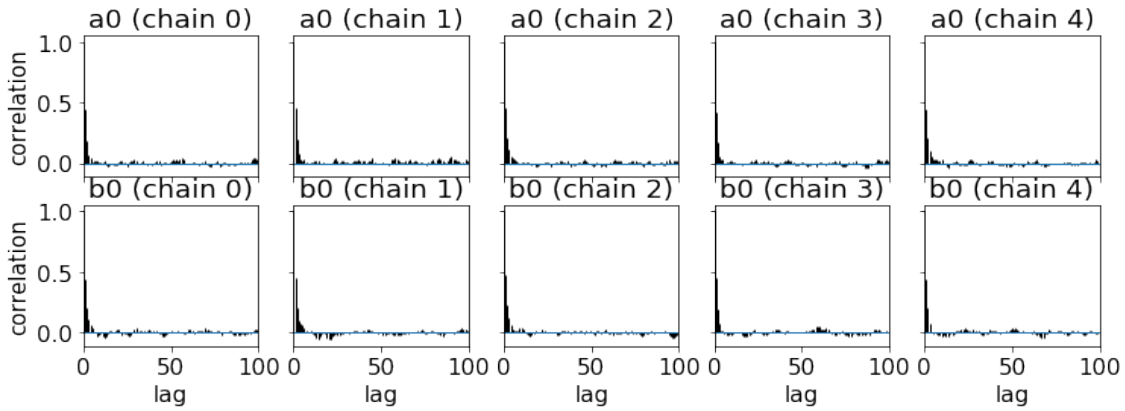

Figure 16.9: Autocorrelation plots for model H_0.

followed: $a = 2.97 \pm 0.038$ with Gelman-Rubin of 1.000113 and $b = 1.995 \pm 0.010$ with Gelman-Rubin 1.000155. Comparing both procedures we observe they provide similar results. In fact, the confidence regions for both approximations, Fig. 16.8 and left panel of Figure 16.10, are similar as well. So, which method is better? We could say that the method with hyperparameters is as good as the one without them, but in order to be sure we compute the evidence ratio K between both models. We obtained from Eqn. (16.49)

$$K = 3. \tag{16.69}$$

Then, comparing with Table 17.2 we can say that the evidence for H_1 to be better than H_0 is weak. In such case it should be equally better to work with H_0 as to H_1, as we explained before.

Finally, in order to exemplify our results, let us plot in the right panel of Figure 16.10 our data with the straight-line inferred by the mean parameters of both models. As we expected our estimation fits well the data for both cases.

16.5.2 Case 2

Here we consider that we have the same theory for the straight-line but different measurements. The data points are given in the right panel of Figure 16.7. These correspond to our dataset D_1 and D_2, but now changing D_2 by 16 new points generated around the line $y = 3.5 + 1.5x$ with a Gaussian noise and standard deviation $\sigma = 0.5$. So, our datasets are not auto-consistent with each other. Let us make again a parameter estimation for the parameters a and b and

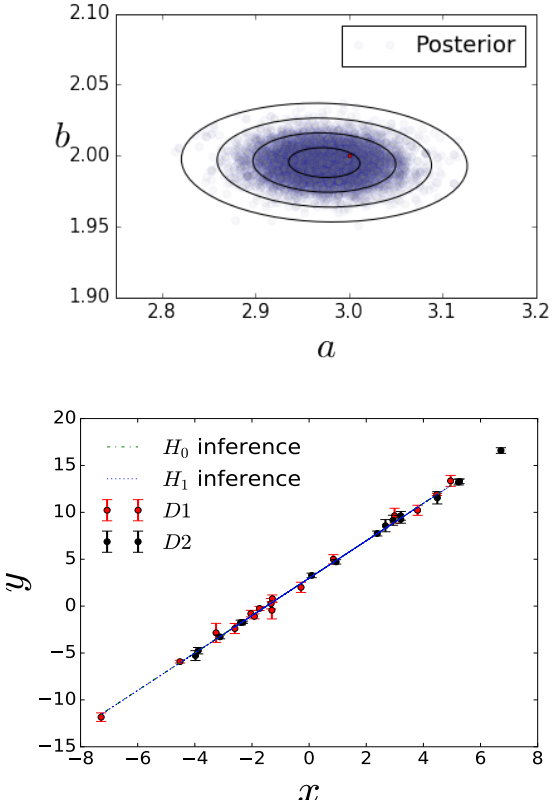

Figure 16.10: Left panel: confidence regions for the parameters in model H_1. Right panel: the best-fit for the straight-lines inferred by the data.

look for the differences in both procedures.

Without hyperparameters. Model H_0.

We follow the same procedure as in Case 1. We computed our posterior and verified that our results converged with the help of the Gelman-Rubin criterion and the autocorrelation plots. Our results are the following: $a = 3.528 \pm 0.056$ and $b = 1.795 \pm 0.014$. Then we plotted our $1 - 4\sigma$ confidence regions in left panel of Figure 16.11. It is easy to see that our estimation differs so much from the real parameters in our datasets (red points). Of course this is because we are trying to fit a model with non auto-consistent datasets and therefore we arrive at incorrect results. Now, let us see what happens in the hyperparameters procedure.

With hyperparameters. Model H_1.

In the top right panel of Figure 16.11 we plotted our posterior distribution. We see immediately that both approximations are very different. While for model H_0 we obtained a single region far away of the real values of our data, for model H_1 we obtained two local maximum regions near the real values for our datasets (red dots). For this example we do not calculate the typical mean and standard deviation for our results.

As the last example we compare both methods. Given the fact that we know *a priori* the real values of our parameters for this example, we could immediately say that the method with hyperparameters is a better approximation than the case without them. However, we confirm this assumption by calculating the ratio K between both models. We obtain

$$K = 37, \tag{16.70}$$

which means that we have a very strong evidence that H_1 is better that H_0.
Finally, we can plot the straight-line inferred by model H_0 and the two inferred by model H_1. Considering parameters inside the two regions in the top right panel of Figure (16.11) we obtain the bottom panel of Figure 16.11.

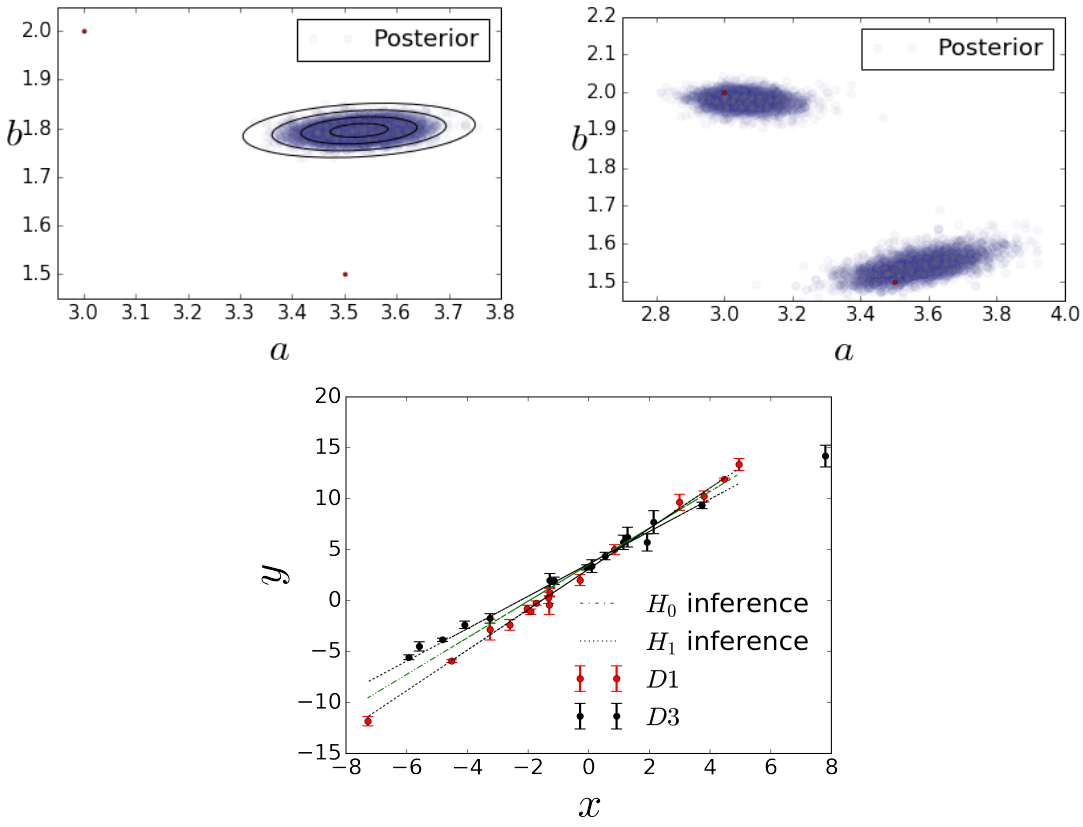

Figure 16.11: Top left panel: confidence regions for the parameters in model H_0. Top right panel: confidence regions for the parameters in model H_1. Bottom panel: Best-fit values for the straight-lines for Case 2 inferred by our with data.

17

Statistics in Cosmology

In the previous chapter we have developed the main equations to describe the evolution of the background and perturbed universe. We noticed, however, that the whole structure of the CMB, matter power spectrum and luminosity distance depend strongly on the initial conditions emerging from the inflationary era ($\mathcal{P}_{\mathcal{R},\mathcal{T}}$), on the matter-energy content ($\Omega_{i,0}$), and on the expansion rate history (H_0). This chapter seeks to give a brief introduction of such quantities used to describe the properties of the universe. We show current and future experimental results used throughout the analysis: CMB, SNe and LSS amongst many others. It also includes a short description of the Bayesian analysis to perform the parameter estimation and model selection. Finally, at the end of the chapter, by making use of the theoretical, observational and statistical tools included in this work, we examine the standard ΛCDM model (spatially flat and non-flat), and present the current constraints on the cosmological parameters.

17.1 The Cosmological Parameters

17.1.1 Base parameters

These parameters, commonly called *standard parameters*, are considered as the principal quantities used describe the universe. They are not, however, predicted by any fundamental theory, rather we have to fit them by hand in order to determine which combination best describes the current astrophysical observations [71, 78]. Variations of these parameters affect the amplitude and shape of the spectra as well as the background evolution in many different ways, yielding to very different universes. They are classified depending on whether they characterise the background or the perturbed universe:

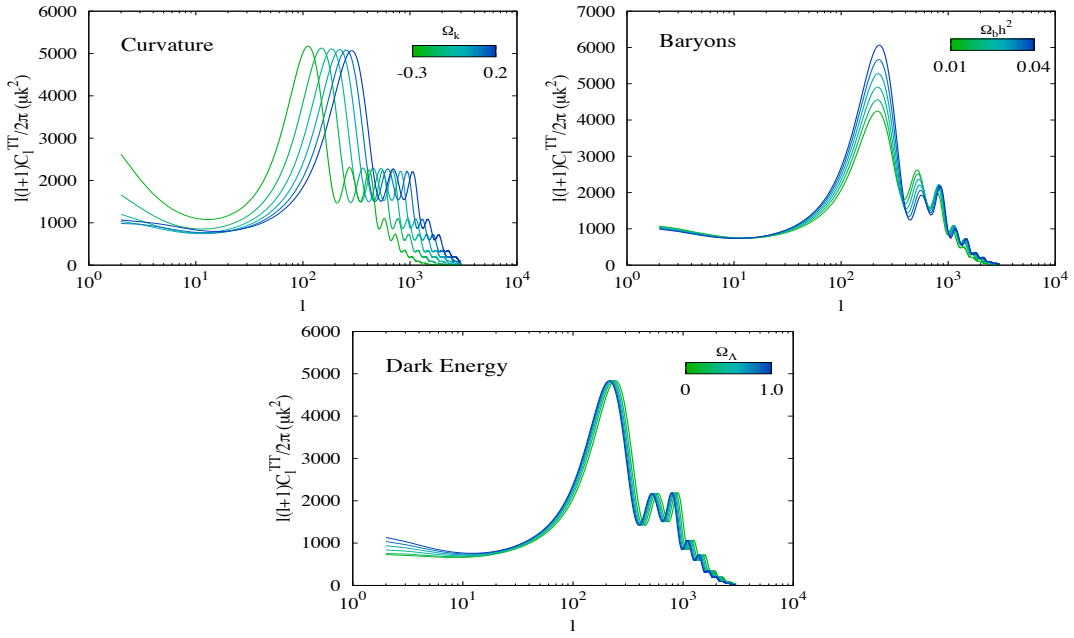

Figure 17.1: Dependence of the temperature power spectrum for three fundamental quantities: Curvature (Ω_k), Baryons (Ω_b) and Dark energy in the form of a cosmological constant (Ω_Λ).

Background parameters

The present description of the homogeneous universe can be given in terms of the density parameters $\Omega_{i,0}$ and the Hubble parameter H_0, through the Friedmann equation (2.155):

$$H^2 = H_0^2 \left[(\Omega_{\gamma,0} + \Omega_{\nu,0})\, a^{-4} + (\Omega_{\mathrm{b},0} + \Omega_{\mathrm{dm},0})\, a^{-3} + \Omega_{k,0} a^{-2} + \Omega_{X,0} a^{-1} + \Omega_{\Lambda,0} \right], \qquad (17.1)$$

From these parameters the radiation contribution is accurately measured, for instance by the WMAP satellite, corresponding to $\Omega_{\gamma,0} = 2.469 \times 10^{-5} h^{-2}$ for $T_\mathrm{cmb} = 2.725K$. Similarly for neutrinos, while taken as relativistic, they can be related to the photon density through (2.144). However, variations of the rest of the parameters imprint different signatures on the background history and evolution of perturbations, observed through the CMB spectrum as it is illustrated in Figure 17.1. We observe that the first peak (and the most prominent, at $l \approx 200$) is particularly related to the spatial geometry $\Omega_{k,0}$; the relative heights of the intermediate peaks probe the baryon density; the largest scales are mainly affected by the dark energy component.

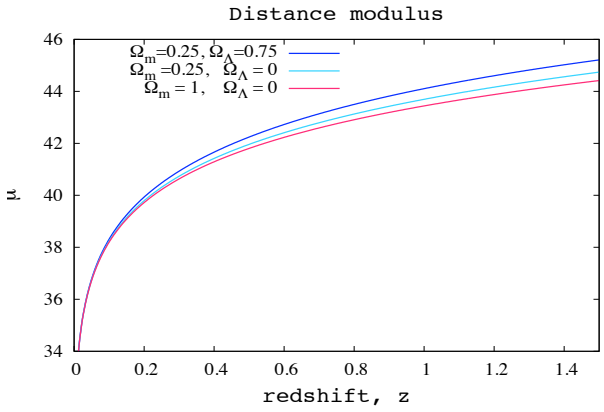

Figure 17.2: Theoretical values of the distance modulus μ for three different models; with various combinations of matter $\Omega_{m,0}$ and dark energy in the form of a cosmological constant $\Omega_{\Lambda,0}$.

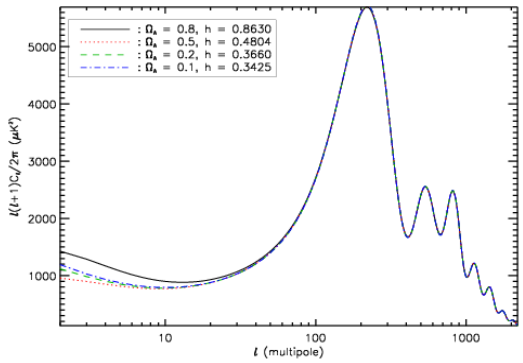

Figure 17.3: Cosmic Degeneracy

These base parameters also play a key role on measurements of the distance modulus μ, through the luminosity distance (2.204). Figure 17.2 shows the theoretical values of the distance modulus for three different models with various combinations of $\Omega_{m,0}$ and $\Omega_{\Lambda,0}$. Note that objects appear to be further away (dimmer) in a universe with cosmological constant than one dominated by only matter today.

The existence of strong degeneracies amongst different combinations of parameters is also noticeable. In particular the well-known *geometrical degeneracy* involving Ω_m, Ω_Λ and the curvature parameter $\Omega_k = 1 - \Omega_m - \Omega_\Lambda$.

To reduce degeneracies it is common to introduce a combination of the cosmological pa-

rameters such that they have orthogonal effects on the power spectrum [68]. For instance, a standard parameterisation is based on the *physical energy-densities* of cold dark matter $\Omega_{\rm dm}h^2$, and baryons $\Omega_{\rm b}h^2$, and the ratio of the sound horizon to the angular diameter distance at decoupling time:

$$\theta = \frac{r_{\rm s}(a_{\rm dec})}{D_A(a_{\rm dec})}. \tag{17.2}$$

There is an extra parameter that accounts for the reionisation history of the universe, the *optical depth to scattering* τ (i.e. the probability that a given photon scatters once), given by

$$\tau = \sigma_{\rm T} \int_{t_r}^{t_0} n_e(t) dt, \tag{17.3}$$

where $\sigma_{\rm T}$ is the Thompson cross-section and $n_e(t)$ is the electron number density as a function of time.

Inflationary parameters

After the horizon exit, H and $\dot{\phi}$ have small variations during few e-folds. Thus, the scalar (**??**) and tensor (**??**) spectra are nearly scale independent. The standard assumption is therefore to parameterise each of the spectra in terms of a power-law

$$\mathcal{P}_{\mathcal{R}}(k) = A_{\rm s} \left(\frac{k}{k_0}\right)^{n_{\rm s}-1}, \tag{17.4}$$

$$\mathcal{P}_{\mathcal{T}}(k) = A_{\rm t} \left(\frac{k}{k_0}\right)^{n_{\rm t}}. \tag{17.5}$$

where $A_{\rm s}$, $A_{\rm t}$ are the *spectral amplitudes*, and $n_{\rm s}$, $n_{\rm t}$ the *spectral indices* or *tilt parameters*, for both scalar and tensor perturbations respectively; k_0 denotes an arbitrary scale at which the tilted spectrum pivots, usually fixed to $k_0 = 0.002$ Mpc^{-1}. A scale-invariant spectrum, called Harrison-Zel'dovich (HZ), has constant variance on all length scales and it is characterised by $n_{\rm s} = 1$, $n_{\rm t} = 0$. Small deviations from scale-invariance are also considered as typical signatures of inflationary models [80]. The spectrum of perturbations is said to be blue if $n_{\rm s} > 0$ (more power in ultraviolet), and red if $n_{\rm s} < 0$ (more power in infrared). The spectral indices, $n_{\rm s}$ and $n_{\rm t}$, and the tensor-to-scalar ratio r can be expressed in terms of the slow-roll parameters $\epsilon_{\rm v}$ and $\eta_{\rm v}$ (3.32), as:

$$n_{\rm s} - 1 \simeq -6\,\epsilon_{\rm v}(\phi) + 2\,\eta_{\rm v}(\phi), \tag{17.6}$$

$$n_{\rm t} \simeq -2\,\epsilon_{\rm v}(\phi), \tag{17.7}$$

$$r \simeq 16\,\epsilon_{\rm v}(\phi). \tag{17.8}$$

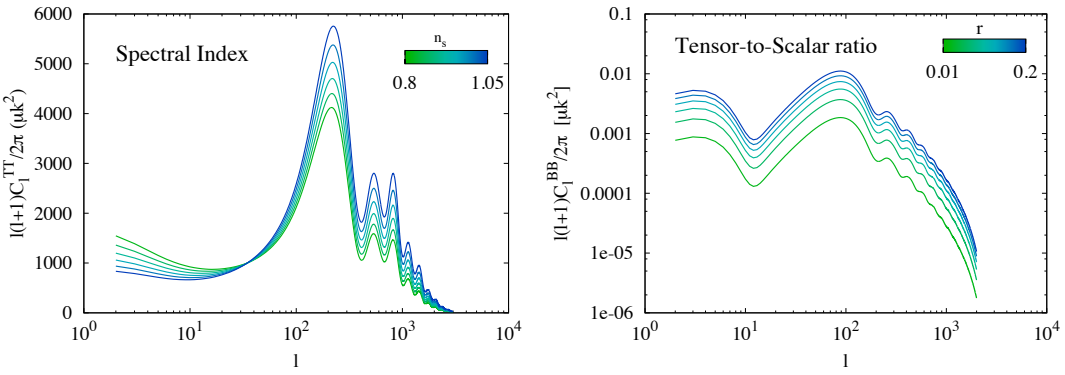

Figure 17.4: Variations of the C^{TT} scalar spectrum for different values of the spectral index n_s (left), and variations of the C^{BB} tensor spectrum with respect to the tensor-to-scalar ratio r (right).

These parameters are not completely independent each other, but the tensor spectral index is proportional to the tensor-to-scalar ratio $r = -8n_{\rm t}$ [30]. This expression is considered as the *consistency relation* for slow-roll inflation. Any single-field inflationary model can hence be described, to the lowest order in slow-roll, in terms of three independent parameters: the amplitude of density perturbations $A_{\rm s}$, the scalar spectral index $n_{\rm s}$, and the tensor-to-scalar ratio r. Variations of the CMB T-spectrum over different values of $n_{\rm s}$ are shown in the left panel of Figure 17.4.

In addition to the temperature T and polarisation E spectra, produced by scalar perturbations, there is also the B-mode polarisation only produced by tensor perturbations. Therefore, measurements of B-modes are important tests for the existence of primordial gravitational waves. Unfortunately, there is no observational evidence of tensor perturbations yet, and r is commonly set to zero. The next generation of CMB polarisation experiments will substantially improve these limits (see Section 17.2.2). Variations of the C^{BB} tensor spectrum with respect to the tensor-to-scalar ratio r are displayed in the right panel of Figure 17.4.

17.1.2 Nuisance parameters

We do not have particular interest on these type of parameters, however they may influence the rest of the parameter-space constraints. These type of parameters may be related to insufficiently constrained aspects of physics, or uncertainties in the measuring process [**?**]. Therefore,

considering their uncertainty is important in order to obtain accurate error-estimates on the physical parameters we are seeking to determine. Examples of nuisance parameters are, for instance, the bias factor in galaxy surveys b, calibrations and beams uncertainties, galactic foregrounds. The new ACT measurements (three seasons of data [121]) incorporate nine parameters describing secondary emissions. Nuisance parameters also control the stretch α and colour β corrections on measurements of distance modulus of SNe Type Ia [93].

17.1.3 Derived parameters

The standard set of parameters, introduced previously, provide an adequate description of the cosmological models in agreement with observational data. However, it is not unique and other parameterisations may be as good as this one. Some parameterisations make use of knowledge about physics or sensitivity of observations and are hence more naturally interpreted. In general we could have used different parameters to describe the universe, those include: the age of the universe, the present neutrino background temperature, the epoch of matter-radiation equality, the reionisation epoch, the baryon to dark matter density ratio, or some other combinations of parameters, i.e. the overall amplitude of the CMB anisotropy $\exp(-2\tau)A_{\rm s}$ [**?**]. In the ΛCDM model, to ameliorate degeneracies, we use as base parameters the physical energy densities $\Omega_{\rm dm,0}h^2$ and $\Omega_{\rm b,0}h^2$, and the ratio of the sound horizon to the angular diameter distance θ; we consider as derived quantities the density parameters $\Omega_{i,0}$ and Hubble parameter H_0.

17.1.4 Beyond the concordance ΛCDM

The best model in agreement with data, at present time, is given by the concordance ΛCDM model. However, this model might not be the final one and several extensions have already been implemented. A non-exhaustive list of candidates beyond the standard cosmological model is shown in Table 17.1. The definite answer on how many parameters we must include or which set of parameters represents the most plausible will be given by high-quality cosmological observations in the coming years. In the same table, we have highlighted the models studied in detail throughout this work.

17.2 Observations

Rapid advance in the development of powerful observational-instruments has led to the establishment of *precision cosmology*. In particular, experiments employed to measure CMB

Table 17.1: Candidate parameters used to describe models beyond the concordance ΛCDM. The highlighted models are studied in detail throughout this work.

αR^n	Modifications to gravity
	[or more complex theories]
$d\tilde{s}^2$	Anisotropic universe
$d\alpha/dz$, dG/dz	Variations of fundamental constants
$f_{\rm NL}$	Non-gaussianity
$n_{\rm run}$	Running of the scalar spectral index
$k_{\rm cut}$	Large-scale cut-off in the spectrum
	[or a more complex parameterisation of $\mathcal{P}_{\mathcal{R}}(k)$]
$r + 8n_{\rm t}$	Violation of the inflationary consistency relation
$n_{\rm t,run}$	Running of the tensor spectral index
	[or a more complex parameterisation of $\mathcal{P}_{\mathcal{T}}(k)$]
$P_{\rm iso}$	CDM isocurvature perturbations
$\Omega_{k,0}$	Spatial curvature
$\Omega_{X,0}$	Additional components
$m_{\rm dm}$	Warm dark matter mass
	[or scalar field dark matter]
m_{ν_i}	Neutrino mass for species 'i'
$w_{\rm DE}$	Dark energy equation-of-state
	[or a more complex parameterisation of $w(z)$]
ρ^α	Polytropic equation of state
Γ	Interacting fluids

anisotropies, luminosity distances and large-scale structure. In this section, we highlight these type of experiments used to impose constraints on the cosmological parameters.

17.2.1 Current observations

CMB experiments

A number of experiments over the past decade or so have been very successful in measuring the anisotropies of the CMB. They include the Cosmic Background Explorer satellite [COBE; 95] as the pioneer of detecting the anisotropy. Nowadays with highly-improved experiments it is possible to find accurate measurements of the temperature and polarisation CMB spectrum from:

Satellite experiments:

- The Wilkinson Microwave Anisotropy Probe [WMAP; 67, 72], with CMB T-spectrum measurements over the multipoles ($2 < l < 1200$). Recently the WMAP collaboration has released the 9-year of observations [52].

Ground-based telescopes:

- The Background Imaging of Cosmic Extragalactic Polarization [BICEP; 27], probes intermediate scales ($21 \leq l \leq 335$).
- The Quest (Q and U Extra-Galactic Sub-mm Telescope) at DASI (Degree Angular Scale Interferometer) [QUAD; 19], improve polarisation constraints, whose primary aim is high resolution measurements ($154 \leq l \leq 2026$) of the polarisation signals.
- The Cosmic Background Imager [CBI; 122], constrains the CMB spectrum in the range ($300 \leq l \leq 1700$).
- The Atacama Cosmology Telescope [ACT; 37], observes the small angle CMB T-spectrum from l= 300 to l=10000, and recently released the three seasons of data [121].
- The South Pole Telescope [SPT; 63], with CMB T-measurements between ($650 < l < 9500$), and recent improved data from the 2500-square-degree SPT-SZ survey [126].

Ballon-borne experiments:

- Balloon Observations Of Millimetric Extragalactic Radiation AND Geophysics [BOOMERanG; 62], measures CMB temperature fluctuations over the multipole range $50 \leq l \leq 1500$.

Figure 17.5 summarises the current status of some experiments constraining the temperature (TT), polarisation (EE) and cross-correlation (T-E) CMB power spectra. In particular the CMB T-power spectrum is now well-constrained over a wide range of scales. For example, WMAP and BICEP observations provide good constraints on the late-time ISW effect arising at the largest scales on the first three acoustic peaks, whilst ACT and SPT data accurately measure the power of higher acoustic peaks and damping tail. Intermediate scales are well constrained by QUAD and CBI experiments, and the overlapping of all of them. In addition to T, E and T-E CMB spectra, Figure 17.6 shows the theoretical B-mode spectrum predicted from a power-law parameterisation, with $r = 0.1$, along with 1σ constraints obtained from

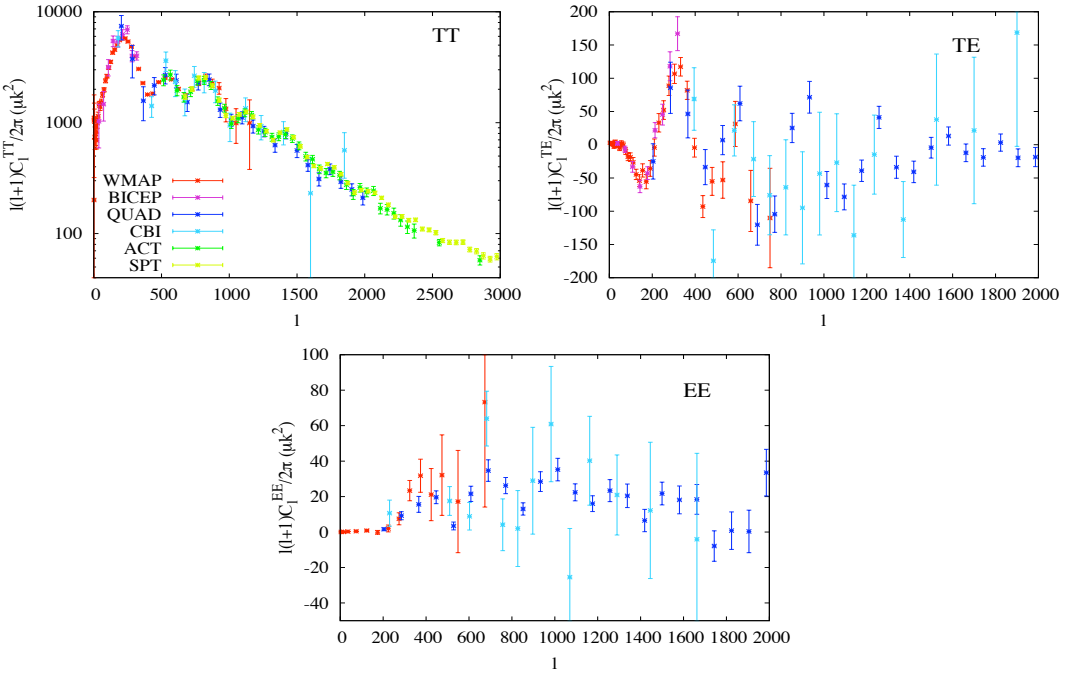

Figure 17.5: Current status of temperature (TT), polarisation (EE) and cross-correlation (T-E) measurements of the CMB power spectra, by various observational probes.

current observations: WMAP, BICEP and QUAD.

At this point it is worthwhile mentioning the existence of an intrinsic uncertainty in the cosmological measurements. This limitation comes from the fact that we have to do statistics with only one universe. For a given multipole l, we expect to have a variance, called the *cosmic variance*, of the C_l's given by

$$(\Delta C_l)^2 = \frac{2}{2l+1} C_l^2. \tag{17.9}$$

In real experiments, the error is increased due to the limited sky coverage by f_{sky}^{-1}.

CMB measurements by themselves cannot, however, place strong constraints on all the parameters because the existence of parameter degeneracies, such as the $\tau - A_s$ and the geometrical degeneracy. Nevertheless, when CMB observations are combined with other cosmological probes, they together increase the constraining power and considerably weaken degeneracies.

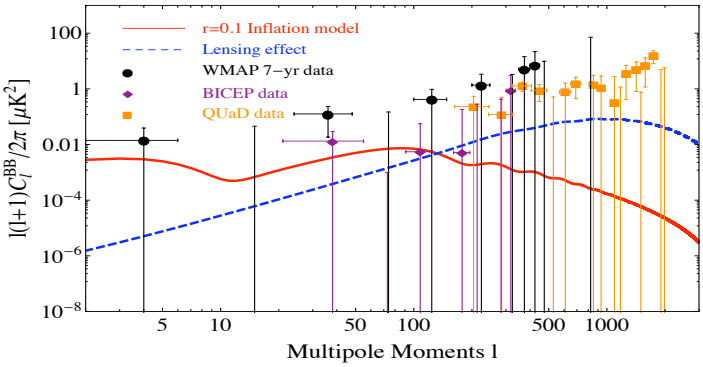

Figure 17.6: WMAP, BICEP and QUaD constraints for the B-mode power spectrum. The solid line represents the theoretical prediction of a $r = 0.1$.

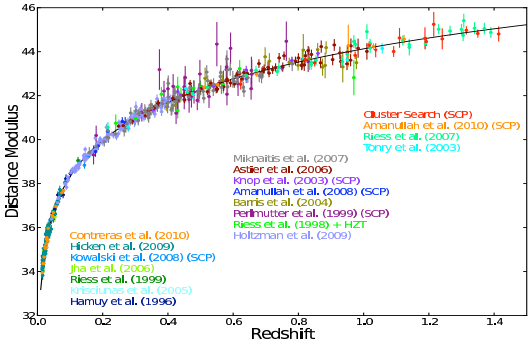

Figure 17.7: Current status of measurements of the Hubble diagram of Type Ia supernovae. Reprinted from the Union 2.1 compilation [128].

Supernovae observations

Throughout the past two decades supernovae observations have provided decisive evidence that the present expansion of the universe is accelerating. In particular studies of Type Ia supernovae as standard candles: they have the same intrinsic magnitude with high accuracy, up to a rescaling factor, e.g. Perlmutter et al. [106], Riess et al. [115]. Hence, the current acceleration suggests the existence of an exotic component or alternative theories which would produce such an effect, as we will see in Chapters **??** and **??**. Branch and Tammann [17] provides a brief introduction to Type Ia supernovae (SNe Ia) as standard candles, and **?**] shows their use in cosmology. Some samples of supernovae Type Ia worth mentioning include:

- The Sloan Digital Sky Survey-II [SDSS-II; 45], discovered and measured multi-band

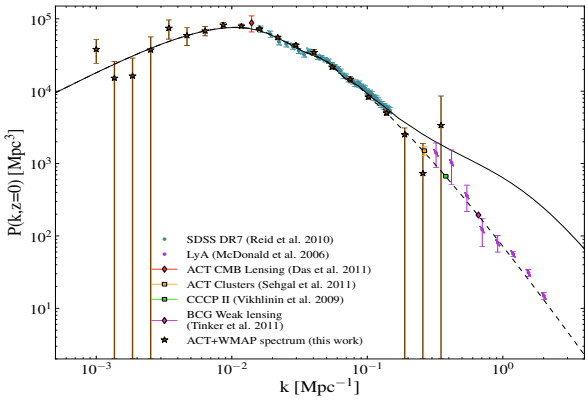

Figure 17.8: Current status of the perturbation power spectrum as measured by different experiments. Figure reproduced from [53].

lightcurves for 327 spectroscopically confirmed Type Ia supernovae in the redshift range $0.05 < z < 0.35$.

- The Equation of State: SupErNovae trace Cosmic Expansion program [ESSENCE; 97], discovered and analysed 60 Type Ia supernovae over the redshift interval $0.15 < z < 0.70$,
- The Supernova Legacy Survey 3-year sample [SNLS; 127], presented 252 high redshift Type Ia supernovae ($0.15 < z < 1.1$).
- The Hubble Space Telescope [HST; 113], discovered 21 Type Ia supernovae at $z \geq 1$.
- Recently the compilation of data from all the above, namely the 'Union' [69], 'Union 2' [4] and 'Union 2.1' [128].

Supernovae measurements can be plotted on a Hubble diagram with distance modulus vs. redshift (as seen in Figure 17.7), and then be used to fit the best cosmological parameters, for instance those shown in Figure 17.2.

LSS measurements

The matter power spectrum is nowadays one of the most important measures of large-scale structure. Many observations have been made to infer the spectrum:

- The sample of Luminous Red Galaxies (LRGs) from the Sloan Digital Sky Survey Seventh Data Release (DR7) [112], provides measurements on the matter spectrum between $0.02 <$

$k < 0.19\text{Mpc}^{-1}$. Nowadays with improved measurements, one has the ninth data released (DR9) of the SDSS-III [2].

- Measurements of the transmitted flux in the Lyα forest probe the smallest scales in the matter power spectrum [96].

An illustration of the matter power spectrum of density fluctuations is shown in Figure 17.8 (see [53] and references therein).

17.2.2 Future surveys

An impressive array of ambitious projects have been implemented, or are underway, to provide high resolution measurements of the physical properties of the universe, and hence the search for possible signatures of new cosmology. The Planck satellite [110] will improve measurements on the E and B polarisation modes. Along with Planck satellite there will be several experiments aiming to provide measurements of small-scale fluctuations and polarisations, such as the E and B EXperiment [EBEX; 102], Q-U-I JOint TEnerife CMB experiment [QUIJOTE; 117] and Spider [32]. Besides CMB experiments, the Euclid satellite [41] will explore the expansion history of the universe and the evolution of cosmic structures over a very large fraction of the sky. The Dark Energy Survey [DES; 130] is designed to probe the origin of the accelerating universe and help uncover the nature of dark energy.

Previously we have shown current constraints of the temperature and polarisation CMB spectra. Here, we aim to explore future constraints coming from Planck satellite and CMB-Pol experiments. Performance assumptions for Planck and CMB-Pol are taken from [110] and [9]. In order to do this we need to simulate these experiments by generating mock data of the $\hat{C}_l^{XY}$'s from a χ^2_{2l+1} distribution with variances [111]:

$$(\Delta\hat{C}_l^{XX})^2 = \frac{2}{(2l+1)f_{sky}}\left(C_l^{XX}+N_l^{XX}\right)^2, \tag{17.10}$$

$$(\Delta\hat{C}_l^{TE})^2 = \frac{2}{(2l+1)f_{sky}}\left[\left(C_l^{TE}\right)^2+\left(C_l^{TT}+N_l^{TT}\right)\left(C_l^{EE}+N_l^{EE}\right)\right], \tag{17.11}$$

where $X = T, E$ and B label the temperature and polarisations; f_{sky} is the fraction of the observed sky. The C_l^{XY}'s represent the theoretical spectra and N_l^{XY} the instrumental noise spectra for each experiment. In experiments with multiple frequency channels c, the noise spectrum is approximated [16] by

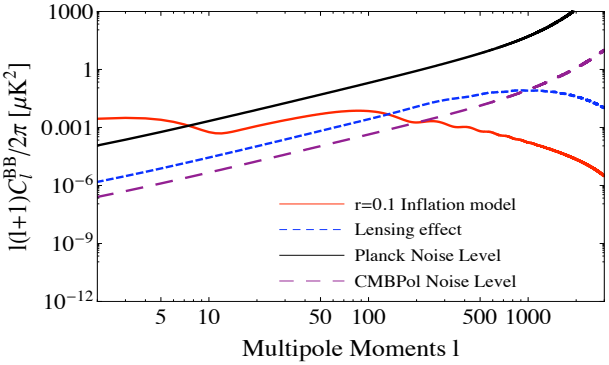

Figure 17.9: Polarisation noise power spectra of forthcoming experiments. Note that these curves include uncertainties associated with the instrumental beam. The red line shows the B-mode power spectrum for the standard inflationary model with $r = 0.1$.

$$N_l^X = \left(\sum_c \frac{1}{N_{l,c}^X} \right)^{-1}, \tag{17.12}$$

where the noise spectrum of an individual frequency channel, assuming a Gaussian beam, is

$$N_{l,c}^X = (\sigma_{\rm pix}\, \theta_{\rm fwhm})^2 \exp\left[l(l+1) \frac{\theta_{\rm fwhm}^2}{8 \ln 2} \right] \delta_{XY}. \tag{17.13}$$

The pixel noise from temperature and polarisation maps are considered as uncorrelated. The noise per pixel $\sigma_{\rm pix}^X$ (and $\sigma_{\rm pix}^P = \sqrt{2}\sigma_{\rm pix}^T$) depends on the instrumental parameters; $\theta_{\rm fwhm}$ is the *full width at half maximum* (FHWM) of the Gaussian beam.

For the Planck experiment, we include three channels with frequencies (100 GHz, 143 GHz, 217 GHz) and noise levels per beam $(\sigma_{\rm pix}^T)^2$= (46.25 μK^2, 36 μK^2, 171 μK^2). The FHWM of the three channels are $\theta_{\rm fwhm}$ =(9.5, 7.1, 5.0) arc-minute. These figures are taken from the values given in [110]. We combine three channels for the CMBPol experiment [9] with frequencies (100 GHz, 150 GHz, 220 GHz), noise levels $(\sigma_{\rm pix}^T)^2$ = (729 nK^2, 676 nK^2, 1600 nK^2) and $\theta_{\rm fwhm}$ = (8, 5, 3.5) arc-minute. Sky coverages of $f_{\rm sky} = 0.65, 0.8$ are respectively assumed and integration time of 14 months. In Figure 17.9, we show the noise levels for these experiments as a function of multipole number l. The blue line corresponds to the B-mode power spectrum using the standard power-law parameterisation with $r = 0.1$. The lensed C_l^B is also shown in the same figure, which can be treated as a part of the total noise power spectrum N_l^B as well as the instrumental noise power spectra [107]. For more information of the noise and beam profile of each frequency channel, refer to [90].

17.3 Bayesian Analysis

Over the last decade or so, the vast amount of information coming from a wide range of sources, including CMB, SNe and LSS, has increased amazingly. We would like to translate this experimental/observational information into constraints of our model(s), summarised by the estimation of the cosmological parameters involved. The concordance ΛCDM model, previously described, depends on a set of cosmological parameters shown in Section 17.1. A primary goal concerning observational cosmology is to determine best-fit parameter values for a given model, as well as to decide which model is in best-agreement with observational data. To do this we focus on *Bayesian inference*. Some excellent reviews of Bayesian statistics applied to cosmology are given by Heavens [51], Liddle [79], Liddle et al. [83], Verde [132, 133], von Toussaint [135**?**], and the textbook for data analysis Sivia and Skilling [123].

17.3.1 Parameter estimation

A Bayesian analysis provides a consistent approach to estimating the values of the parameters $\mathbf{\Theta}$ within a model M, which best describe the data $\mathbf{D}$. The method is based on the assignment of probabilities to the quantities of interest, and then the manipulation of these probabilities given a series of rules, in which Bayes' theorem plays the main role [79]. Bayes' theorem states that

$$P(\mathbf{\Theta}|\mathbf{D}, M) = \frac{P(\mathbf{D}|\mathbf{\Theta}, M)\ P(\mathbf{\Theta}|M)}{P(\mathbf{D}|M)}. \tag{17.14}$$

In this expression, the *prior* probability $\mathrm{P}(\mathbf{\Theta}|\mathrm{M}) \equiv \pi$ represents what we thought the probability of $\mathbf{\Theta}$ was before considering the data. This probability is modified through the *likelihood* $\mathrm{P}(\mathbf{D}|\mathbf{\Theta},\mathrm{M}) \equiv \mathcal{L}$. The posterior probability $\mathrm{P}(\mathbf{\Theta}|\mathbf{D},\mathrm{M})$ represents the state of knowledge once we have taken the experimental data $\mathbf{D}$ into account. The normalisation constant in the denominator is the marginal likelihood or *Bayesian evidence* $\mathrm{P}(\mathbf{D}|\mathrm{M}) \equiv \mathcal{Z}$, as is normally called in cosmology. Since this quantity is independent of the parameters $\mathbf{\Theta}$, it is commonly ignored in parameter estimation but it takes the central role for model comparison.

The central step for parameter estimation is to construct the likelihood function $\mathcal{L}$ for the measurements, and then the exploration of the region around its maximum value $\mathcal{L}_{\max}$. A simple chi-squared function is often used $\chi^2 = -2\ln\mathcal{L}$. when the distributions are Gaussian. However, some current problems in cosmology present obstacles for carrying out this procedure

straightforwardly (some of them discussed by Liddle [79]). Fortunately, models of our interest can be easily tackled by numerical techniques developed on statistical fields, in particular the methods known as *Markov Chain Monte Carlo (MCMC)*. There have been developed different codes employing MCMC techniques to carry out the exploration of the cosmological parameter-space, for instance CosmoMC [75], CosmoHammer [3], CMBEASY [35]. Although some of them use a simple Metropolis-Hasting algorithm by default, nowadays improved algorithms have been adapted to explore complex posterior probability distributions.

Discriminating among models and determining which of them is the most plausible given some data is a task for model comparison techniques, whose application is discussed in the next section.

17.3.2 Model selection

There is nowadays a rich diversity of models trying to describe the vast amount of cosmological information. Some of them might involve complex interactions or introduce a high number of parameters, but provide just as good fit as the standard ΛCDM model (see Table 17.1). So, how can we perform an objective comparison between them and choose the appropriate model?. The solution was proposed by William of Occam: the simplest model which covers all the facts ought to be preferred. That is, a complex model that explains the data slightly better than a simple one should be penalised by the inclusion of extra parameters, because this additional information reflects a lack of predictability in the model. Moreover, if a model is too simple, it might not fit certain data equally well, then it can be discarded [83**?**].

Many attempts have been performed to translate Occam's razor into a mathematical language for model selection. Two major types have been used so far: Bayesian evidence and *Information criteria*; where the latter one can be used as an useful approximation when the Bayesian evidence cannot be computed.

Information criteria is based on some simplifying approximations to the full Bayesian evidence. The method considers the best-fit values and attaches a penalty term for more complex models:

- The Akaike Information criterion (AIC), introduced by Hirotugu Akaike has the form

$$AIC \equiv -2 \ln \mathcal{L}_{max} + 2k, \tag{17.15}$$

where the penalty term is induced by the number of free parameters k to be estimated.

- The Bayesian Information Criterion (BIC), was derived by Gideon E. Schwarz and it is given by

$$BIC \equiv -2 \ln \mathcal{L}_{max} + k \ln N, \tag{17.16}$$

where N is the number of datapoints. It follows from a Gaussian approximation of the Bayesian evidence for a large number of samples.

- The Deviance Information Criterion (DIC), was proposed by David J Spiegelhalter. It is a generalization of the AIC and BIC written as

$$DIC \equiv -2\widehat{D_{KL}} + 2\mathcal{C}_b, \tag{17.17}$$

where the former term is the estimated KL divergence and the latter one is the effective number of parameters.

An extended discussion of the different information criteria can be found in [78, 83**?**].

Bayesian evidence. This is the primordial tool for the model selection we focus on. It applies the same type of analysis as in parameter estimation, but now at the level of models rather than parameters. The Bayesian evidence is the key quantity to bear in mid as it balances the complexity of cosmological models and then, naturally, incorporates Occam's razor. It has been applied to a wide diversity of cosmological contexts, see for example [54, 61**?**].

Let us consider several models M, each of them with prior probability $P(M)$. Bayes' theorem for model selection is

$$P(M|\mathbf{D}) = \frac{P(\mathbf{D}|M)P(M)}{P(\mathbf{D})}. \tag{17.18}$$

The left-hand side denotes the probability of the model given the data, which is exactly what we are looking for in model selection. We need, therefore, to obtain an expression that allows us to compute the Bayesian evidence in terms of the information we already have. As we previously mentioned, the Bayesian evidence is simply the normalisation constant of the posterior distribution expressed by

$$\mathcal{Z} = \int \mathcal{L}(D|\Theta)\pi(\Theta)d^N\Theta. \tag{17.19}$$

Table 17.2: Jeffreys guideline scale for evaluating the strength of evidence when two models are compared.

$\lvert\mathcal{B}_{i,j}\rvert$	Odds	Probability	Strength
< 1.0	$< 3:1$	< 0.750	Inconclusive
1.0-2.5	$\sim 12:1$	0.923	Significant
2.5-5.0	$\sim 150:1$	0.993	Strong
> 5.0	$> 150:1$	> 0.993	Decisive

where N is the dimensionality of the parameter space. More explicitly, it is the average likelihood weighted by the prior for a specific model choice:

$$Evidence = \int (Likelihood \times Prior) d^N\Theta. \tag{17.20}$$

A model containing wider regions of prior parameter-space along with higher likelihoods will have a high evidence and vice versa. Therefore, the Bayesian evidence does provide a natural mechanism to balance the complexity of cosmological models and then, elegantly incorporates Occam's razor.

When comparing two models, M_i and M_j, the important quantity to bear in mind is the ratio of the posterior probabilities, or *posterior odds*, given by

$$\frac{P(M_i|\mathbf{D})}{P(M_j|\mathbf{D})} = \frac{\mathcal{Z}_i}{\mathcal{Z}_j}\frac{P(M_i)}{P(M_j)}, \tag{17.21}$$

where $P(M_i)/P(M_j)$ is the prior probability ratio for the two models, usually set to unity. The ratio of two evidences $\mathcal{Z}_i/\mathcal{Z}_j$ (or equivalently the difference in log evidences $\ln \mathcal{Z}_i - \ln \mathcal{Z}_j$) is often termed the *Bayes factor* $\mathcal{B}_{i,j}$:

$$\mathcal{B}_{i,j} = \ln \frac{\mathcal{Z}_i}{\mathcal{Z}_j}. \tag{17.22}$$

Then, the quantity $\mathcal{B}_{i,j}$ measures the relative probability of how well model i may fit the data when is compared to model j. Jeffreys [60] provided a suitable guideline scale on which we are able to make qualitative conclusions (see Table 17.2). In this work, we refer to positive (negative) values of $\mathcal{B}_{i,j}$ when the i model being favoured (disfavoured) over model j.

The calculation of the integral in Equation (17.19) is a very computationally demanding process, since it requires a multidimensional integration over the likelihood and prior. For many years much progress has been made in the construction of efficient algorithms to allow faster and more accurate computation of the Bayesian evidence. Until recently, algorithms such as simulating annealing or thermodynamic integration [18], required around 10^7 likelihood evaluations making the procedure hardly treatable. A powerful algorithm was recently invented by Skilling [124], known as *nested sampling algorithm*, which has been proven to be ten times more efficient than previous methods. The first computationally-efficient code to compute the Bayesian evidence in cosmology, named CosmoNest, was implemented by Mukherjee et al. [100]. In this work we incorporate into the CosmoMC software [75] a substantially improved and fully-parallelized version of the *nested sampling* algorithm, called the MultiNest algorithm, initially proposed by Feroz & Hobson [43, 44]. The MultiNest algorithm increases the sampling efficiency for calculating the evidence and allows one to obtain posterior samples even from distributions with multiple modes and/or pronounced degeneracies between parameters. There is also CosmoPMC which is based on an adaptative importance sampling method called Population Monte Carlo [64]. For more complex models with high number of parameters, there also exist improved codes to increase the speed of the whole process by employing, for instance, neuronal networks: CosmoNet [7]. BAMBI is an algorithm that combines the benefits of both the nested sampling and artificial neural networks [46].

17.3.3 Dataset consistency

Combining multiple datasets to obtain tight constraints on the cosmological parameters has been a very common practice. Marshall et al. [94] established a test to quantify the consistency of different cosmological datasets analysed under the same model (see also Hobson et al. [55]). The Bayesian consistency analysis relies on partitioning the full combined dataset D into its constituent parts D_i ($i = 1, \ldots, n$), namely CMB, SNe, LSS data, so on, and analyses the model with each dataset independently. The evidence ratio is defined as

$$R = \frac{\Pr(D|H)}{\prod_{i=1}^{n} \Pr(D_i|H)}, \tag{17.23}$$

where the hypothesis H denotes the model under study. This ratio compares the probability that all the datasets were generated from a cosmological model characterised by the same parameter values, with the probability that each dataset was generated from an independent

Parameters	Description	Prior range
Background		
$\Omega_{\rm b,0}h^2$	Physical baryon density	$[0.01, 0.03]$
$\Omega_{\rm dm,0}h^2$	Physical cold dark matter density	$[0.01, 0.3]$
θ	Ratio of the sound horizon to the angular diameter distance	$[1, 1.1]$
τ	Reionization optical depth	$[0.01, 0.3]$
Inflationary		
$\log[10^{10}A_{\rm s}]$	Curvature perturbation amplitude	$[2.5, 4]$
$n_{\rm s}$	Spectral scalar index	$[0.5, 1.2]$
Secondary		
$A_{\rm SZ}$	Sunyaev-Zel'dovich amplitude	$[0, 3]$
$A_{\rm c}$	Total Poisson power	$[0, 20]$
$A_{\rm p}$	Amplitude of the clustered power	$[0, 30]$

Table 17.3: Parameter description along with the flat-uniform priors assumed on the standard ΛCDM.

set of cosmological parameters. Thus, one expects $R > 1$ if the datasets are all consistent, and $R < 1$ otherwise. The Bayes factor for data sets is given by $\mathcal{B}_R = \ln R$.

17.4 The concordance ΛCDM model

In this section, we make use of the theoretical (Section 17.1), Observational (Section 17.2.1) and Statistical (Section 17.3) tools to examine the standard cosmological model. The minimal form of the standard cosmological model, in agreement with several independent observations, considers a FRW background, purely Gaussian adiabatic scalar perturbations and neglect tensor contributions. It also assumes a flat universe fill up with baryons, cold dark matter and a dark energy component in the form of a cosmological constant Λ. The key aspects that describe the standard model here, and throughout the work, are specified by:

- Theory/Parameters

Base parameters: the physical baryon and dark matter densities $\Omega_{\rm b,0}h^2$ and $\Omega_{\rm dm,0}h^2$, $100\times$ the ratio of the sound horizon to angular diameter distance at last scattering surface θ, the optical depth at reionisation τ, the amplitude of the primordial spectrum $A_{\rm s}$ and the spectral index $n_{\rm s}$ defined at a pivot scale $k_0 = 0.002$ Mpc^{-1}. Aside from the base parameters, recent observations include additional secondary parameters: the Sunyaev-Zel'dovich (SZ) amplitude

A_{SZ}, the total Poisson power A_p at $l = 3000$ and the amplitude of the clustered power A_c. The parameters, along with the flat priors, are shown in Table 17.3.

-Observations/Experiments:

To compute posterior probabilities for each model in the light of temperature and polarisation measurements, we use WMAP 7-year data release [67] and the ACT observations [37]. In addition to CMB data, we include distance measurements of 557 Supernovae Type Ia from the Union 2 compilation [69]. We also incorporate large-scale structure data from the SDSS-DR7 [112] power spectrum. We consider baryon density information from BBN [20] and impose a Gaussian prior on H_0 using measurements from the HST [114]. This compromises our dataset I. In addition to dataset I, we include recent results from QUaD [19] and BICEP [27] experiments. Together these observations make up our dataset II.

-Analysis/Codes:

The computation of the CMB spectrum is perform by a modified version of the CAMB code [76] to include any additional components and calculate the predicted power spectra of CMB anisotropies and matter perturbations. The exploration of the parameter-space is carried out by using the CosmoMC software [75] with the addition of the Multinest algorithm [43]. The latter is included to the perform the calculation of the Bayesian evidence.

We have analysed a standard flat ΛCDM model and, for pedagogical purposes, also the same model but with the addition of curvature, with priors $\Omega_{k,0} = [-0.1, 0.1]$. The top panel of Figure 17.10 shows 1D marginalised posterior distributions of the base and some relevant derived parameters, for both models: flat and non-flat ΛCDM. At the top of the same figure, we have included the Bayes factor comparing both of them. For the non-flat model, we notice that the marginalised posteriors of $\Omega_{\mathrm{dm},0}h^2$, H_0 and the Age of the universe have broadened due to correlations created by the inclusion of $\Omega_{k,0}$. These correlations can be observed in the 2D marginalised posterior distribution shown in the bottom panel of Figure 17.10. The constraints on the cosmological parameters are displayed in Table 17.4 along with 1σ confidence levels. In this Table, both models assume the presence of ΛCDM with a scalar power spectrum described by a power-law and no tensor contributions. The first set of rows show the base parameters whereas the second set some derived parameters. Current cosmological observations provide, in general terms, a strong support for a nearly-flat accelerating universe dominated by 72% of

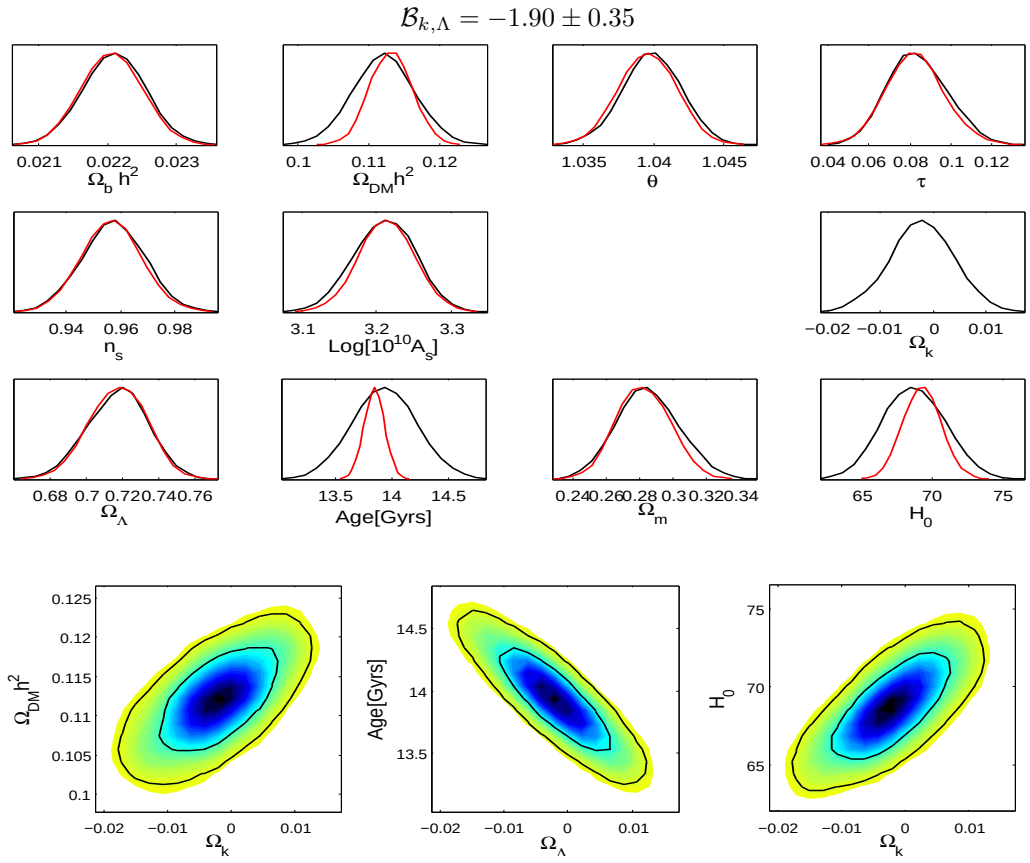

Figure 17.10: Top: 1D marginalised posterior distributions on the standard ΛCDM parameters using current cosmological observations. Bottom: 2D marginalised posterior distributions of non-flat ΛCDM parameters; constraints are plotted with 1σ and 2σ confidence contours.

dark energy in the form of a cosmological constant, 24% of non-baryonic dark matter and 4% of baryon contributions; the primordial spectrum is red ($n_s < 1$) with the Harrison-Zel'dovich excluded with high confidence level. On the other hand, the Bayes factor between these two models, $\mathcal{B}_{\Lambda,\Lambda+\Omega_k} = +1.90 \pm 0.35$, indicates a significant preference for a flat universe, according to the Jeffreys guideline. The last row of Table 17.4 shows that both models are consistent with the full combined dataset I.

Throughout the rest of the chapters we incorporate features beyond the standard ΛCDM model in the search of a better description of cosmological observations. In Chapter **??**, with the use of present data, we determine the structure of the primordial scalar spectrum by implementing an optimal model-free reconstruction. Our aim is to consider models that slightly

Table 17.4: The constraints on the cosmological parameters using our dataset II. We report the mean of the marginalised posterior distribution and 1σ confidence levels. The Bayes factor for models $\mathcal{B}_{\Lambda,\Lambda+\Omega_k}$, and for datasets $\mathcal{B}_R$ are also included.

Description		Flat ΛCDM	Non-flat ΛCDM
Base parameters	$\Omega_{\rm b,0}h^2$	0.02206 ± 0.00042	0.0221 ± 0.00043
	$\Omega_{\rm dm,0}h^2$	0.1130 ± 0.0028	0.112 ± 0.0041
	θ	1.039 ± 0.0019	1.039 ± 0.0020
	τ	0.082 ± 0.013	0.083 ± 0.014
	$n_{\rm s}$	0.956 ± 0.010	0.957 ± 0.011
	$\log[10^{10}A_{\rm s}]$	3.21 ± 0.035	3.21 ± 0.039
	$\Omega_{k,0}$	-	-0.0022 ± 0.0058
Derived parameters	$\Omega_{\rm m,0}$	0.282 ± 0.015	0.285 ± 0.018
	$\Omega_{\Lambda,0}$	0.717 ± 0.015	0.717 ± 0.016
	H_0	69.2 ± 1.27	68.7 ± 2.13
	Age(Gyrs)	13.84 ± 0.086	13.93 ± 0.27
Bayes factor	$-2\ln\mathcal{L}_{\rm max}$	8240.46	8240.80
	$\mathcal{B}_{\Lambda,\Lambda+\Omega_k}$	$+1.6 \pm 0.4$	-
Dataset consistency	$\mathcal{B}_R$	$+5.06 \pm 0.4$	$+5.07 \pm 0.4$

deviate from the simple power-law form. Then, in Chapter **??**, we incorporate tensor contributions to the analysis and present current and future constraints on the scalar spectrum. Chapter **??** explores the possibility of a dynamical behaviour of dark energy. Here, the dark energy equation-of-state $w_{\rm de}(z)$ is modelled as a linear interpolation between a set of 'nodes' with varying amplitudes and redshifts, similarly to the approach used in Chapter **??**. In the search of mechanisms or candidates to explain the mild time-dependence of $w_{\rm de}(z)$, in Chapter **??** we remain focussed on the ΛCDM model but now include a second dark energy component Ω_X with equation-of-state w_X. Finally, in Chapter **??** the Einstein-Hilbert Lagrangian is considered as a limit case of a more general form of it, namely Modified Gravity. We explore these models as an alternative to the dark energy component. The summary of the work done throughout this dissertation is sketched in Figure 17.11.

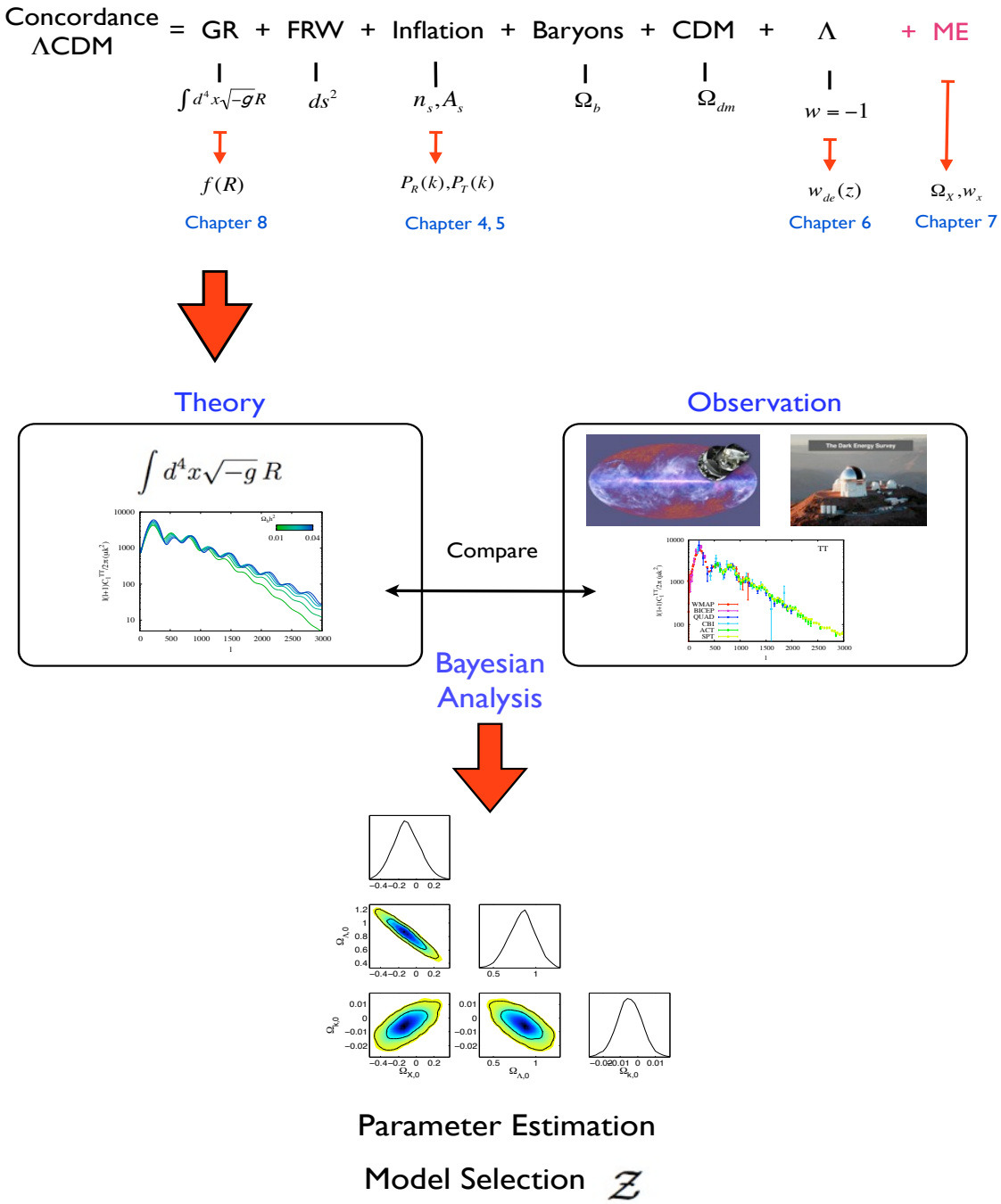

Figure 17.11: Summary of the work performed throughout this dissertation. The top panel of the Figure displays the features beyond the concordance ΛCDM model considered through the following chapters.

Bibliography

[1] Nabila Aghanim, Subhabrata Majumdar, and Joseph Silk. Secondary anisotropies of the CMB. Reports on Progress in Physics, 71(6):066902, 2008. URL http://stacks.iop.org/0034-4885/71/i=6/a=066902. 221

[2] Christopher P. Ahn et al. The Ninth Data Release of the Sloan Digital Sky Survey: First Spectroscopic Data from the SDSS-III Baryon Oscillation Spectroscopic Survey. Astrophys.J.Suppl., 203:21, 2012. doi: 10.1088/0067-0049/203/2/21. 272

[3] Joel Akeret, Sebastian Seehars, Adam Amara, Alexandre Refregier, and Andre Csillaghy. CosmoHammer: Cosmological parameter estimation with the MCMC Hammer. 2012. [arXiv:1212.1721]. 275

[4] R. Amanullah and *et. al.* Spectra and Hubble Space Telescope Light Curves of Six Type Ia Supernovae at $0.511 < z < 1.12$ and the Union2 Compilation. The Astrophysical Journal, 716(1):712, 2010. URL http://stacks.iop.org/0004-637X/716/i=1/a=712. 271

[5] Ambrosio and *et. al.* Final results of magnetic monopole searches with the macro experiment. The European Physical Journal C - Particles and Fields, 25(4):511–522, 2002. URL http://dx.doi.org/10.1140/epjc/s2002-01046-9. 96

[6] Scientific American. Could silicon be the basis for alien life forms, just as carbon is on earth? https://www.scientificamerican.com/article/could-silicon-be-the-basi/, 1998. 19, 48, 109

[7] T. Auld, M. Bridges, and M. P. Hobson. Cosmonet: fast cosmological parameter estimation in non-flat models using neural networks. Monthly Notices of the Royal Astronomical Society, 387(4):1575–1582, 2008. doi: 10.1111/j.1365-2966.2008.13279.x. URL http://mnras.oxfordjournals.org/content/387/4/1575.abstract. 278

[8] Alejandro Aviles, Christine Gruber, Orlando Luongo, and Hernando Quevedo. Cosmography and constraints on the equation of state of the Universe in various parametrizations. Phys. Rev. D, 86:123516, 2012. doi: 10.1103/PhysRevD.86.123516. 60

[9] B-Pol Collaboration.*http://www.b-pol.org/documents.php*, 2010. 272, 273

[10] James M. Bardeen. Gauge-invariant cosmological perturbations. Phys. Rev. D, 22:1882–1905, Oct 1980. doi: 10.1103/PhysRevD.22.1882. URL http://link.aps.org/doi/10.1103/PhysRevD.22.1882. 141

[11] J.D. Barrow and F.J. Tipler. The Anthropic Cosmological Principle. ISSR library. Oxford University Press, 1988. ISBN 9780192821478. URL https://books.google.com.mx/books?id=uSykSbXklWEC. 19

[12] Richard A. Battye, Martin Bucher, and David Spergel. Domain Wall Dominated Universes. [arXiv:9908047]. URL http://arxiv.org/abs/astro-ph/9908047v2. 76

[13] Daniel Baumann. Cosmological Inflation: Theory and Observations. Advanced Science Letters, 2(2):105–120, 2009. doi: doi:10.1166/asl.2009.1019. URL http://www.ingentaconnect.com/content/asp/asl/2009/00000002/00000002/art00002. 93, 103

[14] Gianfranco Bertone, Dan Hooper, and Joseph Silk. Particle dark matter: evidence, candidates and constraints. Physics Reports, 405(5–6):279 – 390, 2005. ISSN 0370-1573. doi: 10.1016/j.physrep.2004.08.031. URL http://www.sciencedirect.com/science/article/pii/S0370157304003515. 75

[15] Krzysztof Bolejko, Marie-Noëlle Célérier, and Andrzej Krasiński. Inhomogeneous cosmological models: exact solutions and their applications. Classical and Quantum Gravity, 28(16):164002, aug 2011. doi: 10.1088/0264-9381/28/16/164002. URL https://dx.doi.org/10.1088/0264-9381/28/16/164002. 18, 48

[16] M. Bowden and et. al. Scientific optimization of a ground-based CMB polarization experiment. Monthly Notices of the Royal Astronomical Society, 349(1):321–335, 2004. ISSN

1365-2966. doi: 10.1111/j.1365-2966.2004.07506.x. URL http://dx.doi.org/10.1111/j.1365-2966.2004.07506.x. 272

[17] D Branch and G A Tammann. Type Ia Supernovae as Standard Candles. Annual Review of Astronomy and Astrophysics, 30(1):359–389, 1992. doi: 10.1146/annurev.aa.30.090192.002043. URL http://www.annualreviews.org/doi/abs/10.1146/annurev.aa.30.090192.002043. 270

[18] M. Bridges, A. N. Lasenby, and M. P. Hobson. A Bayesian analysis of the primordial power spectrum. Monthly Notices of the Royal Astronomical Society, 369(3):1123–1130, 2006. ISSN 1365-2966. doi: 10.1111/j.1365-2966.2006.10351.x. URL http://dx.doi.org/10.1111/j.1365-2966.2006.10351.x. 278

[19] M. L. Brown and et. al. Improved Measurements of the Temperature and Polarization of the Cosmic Microwave Background from QUaD. The Astrophysical Journal, 705(1):978, 2009. URL http://stacks.iop.org/0004-637X/705/i=1/a=978. 268, 280

[20] Scott Burles, Kenneth M. Nollett, and Michael S. Turner. Big Bang Nucleosynthesis Predictions for Precision Cosmology. The Astrophysical Journal Letters, 552(1):L1, 2001. URL http://stacks.iop.org/1538-4357/552/i=1/a=L1. 280

[21] Sean M. Carroll. The Cosmological Constant. Living Reviews in Relativity, 4(1), 2001. URL http://www.livingreviews.org/lrr-2001-1. 69, 75

[22] Brandon Carter. Large Number Coincidences and the Anthropic Principle in Cosmology, pages 291–298. Springer Netherlands, Dordrecht, 1974. ISBN 978-94-010-2220-0. doi: 10.1007/978-94-010-2220-0_25. URL https://doi.org/10.1007/978-94-010-2220-0_25. 19

[23] Marius Cautun, Alis J Deason, Carlos S Frenk, and Stuart McAlpine. The aftermath of the Great Collision between our Galaxy and the Large Magellanic Cloud. Monthly Notices of the Royal Astronomical Society, 483(2):2185–2196, 11 2018. ISSN 0035-8711. doi: 10.1093/mnras/sty3084. URL https://doi.org/10.1093/mnras/sty3084. 11

[24] Anthony Challinor. Part III- Large Scale Strucutre Formation. *http://nefertiti.hpc.phys.ucl.ac.uk/cosmology/cosmology.html*, 2008. 15, 141, 213

[25] Anthony Challinor and Hiranya Peiris. Lecture notes on the physics of cosmic microwave background anisotropies. AIP Conference Proceedings, 1132(1):86–140, 2009. doi: 10.1063/1.3151849. URL http://link.aip.org/link/?APC/1132/86/1. 218, 220

[26] M. Chevallier and D. Polarski. Accelerating Universes with Scaling Dark Matter. International Journal of Modern Physics D, 10(2):213–223, 2001. URL http://arxiv.org/abs/gr-qc/0009008v2. 91

[27] H. C. Chiang and et. al. Measurement of Cosmic Microwave Background Polarization Power Spectra from Two Years of BICEP Data. The Astrophysical Journal, 711(2):1123, 2010. URL http://stacks.iop.org/0004-637X/711/i=2/a=1123. 268, 280

[28] Shaun Cole and *et. al.* The 2dF Galaxy Redshift Survey: power-spectrum analysis of the final data set and cosmological implications. Monthly Notices of the Royal Astronomical Society, 362(2):505–534, 2005. ISSN 1365-2966. doi: 10.1111/j.1365-2966.2005.09318.x. URL http://dx.doi.org/10.1111/j.1365-2966.2005.09318.x. 16

[29] P. Coles and F. Lucchin. Cosmology. WILEY, 1995. 96

[30] Marina Cortês, Andrew R. Liddle, and David Parkinson. On the prior dependence of constraints on the tensor-to-scalar ratio. Journal of Cosmology and Astroparticle Physics, 2011(09):027, 2011. URL http://stacks.iop.org/1475-7516/2011/i=09/a=027. 265

[31] Ron Cowen. Andromeda on collision course with the milky way. Nature, 2012. doi: 10.1038/nature.2012.10765. URL https://doi.org/10.1038/nature.2012.10765. 11

[32] B. P. Crill and *et. al.* SPIDER: a balloon-borne large-scale CMB polarimeter. Proc. SPIE 7010, Space Telescopes and Instrumentation 2008, pages 70102P–70102P–12, 2008. doi: 10.1117/12.787446. URL +http://dx.doi.org/10.1117/12.787446. 272

[33] Scott Dodelson. Modern Cosmology. Academic Press, 2003. 15, 85, 141

[34] A.D. Dolgov. Neutrinos in cosmology. Physics Reports, 370:333 – 535, 2002. ISSN 0370-1573. doi: 10.1016/S0370-1573(02)00139-4. URL http://www.sciencedirect.com/science/article/pii/S0370157302001394. 74

[35] Michael Doran. CMBEASY: an object oriented code for the cosmic microwave background. Journal of Cosmology and Astroparticle Physics, 2005(10):011, 2005. URL http://stacks.iop.org/1475-7516/2005/i=10/a=011. 212, 218, 275

[36] Michael Doran. The Theory of the Cosmic Microwave Background. *http://www.thphys.uni-heidelberg.de/ cosmo/view/main/cmbdoran*, 2010. 141, 210, 211, 213, 217

[37] J. Dunkley and *et. al.* The Atacama Cosmology Telescope: Cosmological Parameters from the 2008 Power Spectra. [arXiv:1009.0866], 2010. URL http://arxiv.org/abs/1009.0866v1. 268, 280

[38] Ruth Durrer. The theory of CMB anisotropies. [arXiv:0109522], 2001. 141

[39] Øystein Elgarøy and Ofer Lahav. Neutrino masses from cosmological probes. New Journal of Physics, 7(1):61, 2005. URL http://stacks.iop.org/1367-2630/7/i=1/a=061. 74

[40] Kari Enqvist. Lemaitre–tolman–bondi model and accelerating expansion. General Relativity and Gravitation, 40(2):451–466, 2008. doi: 10.1007/s10714-007-0553-9. URL https://doi.org/10.1007/s10714-007-0553-9. 18

[41] Euclid Missin Consortium.*http://www.euclid-ec.org/*, 2012. 272

[42] Antonio De Felice and Shinji Tsujikawa. f(R) Theories. Living Reviews in Relativity, 13 (3), 2010. URL http://www.livingreviews.org/lrr-2010-3. 56, 91

[43] F. Feroz and M. P. Hobson. Multimodal nested sampling: an efficient and robust alternative to Markov Chain Monte Carlo methods for astronomical data analyses. Monthly Notices of the Royal Astronomical Society, 384(2):449–463, 2008. ISSN 1365-2966. doi: 10.1111/j.1365-2966.2007.12353.x. URL http://dx.doi.org/10.1111/j.1365-2966.2007.12353.x. 278, 280

[44] F. Feroz, M. P. Hobson, and M. Bridges. MultiNest: an efficient and robust Bayesian inference tool for cosmology and particle physics. Monthly Notices of the Royal Astronomical Society, 398(4):1601–1614, 2009. ISSN 1365-2966. doi: 10.1111/j.1365-2966.2009.14548.x. URL http://dx.doi.org/10.1111/j.1365-2966.2009.14548.x. 278

[45] Joshua A. Frieman and *et. al.* The Sloan Digital Sky Survey-II Supernova Survey: Technical Summary. The Astronomical Journal, 135(1):338, 2008. URL http://stacks.iop.org/1538-3881/135/i=1/a=338. 270

[46] Philip Graff, Farhan Feroz, Michael P. Hobson, and Anthony Lasenby. BAMBI: blind accelerated multimodal Bayesian inference. Monthly Notices of the Royal Astronomical Society, 421(1):169–180, 2012. doi: 10.1111/j.1365-2966.2011.20288.x. URL http://mnras.oxfordjournals.org/content/421/1/169.abstract. 278

[47] A.H. Guth. The Inflationary Universe. Ed. Vintage, 1997. 96

[48] Alan H. Guth. Inflationary universe: A possible solution to the horizon and flatness problems. Phys. Rev. D, 23:347–356, Jan 1981. doi: 10.1103/PhysRevD.23.347. URL http://link.aps.org/doi/10.1103/PhysRevD.23.347. 93

[49] Steen Hannestad. Primordial Neutrinos. Annual Review of Nuclear and Particle Science, 56(1):137–161, 2006. doi: 10.1146/annurev.nucl.56.080805.140548. URL http://www.annualreviews.org/doi/abs/10.1146/annurev.nucl.56.080805.140548. 74

[50] Alex Harvey, Engelbert L. Schucking, and Eugene J. Surowitz. Redshifts and killing vectors. Am. J. Phys., 74:1017–1024, 2006. doi: 10.1119/1.2338544. 58

[51] Alan Heavens. Statistical techniques in cosmology. [arXiv:0906.0664], 2010. 274

[52] G. Hinshaw and *et. al.* Nine-Year Wilkinson Microwave Anisotropy Probe (WMAP) Observations: Cosmological Parameter Results. [arXiv:1212.5226], 2013. 268

[53] R. Hlozek and *et. al.* The Atacama Cosmology Telescope: a measurement of the primordial power spectrum. [arXiv:1105.4887], 2011. URL http://arxiv.org/abs/1105.4887v1. 271, 272

[54] M. P. Hobson and C. McLachlan. A Bayesian approach to discrete object detection in astronomical data sets. Monthly Notices of the Royal Astronomical Society, 338(3): 765–784, 2003. ISSN 1365-2966. doi: 10.1046/j.1365-8711.2003.06094.x. URL http://dx.doi.org/10.1046/j.1365-8711.2003.06094.x. 276

[55] M. P. Hobson, S. L. Bridle, and O Lahav. Combining cosmological data sets: hyperparameters and bayesian evidence. Monthly Notices of the Royal Astronomical Society, 335(2):377–388, 2002. ISSN 1365-2966. doi: 10.1046/j.1365-8711.2002.05614.x. URL http://dx.doi.org/10.1046/j.1365-8711.2002.05614.x. 278

[56] M.P. Hobson, G. P. Efstathiou, and A. N. Lasenby. General Relativity: An Introduction for Physicists. Cambridge University Press, 2006. 15, 86

[57] Wayne Hu and Scott Dodelson. COSMIC MICROWAVE BACKGROUND ANISOTROPIES. Annual Review of Astronomy and Astrophysics, 40(1):171–216, 2002. doi: 10.1146/annurev.astro.40.060401.093926. URL http://www.annualreviews.org/doi/abs/10.1146/annurev.astro.40.060401.093926. 141

[58] Wayne Hu, Uro š Seljak, Martin White, and Matias Zaldarriaga. Complete treatment of CMB anisotropies in a FRW universe. Phys. Rev. D, 57:3290–3301, Mar 1998. doi: 10.1103/PhysRevD.57.3290. URL http://link.aps.org/doi/10.1103/PhysRevD.57.3290. 211

[59] Edwin Hubble. A relation between distance and radial velocity among extra-galactic nebulae. Proceedings of the National Academy of Sciences, 15(3):168–173, 1929. doi: 10.1073/pnas.15.3.168. URL http://www.pnas.org/content/15/3/168.short. 42, 89

[60] Harold Jeffreys. Theory of Probability. Oxford University Press, 1998. 277

[61] Moncy V. John and J. V. Narlikar. Comparison of cosmological models using Bayesian theory. Phys. Rev. D, 65:043506, Jan 2002. doi: 10.1103/PhysRevD.65.043506. URL http://link.aps.org/doi/10.1103/PhysRevD.65.043506. 276

[62] W. C. Jones and *et. al.* A Measurement of the Angular Power Spectrum of the CMB Temperature Anisotropy from the 2003 Flight of BOOMERANG. The Astrophysical Journal, 647(2):823, 2006. URL http://stacks.iop.org/0004-637X/647/i=2/a=823. 268

[63] R. Keisler and *et. al.* A Measurement of the Damping Tail of the Cosmic Microwave Background Power Spectrum with the South Pole Telescope. [arXiv:1105.3182], 2011. URL http://arxiv.org/abs/1105.3182v2. 268

[64] Martin Kilbinger, Karim Benabed, Olivier Cappe, Jean-Francois Cardoso, Gersende Fort, et al. CosmoPMC: Cosmology Population Monte Carlo. arXiv:1101.0950, 2011. 278

[65] Christian Knobel. An introduction into the theory of cosmological structure formation. 2012. [arXiv:1208.5931]. 141

[66] Hideo Kodama and Misao Sasaki. Cosmological Perturbation Theory. Progress of Theoretical Physics Supplement, 78:1–166, 1984. doi: 10.1143/PTPS.78.1. URL http://ptp.ipap.jp/link?PTPS/78/1/. 141

[67] E. Komatsu and *et. al.* Seven-year Wilkinson Microwave Anisotropy Probe (WMAP) Observations: Cosmological Interpretation. The Astrophysical Journal Supplement Series, 192(2):18, 2011. URL http://stacks.iop.org/0067-0049/192/i=2/a=18. 16, 94, 268, 280

[68] Arthur Kosowsky, Milos Milosavljevic, and Raul Jimenez. Efficient cosmological parameter estimation from microwave background anisotropies. Phys. Rev. D, 66:063007, Sep 2002. doi: 10.1103/PhysRevD.66.063007. URL http://link.aps.org/doi/10.1103/PhysRevD.66.063007. 264

[69] M. Kowalski and *et. al.* Improved Cosmological Constraints from New, Old, and Combined Supernova Data Sets. The Astrophysical Journal, 686(2):749, 2008. URL http://stacks.iop.org/0004-637X/686/i=2/a=749. 271, 280

[70] Hannu Kurki-Suonio. Cosmological Perturbation Theory. *http://www.helsinki.fi/∼hkurkisu/*, 2008. 141

[71] Ofer Lahav and Andrew R Liddle. The Cosmological Parameters 2010. 2010. [arXiv:1207.4898]. 261

[72] D. Larson and *et. al.* Seven-year Wilkinson Microwave Anisotropy Probe (WMAP) Observations: Power Spectra and WMAP-derived Parameters. The Astrophysical Journal Supplement Series, 192(2):16, 2011. URL http://stacks.iop.org/0067-0049/192/i=2/a=16. 94, 95, 268

[73] Julien Lesgourgues. The Cosmic Linear Anisotropy Solving System (CLASS) I: Overview. arXiv:1104.2932, 2011. 212, 218

[74] Julien Lesgourgues and Sergio Pastor. Massive neutrinos and cosmology. Physics Reports, 429(6):307 – 379, 2006. ISSN 0370-1573. doi: 10.1016/j.physrep.2006.04.001. URL http://www.sciencedirect.com/science/article/pii/S0370157306001359. 74

[75] Antony Lewis and Sarah Bridle. Cosmological parameters from CMB and other data: A Monte Carlo approach. Physical Review D, 66(10), 2002. doi: 10.1103/PhysRevD.66.103511. 275, 278, 280

[76] Antony Lewis, Anthony Challinor, and Anthony Lasenby. Efficient Computation of Cosmic Microwave Background Anisotropies in Closed Friedmann-Robertson-Walker Models. The Astrophysical Journal, 538(2):473, 2000. URL http://stacks.iop.org/0004-637X/538/i=2/a=473. 212, 218, 280

[77] Andrew R. Liddle. An Introduction to cosmological inflation. pages 260–295, 1999. astro-ph/9901124. 93

[78] Andrew R. Liddle. How many cosmological parameters? Monthly Notices of the Royal Astronomical Society, 351(3):L49–L53, 2004. ISSN 1365-2966. doi: 10.1111/j.1365-2966.2004.08033.x. URL http://dx.doi.org/10.1111/j.1365-2966.2004.08033.x. 261, 276

[79] Andrew R. Liddle. Statistical Methods for Cosmological Parameter Selection and Estimation. Annual Review of Nuclear and Particle Science, 59(1):95–114, 2009. doi: 10.1146/annurev.nucl.010909.083706. URL http://www.annualreviews.org/doi/abs/10.1146/annurev.nucl.010909.083706. 274, 275

[80] Andrew R. Liddle and David H. Lyth. COBE, gravitational waves, inflation and extended inflation. Physics Letters B, 291(4):391 – 398, 1992. ISSN 0370-2693. doi: 10.1016/0370-2693(92)91393-N. URL http://www.sciencedirect.com/science/article/pii/037026939291393N. 102, 103, 264

[81] Andrew R. Liddle and David H. Lyth. Cosmological Inflation and Large-Scale Structure. Cambridge University Press, 2000. 15, 58, 93, 97, 104, 141

[82] Andrew R. Liddle, Paul Parsons, and John D. Barrow. Formalizing the slow-roll approximation in inflation. Phys. Rev. D, 50:7222–7232, Dec 1994. doi: 10.1103/PhysRevD.50.7222. URL http://link.aps.org/doi/10.1103/PhysRevD.50.7222. 102

[83] Andrew R. Liddle, Pia Mukherjee, and David Parkinson. Cosmological model selection. [arXiv:0608184], 2006. 274, 275, 276

[84] A.D. Linde. A new inflationary universe scenario: A possible solution of the horizon, flatness, homogeneity, isotropy and primordial monopole problems. Physics Letters B, 108(6):389 – 393, 1982. ISSN 0370-2693. doi: 10.1016/0370-2693(82)91219-9. URL http://www.sciencedirect.com/science/article/pii/0370269382912199. 93

[85] Andrei Linde. Particle Physics and Inflationary Cosmology. CRC Press, 1990. 93

[86] Andrei D. Linde. Inflationary Cosmology. Lect.Notes Phys., 738:1–54, 2008. doi: 10.1007/978-3-540-74353-8_1. 100

[87] Eric V. Linder. Exploring the Expansion History of the Universe. Phys. Rev. Lett., 90: 091301, Mar 2003. doi: 10.1103/PhysRevLett.90.091301. URL http://link.aps.org/doi/10.1103/PhysRevLett.90.091301. 91

[88] David H. Lyth and Antonio Riotto. Particle physics models of inflation and the cosmological density perturbation. Physics Reports, 314(1–2):1 – 146, 1999. ISSN 0370-1573. doi: 10.1016/S0370-1573(98)00128-8. URL http://www.sciencedirect.com/science/article/pii/S0370157398001288. 93, 100, 104

[89] Chung-Pei Ma and Edmund Bertschinger. Cosmological Perturbation Theory in the Synchronous and Conformal Newtonian Gauges. [arXiv:9506072], 1995. 141

[90] Yin-Zhe Ma, Wen Zhao, and Michael L. Brown. Constraints on standard and non-standard early universe models from CMB B -mode polarization. Journal of Cosmology and Astroparticle Physics, 2010(10):007, 2010. URL http://stacks.iop.org/1475-7516/2010/i=10/a=007. 273

[91] Roy Maartens. Brane-World Gravity. Living Reviews in Relativity, 7(7), 2004. URL http://www.livingreviews.org/lrr-2004-7. 56

[92] Gianpiero Mangano, Gennaro Miele, Sergio Pastor, Teguayco Pinto, Ofelia Pisanti, and Pasquale D. Serpico. Relic neutrino decoupling including flavour oscillations. Nuclear Physics B, 729:221 – 234, 2005. ISSN 0550-3213. doi: 10.1016/j.nuclphysb.2005.09.041. URL http://www.sciencedirect.com/science/article/pii/S0550321305008291. 74

[93] M. C. March, N. V. Karpenka, F. Feroz, and M. P. Hobson. Comparison of cosmological parameter inference methods applied to supernovae lightcurves fitted with SALT2. [arXiv: 1207.3705], 2012. 266

[94] Phil Marshall, Nutan Rajguru, and An že Slosar. Bayesian evidence as a tool for comparing datasets. Phys. Rev. D, 73:067302, Mar 2006. doi: 10.1103/PhysRevD.73.067302. URL http://link.aps.org/doi/10.1103/PhysRevD.73.067302. 278

[95] J. C. Mather and *et. al.* Calibrator design for the cobe far infrared absolute spectrophotometer (firas). The Astrophysical Journal, 512(2):511, 1999. URL http://stacks.iop.org/0004-637X/512/i=2/a=511. 267

[96] Patrick McDonald, Uroš Seljak, Scott Burles, and et al. The lya forest power spectrum from the sloan digital sky survey. The Astrophysical Journal Supplement Series, 163(1): 80, 2006. URL http://stacks.iop.org/0067-0049/163/i=1/a=80. 272

[97] G. Miknaitis and *et. al.* The ESSENCE Supernova Survey: Survey Optimization, Observations, and Supernova Photometry. The Astrophysical Journal, 666(2):674, 2007. URL http://stacks.iop.org/0004-637X/666/i=2/a=674. 271

[98] V. Mukhanov. Physical Foundations of Cosmology. Cambridge University Press, 2005. 15, 93, 141

[99] V.F. Mukhanov, H.A. Feldman, and R.H. Brandenberger. Theory of cosmological perturbations. Physics Reports, 215:203 – 333, 1992. ISSN 0370-1573. doi: 10.1016/0370-1573(92)90044-Z. URL http://www.sciencedirect.com/science/article/pii/037015739290044Z. 141

[100] Pia Mukherjee, David Parkinson, and Andrew R. Liddle. A Nested Sampling Algorithm for Cosmological Model Selection. The Astrophysical Journal Letters, 638(2):L51, 2006. URL http://stacks.iop.org/1538-4357/638/i=2/a=L51. 278

[101] Keith A. Olive. Inflation. Physics Reports, 190(6):307 – 403, 1990. ISSN 0370-1573. doi: 10.1016/0370-1573(90)90144-Q. URL http://www.sciencedirect.com/science/article/pii/037015739090144Q. 93, 100

[102] Paul Oxley, Peter A. Ade, and et al. The EBEX experiment. Proc. SPIE 5543, Infrared Spaceborne Remote Sensing XII, pages 320–331, 2004. doi: 10.1117/12.563447. URL +http://dx.doi.org/10.1117/12.563447. 272

[103] T. Padmanabhan. Cosmological constant—the weight of the vacuum. Physics Reports, 380(5–6):235 – 320, 2003. ISSN 0370-1573. doi: 10.1016/S0370-1573(03)00120-0. URL http://www.sciencedirect.com/science/article/pii/S0370157303001200. 69, 75

[104] P. J. E. Peebles and Bharat Ratra. The cosmological constant and dark energy. Rev. Mod. Phys., 75:559–606, Apr 2003. doi: 10.1103/RevModPhys.75.559. URL http://link.aps.org/doi/10.1103/RevModPhys.75.559. 75

[105] Hiranya Peiris. Cosmology Part I: The Unperturbed Universe. *http://nefertiti.hpc.phys.ucl.ac.uk/cosmology/cosmology.html*, 2008. 15

[106] S. Perlmutter, G. Aldering, G. Goldhaber, and et al. Measurements of Ω and Λ from 42 High-Redshift Supernovae. The Astrophysical Journal, 517(2):565, 1999. URL http://stacks.iop.org/0004-637X/517/i=2/a=565. 42, 270

[107] Laurence Perotto, Julien Lesgourgues, Steen Hannestad, Huitzu Tu, and Yvonne Y Y Wong. Probing cosmological parameters with the CMB: forecasts from Monte Carlo simulations. Journal of Cosmology and Astroparticle Physics, 2006(10):013, 2006. URL http://stacks.iop.org/1475-7516/2006/i=10/a=013. 273

[108] Max Pettini. Physical Cosmology. *http://www.ast.cam.ac.uk/∼pettini/physical%20cosmology*, 2008. 15

[109] Cyril Pitrou. The package CMBquick. 2011. *http://www2.iap.fr/users/pitrou/*. 212, 218

[110] Planck Collaboration. The Science Programme of Planck. [astro-ph/0604069], 2012. 272, 273

[111] Brian A. Powell. Tensor tilt from primordial b-modes. [arXiv:1106.5059], 2011. 272

[112] Beth A. Reid and *et. al.* Cosmological constraints from the clustering of the Sloan Digital Sky Survey DR7 luminous red galaxies. Monthly Notices of the Royal Astronomical Society, 404(1):60–85, 2010. ISSN 1365-2966. doi: 10.1111/j.1365-2966.2010.16276.x. URL http://dx.doi.org/10.1111/j.1365-2966.2010.16276.x. 271, 280

[113] Adam G. Riess and *et. al.* New Hubble Space Telescope Discoveries of Type Ia Supernovae at $z \geq 1$ Narrowing Constraints on the Early Behavior of Dark Energy. The Astrophysical Journal, 659(1):98, 2007. URL http://stacks.iop.org/0004-637X/659/i=1/a=98. 271

[114] Adam G. Riess and *et. al.* A Redetermination of the Hubble Constant with the Hubble Space Telescope from a Differential Distance Ladder. The Astrophysical Journal, 699(1): 539, 2009. URL http://stacks.iop.org/0004-637X/699/i=1/a=539. 280

[115] Adam G. Riess, Alexei V. Filippenko, Peter Challis, and et al. Observational evidence from supernovae for an accelerating universe and a cosmological constant. The Astronomical Journal, 116(3):1009, 1998. URL http://stacks.iop.org/1538-3881/116/i=3/a=1009. 42, 270

[116] Antonio Riotto. Inflation and the theory of cosmological perturbations. pages 317–413, 2002. arXiv:0210162. 93

[117] J.A. Rubino-Martin, R. Rebolo, M. Tucci, R. Genova-Santos, S.R. Hildebrandt, et al. The Quijote CMB Experiment. 2008. arXiv:0810.3141. 272

[118] R.K. Sachs and A.M. Wolfe. Perturbations of a cosmological model and angular variations of the microwave background. Astrophys.J., 147:73–90, 1967. doi: 10.1007/s10714-007-0448-9. 213

[119] Uros Seljak and Matias Zaldarriaga. A Line of sight integration approach to cosmic microwave background anisotropies. Astrophys.J., 469:437–444, 1996. doi: 10.1086/177793. 211, 216, 218

[120] J.A. Sellwood and A. Kosowsky. Does dark matter exist? 2000. astro-ph/0009074. 75

[121] Sievers and *et. al.* The Atacama Cosmology Telescope: Cosmological parameters from three seasons of data. [arXiv: 1301.0824], 2013. 266, 268

[122] J. L. Sievers and *et. al.* Cosmological Parameters from Cosmic Background Imager Observations and comparisons with boomerang, dasi, and maxima. The Astrophysical Journal, 591(2):599, 2003. URL http://stacks.iop.org/0004-637X/591/i=2/a=599. 268

[123] Devinderjit Sivia and John Skilling. Data Analysis: A Bayesian Tutorial. OUP Oxford, 2006. 274

[124] J. Skilling. Nested sampling for general Bayesian computation. Bayesian Analysis, 1(4):833–860, 2006. 278

[125] Gary Steigman. Primordial Nucleosynthesis in the Precision Cosmology Era. Annual Review of Nuclear and Particle Science, 57(1):463–491, 2007. doi: 10.1146/annurev.nucl.56.080805.140437. URL http://www.annualreviews.org/doi/abs/10.1146/annurev.nucl.56.080805.140437. 75

[126] K. T. Story and *et. al.* A Measurement of the Cosmic Microwave Background Damping Tail from the 2500-square-degree SPT-SZ survey. [arXiv:1210.7231], 2012. 268

[127] M. Sullivan and *et. al.* SNLS3: Constraints on Dark Energy Combining the Supernova Legacy Survey Three-year Data with Other Probes. The Astrophysical Journal, 737(2):102, 2011. URL http://stacks.iop.org/0004-637X/737/i=2/a=102. 271

[128] N. Suzuki and *et. al.* The Hubble Space Telescope Cluster Supernova Survey. V. Improving the Dark-energy Constraints above $z > 1$ and Building an Early-type-hosted Supernova Sample. The Astrophysical Journal, 746(1):85, 2012. URL http://stacks.iop.org/0004-637X/746/i=1/a=85. 270, 271

[129] P. Szekeres. A class of inhomogeneous cosmological models. Communications in Mathematical Physics, 41(1):55–64, 1975. doi: 10.1007/BF01608547. URL https://doi.org/10.1007/BF01608547. 18

[130] The Dark Energy Survey.*http://www.darkenergysurvey.org/index.shtml*, 2012. 272

[131] J. Alberto Vazquez, S. Hee, M. P. Hobson, A. N. Lasenby, M. Ibison, and M. Bridges. Observational constraints on conformal time symmetry, missing matter and double dark energy. JCAP, 07:062, 2018. doi: 10.1088/1475-7516/2018/07/062. 76

[132] Licia Verde. A practical guide to Basic Statistical Techniques for Data Analysis in Cosmology. [arXiv:0712.3028], 2008. 274

[133] Licia Verde. Statistical methods in cosmology. [arXiv:0911.3105], 2009. 274

[134] Alexander Vilenkin. Cosmic strings and domain walls. Physics Reports, 121(5):263 – 315, 1985. ISSN 0370-1573. doi: 10.1016/0370-1573(85)90033-X. URL http://www.sciencedirect.com/science/article/pii/037015738590033X. 76

[135] Udo von Toussaint. Bayesian inference in physics. Rev. Mod. Phys., 83:943–999, Sep 2011. doi: 10.1103/RevModPhys.83.943. URL http://link.aps.org/doi/10.1103/RevModPhys.83.943. 274

[136] Matias Zaldarriaga and Uro š Seljak. All-sky analysis of polarization in the microwave background. Phys. Rev. D, 55:1830–1840, Feb 1997. doi: 10.1103/PhysRevD.55.1830. URL http://link.aps.org/doi/10.1103/PhysRevD.55.1830. 211, 217